

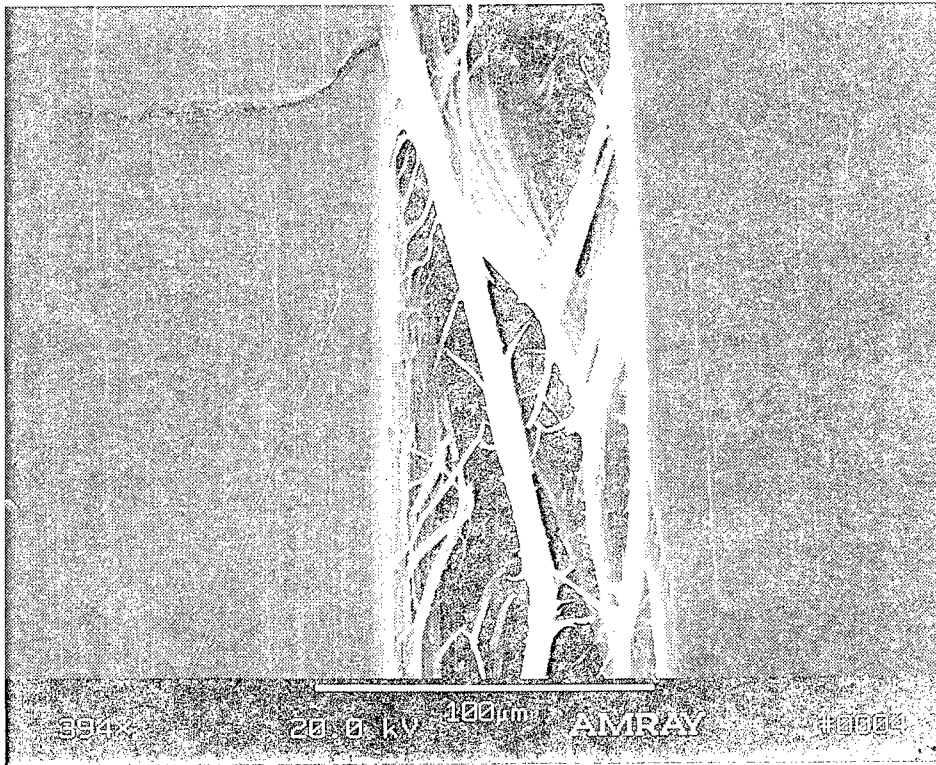
Stress Cracking Potential of HDPE Geogrids



PB99-105512

PUBLICATION NO. FHWA-RD-97-142

AUGUST 1998



U.S. Department of Transportation
Federal Highway Administration

Research and Development
Turner-Fairbank Highway Research Center
6300 Georgetown Pike
McLean, VA 22101-2296

REPRODUCED BY: **NTIS**
U.S. Department of Commerce
National Technical Information Service
Springfield, Virginia 22161



FOREWORD

This report documents part of a comprehensive study entitled, "Durability of Geosynthetics for Highway Applications". The research described here was concerned with evaluating the stress-cracking potential of uniaxially drawn high-density polyethylene (HDPE) geogrid. Assessing the long-term performance of such geogrids is necessary in order to provide rational design procedures for their use in highway applications. This report will be of interest to engineers and technologists charged with the design and construction of highway structures using HDPE geogrids.



Charles J. Nemmers, P.E.
Director, Office of Engineering
Research and Development

PROTECTED UNDER INTERNATIONAL COPYRIGHT
ALL RIGHTS RESERVED.
NATIONAL TECHNICAL INFORMATION SERVICE
U.S. DEPARTMENT OF COMMERCE

NOTICE

This document is disseminated under the sponsorship of the Department of Transportation in the interest of information exchange. The United States Government assumes no liability for its contents or use thereof. This report does not constitute a standard, specification, or regulation.

The United States Government does not endorse products or manufacturers. Trade and manufacturers' names appear in this report only because they are considered essential to the object of the document.

Reproduced from
best available copy.



1. Report No. FHWA-RD-97-142	2  PB99-105512	3. Recipient's Catalog No.	
4. Title and Subtitle STRESS CRACKING POTENTIAL OF HDPE GEOGRIDS		5. Report Date August 1998	6. Performing Organization Code
7. Author(s) Victor Elias, Daniel Carlson, Robert Bachus, and J.P. Giroud		8. Performing Organization Report No. 91-239	
9. Performing Organization Name and Address Earth Engineering and Sciences, Inc. 3401 Carlins Park Drive Baltimore, MD 21215		10. Work Unit No. (TRAIS) 3E3B0772	11. Contract or Grant No. DTFH 61-91-R-00054
12. Sponsoring Agency Name and Address Office of Engineering R & D Federal Highway Administration 6300 Georgetown Pike McLean, VA 22101-2296		13. Type of Report and Period Covered Final Report April 1993 - July 1997	
15. Supplementary Notes FHWA Contracting Officer's Technical Representative: Albert F. DiMillio, HNR-10 Research Subcontractor: GeoSyntec Consultants Technical Consultant: Jerry DiMaggio, HNG-31		14. Sponsoring Agency Code	
16. Abstract This report presents the development of a testing protocol to measure the potential for stress cracking of high-density polyethelene (HDPE) geogrids used for soil reinforcement. The developed data demonstrate that local stress cracking in the unoriented transverse node of HDPE geogrids can occur as a result of construction-induced damage. Undamaged geogrids are not prone to stress cracking at load levels below their 100-year limiting creep load. Cover photo: Scanning electron micrograph of HDPE geogrid test specimen showing shear rupture (Figure 7.28 in text).			
17. Key Words Geosynthetics, testing for stress cracking of geogrids, testing protocols		18. Distribution Statement This document is available to the public through the National Technical Information Service, Springfield, Virginia 22161.	
19. Security Classif. (of this report) Unclassified	20. Security Classif. (of this page) Unclassified	21. No. of Pages 192	22. Price

SI* (MODERN METRIC) CONVERSION FACTORS

APPROXIMATE CONVERSIONS TO SI UNITS

APPROXIMATE CONVERSIONS FROM SI UNITS

Symbol	When You Know	Multiply By	To Find	Symbol	When You Know	Multiply By	To Find	Symbol
LENGTH								
in	inches	25.4	millimeters	mm	millimeters	0.039	inches	in
ft	feet	0.305	meters	m	meters	3.28	feet	ft
yd	yards	0.914	meters	m	meters	1.09	yards	yd
mi	miles	1.61	kilometers	km	kilometers	0.621	miles	mi
AREA								
in ²	square inches	645.2	square millimeters	mm ²	square millimeters	0.0016	square inches	in ²
ft ²	square feet	0.093	square meters	m ²	square meters	10.764	square feet	ft ²
yd ²	square yards	0.836	square meters	m ²	square meters	1.195	square yards	yd ²
ac	acres	0.405	hectares	ha	hectares	2.47	acres	ac
mi ²	square miles	2.59	square kilometers	km ²	square kilometers	0.386	square miles	mi ²
VOLUME								
fl oz	fluid ounces	29.57	milliliters	mL	milliliters	0.034	fluid ounces	fl oz
gal	gallons	3.785	liters	L	liters	0.264	gallons	gal
ft ³	cubic feet	0.028	cubic meters	m ³	cubic meters	35.71	cubic feet	ft ³
yd ³	cubic yards	0.765	cubic meters	m ³	cubic meters	1.307	cubic yards	yd ³
NOTE: Volumes greater than 1000 l shall be shown in m ³ .								
MASS								
oz	ounces	28.35	grams	g	grams	0.035	ounces	oz
lb	pounds	0.454	kilograms	kg	kilograms	2.202	pounds	lb
T	short tons (2000 lb)	0.907	megagrams (or "metric ton")	Mg (or "t")	megagrams (or "metric ton")	1.103	short tons (2000 lb)	T
TEMPERATURE (exact)								
°F	Fahrenheit temperature	5(F-32)/9 or (F-32)/1.8	Celsius temperature	°C	Celsius temperature	1.8C + 32	Fahrenheit temperature	°F
ILLUMINATION								
fc	foot-candles	10.76	lux	lx	lux	0.0929	foot-candles	fc
fl	foot-Lamberts	3.426	candela/m ²	cd/m ²	candela/m ²	0.2919	foot-Lamberts	fl
FORCE and PRESSURE or STRESS								
lbf	poundforce	4.45	newtons	N	newtons	0.225	poundforce	lbf
lbf/in ²	poundforce per square inch	6.89	kilopascals	kPa	kilopascals	0.145	poundforce per square inch	lbf/in ²

* SI is the symbol for the International System of Units. Appropriate rounding should be made to comply with Section 4 of ASTM E380. (Revised September 1993)

TABLE OF CONTENTS

<u>Section</u>		<u>Page</u>
CHAPTER 1	INTRODUCTION	1
1.1	Project Overview	1
1.2	Report Organization	2
1.3	Reviews	2
CHAPTER 2	PROJECT BACKGROUND	3
2.1	Overview	3
2.2	Polyethylene Materials and Their Use in Geosynthetics.	3
2.3	Ductile and Brittle Fracture in HDPE	8
2.4	Constant Tensile Load (CTL) Testing Overview and Equipment	11
2.5	A Comparison of NCTL and UCTL Testing	13
2.6	A Comparison of UCTL Testing and Creep Rupture Testing	15
CHAPTER 3	SCOPE OF WORK	17
3.1	Purpose of Testing Program	17
3.2	Summary of the Research Program's Activities	19
CHAPTER 4	MATERIALS	21
4.1	Selection of Geogrid	21
4.2	Selection of Resins	21
4.3	Resin and Geogrid Index Tests	25
CHAPTER 5	GEOGRID SPECIMEN SELECTION PROCESS	27
5.1	Overview	27
5.2	Investigation of Different Geogrid Specimen Characteristics	27
a.	Specimen Configuration	27
b.	Notch Location	28
c.	Notch Length and Orientation	28
d.	Notch Depth	33
e.	Center Node Width	34

TABLE OF CONTENTS
(continued)

<u>Section</u>	<u>Page</u>	
5.3	Overview of the Geogrid Specimen Selection Process CTL Testing	35
5.4	Geogrid Specimen Selection Process Results	37
a.	Type 1 Configuration (Notch In Rib Material)	37
b.	Type 2 Configuration (Notch in Material Between the Node and the Rib)	39
c.	Type 3 Configuration (Notch In Single-Rib-Wide Node Material)	41
d.	Type 4 Configuration (Notch In Three-Rib-Wide Node Material)	42
5.5	Summary of the Geogrid Specimen Selection Process and Recommendations	45
a.	Summary Regarding Configuration Types 1 to 4	46
b.	Detailed Summary Regarding Type 3 Configuration (Selected)	47
c.	Recommended HDPE Geogrid CTL Testing Protocols	47
CHAPTER 6	CTL TESTING PROGRAM	49
6.1	Overview and Objectives	49
a.	NCTL Resin Testing Objectives	49
b.	UCTL Resin Testing Objectives	50
c.	NCTL Geogrid Testing Objectives	51
d.	UCTL Geogrid Testing Objectives	51
e.	Post-CTL Testing Activities and Objectives	52
6.2	Details of the CTL Testing Program	52
a.	CTL Testing Equipment	52
b.	Procedures for NCTL Resin Specimen Preparation	53
c.	Procedures for UCTL Resin Specimen Preparation	55
d.	Procedures for Geogrid Specimen Preparation	55
e.	Parameters and Procedures for CTL Testing	55
6.3	Discussion of Interpretation Procedures for CTL Testing Results	57
a.	Reliability of Test Results	57
b.	Interpretation of NCTL Strength Rupture Curves	59
c.	Interpretation of UCTL Strength Rupture Curves	63

TABLE OF CONTENTS (continued)

<u>Section</u>	<u>Page</u>
CHAPTER 7	CTL RESIN AND GEOGRID TEST RESULTS AND DATA ANALYSIS 65
7.1	Introduction 65
7.2	CTL Test Results for the Resins 66
a.	Overview 66
b.	NCTL Test Results for the Resins 66
c.	UCTL Test Results for the Resins 80
7.3	CTL Test Results for P-1 Geogrid 83
a.	Overview 83
b.	NCTL Test Results for P-1 Geogrid 92
c.	UCTL Test Results for P-1 Geogrid 95
7.4	Geogrid Failure Mechanisms 100
a.	NCTL Failure Mechanisms in Node Material 103
b.	UCTL Failure Mechanisms in Geogrid 106
7.5	Summary of NCTL and UCTL Tests Results and Failure Mechanisms 113
a.	Summary of CTL Test Results for the Resins 113
b.	Summary of CTL Test Results for the P-1 Geogrid Sample 117
c.	Comparisons 119
d.	Summary of CTL P-1 Geogrid Failure Mechanisms 120
CHAPTER 8	PREDICTING LONG-TERM PERFORMANCE 123
8.1	Introduction 123
8.2	Geogrid Performance Prediction using the Rate Process Method . 125
a.	RPM Predictions from NCTL (Worst Case) Geogrid Data 126
b.	RPM Predictions from UCTL Geogrid Data 130
8.3	Performance Prediction using Popelar et al. 1991 Bidirectional Shifting 135
a.	Popelar et al. Shifting of NCTL Geogrid Data 138
b.	Popelar et al. Shifting of UCTL (Performance) Geogrid Data 140
c.	Comparison of 20°C NCTL and UCTL Master Curves 142

TABLE OF CONTENTS
(continued)

<u>Section</u>	<u>Page</u>
8.4	Conclusions on Geogrid Performance Predictions 145
a.	Comparison Between CTL Predictions 145
b.	Creep Prediction from the Literature 147
c.	Comparison Between CTL and Literature Creep Predictions 148
d.	Significance of NCTL Testing 148
e.	Conclusions 149
8.5	Closure of the Research Program 151
REFERENCES	152
GLOSSARY	155
APPENDICES	
A	- Index Data 160
B	- Resin CTL Data 169
C	- Geogrid CTL Data 177

LIST OF FIGURES

<u>Figure</u>		<u>Page</u>
2.1	The 60-station NCTL testing apparatus used to test resin specimens	14
2.2	A 30-station NCTL testing apparatus, modified to accommodate P-1 geogrid	14
3.1	Isotherms in a reinforced earth structure in July 1983 [Segrestin and Jailloux, 1988]	17
5.1	Type 1 configuration: notch in rib material	29
5.2	Type 2 configuration: notch in material between the node and the rib . . .	30
5.3	Type 3 configuration: notch in single-rib-wide node material	31
5.4	Type 4 configuration: notch in three-rib-wide node material	32
5.5	Ruptured geogrid specimen notched in the rib	40
5.6	Deformation in geogrid specimens notched in the transition zone	40
5.7A&B	Ruptured 80°C geogrid specimens notched across single-rib-wide node . .	43
5.8A&B	Ruptured 80°C geogrid specimens notched in triple-rib-wide node	44
6.1	Typical resin specimen	54
6.2	Typical geogrid specimen	54
6.3	Reproduction of Figure 4 of ASTM D5397-93 showing idealized shapes of NCTL strength-rupture curves	60
6.4	Reproduction of a selected page from Appendix B of Standard Method GRI-GM5(a) showing four examples of transition point selection from NCTL strength rupture curves	62
7.1	NCTL data for resin L, tested at 50°C in water	67
7.2	NCTL data for resin M, tested at 50°C in water	68
7.3	NCTL data for resin H, tested at 50°C in water	69
7.4	NCTL data for resins L, M, and H, tested at 50°C in water	70
7.5	UCTL data for resin L, tested at 50°C in water	71
7.6	UCTL data for resin M, tested at 50°C in water	72
7.7	UCTL data for resin H, tested at 50°C in water	73
7.8	UCTL data for resins L, M, and H, tested at 50°C in water	74
7.9	Selected transition time versus crystallinity, for 50°C NCTL resins L and M, and P-1 geogrid	77
7.10	Selected transition strength versus melt flow index, for 50°C NCTL resins L and M, and P-1 geogrid	79
7.11	NCTL data for P-1 geogrid, tested at 50°C in water	84
7.12	NCTL data for P-1 geogrid, tested at 65°C in water	85
7.13	NCTL data for P-1 geogrid, tested at 80°C in water	86
7.14	NCTL data for P-1 geogrid, tested at 50°C, 65°C, and 80°C in water . . .	87
7.15	UCTL data for P-1 geogrid, tested at 50°C in water	88
7.16	UCTL data for P-1 geogrid, tested at 65°C in water	89
7.17	UCTL data for P-1 geogrid, tested at 80°C in water	90
7.18	UCTL data for P-1 geogrid, tested at 50°C, 65°C, and 80°C in water . . .	91

LIST OF FIGURES (continued)

<u>Figure</u>		<u>Page</u>
7.19	Trend in transition time for NCTL P-1 geogrid test series.	94
7.20	NCTL data for resin M and P-1 geogrid, tested at 50°C in water	96
7.21	Relationship between 65°C NCTL and 65°C UCTL brittle zone P-1 geogrid data	101
7.22	Relationship between 80°C NCTL and 80°C UCTL brittle zone P-1 geogrid data	102
7.23A,B&C	Ductile ruptures in NCTL P-1 geogrid specimens	104
7.24A,B&C	Transitional ruptures in NCTL P-1 geogrid specimens	105
7.25A,B&C	Brittle ruptures in NCTL P-1 geogrid specimens	107
7.26A,B&C	Shear ruptures in 50°C UCTL P-1 geogrid specimens	109
7.27	Closeup of shear rupture in UCTL P-1 geogrid specimen	110
7.28A,B&C	Shear ruptures in 50°C, 65°C, and 80°C UCTL P-1 geogrid specimens	111
7.29A&B	Brittle ruptures in 65°C and 80°C UCTL P-1 geogrid specimens	114
7.30A&B	Brittle ruptures in 80°C UCTL P-1 geogrid specimen compared with brittle rupture in 80°C NCTL P-1 geogrid specimen	115
7.31A,B,C&D	Brittle ruptures in 80°C UCTL P-1 geogrid specimens	116
8.1	Idealizations of NCTL (“worst case”) P-1 node material test data	127
8.2	Idealizations of NCTL (“worst case”) P-1 node material test data, showing equations of lines, center points, and corner points	128
8.3	Predicted NCTL (“worst case”) behavior of P-1 node material using the RPM (20°C)	129
8.4	Idealizations of UCTL P-1 geogrid test data	131
8.5	Idealizations of UCTL P-1 geogrid test data, showing equations of lines, center points, and corner points	133
8.6	Predicted UCTL behavior of P-1 geogrid product using the RPM (20°C)	134
8.7	Predicted NCTL (“worst case”) behavior of P-1 node material using Popelar et al. shifting functions (20°C)	139
8.8	Predicted UCTL behavior of P-1 geogrid product using Popelar et al. shifting functions (20°C)	141
8.9	Predicted UCTL behavior of P-1 geogrid product using Popelar et al. shifting functions (20°C), based on an overall trend	143
8.10	Relationship between 20°C NCTL and 20°C UCTL P-1 geogrid trends obtained using Popelar et al. shifting functions	144

LIST OF TABLES

<u>Table</u>		<u>Page</u>
1	Generalized summary of the five HDPE materials used in the research program .	8
2	Number of specimens tested for program	20
3	Summary of mean resin and geogrid index test data	23
4	Investigation of effect of center node width on failure mechanism and time to rupture	36
5	Summary of results of the geogrid specimen selection process	38
6	Summary of slopes and transition points for CTL results	75
7	NCTL (“worst case”) geogrid data used for RPM calculations	130
8	UCTL geogrid data used for RPM calculations	135
9	Summary of calculated natural exponentials used for Popelar et al. shifting . . .	137
10	20°C, 100-yr strength levels predicted using different methods	146
11	Long-term performance strength levels at 20°C	148

CHAPTER 1

INTRODUCTION

This report provides an evaluation of the notched and unnotched stress rupture characteristics of three high-density polyethylene (HDPE) resins, one used to produce geogrids, and one oriented, HDPE geogrid product. This research initiative was conducted for the development of a methodology that can be used to predict long-term performance, with reference to stress-cracking resistance of uniaxially drawn HDPE geogrid products.

The data presented in this report are consistent with the scope of work for Task G, Federal Highway Administration (FHWA) Project - DTFH 61-91-R-00054 *“Durability of Geosynthetics for Highway Applications.”* The research was primarily conducted by GeoSyntec Consultants.

1.1 PROJECT OVERVIEW

Geosynthetics are manmade products installed in the ground or in structures made of earth. A typical modern geosynthetic product is designed to perform specific engineering functions and is a compound composed of a specific plastic resin and specific additives. Engineers commonly use geosynthetic products in highway applications to provide soil reinforcement, soil filtration, soil/aggregate separation, and water transmission. The types of plastic compounds used in geosynthetics have unique material properties that must be considered by the designer. It is necessary for the engineer to understand the performance characteristics and material properties of the geosynthetic products that will be used for a functional use.

Geogrids are geosynthetic products commonly used in highway applications and are the subject of this research. Geogrids are primarily used for soil reinforcement applications in which the tensile strength characteristics of the geogrid are utilized. Different materials and different manufacturing techniques are used to produce geogrids. One frequently used geogrid product is manufactured from HDPE. It has been observed in geosynthetic applications other than highway soil reinforcement that certain HDPE materials are susceptible to a phenomenon known as environmental stress cracking (ESC). ESC occurs when a material cracks in a relatively abrupt, brittle fashion. To date, there are no known instances or reports of this type of failure in installed HDPE geogrids. However, because of

the widespread use of HDPE in engineering applications, it is desirable to gain a better understanding of the material properties of HDPE, particularly as it is used in geogrid products. Accordingly, a research program was developed to improve the understanding of the ESC resistance and the long-term performance of uniaxially drawn, HDPE geogrid products. This report presents the results of the research program.

1.2 REPORT ORGANIZATION

This report is organized as follows:

- project background is presented in chapter 2;
- scope of work is described in chapter 3;
- selection of test materials is discussed in chapter 4;
- geogrid specimen selection process is discussed in chapter 5;
- CTL testing program is described in chapter 6;
- data analysis is discussed in chapter 7; and
- long-term performance prediction is presented in chapter 8.

1.3 REVIEWS

The research tasks reported were developed initially by a project Interdisciplinary Advisor Team and formalized on a Task A Final Report, which formed the basis of the research program.

The Task A Final Report was then reviewed by a Peer Advisory Group whose valuable suggestions were incorporated whenever possible prior to the commencement of the research. The Peer Advisory Group consisted of:

1. Dr. Robert Koerner - Geosynthetic Research Institute
2. Dr. Robert Holtz - University of Washington
3. Dr. Robert Duvall - Engineering Systems, Inc.

Prior to finalizing the results of the research, a draft report was further reviewed by Drs. Koerner and Duvall of the Peer Advisory Group who made a number of suggestions to clarify some issues and improve the final product. These suggestions were incorporated whenever possible in this final report.

CHAPTER 2

PROJECT BACKGROUND

2.1 OVERVIEW

To better understand the research program and the rationale for its development, a background is presented. This section is organized to provide: (1) a discussion of polyethylene and its use in engineering geosynthetics (including geogrids); (2) an introduction to environmental stress cracking and the mechanisms of ductile and brittle fracture; (3) a description of constant tensile load (CTL) testing equipment that is used to evaluate the stress cracking resistance of materials; and (4) a comparison of notched constant tensile load (NCTL) and unnotched constant tensile load (UCTL) testing. Whenever appropriate, reference is made in this background section to specific elements of the actual laboratory testing program.

2.2 POLYETHYLENE MATERIALS AND THEIR USE IN GEOSYNTHETICS

Polyethylene is a manmade material, classified as a polymer, which consists of polyethylene molecules. The polyethylene molecule can be thought of as a chain in which the individual links, referred to as ethyl units, have a simple molecular structure consisting of two carbon atoms bonded to each other and two hydrogen atoms bonded to each carbon atom. The subsequent bonding of carbon atoms of adjacent ethyl units occurs in a linear (i.e., chain-like) fashion, forming the backbone of the polyethylene chain. Polyethylene is, therefore, referred to as a linear polymer.

Linear polymers can exist in any combination of three specific states: crystalline, amorphous, and oriented. The crystalline state, also called the ordered state, is characterized by three-dimensional order over at least a portion of the chains.⁽⁵⁾ The amorphous state, also called the liquid state, is characterized by randomly arranged chains. Because both crystalline and amorphous states are present, polyethylene material, for example, is generally referred to as having a semicrystalline structure.

The oriented state is a more recent concept of order. The oriented state results when a mechanical stress is applied to a linear polymer during crystallization; this is a process sometimes called oriented crystallization.

Studies of the semicrystalline nature of standard linear polymers (i.e., polymers not having undergone oriented crystallization) have identified three major regions of molecular organization: the crystalline region, the interfacial region, and the amorphous region.⁽⁵⁾ These regions are described as follows:

- ***Crystalline Region:*** In certain regions of a polyethylene material, portions of polyethylene molecules are highly ordered and densely packed into lamellar-like crystallites. (The non-ordered portions of these molecules then make up, and interact with, interfacial regions and amorphous regions).⁽⁵⁾ The degree of crystallinity in a linear polymer affects the material properties (e.g., flexibility) of the resin.
- ***Interfacial Region:*** An interfacial region can be thought of as representing the boundary between a crystalline region and an amorphous region. However, the interfacial region is diffuse; it is not sharp or clearly defined.⁽⁵⁾ The relationship between the interfacial region and material properties is not well understood.
- ***Amorphous Region:*** The amorphous region is situated between crystallites and is, therefore, also known as the interlamellar region. The interlamellar region consists of molecules and portions of molecules that are much less organized than crystalline regions and that can be loosely thought of as the connecting regions between crystallites. Note: the term tie molecule is associated with this region. However, Mandelkern points out: “The term tie molecules... is a misnomer. It implies that the connections are extended or straight and represent complete molecules. These connections represent only portions of molecules and are clearly in random conformation.” This region is considered generally isotropic; that is, molecules and portions of molecules in the interlamellar region are without preferential orientation. (An exception to this may be the interlamellar regions of an oriented linear polymer, such as the P-1 material tested in this research program.) The amorphous region plays a crucial role in governing many properties.⁽⁵⁾

A fourth microstructural region, the oriented region, also can be distinguished and is briefly discussed. Mechanically stretching a polyethylene resin at temperatures near its melting point aligns, or orients, both crystalline and amorphous regions in the direction of the mechanical stretching. Because crystalline regions are affected by the warming and stretching, some new crystallization processes are imparted to the material. Immediate cooling of the material then locks the molecules into the oriented state. The process of applying a mechanical stress to a linear polymer during warming at temperatures near its

melting point is sometimes called oriented crystallization. The addition of oriented-crystallization processes to the microstructural domain of a standard linear polymer appears to further complicate a picture of the microstructure. This discussion is presented, however, because the amount of orientation affects material properties.

Material properties are also affected by the supermolecular structure. Crystalline and oriented regions can be found organized in patterns, indicating a larger scale of organization (i.e., the supermolecular structure); spherulitic structures in polyethylene, for example, evidence a larger scale of organization. The supermolecular structure is largely dependent on molecular weight, crystallization conditions (e.g., quenching temperature), and density.⁽⁵⁾ Some understanding of supermolecular structure is important to this research program because the different portions of the geogrid tested in this program underwent different crystallization conditions (i.e., different degrees of oriented crystallization).

As indicated in the above discussions, the material properties of linear polyethylene are dependent on a large number of variable manufacturing processes and variable material characteristics (e.g., molecular weight). Of these many variables, the material properties of linear polyethylene are perhaps most influenced by the following characteristics:

- density;
- molecular weight and molecular weight distribution; and
- crystallization conditions.

Bourgeois and Blacket and the Plastic Pipe Institute (PPI) each identify density, molecular weight (MW), and molecular weight distribution (MWD) as the three material characteristics most influencing material properties.^(6,7) Mandelkern includes crystallization conditions, as well as molecular constitution, as the primary variables affecting molecular structure and, thus, material properties. Furthermore, Mandelkern shows how molecular weight and crystallization conditions can be strategically controlled in order to isolate independent structural variables and assess the influence of each such variable on a given property.⁽⁵⁾

Density is defined as the mass in air of a unit volume of the material, as defined by the American Society for Testing and Materials (ASTM) D 883-90. ASTM D 1248 requires that polyethylene resins with a density 0.941 g/cm^3 and higher be classified by the term high-density. The polyethylene materials tested in this research program each possessed a density greater than 0.941 g/cm^3 , with the exception of the resin H material, which had a density of approximately 0.936 g/cm^3 when corrected for carbon black content.

The density of a polyethylene material is determined by the amount of side branching on the main polymer chains (i.e., by the level of comonomer used). Polymer chains with only a few, short side branches can pack tightly together; i.e., in a *dense* arrangement. Because side branches act as obstacles to tight packing, polymer chains with more or longer side branches are not able to pack as tightly together. Hence, the more side branches, the lower the density. This discussion of density is important because it is well established that stress cracking resistance, the property primarily studied in this research program, correlates strongly with density.^(6,7,8) For this research program, density and degree of orientation will be considered the two characteristics most affecting stress cracking resistance.

MW and MWD are two other important variables the control of which, in conjunction with the control of crystallization processes, influences material properties.^(5,6) MW represents an average polymer molecule size, and MWD represents a statistical range of molecule lengths. The MW and MWD of the materials tested for this research program were not determined, and it is likely that these materials had different MWs and MWDs. MW and MWD cannot, therefore, be considered variables that were kept constant in this research program.

In light of not knowing the MWs and MWDs of the materials tested for this research program, and in light of the well-established correlation between density and stress cracking resistance, it was assumed that the influence of MW and MWD (on stress cracking resistance) is subordinate to the influence of density. Therefore, this report emphasizes density and excludes correlation of results with MW or with MWD.

Prior to its use in manufacturing a geosynthetic product, polyethylene resin is in the form of small, white pellets. A representative quantity of these pellets can be set aside and later molded into a flat sheet, referred to as a plaque. A plaque is tested in a laboratory to verify the material properties of the batch of polyethylene resin from which the plaque was molded. Plaques of two specific polyethylene resins (i.e., resins L and M) were produced for this laboratory testing program.

Plaques further enable the commercial identification of a polyethylene resin. A specified system of identifying PE plastics molding and extrusion materials by type, class, category, and grade is detailed in ASTM D1248.⁽⁹⁾ According to ASTM D1248, type identifies nominal density, class identifies color, category identifies nominal flow rate, and grade distinguishes between a variety of different characteristics or properties such as resistance to ESC. Commercial identification of polyethylene resins is important to manufacturers who are concerned with the characteristics and properties of the final materials and products made from the resins.

Reference is also made to the more recent standards for classification such ASTM D 3350-96, "Standard Specification for Polyethylene Plastic Pipe and Fittings Materials," and ASTM D 4000-95a, "Standard Classification System for Specifying Plastic Materials."

Polyethylene is commonly used in the manufacturing of geomembranes as well as in geogrids. Geomembranes are typically used for liquid retention applications, while geogrids are most commonly used for reinforcement applications. Most geomembranes have a small degree of biaxial orientation due to stretching that occurs during their manufacturing. The biaxial orientation in most geomembranes is normally slightly stronger in one direction. The direction commonly referred to as the machine direction is usually the most oriented and, therefore, stronger direction in a geomembrane. Geomembrane is fabricated from polyethylene ranging from very low to high-density.

Certain types of geogrids are manufactured using HDPE. Due to the manufacturing process, HDPE geogrids are different from HDPE geomembranes in both form and microstructure. The manufacturing process for the HDPE geogrid used in this research program involves: (1) punching rows of holes in a thick, extruded sheet of HDPE; (2) stretching the heated, softened sheet to form elongated, parallel ribs separated by elongated holes; and (3) cooling the resulting grid in this stressed condition. This product is referred to as an uniaxially drawn HDPE geogrid. It is noted that a punched HDPE sheet can be stretched in two directions to form a biaxially drawn HDPE geogrid.

The thick crossbars of a uniaxially drawn geogrid, representing the original HDPE sheet material from which the ribs were stretched, are commonly referred to as nodes or as bars. The material in the area between a rib and a node is sometimes called the transition zone or transition zone material. This term can be confusing, however, because the term transition zone also is used to refer to a certain part of a stress rupture curve. Therefore, to reduce potential confusion, transition zone material will be referred to as the material in the area between the rib and the node in this report. The geogrid manufacturing process is important to understand because it results in a high degree of orientation in the rib material, and a lesser degree of orientation in the node material. This high degree of orientation in the ribs makes this type of geogrid product strong in the direction of stretching, thus enabling its use in reinforcement applications.

For reference, table 1 provides a generalized summary of the five polyethylene materials tested in this research program. The commercial identifications of the HDPE materials tested in this research program are summarized as follows:

base resin for P-1
 and P-1a geogrid - D1248-IIIA5-E5
 resin L - D1248-IIIA5-E10/low ESCR
 resin M - D1248-IIIA5-E5
 resin H - D1248-IIIC4-W7/W8

Table 1. Generalized summary of the five HDPE materials used in the research program.

Material Identification	Polyethylene Density	Geosynthetic Product Type	Color	Approximate Thickness (mm)	Other Dimensions (mm)
Resin L	High-density	Plaque	Milky-White	1.8	N/A
Resin M	High-density	Plaque	Translucent-White	2.1	N/A
Resin H	High-density	Geomembrane	Black	1.5	N/A
Geogrid P-1	High-density	Uniaxially Drawn Oriented-Geogrid	Black	node: 2.75 rib: 0.9	node width: 16 rib width: 6.0 rib length: 147
Geogrid P-1a	High-density	Uniaxially Drawn Oriented-Geogrid	Black	node: 5.8 rib: 2.0	node width: 17 rib width: 6.2 rib length: 150

For the purposes of this research program, it is important to notice that resin M had the same commercial identification as that of the base resin used to make the P-1 geogrid, and also that resin L was commercially identified as having a low resistance to ESC when tested in accordance with ASTM D1693, while resin H was identified as having a high resistance to ESC.

2.3 DUCTILE AND BRITTLE FRACTURE IN HDPE

This section presents descriptions of ductile and brittle fracture, and of stress cracking initiation and propagation, in basically non-oriented HDPE material. It is emphasized,

however, that these descriptions do not necessarily describe fracture appearances and processes in highly oriented HDPE material, as will be revealed in this research program. The subject of ductile and brittle fracture in HDPE is closely related to the subject known as creep rupture of the material.

When a polyethylene product is loaded in tension, the material stretches and the object's cross-section becomes smaller than it was in the original unloaded state. Under sustained loading, polyethylene can stretch to several times its original length, resulting in a large amount of plastic, or irrecoverable, deformation. Ductile rupture results when continuing plastic deformation leads to the separation of the material into two pieces. The two new surfaces in the ruptured material are called fracture faces. The terminal condition of a material that has experienced stress cracking, rapid crack propagation, an extensive degree of plastic deformation, or a combination of these failure modes is called a fracture. Fractures in polyethylene are characterized as being either ductile, brittle, or transitional. These type of fractures are briefly described:

- *Ductile Fracture:* A ductile fracture in polyethylene is characterized by obvious plastic deformation. The material appears to stretch until it breaks. The resulting final cross-sectional area is smaller than the original cross-sectional area.
- *Brittle Fracture:* A brittle fracture in polyethylene is characterized by fracture faces showing no obvious plastic deformation of the bulk material. Brittle fractures in HDPE can be further subdivided as quasi-brittle and truly brittle. A quasi-brittle fracture in HDPE is characterized by a multitude of tiny plastic deformation points observable on a microscopic level; thus causing the quasi-brittle fracture to appear velvety to the naked eye. A truly brittle fracture in HDPE is characterized by very smooth, often shiny and glass-like, fracture faces. The brittle fractures observed in this research program were all quasi-brittle.
- *Transitional Fracture:* the third type of fracture that can occur in polyethylene is called a transitional fracture. A transitional fracture is characterized by roughly equal degrees of both ductile and quasi-brittle characteristics.

In general, ductile fractures occur when HDPE is subjected to relatively high stress. Brittle fractures may occur in HDPE subjected to relatively low stress. The terms high and low are relative to the short-term yield stress. Transitional fractures may occur in HDPE subjected to a stress falling within a narrow window that is between the minimum stress required to

produce ductile rupture and the maximum stress producing brittle rupture. The precise values of these stress levels vary according to the variations in material properties between specific resins.

Quasi-brittle fracture planes are created by the development of slowly growing cracks in the material. The slow crack growth rate can be as slow as a fraction of an inch (25 mm) per day.⁽³⁾ This slow crack growth process occurs at stress levels that are not high enough to cause observable plastic deformation in the bulk material, but that are high enough to cause very slow separation between crystalline regions of the material's microstructure. This phenomenon is referred to as stress cracking. Stress cracking represents slow, microscopic-scale, plastic deformation that propagates in a more or less planar manner between crystalline regions, or along crystalline planes, in a material's microstructure. Therefore, resistance to stress cracking propagation is considered a material property, and is simply referred to as stress cracking resistance.

Stress cracking usually initiates at a stress raiser, such as a notch, hole, or other discontinuity in the material. A stress raiser is a location that causes localized stress concentration, providing a *potential* initiation site for stress cracking. The term flaw is also sometimes used to identify a potential initiation site for stress cracking. A flaw can be a material defect, a manufacturing defect, or post-production damage and can be microscopic or macroscopic in size.⁽⁷⁾ In this report, the term stress raiser will be used, rather than flaw, because flaw implies a mistake or unintended occurrence. A stress raiser, however, also can occur at a location of *intended* change in product shape or *intended/unavoidable* change in (internal) morphology. Frequently, inclusion of a stress raiser in a product cannot be avoided. (A corner or hole are examples of stress raisers.) Minimizing the local stress concentration at such a stress raiser may then become desirable (e.g., using a radius at a corner).

Quasi-brittle fracture can occur without any apparent stress raiser.⁽⁸⁾ In usage, however, quasi-brittle fracture initiates at obvious stress raisers, such as at the edge of a weld, or in the valley of a deep gouge. Therefore, for simplicity, it will be herein stated that stress cracking initiation *requires* a stress raiser.

Through microscopic analysis, it is known that stress cracking initiates when crystalline regions abutting a stress raiser begin to slowly stretch apart in a shape that looks like a narrow arrowhead pointing sharply away from the stress raiser. This arrowhead-shaped, microscopically small region of plastic deformation is called a craze. As the crystalline regions on either side of the craze continue to separate, the wider end of the craze will

rupture, forming the start of a crack. The sharp tip of the craze will provide the new location of a new stress raiser. As a result, the stress cracking process will perpetuate itself through the material until either rupture occurs or until the craze is arrested. A craze can therefore be viewed as the precursor of quasi-brittle rupture.

Stress cracking in polyethylene materials may be further accelerated by the presence of some chemical agents and by an increase in ambient temperature. Stress cracking that is accelerated in a chemical environment is called environmental stress cracking. The testing performed for this report is best referred to simply as stress cracking, rather than environmental stress cracking, because the testing was performed in a water bath. The terms are, however, sometimes used interchangeably as they relate to the same fundamental material property.

In summary, there are three elements necessary for stress cracking to occur in practical situations : (1) a stress, (2) a stress raiser, and (3) a material susceptible to stress cracking.

2.4 CONSTANT TENSILE LOAD (CTL) TESTING OVERVIEW AND EQUIPMENT

Procedures for evaluating the stress cracking resistance of product specific PE materials were developed by the plastic pipe industry before they were adopted by the geosynthetics industry. Mention is therefore made to ASTM D 1598, "*Test Method for Time-to-Failure of Plastic Pipe Under Constant Internal Pressure,*" and ASTM D 2837, "*Standard Test Method for Obtaining Hydrostatic Design Basis for Thermoplastic Pipe Materials.*" While these plastic pipe methods have been used and refined for several decades, it has only been in the last 5 to 10 years that the geosynthetics industry has established a standard method for evaluating stress cracking resistance of PE geomembrane. This method involves a laboratory test called the CTL test.

A CTL test is a laboratory test in which a force of constant magnitude and direction is continuously applied to one end of an anchored specimen; the force is intended to produce stretching or rupture in the specimen's gauge length. In this report, the term CTL is used in a generic sense to encompass both NCTL testing and UCTL testing.

The stress cracking resistance of polyethylene resins and geomembranes is now commonly evaluated using ASTM D 5397, "*Standard Test Method for Evaluation of Stress Crack*

Resistance of Polyolefin Geomembranes Using Notched Constant Tensile Load Test.” This method consists of: (1) applying a range of constant tensile loads to carefully notched, dumbbell-shaped specimens while exposing these specimens to a specific surface-active solution and to a controlled, elevated temperature; and (2) accurately recording the time to rupture for each specimen and plotting percent of yield strength versus time to rupture data points on log-log axes. The purpose of this test method is to provide for relative comparisons of the stress cracking resistances of different geomembrane sheets. Section 5.2 of ASTM D 5397-93 states, “This test method is intended as an index test and may be used for grading polyolefin geomembrane sheets in regard to their stress cracking sensitivity.” The CTL testing performed for this research program followed ASTM D 5397 methodology with the following deviations in specified test conditions: (1) no notch was employed for UCTL testing, and (2) immersion in a water bath was employed for all CTL testing performed for the main CTL testing program.

Standard CTL testing equipment requirements also are described in ASTM D 5397 and were employed for this research program. These equipment requirements included:

- D 1822 Type L die (for cutting test specimens from sheet samples);
- Notching device (for making accurate, consistent notches in specimens);
- Immersion cell with:
 - ability to hold a fluid,
 - a distinct station for each specimen,
 - accommodation for 10 or more stations per cell,
 - construction materials resistant to the immersion solution,
 - heating system, controller, and insulation, and
 - circulation or agitation device;
- Loading system with:
 - simple lever arms,
 - weights (individually calculated and weighed), and
 - clamps or hooks (for gripping test specimens); and
- Timer system with:
 - on and off switches, and
 - hour meters.

Two of the actual testing apparatus used for this research program are shown in figures 2.1 and 2.2. These figures show immersion cells, loading systems, and timer systems. The CTL testing equipment, and modifications made to the equipment to accommodate CTL testing on geogrid, are further described in chapter 6.

2.5 A COMPARISON OF NCTL AND UCTL TESTING

The stress cracking resistance of a material is evaluated in the laboratory by the CTL test using the testing equipment previously described. In this test, a CTL is applied to a specimen containing a stress concentrator potentially sufficient to induce stress cracking. CTL testing that employs a reproducible, artificial notch as a stress concentrator is called NCTL testing; if testing proceeds on a specimen without introducing an artificial stress concentrator, the test is referenced as UCTL test. The testing performed in this research program consisted of both NCTL and UCTL tests.

A detailed discussion of the NCTL and UCTL tests will be presented in subsequent sections of this report. For purposes of this background, however, it is useful to briefly compare and contrast the two testing techniques. The primary purpose of the NCTL test is to assess the relative stress cracking resistance of a material. This is accomplished by placing a stress concentrator (usually a sharp notch) at a critical location on the specimen. The notch shape and location is pre-selected to induce stress cracking initiation at that location.

The UCTL test procedures are essentially identical to those of an NCTL test, except that an artificial stress concentrator (i.e., the notch) is not introduced to the (UCTL) specimen. The stress concentrator in a UCTL specimen may be some inherent feature of the product (i.e., node, hole, seam, scratch, etc.). Therefore, the results may have a more direct design application:

With specific reference to the testing program described in this research project, both NCTL and UCTL testing were conducted on specimens from two HDPE plaques, one HDPE geomembrane, and one HDPE geogrid product. The reasons for this type of testing program are summarized as follows:

- The NCTL tests on the two HDPE plaques and one geomembrane were conducted to provide baseline reference information regarding the relative stress cracking resistance of HDPE resin, including the resistance of the specific HDPE resin type (i.e., a base resin) used to manufacture the HDPE geogrid.

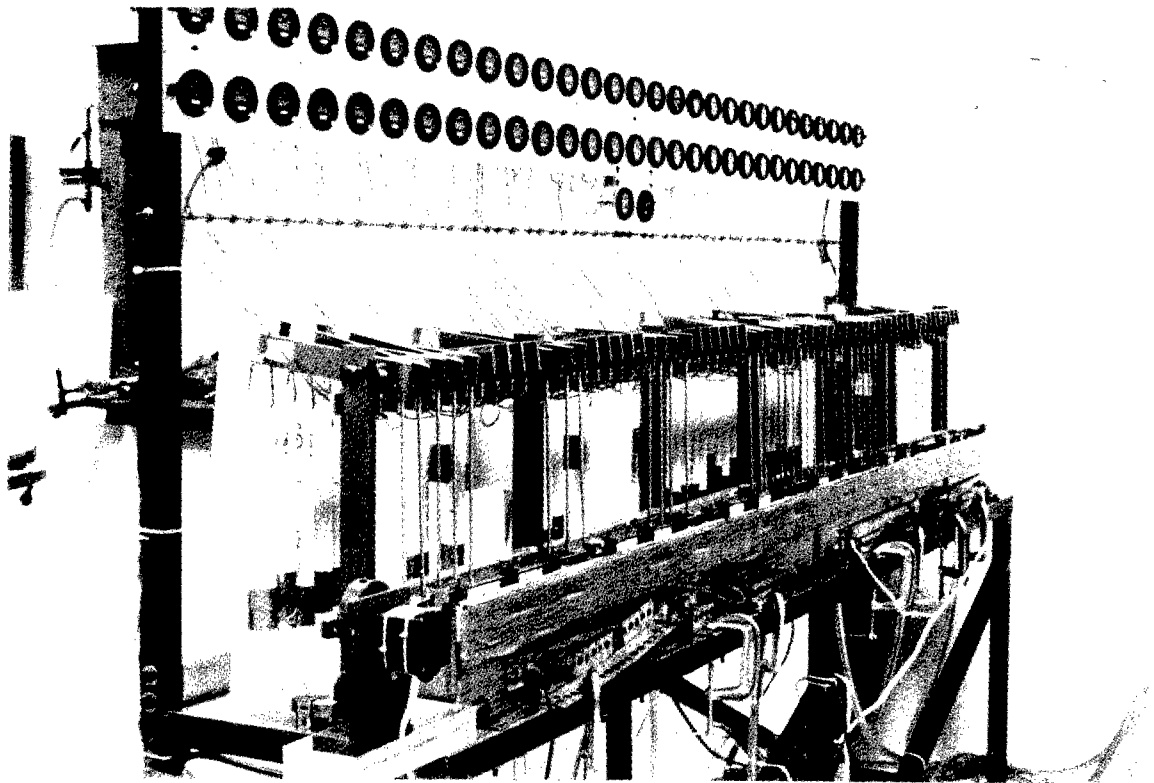


Figure 2.1 The 60-station NCTL testing apparatus used to test resin specimens.

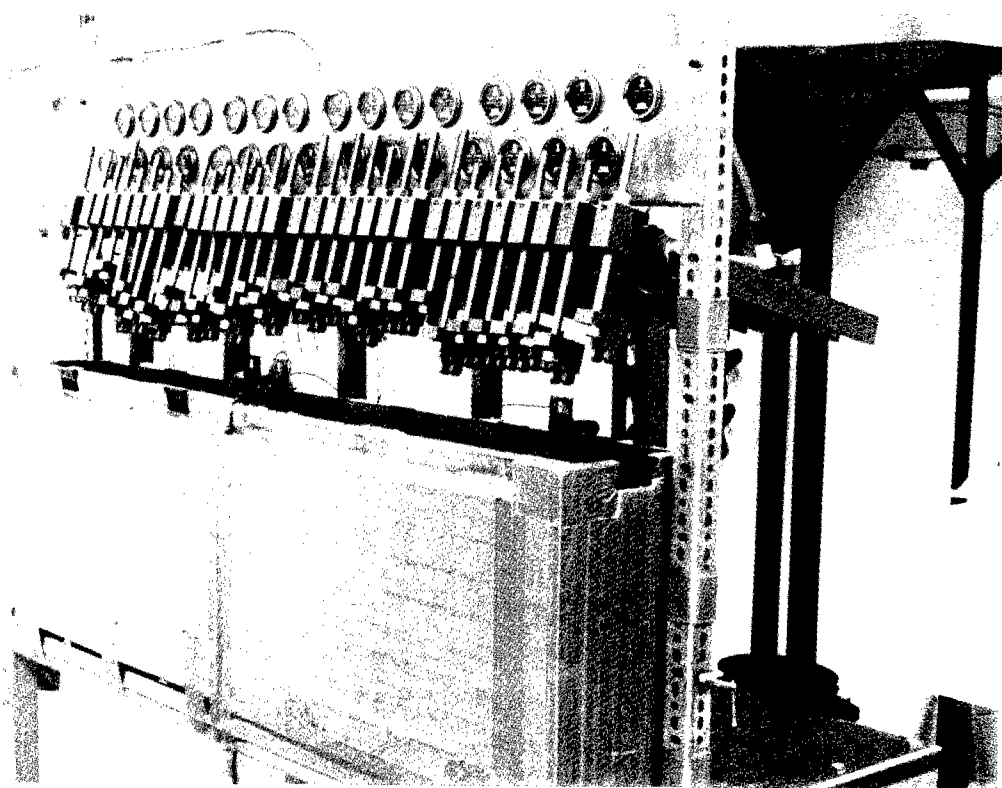


Figure 2.2 A 30-station NCTL testing apparatus, modified to accommodate P-1 geogrid.

- The UCTL tests on the two HDPE plaques and one geomembrane were conducted to provide for a comparative analysis of NCTL and UCTL testing results and provide baseline data for long-term prediction for stress cracking resistance of non-oriented HDPE materials.
- The NCTL tests on the HDPE geogrid were conducted to assess the inherent stress cracking resistance of the partially oriented node material. Again, this testing was conducted to assess the fundamental material property, stress cracking resistance, of the node material of the HDPE geogrid.
- The UCTL tests on geogrid were conducted to assess whether any feature or portion of the node, the material in the area between the rib and the node, or rib of the HDPE geogrid product can serve as an inherent stress concentrator sufficient to induce stress cracking. This testing also allowed for comparison of UCTL geogrid results with NCTL geogrid results.
- The UCTL tests on geogrid also were conducted to provide for a long-term prediction that engineers can use to preclude stress cracking failures in the geogrid; this was the primary goal of the UCTL testing and of the research program.

A detailed discussion of the NCTL and UCTL testing program is described in chapter 6 of this report. Results of the laboratory testing and of the interpretation of the test results are provided in chapters 7 and 8, respectively.

2.6 A COMPARISON OF UCTL TESTING AND CREEP RUPTURE TESTING

Standard creep rupture testing involves applying a CTL to an unnotched specimen exposed to air at room temperature, and measuring strain with time until specimen rupture or a preset maximum strain for durations of up to 10,000 hr.⁽¹⁰⁾ UCTL testing also involves applying a constant load to an unnotched specimen. In UCTL testing, however, the specimen is exposed to a chemical environment (e.g., water) at an elevated temperature, and the time to rupture is recorded.⁽⁴⁾ The test conditions involved in this comparison are:

<u>Test Condition</u>	<u>Creep Rupture Testing</u>	<u>UCTL Testing</u>
undamaged product	✓	✓
unnotched specimen	✓	✓
constant load	✓	✓
specimen allowed to creep until rupture	✓	✓
chemical environment	X	✓
elevated temperature	X	✓

Note that ✓ indicates a condition normally incorporated, and X indicates a condition not normally incorporated. The UCTL test is very similar to a creep rupture test but differs from a creep rupture test in that strain is not measured in the UCTL test and in that the UCTL test is performed at an elevated temperature (rather than at, or near, room temperature) in a chemical environment (e.g., in water). The intent of exposing the geogrid to a chemical environment (e.g., water) in the UCTL test is to simulate the actual chemical environment to which the installed geogrid may be exposed. The intent of exposing the geogrid to an elevated temperature in the UCTL test is to accelerate the test (i.e., to decrease its duration).

CHAPTER 3

SCOPE OF WORK

3.1 PURPOSE OF TESTING PROGRAM

The primary goal of this research program is to conservatively predict a strength value that engineers can use as a design parameter to preclude stress cracking failures in the selected, uniaxially drawn, HDPE geogrid product exposed to a baseline ambient temperature of 20°C for 100 yrs. The 20°C/100-yr conditions for prediction are consistent with 1992 American Association of State Highway and Transportation Officials (AASHTO) criteria. The impetus for this research program is the need to investigate the possibility of stress cracking failure in HDPE geogrids in light of the known capability of stress cracking failure inherent in HDPE pipes in HDPE geomembranes.

It is beyond the scope of this report to discuss the 20°C/100-yr conditions. It is only noted that the temperature of a geogrid in a reinforced soil structure can be significantly lower or higher than 20°C, as illustrated by figure 3.1.⁽¹⁾ This figure shows isotherms in the summer in a reinforced earth structure in the Europe, although even higher temperatures have been measured in a similar structure in Arizona.

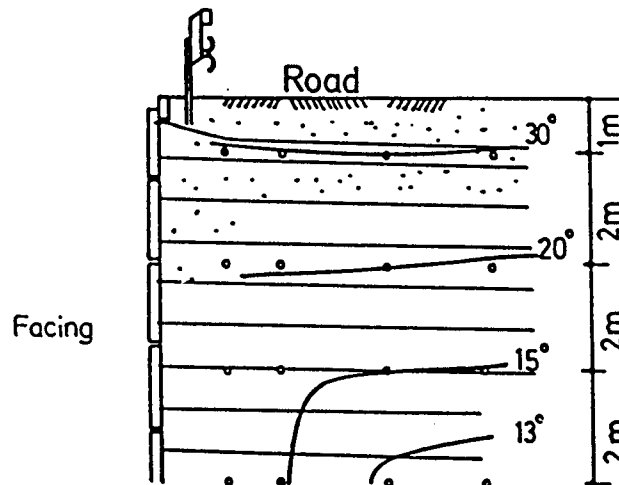


Figure 3.1. Isotherms in a reinforced earth structure in July 1983.⁽¹⁾

Stress cracking resistance may be an important criterion for the selection of most HDPE geosynthetic materials used in engineering applications. A survey of the literature indicates, however, that very little notched stress rupture testing has been performed directly on oriented HDPE geogrids, although limited NCTL testing has been conducted on the base resins used to produce HDPE geogrids. Therefore, NCTL testing procedures similar to those used on HDPE geomembranes were necessarily developed and applied to allow NCTL testing of oriented HDPE geogrid material. The specific investigative purpose of this testing program can, therefore, be summarized as follows:

- investigate the stress cracking resistance properties of different parts of a selected uniaxially drawn, HDPE geogrid product;
- investigate three HDPE resins of varying environmental stress cracking resistance (i.e. low, medium, high) to provide a base of reference for interpreting the stress cracking resistance test results for the selected geogrid; and
- investigate the long-term stress cracking-resistance performance characteristics of the selected, uniaxially drawn, HDPE geogrid product.

This contracted scope of work included limiting testing times to approximately 10,000 hours.

Accordingly, the scope of work for the research project required: (1) developing a test protocol to evaluate the NCTL characteristics of different parts of uniaxially drawn, HDPE geogrids; (2) conducting an NCTL and UCTL elevated temperature testing program on three HDPE resin materials and on one uniaxially drawn, HDPE geogrid product; and (3) evaluating the data from the testing program to assess the selection of a long-term design strength for the subject uniaxially drawn, HDPE geogrid.

The specific scope of work completed in the testing program includes:

- selecting HDPE geogrid and resin materials;
- developing a uniaxially drawn, HDPE geogrid test protocol for notched and unnotched geogrid specimens;
- conducting NCTL and UCTL testing on the three resin materials at 50°C and on the one geogrid product at 50°C, 65°C, and 80°C; and

- preparing a report, including an analysis of the NCTL and UCTL data, to include practical recommendations concerning long-term design strength of the geogrid in regard to stress cracking resistance.

3.2 SUMMARY OF THE RESEARCH PROGRAM'S ACTIVITIES

The scope of work evolved in minor ways from the original scope of work as a result of on-going periodic discussions between the investigators and new insights obtained from early test results and observations. The two most significant evolutions from the original scope of work were:

- the testing of a larger quantity of CTL specimens than originally anticipated; and
- CTL testing over a broader range of strength levels than originally expected.

The purpose of these evolutionary changes was to enhance the ability of the CTL testing program to meet the research program's objectives.

A detailed matrix of the CTL testing groups is presented in table 2.

Table 2. Number of specimens tested for program.

	Percent of Yield Strength (%)																		Total Specimens Tested				
	6	7.5	9	12	15	18	21	24	27	30	33	36	39	42	45	48	51	54		57	60	63	66
Notched Resins L M H	2	2	2	4	2	4	2	4	2	4	2	4	2	2	2	2	2	2	2	2	2	2	38
			2	2	2	5	3	5	5	5	5	5	2	2	2	3	2	2	1	0	1	1	48
Unnotched Resins L M H					2	2	2	4	2	4	2	5	2	4	2	2	2	2	2	2	2	2	33
				2	2	2	3	4	5	5	4	4	4	5	5	2	2	2	5	2	0	1	45
					2	2	2	2	2	1	1	1	1	0	2	2	2	2	5	2	0	1	28

	Percent of Yield Strength (%)																		Total Specimens Tested			
	3.98	4.78	5.57	7.17	8.76	10.35	11.94	13.53	15.13	16.72	18.31	19.90	22.29	24.68	27.07	29.46	31.85	34.23		36.62		
Notched P-1 Geogrid 50°C 65°C 80°C	1	0	1	2	3	5	5	5	5	2	5	2	5	2	4	2	5	2	2	2	2	58
		2	0	2	1	5	2	5	4	5	2	6	2	2	0	0	3	0	0	2	2	43
		2	3	5	2	5	2	5	1	5	2	5	2	2	5	2	2	2	5	2	2	2
	Percent of Yield Strength (%)																					
	5	7	9	11	13	15	17	19	21	23	25	28	31	34	37	41	44	48	51			
Unnotched P-1 Geogrid 50°C 65°C 80°C	1	1	1	1	1	1	1	1	1	1	1	2	2	3	3	5	2	2	2	2	2	31
		1	1	1	1	1	1	2	2	2	2	1	1	5	2	2	2	2	2	2	2	26
		1	1	1	1	1	1	1	4	3	3	1	6	2	2	2	2	2	2	2	2	32

CHAPTER 4

MATERIALS

4.1 SELECTION OF GEOGRID

The representative geogrid selected for this testing program is a uniaxially drawn, HDPE product designated herein as P-1. This geogrid was selected to maintain continuity within the *Durability of Geosynthetics for Highway Applications* project and is considered typical of presently available uniaxially drawn, HDPE geogrids of this type. A second uniaxially drawn, HDPE geogrid product was employed to a limited degree in this testing program; it was used in the geogrid specimen selection testing program (see chapter 5). This second geogrid product is designated herein as P-1a. Geogrid P-1a was only used in the geogrid specimen selection process and was not used in the CTL testing program. For the purpose of this report, geogrids P-1 and P-1a are considered identical products with two exceptions: (1) P-1a was substantially thicker than P-1, and (2) P-1a exhibited significantly higher tensile strength than P-1.

4.2 SELECTION OF RESINS

Resin Description

Three HDPE resins were selected for this testing program and are identified in the report as: resin L, resin M, and resin H. The commercial classifications of the HDPE materials tested in this research program, as presented previously in chapter 2, are reiterated here:

base resin for P-1 and P-1a geogrid	- D1248-IIIA5-E5
resin L	- D1248-IIIA5-E10/low ESCR
resin M	- D1248-IIIA5-E5
resin H	- D1248-IIIC4-W7/W8

The letters L, M, and H refer to the low, medium, and high resistance to environmental stress cracking (ESC), respectively, as measured using ASTM D 1693 “*Test Method for Environmental Stress Cracking of Ethylene Plastics.*” Resins L and M were in plaque form, and resin H was in geomembrane form. Resin H was in geomembrane form because that is the form in which it was most readily available at the time of resin H procurement.

It is noted that the medium resistant resin, resin M, has the same commercial identification as that of the base resin used to make the P-1 geogrid; i.e., D1248-III A5-E5. Resin M is therefore sometimes referred to as the base resin in this report. However, two resins having the same commercial designation (in accordance with ASTM D 1248) are not necessarily exactly equivalent due to the broad ranges of many properties (specified in ASTM D 1248) used to delineate the different areas of classification.⁽⁸⁾ (For example, a Category III polyethylene resin is defined by a very broad melt flow range: > 1.0 g/10 min to 10 g/10 min.) While the resin M and the P-1 geogrid base resin have the same commercial classification, the authors were unable to verify if resin M and the P-1 geogrid base resin were manufactured by the same resin manufacturer, under the same trade name, etc. It is, therefore, important to compare the properties of these two resins to determine the extent to which they are similar.

Comparison Between Resin M and P-1 Geogrid Resin

It is expected that polymer density (and the associated degree of crystallinity) in the geogrid node will be virtually unaffected by the geogrid manufacturing process (i.e., a warming/shaping/quenching process) because the geogrid warming/shaping/quenching process does not involve processes, such as copolymerization, which result in modification to polymer chain structure and because the geogrid node experiences a significantly lesser degree of oriented crystallization than, for example, the rib material does. Accordingly, density and crystallinity measurements were made for resin M and for P-1 geogrid node material. The melt flow index also was measured. The results presented below are excerpted from table 3.

Table 3. Summary of mean resin and geogrid index test data.

Index Test (Standard)	Units	Resin L Plaque	Resin M Plaque	Resin H Geomembrane	P-1 Geogrid
Specific Gravity (ASTM D 792)		0.955	0.951	0.949	0.965 ¹
Resin Density (ASTM D 792)	g/cm ³	0.953	0.949	0.947	0.962 ¹
Polymer Density (calculated)	g/cm ³	0.953	0.949	= 0.935 ⁴	= 0.950 ⁴
Crystallinity (ASTM E 793 ²)	%	60.5	59.7	54.1	58.7 ¹
Melt Flow Index (ASTM D 1238)	g/10 min	0.084	0.127	0.433	0.079 ¹
Yield Strength ⁵ (ASTM D 638 ³)	lb/in	280.4	279.2	136.1	
Yield Strain (ASTM D 638 ³)	%	14.0	16.4	18.3	
Rib Tensile Strength (GRI-GG1 ³)	lb				300.8
Wide-Width Tensile Property: Ultimate Strength (ASTM D 4595)	lb/in				295.6
Wide-Width Tensile Property: Strain @ Ultimate (ASTM D 4595)	%				38.3

NOTES:

- ¹ Node material sampled.
- ² Differential Scanning Calorimetry, at scan rate = 10°C/min, in nitrogen atmosphere.
- ³ Room temperature; cross-roll direction for resins.
- ⁴ Density value calculated assuming carbon black content ≈ 2.5 percent.
- ⁵ The strengths are not normalized for thickness because there is a need, in this report, to present mechanical properties as load per-unit-width instead of as a stress in psi. For easier reference, however, average material thicknesses are : Resin L, 0.0709 in; Resin H, 0.0591 in; and Resin M, 0.0827 in.

Material	Density (g/cm ³)	Degree of Crystallinity (%)	Melt Flow Index (g/10 min)
resin M	0.949	59.7	0.127
P-1 node material	0.962	58.7	0.079
P-1 node polymer	≈ 0.950	58.7	?

It is important to note that resin M does not include carbon black, while the P-1 geogrid material does contain carbon black. To accurately compare resin M and the P-1 geogrid resin, the influence of carbon black must be eliminated from the P-1 geogrid material results. Accordingly, the density of the P-1 polymer has been derived from the density of the P-1 geogrid material, as shown in chapter 4. The degree of crystallinity is not affected by carbon black. The melt flow index is affected by carbon black, but this effect is not easy to quantify. Therefore, to compare resin M and the P-1 geogrid resin, only the density and degree of crystallinity can be used. It now appears that they are very close (≈ 0.950 vs 0.949 g/cm³ for the density, and 58.7 vs 59.7 percent for the degree of crystallinity). Furthermore, density and crystallinity are the resin characteristics that are the most closely related to stress cracking resistance. Therefore, for the purpose of this study, resin M and the P-1 geogrid resin can be considered equivalent.

Selection of Resin Samples

Non-oriented plaques of base resin (M) were selected to provide for investigation of the beneficial effects (if any) of the geogrid manufacturing process to the base resin's stress cracking resistance. In this sense, resin M was selected for the testing program as a baseline reference. Resins L and H were selected for the testing program to further gauge the stress cracking resistance of different parts of the oriented geogrid product, as well as to gauge the stress cracking resistance of the base resin (M) used to manufacture the geogrid. Therefore, resins L and H were selected as resins expected to exhibit relatively low and high resistance, respectively, to stress cracking when subjected to NCTL testing.

The resin L and M plaques were made by a compression molding process. This method for making plaques results in a resin sample that has not experienced stretching and that, therefore, has virtually no molecular orientation. The resin H geomembrane was made by the cast sheet process. The cast sheet process is extrusion followed by calendaring. It is also known as a flat die process.⁽¹²⁾ The cast sheet process results in a resin sample that has not experienced stretching and that has virtually no molecular orientation.⁽¹²⁾ Even though the resin H sample was made by a different process than resins L and M, the resin H sample is satisfactory for this research program because it has virtually no orientation.

4.3 RESIN AND GEOGRID INDEX TESTS

A series of index tests was conducted to document and quantify relevant material properties of the three resins and the P-1 geogrid used in the testing program. The primary purpose of the index tests was to provide for comparison of NCTL behavior with basic material properties in order to look for trends or correlations between stress cracking resistance and one or more specific material properties. The index tests conducted on the three resins included: density, tensile properties, percent crystallinity, and melt flow index. The index tests conducted on the P-1 geogrid included: density, wide-width tensile properties, rib tensile strength, percent crystallinity, and melt flow index.

The results of the index testing are summarized in table 3. Detailed resin and geogrid index test results are included in appendix A. The primary objective of the index testing was to provide basic data for comparison of resin M with P-1 node material to aid in understanding the influence of the geogrid manufacturing process on the base resin's stress cracking resistance. This comparison is presented in chapter 7.

Density Correction

The measured density of the resin H geomembrane was 0.947 g/cm³, and the measured density of the P-1 geogrid node material was 0.962 g/cm³. Both the resin H and the P-1 geogrid sample contained standard (i.e., 2 to 3 percent) carbon black pigmentation. The density of the polymer was derived using the following equation developed by Giroud.⁽¹³⁾

$$\rho_R - \rho_P = 0.0047 C_B$$

where: ρ_R = resin density (g/m³);
 ρ_P = polymer density (g/m³); and
 C_B = carbon black content (%).

Using the above values of resin densities and an average value of 2.5 percent for C_B , the following values were obtained for the polymer density:

$$\rho_P \approx 0.935 \text{ g/cm}^3 \text{ for resin H ; and}$$

$$\rho_P \approx 0.950 \text{ g/cm}^3 \text{ for P-1 resin.}$$

CHAPTER 5

GEOGRID SPECIMEN SELECTION PROCESS

5.1 OVERVIEW

Prescribed specimen geometry and notch parameters do not exist for NCTL tests on oriented HDPE geogrid. For NCTL tests on plaque or geomembrane samples, the geometry of the specimen, and the notch depth, orientation, and location are prescribed in the standard testing protocol ASTM D 5397. Therefore, the initial portion of this testing program involved selecting specimen configuration, notch depth, orientation, and location, and center node width suitable to reproducible CTL testing and the objectives of the program.

The ultimate goal of the geogrid specimen selection process was to select an NCTL geogrid specimen that would produce valid, accurate, and repeatable NCTL data. In order for the NCTL geogrid data to be valid and conducive to comparison with data produced from NCTL resin specimens, tested NCTL geogrid specimens needed to exhibit failure characteristics similar to those in the resins. Therefore, a NCTL geogrid specimen configuration was sought that could potentially reveal ductile and brittle failure mechanisms, *as well as* promote repeatable rupture times and consistent fracture patterns. To investigate potential ductile and brittle failure mechanisms, as well as fracture pattern repeatability (consistency), a testing program was developed and conducted for different, logically selected specimen configurations. It is noted that full stress rupture curves were not developed if preliminary testing results precluded continued testing of a particular specimen configuration.

5.2 INVESTIGATION OF DIFFERENT GEOGRID SPECIMEN CHARACTERISTICS

a. Specimen Configuration

Four specimen configurations were considered during the selection process. These specimen configurations are identified as Type 1 through Type 4 and are illustrated in figures 5.1

through 5.4, respectively. Type 1, 3, and 4 configurations required no modifications to the as-manufactured geometry (profile) of the P-1 geogrid product. Type 2 specimens required the removal of lateral portions of the material in the area between the rib and the node in order to create a rectangular and reproducible cross-sectional area at the notch location.

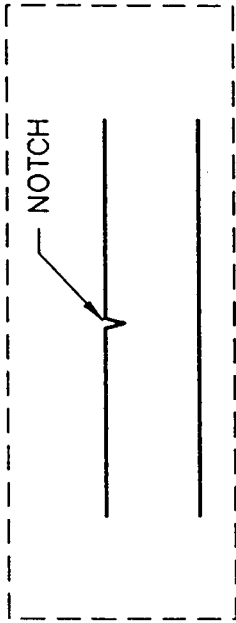
b. Notch Location

The investigation for an appropriate notch location for NCTL geogrid testing included: (1) specimens with notches located in the rib (Type 1); (2) specimens with notches in the material in the area between the rib and the node (Type 2); and (3) specimens with notches in the node (Types 3 and 4). These locations were selected because they represent zones of differing degrees of molecular orientation within the geogrid products. Rib material exhibits the highest degree of molecular orientation and is the strongest portion of the product. The material in the area between the rib and the node also includes a high degree of molecular orientation because it represents material transitioning from node to rib material. Node material exhibits the least degree of orientation, though significant orientation is present in center node material. These three notch locations are illustrated in figures 5.1 through 5.4.

c. Notch Length and Orientation

The notch length for standard NCTL testing of non-oriented geomembranes or compression molded sheet material (plaques) is across the entire width of the specimen. This practice helps minimize effects caused by the specimen's edges and precludes the possibility of stress re-distribution through unnotched material beyond the notch's endpoints. Therefore, by conventional notching practice, the notches used in Type 1, 2, and 3 configurations were inscribed completely across the specimen (figures 5.1 to 5.3). The Type 4 specimens were notched approximately in the center of the node, leaving some unnotched material extending beyond the notch's endpoints (figure 5.4).

The Type 4 specimen was investigated after commencement of the geogrid specimen selection process when some early tested, single-rib, Type 3 specimens exhibited brittle failure originating in rough grooves in the roughly cut, outer edges of the center node. It was anticipated that this localized response in some initial Type 3 specimens might produce inconsistent data and that the Type 4 configuration might eliminate edge failures and the accompanying potential problems for data repeatability. However, a razor cutting technique



CROSS-SECTION A-A'
NOT TO SCALE

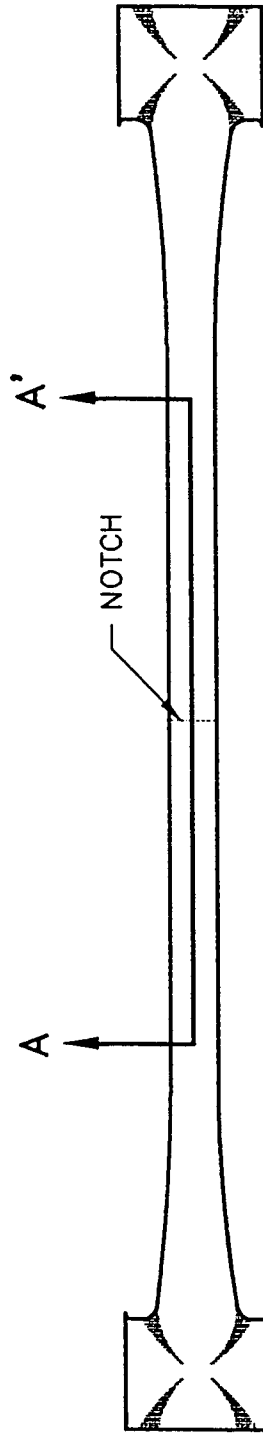


Figure 5.1. Type 1 configuration: notch in rib material.

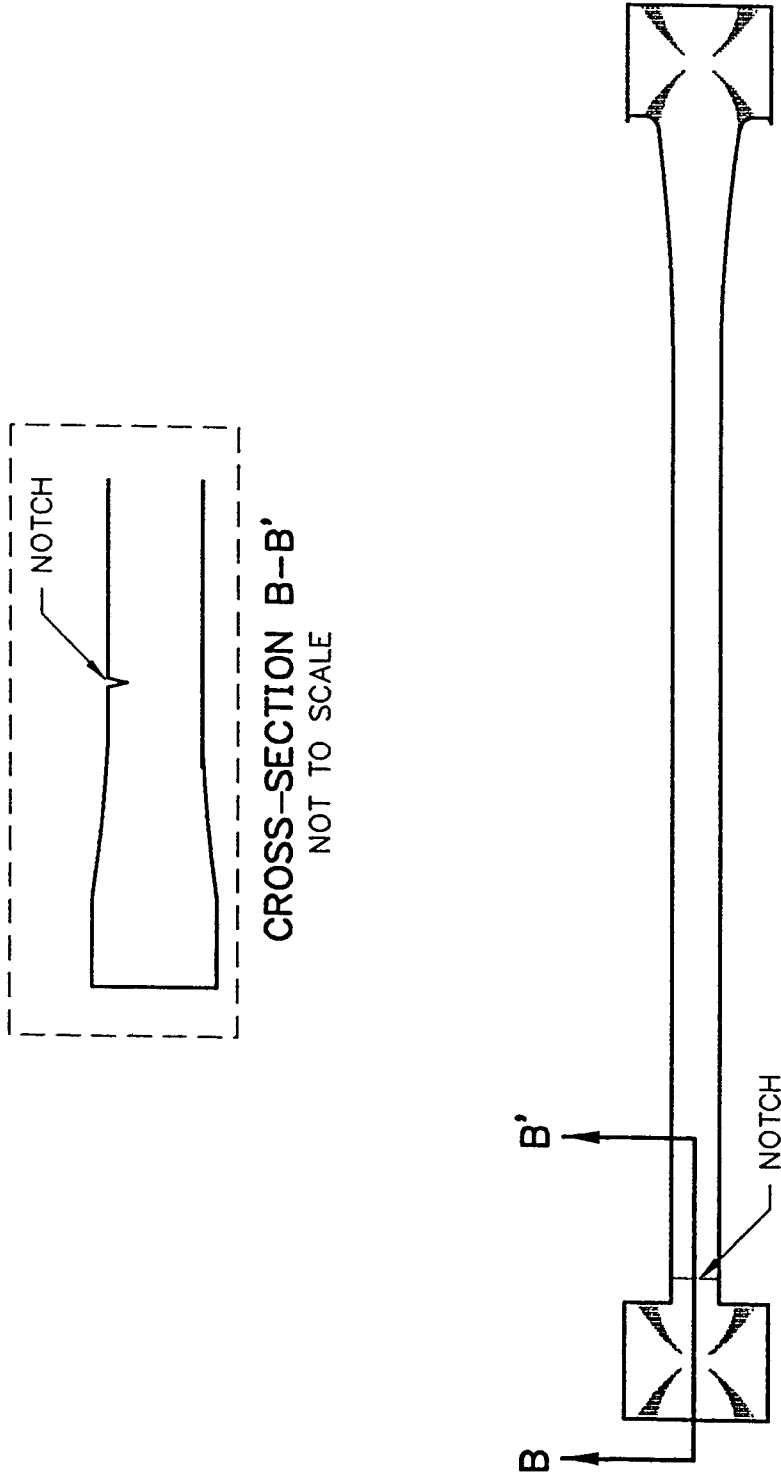
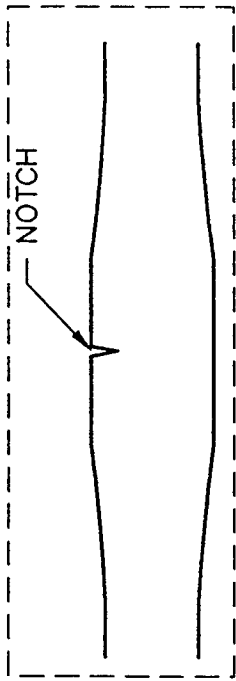


Figure 5.2. Type 2 configuration: notch in transition zone material.



CROSS-SECTION C-C'
NOT TO SCALE

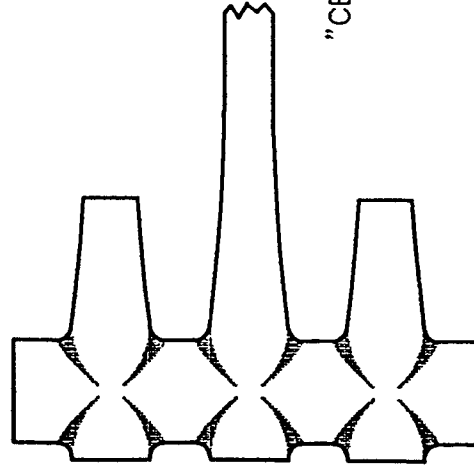
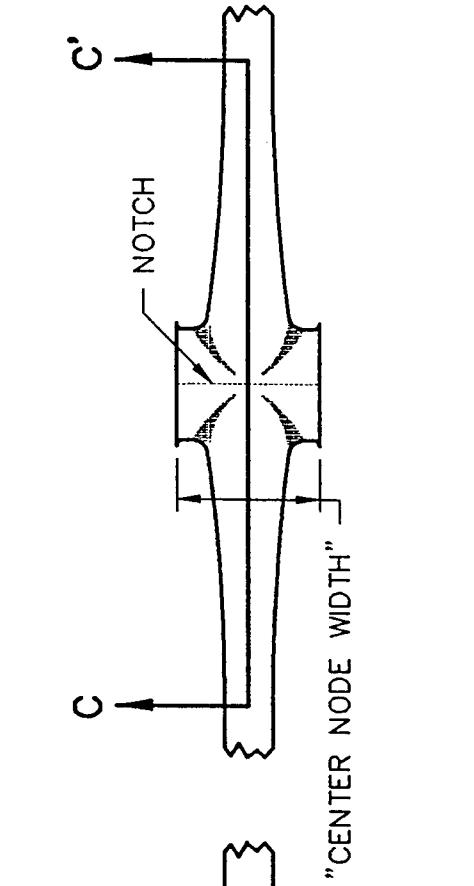
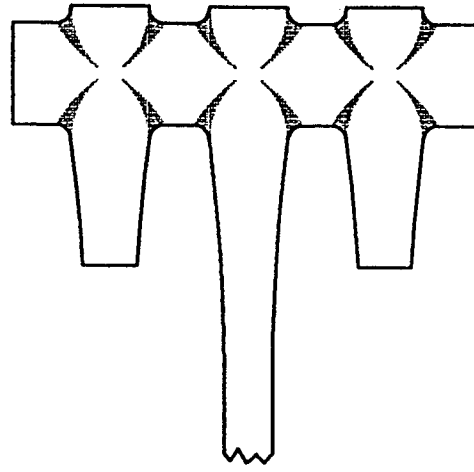


Figure 5.3. Type 3 configuration: notch in single-rib-wide node material.

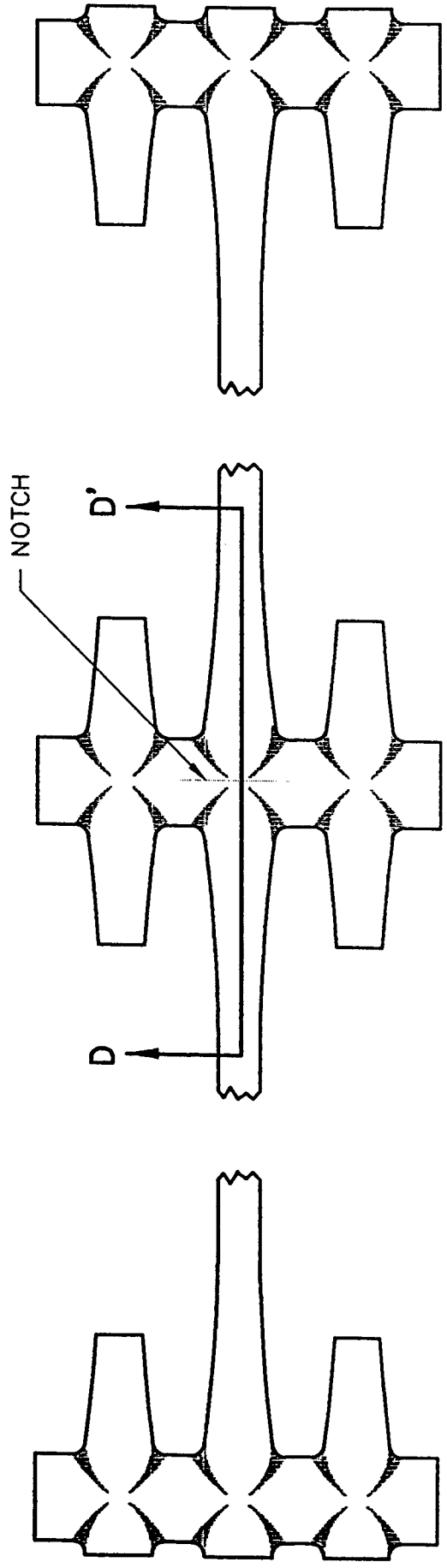
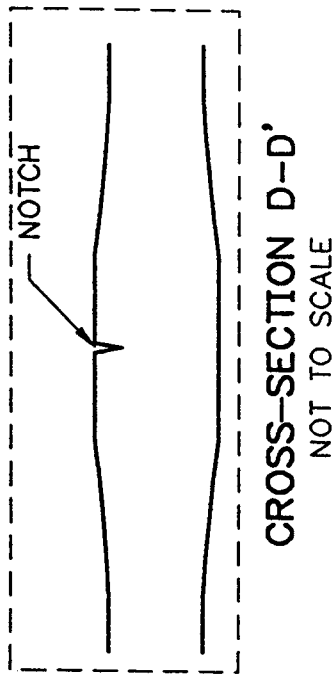


Figure 5.4. Type 3 configuration: notch in three-rib-wide node material.

was later developed for leaving very smooth cuts on the outer edges of the center node of Type 3 specimens. Subsequent testing using the razor cutting technique demonstrated the practical elimination of undesired effects caused by the cut edge.

All notches were oriented normal to (perpendicular to) the plane of the geogrid product when it is lying flat. Notches in rib and the material in the area between the rib and the node were oriented normal to the direction of rib elongation and therefore normal to the direction of the applied load. Notches in the node material were inscribed coincident to the center line of the crossbar in the node area.

d. Notch Depth

Notch depth was investigated and selected last in the geogrid specimen selection process. The notch depth investigation was only performed on Type 3 specimens (notch in single-rib-wide node material), after the Type 3 configuration had been selected as the most acceptable specimen configuration for NCTL geogrid testing. This investigation consisted of varying the depths to which notches were cut into the node material of Type 3 specimens (i.e., one notch per specimen). NCTL Type 3 specimens with the following notch depths were tested: 2.5, 5, 10, 15, 20, 25, and 30 percent. The following NCTL test conditions were used in the notch depth investigation:

- notch depths: 2.5 to 30 percent of material thickness
- stress level: 350 psi ⁽¹⁾ (2400 kPa)
- bath temperature: 80°C
- bath medium: water

Note: ⁽¹⁾ The load on each specimen was varied, in accordance with notch depth, in order to achieve a 350 psi (2400 kPa) stress over the remainder of the cross-section in the plane of the notch.

Performing all testing at 350 psi (2400 kPa) was important because it was desired to vary only the notch depth parameter in order to establish a range of notch depths over which failure times would be about the same. The results of the notch depth investigation are

summarized below. Notch depths are expressed as a percent of approximate node thickness, and times to specimen rupture are expressed in hours.

2.5%	335.8 hr
5%	134.2 hr
10%	119.4 hr
15%	115.9 hr
20%	104.0 hr
25%	95.6 hr
30%	74.0 hr

These results indicate that a 10- to 25-percent notch depth range produces acceptably repeatable times to failure (all other parameters being equal). The notch depth investigation confirmed that repeatable NCTL results can be obtained for node material using a 20-percent notch depth. A 20-percent notch depth was considered most desirable because a notch depth of 20-percent is specified in ASTM D 5397-93, Section 9.2, and data obtained from 20-percent notch depth NCTL geogrid testing are more conducive to comparison with NCTL geomembrane databases tested in accordance with ASTM D 5397. A notch depth of 20 percent was, therefore, selected.

e. Center Node Width

The term center node width refers to the width of the center node bar portion of a Type 3 specimen, whereby the width is the dimension normal to the direction of the specimen length when the specimen is lying flat. This dimension is more clearly identified in figure 5.3.

An investigation of the effect of the center node width on failure mechanism and time to rupture was not performed as part of the formal geogrid specimen selection process due to the focus of the selection process on *notched* CTL testing. *Unnotched* CTL geogrid test results obtained early in the CTL testing program, however, indicated that a minimum center node width needed to be defined for unnotched Type 3 specimens. The investigation of a minimum center node width is therefore logically included here.

Some early UCTL geogrid specimens were prepared with relatively narrow center node widths ranging between approximately 17 and 19 mm. The center node width was experimented with for two reasons: (1) to further define an acceptable Type 3 UCTL geogrid specimen, and (2) to investigate trends (if any) in failure mechanisms that may be related to specimen preparation.

Severe plastic deformation of center node material occurred in the early UCTL geogrid specimens that had been prepared with center node widths of approximately 17 to 19 mm. Noticeable plastic deformation of node material did not, however, occur in early UCTL specimens with center node widths greater than approximately 22 mm. These observations are presented in table 4. In this table, the column heading Node Width means center node width as defined above, and bold lines are used to draw attention to the specimens that were prepared with 17- to 19-mm center node widths.

Due to the observations summarized in table 4, the plastic deformation of node material was considered an artifact of the specimen preparation process. Because UCTL testing is a performance test that strives to avoid artificially induced behavior such as the subject node material elongation, a minimum center node width of 22 mm was adopted for all subsequent UCTL geogrid testing, and non-valid results obtained from the small number of earlier (17 to 19 mm) UCTL specimens were not included in the final results presented in this report.

A minimum center node width of 22 mm is recommended to ensure valid and repeatable UCTL performance results.

5.3 OVERVIEW OF THE GEOGRID SPECIMEN SELECTION PROCESS FOR CTL TESTING

Four combinations of test conditions and notch locations for potential use in the NCTL geogrid portion of the main CTL testing program were investigated in the geogrid specimen selection process. The main CTL testing program is distinguished from the CTL testing performed for the geogrid specimen selection process. The main CTL testing program is presented later in chapters 6 and 7. Each of these four combinations was evaluated for: (1) failure mechanisms exhibited, (2) repeatability of rupture times, and (3) consistency of fracture morphology. The NCTL specimen types and exposure conditions for the geogrid specimen selection process consisted of:

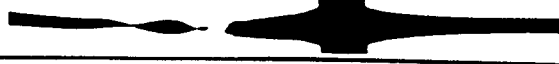
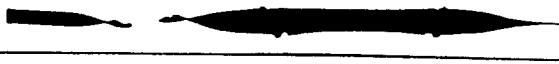
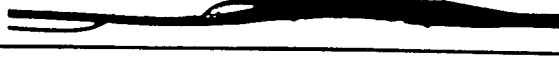
- Type 1 single rib P-1a specimens notched in rib material, tested in an Igepal solution at 80°C;
- Type 2 single rib P-1a specimens notched in the material in the area between the rib and the node, tested in an Igepal solution at 80°C;

Table 4. Investigation of effect of center node width on failure mechanism and time to rupture.

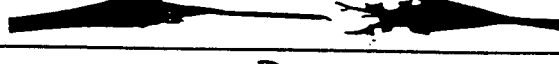
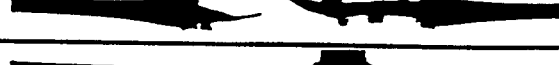
PROJECT: <i>Federal Highway Administration</i>	MATERIAL: <i>P-1 Geogrid</i>	REPORT DATE: <i>10/24/96</i>
JOB NO.: <i>MP5548/03</i>	TEST PARAMETERS: <i>Unnotched, in Water</i>	

Specimen ID.	% of Y.S. (%)	Node Width (mm)	Stress Over Node (psi)	Time to Failure (hr)	Failure Location and Failure Mechanism(s)
--------------	---------------	-----------------	------------------------	----------------------	---

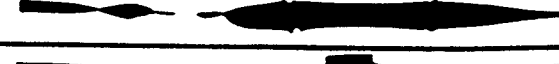
50° C

505	37	22.7	1156	209	
506	40	22.5	1257	216	
516	40	17.7	1596	256	
518	40	17.6	1605	189	

65° C

651	25	23.4	760	1213	
653	31	22.5	987	80	
670	31	17.0	1293	97	
671	31	18.3	1190	105	
672	31	18.0	1216	119	
654	34	22.4	1084	100	
655	37	21.9	1205	41	

80° C

801	25	23.2	731	324	
802	28	23.3	855	103	
816	28	18.2	1091	59	
817	28	17.6	1116	54	
803	31	22.0	981	8.3	
804	34	22.7	1065	7.5	

- Type 3 single rib P-1 and P-1a specimens notched in single-rib-wide node material, tested in water at 80°C; and
- Type 4 single rib P-1a specimens notched in three-rib-wide node material, tested in water at 80°C.

Igepal solution was used in the geogrid specimen selection process in order to facilitate rapid results. However, Igepal was not used in the main CTL testing program because water was selected to more satisfactorily model the anticipated in-service environmental chemical exposure as the use of Igepal solutions to accelerate stress cracking in HDPE is well known.⁽¹⁴⁾ The highest proposed testing temperature of 80°C was also employed in order to obtain rapid results. Higher water bath temperatures, such as 90°C or 100°C, were not used because HDPE can begin to exhibit morphological changes at temperatures above 80°C.⁽¹⁴⁾

The NCTL geogrid testing on the Type 3 and 4 specimens was conducted in water for the following two reasons:

- to verify the ability of a deviated testing protocol (i.e., water environment) to not preclude the development of stress cracking under proposed NCTL geogrid testing conditions. Water is believed to better represent in-service conditions relative to an aggressive Igepal solution; and
- to verify rupture time repeatability for P-1 NCTL testing in water. This was a potential concern since most geogrid specimen selection process testing was conducted on P-1a in Igepal.

5.4 GEOGRID SPECIMEN SELECTION PROCESS RESULTS

Results of the geogrid specimen selection process are summarized in table 5. This summary table presents information critical to the selection process. A discussion of this information is presented below.

a. Type 1 Configuration (Notch In Rib Material)

A photograph of a representative Type 1 fracture is presented in figure 5.5. Visual observation of Type 1 specimens after NCTL testing revealed the following:

Table 5. Summary of results of the geogrid specimen selection process.

PROJECT : Federal Highway Administration	MATERIAL : P-1 & P-1a Geogrids
JOB NO. : MP5648 / 02	REPORT DATE : 12/11/88

Specimen Geometry & Notch Location	Specimen Configuration Selection Process						Notch Depth Selection Process		
	Material Tested & Test Parameters	Failure Mechanisms Exhibited ?			Failure Time (hr)	Repeatability of Fracture Morphology	Material Tested & Test Parameters	Notch Depth as Percent of Node Thickness	Failure Time (hr)
		Quasi-Brittle	Shear-Rupture	Ductile or Creep					
Type 1 Rib	P-1a 80°C 1% Igepal 30% Notch Depth	No	Yes	Yes	10 - 1000	Repeatable	not tested	not tested	not tested
Type 2 Transition Zone	P-1a 80°C 1% Igepal 30% Notch Depth	No	Yes	Yes	0.1 - 100	Repeatable	not tested	not tested	not tested
Type 3 Single Node	P-1 & P-1a 80°C Water 25% Notch Depth	Yes	No	Yes	5 - 200	Repeatable	P-1 80°C Water	2.5% 5% 10% 15% 20%* 25% 30%	335.8 134.2 119.4 115.9 104.0 95.6 74
Type 4 Triple Node	P-1a 80°C Water 25% Notch Depth	Yes	No	Yes	5 - 200+	Not Repeatable	not tested	not tested	not tested

Notes: * A notch depth of 20 percent is specified in ASTM D5397-93, section 9.2.

- notched rib material demonstrated plastic deformation (creep) and/or ductile fracture accompanied by shear rupture occurring between oriented fibers parallel to the applied load;
- quasi-brittle (stress cracking) fracture was not observed in the rib material in the remainder of the cross-section in the plane of the notch; and
- a number of specimens exhibited quasi-brittle fracture in clamped (unnotched) node material (i.e., away from the notch that is located in the rib).

Examination of the notch roots in the Type 1 specimens revealed a notch blunting process (figure 5.5) due to macroscopic, plastic deformation (creep) between the walls of the notch. This is an important observation because blunting of the notch severely reduces the effectiveness of the notch to concentrate stress. Under notch blunting conditions, the craze growth rate, which depends on the stress field near the notch root, is suppressed.⁽¹⁵⁾ No stress cracking initiations or quasi-brittle fractures were observed in the remainder of the cross-section in the plane of the notch in the highly oriented rib material of the tested Type 1 specimens.

The observed failure mechanisms for the Type 1 specimens indicate, therefore, that the rib is a poor candidate as the notch location for NCTL geogrid testing. More importantly, though, the observations of Type 1 specimens indicate that relatively homolithic, highly oriented HDPE material (i.e., rib material) may be very resistant to quasi-brittle fracture (i.e., to the kind of stress cracking failure investigated in this research program, occurring normal to load and orientation directions, and occurring under similar conditions to those used in the testing program). The Type 1 specimen test results indicate that, even if there are scratches on the ribs of an installed HDPE geogrid sample, these scratches should not be expected to initiate stress cracking type failure in the rib material.

b. Type 2 Configuration (Notch in Material Between the Node and the Rib)

A photograph of a representative Type 2 fracture is presented in figure 5.6. Visual observation of Type 2 specimens after NCTL testing revealed the following:

- notched material in the area between the rib and the node demonstrated plastic deformation (creep) and ductile fracture accompanied by shear rupture, as shown in figure 5.6;

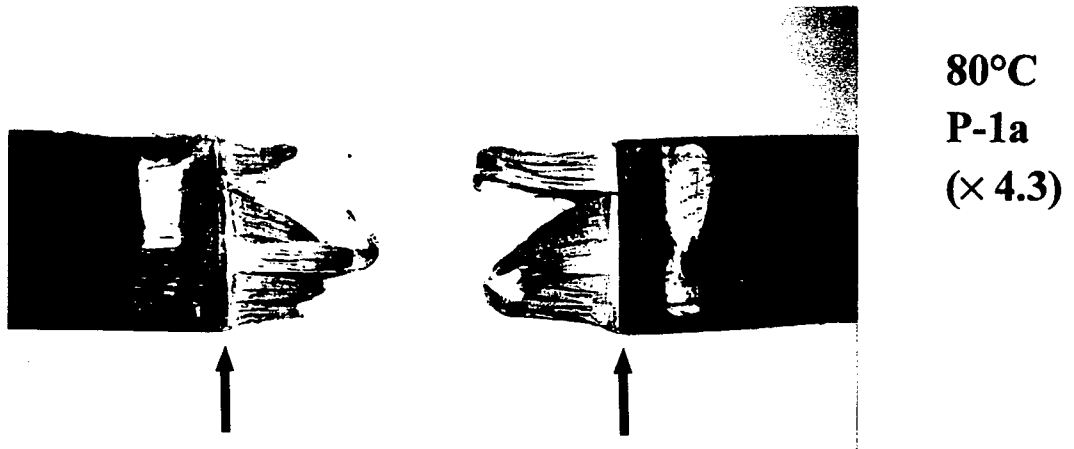


Figure 5.5. Ruptured geogrid specimen notched in the rig (notch walls arrowed).

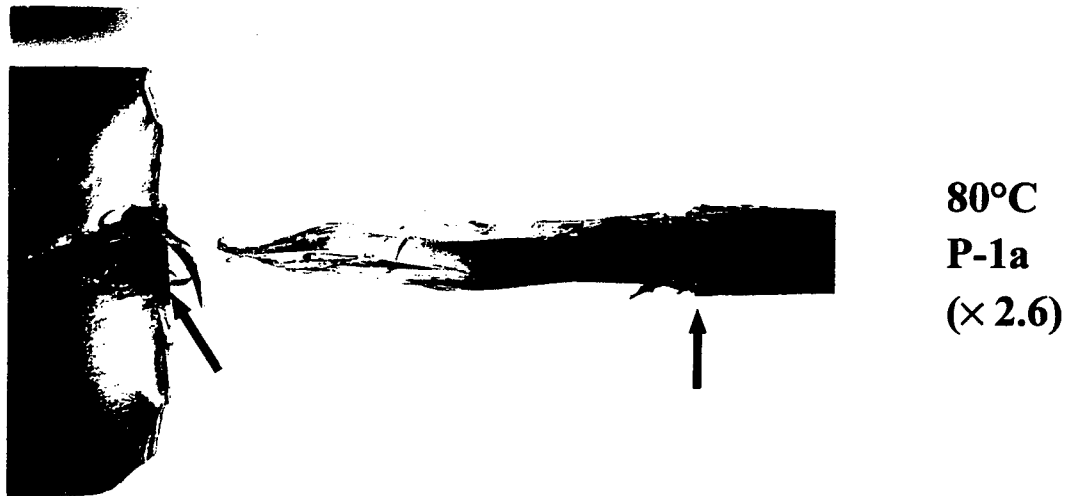


Figure 5.6 Deformation in geogrid specimens notched in the transition zone. Note fibrous, drawn material between notch walls (arrowed); also note abutting node material that has been removed (or drawn).

- quasi-brittle fracture was not observed in the material in the area between the rib and the node in the remainder of the cross-section in the plane of the notch; and
- a number of specimens exhibited quasi-brittle fracture in clamped (unnotched) node material nearby, but away from, the notch.

The presence of significant molecular orientation in the material in the area between the rib and the node was evidenced by the fibrous nature of the elongated material in ruptured NCTL specimens.

The void in the nearby node material, with multiple tongues of plastically deformed material extending out of it, is evidence that abutting node material was pulled out as plastic deformation in the material in the area between the rib and the node progressed. This observation, along with the triangular shape of the void in the node material, indicates that the removal of the abutting node material (in the observed manner) may have been an artifact of the trimming performed on the material in the area between the rib and the node prior to notching and testing, and as illustrated in figure 5.2. It appears that the trimming of lateral material in the area between the rib and the node was potentially a bad testing practice because it may have influenced the response in the abutting node material.

The observed failure mechanisms for the Type 2 specimens indicate that the material in the area between the rib and the node is a poor candidate as the notch location for NCTL geogrid testing. No stress cracking initiations or quasi-brittle fractures were observed in the remainder of the cross-section in the plane of the notch in the highly oriented material of the tested Type 2 specimens. These observations of Type 2 specimens collaborate the above speculation that homolithic, highly oriented HDPE material (i.e., rib material *or* the material in the area between the rib and the node) may be *impervious* to quasi-brittle fracture. The Type 2 specimen test results show that, even if there are scratches in transition zone material (and the scratches do not extend near or into node material) of an installed HDPE geogrid sample, these scratches should not be expected to initiate stress cracking failure in the material in the area between the rib and the node.

c. **Type 3 Configuration (Notch In Single-Rib-Wide Node Material)**

Due to many brittle failures in clamped node material of Type 1 specimens, single-rib-wide clamping was determined to be inadequate. Three-rib-wide clamping was, therefore, developed and implemented for Type 3 and 4 configuration testing.

Photographs of representative Type 3 fractures are presented in figures 5.7A & B. Visual observation of Type 3 specimens after NCTL testing revealed the following:

- notched node material demonstrated both ductile (figure 5.7A) and quasi-brittle (figure 5.7B) fracture;
- failure mechanisms and fracture morphologies were consistent and repeatable;
- repeatability of P-1 and P-1a NCTL rupture time data was satisfactory;
- it was confirmed that a water environment will not preclude the development of stress cracking under proposed NCTL geogrid testing conditions; and
- experimental unnotched Type 3 specimens, whose node edges were smoothly cut with a razor, produced no edge failures.

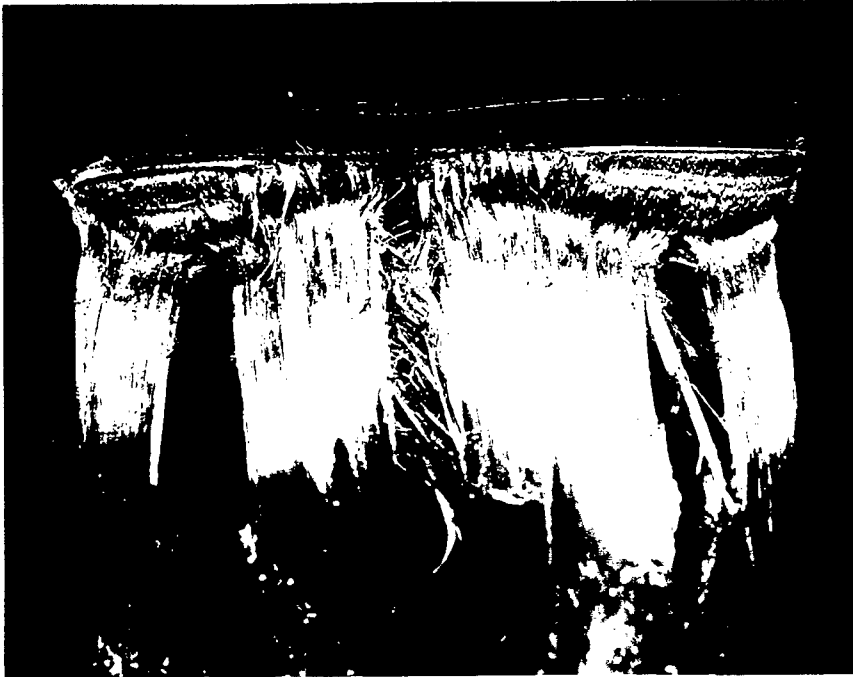
Ductile to brittle range of failure mechanisms, repeatable failure times, and repeatable fracture morphologies indicate that the Type 3 configuration is a good candidate for NCTL geogrid testing.

A small number of experimental unnotched Type 3 specimens were tested. The center node portions of these experimental specimens were cut using tin snips. A large number of quasi-brittle fractures, apparently initiating in irregularities from the coarsely cut edges, occurred in these specimens. These fractures are referred to as edge failures. A method for smoothly cutting the center node portion of unnotched Type 3 specimens was, therefore, developed and instituted. The occurrence of edge failures in all subsequently tested unnotched Type 3 specimens was dramatically reduced.

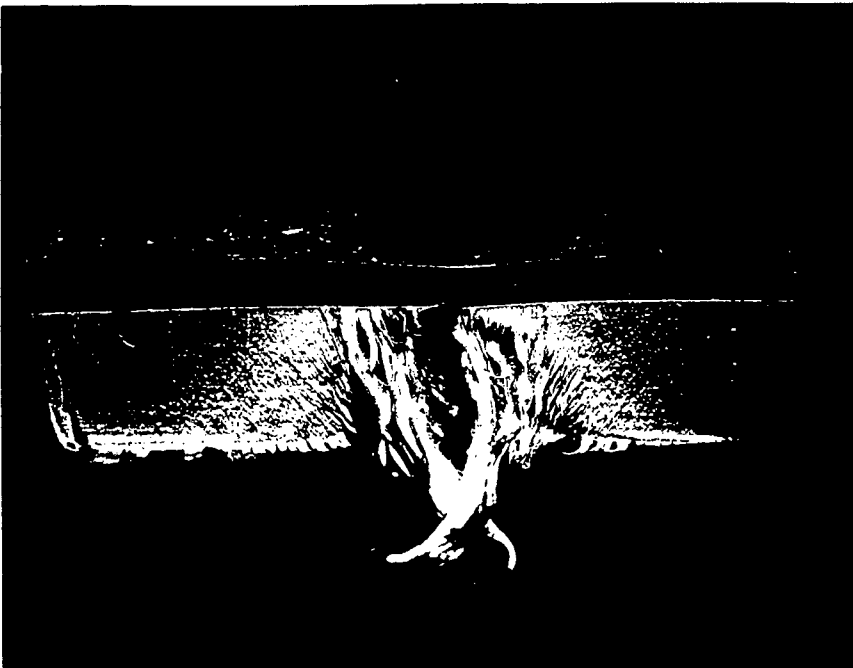
The notch depth investigation performed on Type 3 specimens confirmed that repeatable results can be obtained using a 20-percent notch depth. The 20-percent notch depth specimen failure times fell into an acceptably repeatable range of failure times obtained from specimens with notch depths ranging from 10 percent to 25 percent.

d. Type 4 Configuration (Notch in Three-Rib-Wide Node Material)

Photographs of representative Type 4 fractures are presented in figures 5.8A & B. The Type 4 configuration included a wider center node section (i.e., three ribs in width). Visual observation of Type 4 specimens after NCTL testing revealed the following:

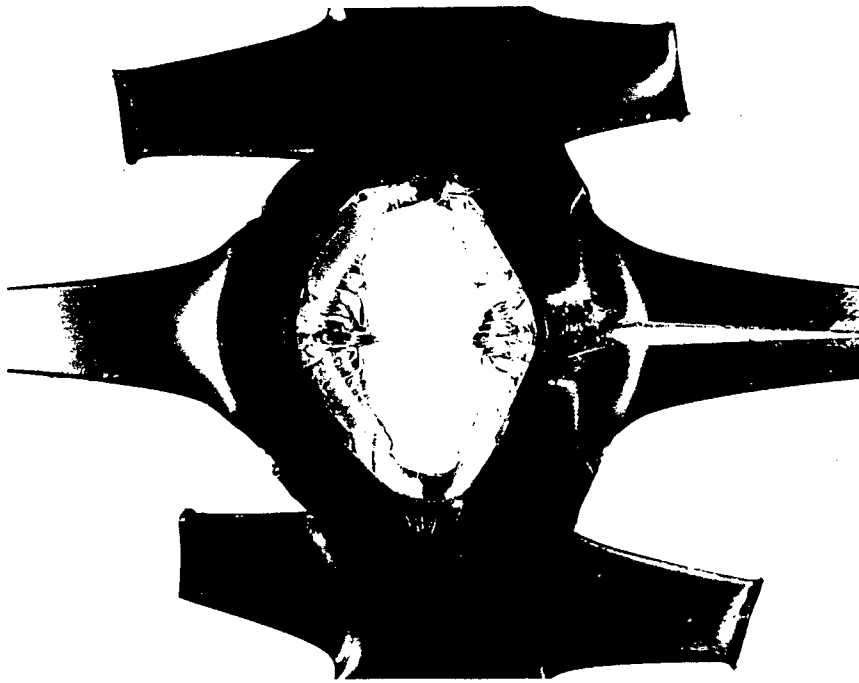


80°C
P-1a
(223, × 4.5)
Figure 5.7A

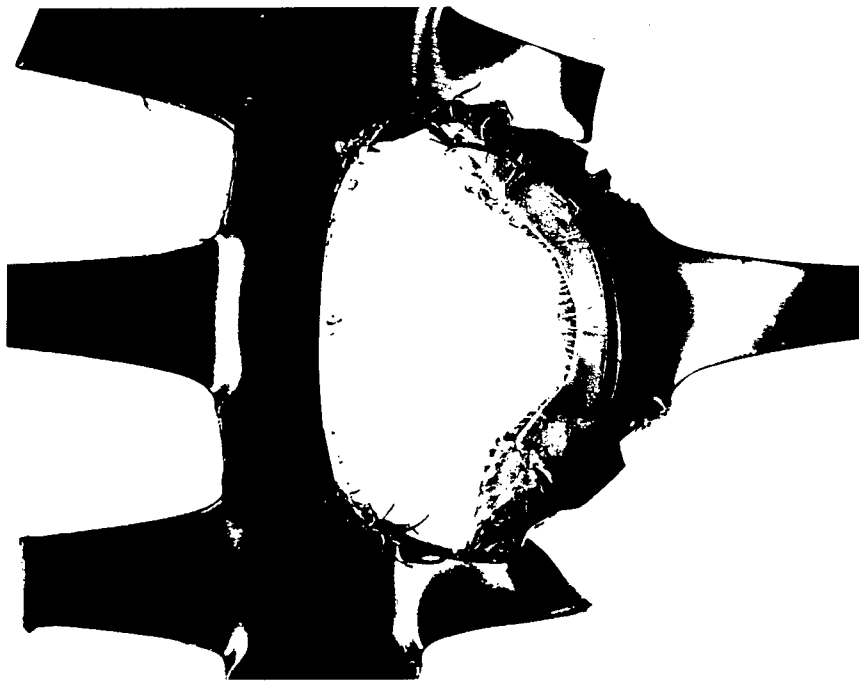


80°C
P-1a
(219, × 5.1)
Figure 5.7B

Figures 5.7A&B. Ruptured 80°C geogrid specimens notched across single-rib node. Note ductile (figure 5.7A) and quasi-brittle (figure 5.7B) fracture faces.



80°C
P-1a
(212, × 1.5)
Figure 5.8A



80°C
P-1a
(214, × 1.35)
Figure 5.8B

Figure 5.8A&B. Ruptured 80°C geogrid specimens notched in triple-rib node. Note stress redistribution around the notch (figure 5.8A); also note inconsistent rupture patterns (figure 5.8B).

- the Type 4 configuration eliminated the undesirable initiation of brittle failures at the edges of a geogrid specimen's center node portion by leaving a center node portion so wide that its edges are practically removed from exposure to stress (figure 5.4 and figures 5.8A & B);
- redistribution of stress occurring after brittle rupture (i.e., opening) resulted in rounding of the lateral endpoints of brittle ruptures in the node material at and beyond the endpoints of the opened brittle rupture (figure 5.8A);
- lateral stress cracking growth from the notch appeared to be arrested; and
- brittle fracture morphologies occurred through node material in non-repeatable directions and patterns (figure 5.8B).

The stress redistribution through lateral node material was further evidenced by an increased time to rupture for Type 4 specimens relative to Type 3 specimens. The complex process of stress redistribution (around the developing brittle fracture) and non-repeatable fracture morphologies observed in the ruptured Type 4 specimens were considered to hinder data interpretation and data repeatability. The Type 4 configuration is, therefore, a poor candidate for NCTL geogrid testing.

The apparent arrest of lateral stress cracking growth from the notch is hypothesized to have resulted from a combination of:

- plastic deformation (creep) occurring in the node material beyond the endpoints of the opened brittle rupture, resulting in notch blunting as evidenced by the rounding of the endpoints of the opened brittle rupture (figure 5.8A); and
- a higher degree of orientation in the node material coincident with the outer ribs, where material is (apparently) more resistant to stress cracking, and where material created a barrier, arresting crack growth in that direction.

5.5 SUMMARY OF THE GEOGRID SPECIMEN SELECTION PROCESS AND RECOMMENDATIONS

A study was conducted to select the best notch location, specimen geometry, and notch depth

for NCTL testing of the geogrid in order to develop a test protocol that can achieve repeatable stress rupture times and to achieve repeatable ductile, transitional, and quasi-brittle fractures. The specimen configuration selected for the NCTL testing also was qualified for use in UCTL testing of the geogrid. By qualifying a geogrid UCTL specimen preparation protocol, the geogrid specimen selection study fulfilled an important part of the research program's ultimate purpose.

a. Summary Regarding Configuration Types 1 to 4

The results of the geogrid specimen selection process can be summarized as follows:

- Type 1 configuration, with a notch located in rib material, did not produce the required ductile to brittle range of failure mechanisms. Therefore, this configuration was considered unacceptable for use in this research program.
- Type 2 configuration, with a notch located in the material in the area between the rib and the node, exhibited failures in node material near the clamp (away from the notch). Therefore, this configuration was considered unacceptable for the program. Furthermore, the trimming of lateral material in the area between the rib and the node was potentially a bad testing practice.
- Type 3 configuration, with a notch located in single-rib-wide node material, produced an acceptable range of ductile to brittle failure mechanisms, repeatable rupture times, and consistent fracture morphologies. Therefore, this configuration was considered acceptable for the research program.
- Type 4 configuration, with a notch location in three-rib-wide node material, evidenced stress redistribution around the notch and exhibited inconsistent fracture patterns in ruptured specimens. Therefore, this configuration was considered unacceptable for the research program.
- A clamping device capable of gripping a three-rib-wide node bar portion of a geogrid specimen's ends is required to load Type 3 specimens. Such a clamp securely holds the specimen while minimizing grip failures.
- Water was verified to not preclude the development of stress cracking in P-1 and P-1a geogrid node material.

b. Detailed Summary Regarding Type 3 Configuration (Selected)

Single node specimen geometry, consisting of two aligned ribs and a single center node with smooth razor cut edges, provides for repeatable NCTL and UCTL failure times. However, there are two conditions that must be met: the center node for UCTL testing must have a minimum centered width of 22 mm and it must have very smooth edges.

Type 3 notch location, a line coincident to the center line of the crossbar in the node area and extending the full width of the center node, provides for repeatable failure times and an acceptable range of ductile, transitional, and brittle fracture characteristics.

The 20-percent notch depth provides for more reliable comparisons of NCTL geogrid data with NCTL resin data.

c. Recommended HDPE Geogrid CTL Testing Protocols

Recommendation of NCTL and UCTL testing protocols for uniaxially drawn HDPE geogrid fulfills one requirement of this research program. The standard test procedures described in ASTM D 5397, *“Evaluation of Stress Crack Resistance of Polyolefin Geomembranes Using Notched Constant Tensile Load Test,”* provide the basis for these protocols. The following protocols therefore summarize deviations from, and additions to, standard test method ASTM D 5397, necessary for CTL testing of HDPE geogrids.

NCTL Geogrid Testing Protocols

Standard test method ASTM D 5397 shall provide the basis for NCTL testing of a uniaxially drawn HDPE geogrid product with the following recommended deviations and additions:

- Type 3 configuration specimen preparation (i.e., single node), including smooth razor cut edges, and including notch placement across the entire width of the center node;
- three-rib-wide clamping of the specimen’s ends;
- a water bath (as opposed to an Igepal solution);

- selection of testing temperature(s) that facilitate achieving the goal of the testing (i.e., testing at two or more elevated temperatures is necessary for producing data in a reasonable period of time that can be used to make predictions for lower temperatures and for longer periods of time; 50°C is one convenient temperature);
- selection of testing loads required to produce a full range of ductile to brittle fractures at the selected temperature(s) (i.e., a load range other than 20 to 65 percent of room temperature yield strength will be necessary); and
- modification of the CTL apparatus loading arms to absorb enough strain (in a geogrid specimen) to obtain ductile stress rupture data points.

UCTL Geogrid Testing Protocols

Standard test method ASTM D 5397 shall provide the basis for UCTL testing of a uniaxially drawn HDPE geogrid product, with the following recommended deviations and additions:

- unnotched Type 3 configuration specimen preparation (i.e., single node), with a minimum center node width of 22 mm, and with very smooth razor cut edges;
- three-rib-wide clamping of the specimen's ends;
- a water bath (as opposed to an Igepal solution);
- selection of testing temperature(s) that facilitate achieving the goal of the testing (i.e., testing at two or more elevated temperatures is necessary for producing data in a reasonable period of time that can be used to make predictions for lower temperatures and for longer periods of time);
- selection of testing loads required to produce a full range of shear rupture to brittle fractures at the selected temperature(s) (i.e., a load range other than 20 to 65 percent of room temperature yield strength will be necessary); and
- modification of the CTL apparatus loading arms to absorb enough strain (in a geogrid specimen) to obtain ductile stress rupture data points.

CHAPTER 6

CTL TESTING PROGRAM

6.1 OVERVIEW AND OBJECTIVES

In this report, the term CTL is used in a generic sense to encompass both notched constant tensile load (NCTL) testing and unnotched constant tensile load (UCTL) testing.

Four series of CTL tests were conducted. These series constitute the bulk of the work performed for this research program and the data derived from them constitute the basis of the conclusions drawn. The four series of CTL testing consisted of: (1) NCTL resin testing, (2) UCTL resin testing, (3) NCTL geogrid testing, and (4) UCTL geogrid testing. Data derived from these four series are tabulated and presented as log-log scale plots of percent of yield strength versus time to rupture. A majority of the interpretations of the CTL data were made from these strength rupture plots and from fracture face examinations.

A total of 212 resin specimens and 240 geogrid specimens were tested in this program. The matrix of test conditions for these specimens is presented in appendix B (resins) and appendix C (geogrid), and in table 2.

a. NCTL Resin Testing Objectives

The NCTL testing was performed on resins L, M, and H according to ASTM D 5397 procedures (50°C, 20 percent notch), with the following deviations: (1) testing in a water bath, whereas ASTM D 5397 specifies testing in Igepal solution; (2) testing over a selective set of yield strength levels, whereas ASTM D 5397 specifies testing at a specific set of stress levels; and (3) testing a selective number of specimens at each strength level, whereas ASTM D 5397 specifies testing three specimens at each strength level. The first deviation, testing in a water bath, is considered a deviation of ASTM test conditions, because this deviation impacts the use to which the results are applied. The last two deviations are considered deviations of ASTM test scope, because they do not impact the use to which the results are applied.

A total of 106 specimens were tested in this series. The objectives of this testing series were to:

- verify the ability of deviated test conditions (i.e., water environment) to distinguish variance in stress cracking resistance between resins;
- provide strength rupture data for the quantitative comparison of the stress cracking resistances at 50°C of resin M (a base resin) with P-1 node material (part of the manufactured product) since the P-1 geogrid is made from a resin like resin M; and
- compare the strength rupture characteristics of resins of different composition as differentiated by ASTM D1248.

b. UCTL Resin Testing Objectives

The UCTL testing was performed on resins L, M, and H in general accordance with ASTM D 5397 procedures (50°C), with the following deviations: (1) no notch, (2) testing in a water bath, (3) testing over a selective set of yield strength levels, and (4) testing a selective number of specimens at each strength level. The first two deviations, testing without a notch and in a water bath, are considered deviations of ASTM test conditions, because these deviations impact the use to which the results are applied. The last two deviations are considered deviations of ASTM test scope.

A total of 106 specimens were tested in this series. The objectives of this testing series were to:

- verify the ability of deviated test conditions (i.e., water environment plus no notch) to distinguish variance in UCTL stress cracking resistance between resins;
- obtain strength rupture data for resins in a test that includes the crack initiation step (in the absence of an artificial stress raiser such as the notch) in order to provide data for quantitative comparison of a base resin with its associated geogrid product to investigate the potential beneficial effects on stress cracking resistance that might result from the geogrid manufacturing process; and
- provide strength rupture data which, when compared with NCTL resin data, may further qualify the shorter term NCTL test as a preferred test for ranking resins with respect to stress cracking resistance.

c. NCTL Geogrid Testing Objectives

NCTL geogrid testing was performed at three elevated temperatures, 50°C, 65°C, and 80°C, on notched geogrid product P-1 according to the testing protocols selected in the geogrid specimen selection process. A total of 151 specimens was tested in this series. The objectives of this testing series were to:

- provide strength rupture data for P-1 geogrid specimens notched in the center node to investigate the possibility of stress cracking propagation in the less oriented node material of uniaxially drawn HDPE geogrids;
- provide strength rupture data for quantitatively comparing the stress cracking resistances (at 50°C) of resin M with P-1 node material; and
- obtain strength rupture data to provide for comparison of NCTL geogrid testing results with UCTL geogrid testing results to potentially qualify the NCTL geogrid test as an acceptable procedure for yielding quantitative, design-oriented results in a relatively short period of time.

d. UCTL Geogrid Testing Objectives

UCTL testing was performed at three elevated temperatures, 50°C, 65°C, and 80°C, on unnotched geogrid product P-1 according to the testing protocols qualified in the geogrid specimen selection process. A total of 89 specimens was tested in this series. The objectives of this testing series were to:

- provide strength rupture data for unnotched and undamaged P-1 geogrid specimens tested at elevated temperatures in order to investigate the possibility of stress cracking initiation and propagation in uniaxially drawn HDPE geogrids;
- obtain UCTL strength rupture data for geogrid tested at 50°C, in order to provide data for comparison of a base resin with its associated geogrid product to investigate the potential beneficial effects on stress cracking resistance that might result from the geogrid manufacturing process; and
- provide data to generate the strength rupture curves necessary for analytically calculating a master curve from which a long-term safe strength level can be selected as a design parameter for geogrid applications.

e. Post-CTL Testing Activities and Objectives

Examination of fracture faces were conducted to: (1) verify mode of failure interpretations (i.e., ductile/shear, transitional, quasi-brittle) made from strength rupture curves; (2) select a transition point for each unnotched geogrid curve; and (3) investigate the fracture characteristics of ruptured notched and unnotched geogrid specimens.

Data analysis procedures were performed on strength rupture data, with an emphasis on brittle zone trends. The data analysis procedures included: (1) the rate process method (RPM), and (2) Popelar et al. bidirectional shifting.⁽¹⁶⁾ Linear regression analysis was then performed on analyzed data in order to predict a 100-yr/20°C strength level that can be used as a design parameter to preclude stress cracking failures in HDPE geogrids.

6.2 DETAILS OF THE CTL TESTING PROGRAM

a. CTL Testing Equipment

One 60-station CTL testing apparatus was used to test resin specimens, as shown in figure 2.1. Specimens were mounted and immersed in the stainless steel tank located in the front of the apparatus. The load area in the rear of the apparatus contained weights and the extended portions of the lever arms. Low friction roller bearings provided for good load transmission and lack of stick slip phenomenon. Stainless steel, hook end mounting rods attached to the lever arms provided for specimen mounting. Timer switches were located under each lever arm near the roller bearings (pivot point).

Two 30-station CTL test apparatus, as shown in figure 2.2, were modified specifically to accommodate the geogrid loading and immersion requirements of this program. Because HDPE geogrids are known to strain appreciably, particularly at high loads and at elevated temperatures, and because a straining geogrid specimen will quickly use up all of the available travel distance of its associated lever arm, strain compensating mounting rods were designed, manufactured, and installed. These rods each consisted of a long threaded rod with end brackets and nuts, as clearly visible in the front of the apparatus photographed in figure 2.2. One wrench was used to secure the bottom bracket (attached to the upper specimen grid) from movement while a second wrench was used to tighten the top nut in order to take up the strain as necessary. Periodic adjustments of the strain compensating mounting rods accommodated the strains that occurred in the geogrid specimens while maintaining a constant load condition. These rods worked very well in that their use had an apparent minimal impact on the specimens.

b. Procedures for NCTL Resin Specimen Preparation

Specimen Preparation

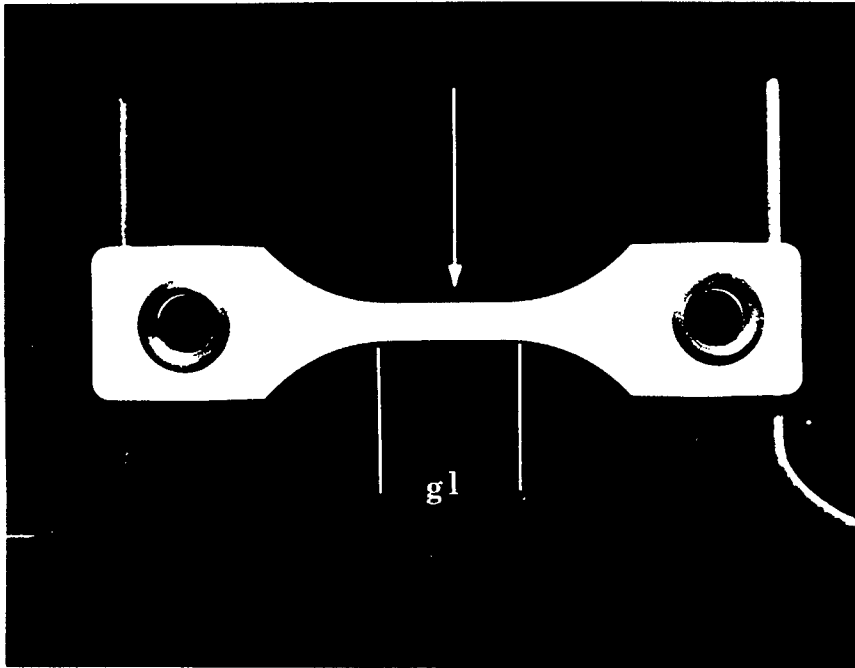
For resin testing, specimens were prepared in accordance with ASTM D 5397. The specimens were individually die cut and notched on one side to predetermined depths equal to 20 percent of each specimen's thickness in the gauge length center. For all resin testing, the gauge length of a specimen was the portion of a specimen between grips; the portion has an intentionally reduced cross-sectional area of uniform dimensions along the length of the portion. Resin specimen gauge length is identified in figure 6.1. (The gauge length of the P-1 geogrid specimens, however, included all material between the grip faces.) A typical unnotched resin (M) specimen used in the testing program is shown in figure 6.1.

A discussion of specimen gauge length is necessary because, for the die cut resin specimens, the cross-sectional area of the gauge length material can be pre-measured in order to calculate an initial stress condition at the location of subsequent rupture. This measured cross-sectional area, therefore, provides for calculation of the various CTL strength levels in terms of percent of yield stress of the material. For NCTL geogrid specimens, an initial stress condition at the location of rupture can also be pre-measured because the NCTL specimens will fail in the remainder of the cross-section in the plane of the notch. For UCTL geogrid specimens, location of specimen rupture(s) are not known prior to testing. Because it is not practical to accurately pre-measure all dimensions in a P-1 geogrid specimen's gauge length, the initial stress condition at the location of rupture is not known.

Notching

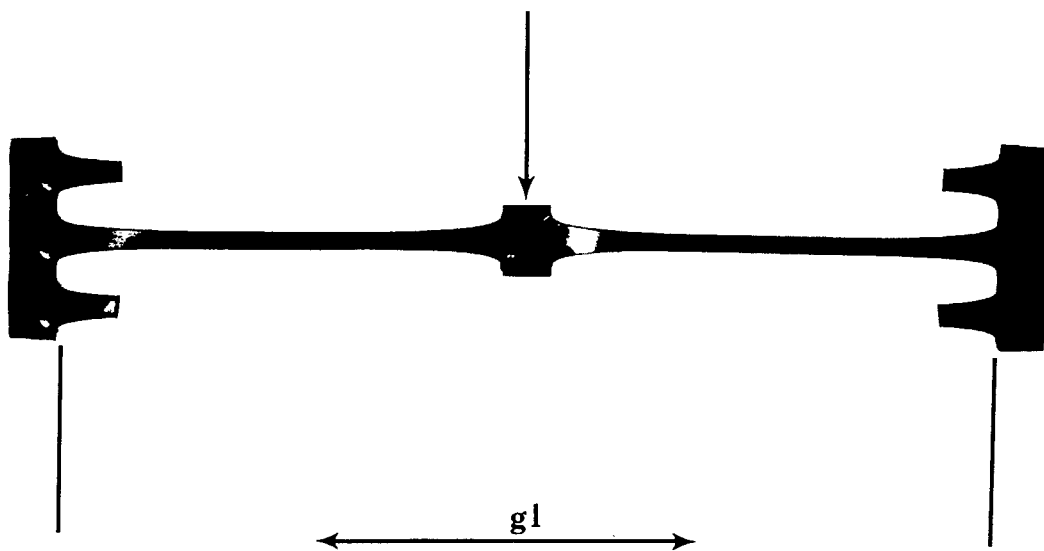
A notch was cut in each NCTL specimen by slowly pressing a fresh razor blade into the top surface of the material to a controlled depth. The depth of the notch was controlled using a dial gauge with a marked least reading of 0.01 mm, and a practical least reading of approximately 0.002 mm. The notch was cut normal to the plane of the specimen when it is lying flat and normal to the direction of the anticipated applied load.

The purpose of the notch is to initiate stress cracking propagation, or to act as a distinct stress raiser to provide for potential stress cracking propagation through a material.



**Resin M notched
untested
(top view, x 1.6)**

Figure 6.1. Typical specimen (notch location arrowed).



**P-1 notched
untested
(top view)**

Figure 6.2. Typical geogrid specimen (notch location arrowed).

c. Procedures for UCTL Resin Specimen Preparation

The procedures for UCTL specimen preparation were the same as for NCTL specimen preparation, except for absence of a notch in UCTL specimens. For all geogrid testing, however, the gauge length of a specimen was considered to be the entire portion of a specimen between grips. Geogrid specimen gauge length is identified in figure 6.2.

For UCTL testing, a product is tested whenever possible. Unlike the NCTL test, no artificial stress raiser (i.e., notch) is employed; rather, the UCTL test's intent is to challenge the stress concentration factors inherent in the exterior contours and interior microstructure(s) of the normal product.

d. Procedures for Geogrid Specimen Preparation

The protocols developed in the geogrid specimen selection process, described in chapter 5, were used to prepare the geogrid specimens. A typical notched P-1 geogrid Type 3 specimen, as used in this program, is shown in Figure 6.2.

e. Parameters and Procedures for CTL Testing

The CTL testing of resins was conducted in general accordance with ASTM D 5397, "*Test Method for Evaluation of Stress Crack Resistance of Polyolefin Geomembranes Using Notched Constant Tension Load Test*," with deviations from the specified test conditions as previously outlined in this chapter. The CTL testing of the geogrid followed the protocols developed during the geogrid specimen selection process, described in chapter 5. The following test conditions were used in the testing program:

- Resins Test Conditions

- notch depth: none and 20 percent of plaque thickness
- strength levels: from 6 to 66 percent of material yield strength⁽¹⁾
- bath temperature: 50°C
- bath medium: water⁽²⁾

- Geogrid Test Conditions

- notch depth: none and 20 percent of material thickness ⁽³⁾

- strength levels: from 4 to 51 percent of single-rib yield strength ⁽¹⁾
- bath temperatures: 50°C, 65°C, and 80°C
- bath medium: water⁽²⁾

Notes: ⁽¹⁾ This refers to room-temperature yield strength.

⁽²⁾ It is noted that an Igepal solution was used as the immersion bath for some of the geogrid specimen selection process tests. Water was selected as the immersion medium for the main CTL testing program to better model in-service conditions.

⁽³⁾ Because the thickness of the geogrid nodes (i.e., crossbars) varies moderately from point to point, an average thickness was measured for each specimen and was used for all calculations regarding notch depth and loading levels.

Procedures for Resin CTL Testing

Placement in Bath. After preparation, each NCTL specimen was mounted in a water bath that was maintained at 50°C ± 1°C. Each water bath was gently and continuously stirred to promote uniform temperature within the bath. Mounted specimens were left immersed and unloaded in the 50°C bath for a minimum of 30 min prior to loading.

Loading. Once each NCTL specimen had been immersed for a minimum of 30 min, it was loaded by means of a weight placed on its associated lever arm. Each load was calculated to achieve either a desired stress in the remainder of the cross-section in the plane of the notch, or a desired strength level applied to the specimen. In this report, the phrase strength level means the constant load applied to a specimen expressed as a percent of the sample's room-temperature yield strength. It is important to recognize that strength level, as such, does not take cross-sectional area into consideration; i.e., strength level is simply a ratio, expressed as a percent, of two loads.

The loads employed were selected in order to achieve rupture times between 0.001 hr and 10,000 hr, and representative ductile, transitional, and brittle fractures in specimens. Loads for NCTL tests were calculated to provide a round number increment of initial *stress* in the remainder of the material below the notch (e.g., psi or kPa). Loads for UCTL tests were, in some cases, calculated to provide a round number strength level increment (e.g., 7.00, 13.00, and 17.00 percent).

Yield strength is defined as: the strongest response of a specimen, measured by force or by force per unit width, where response occurs at the moment when plastic (unrecoverable) deformation begins to occur in the specimen's gauge length; in other words, yield strength is the maximum force, or force per unit width, required to stretch the specimen beyond its elastic limit. Yield strength is also defined as the maximum force, or force per unit width, at the apex of the first, major peak that occurs early in a tensile strength-strain curve. The room-temperature yield strength values were determined by index testing for the materials tested in this program, as shown previously in table 3.

Recording Time. Once a NCTL specimen was loaded, the test continued until the specimen ruptured or until the test was terminated by unloading the specimen. This time duration was recorded as elapsed time in hours. The following devices were used to measure time: (1) dedicated hour meters accurate to 0.1 hr, and (2) a digital readout clock with a seconds counter.

Plotting Results. The results of each test were plotted on a log-log scale of strength level (%) versus elapsed time (hr). The resultant strength rupture curves provided the primary means for data interpretation presented in this report. The intent of plotting all results in this report as percent of yield *strength* (i.e., strength level) versus time was to eliminate secondary conversions of *stress* values into *strength* values, since end-result *strength* values were desired for comparison with engineering design strengths.

Procedures for Geogrid CTL Testing

The CTL testing of the geogrid followed the protocols developed during the geogrid specimen selection process, described in chapter 5. The single-rib yield strength of the geogrid product was previously assessed at room temperature (23°C) in accordance with method GRI-GG1. (Index test results are provided in appendix A.) Geogrid specimens were secured in water baths where the temperature was controlled to either 50°C, 65°C, or 80°C \pm 2°C throughout the CTL testing program. Specimens were tested to rupture (separation into two pieces). Elapsed time to rupture was recorded for each specimen.

6.3 DISCUSSION OF INTERPRETATION PROCEDURES FOR CTL TESTING RESULTS

a. Reliability of Test Results

Repeatability of Test Data

Repeatability of within laboratory test results is gauged by a computation of standard deviation for a large set of test results obtained from specimens tested under the same conditions and with the same levels of precision. Generally, determining repeatability requires a set of at least 30 test results to provide a good approximation to the standard deviation of all test results that could be obtained.

Repeatability testing is testing performed in the same laboratory by the same technician using the same apparatus and repeating the same procedures. Repeatable results means that, if the technician who produced the original results were to test more like specimens on the same apparatus using the same procedures, then that technician could expect to produce results that are the same as, or very similar to, the original results. Results described as repeatable in this report indicate results that were (subjectively) found to be predictable and reasonably consistent for like specimens tested under the same conditions. The standard deviations listed in the data tables in appendices B and C give quantitative indications of repeatability. The observations and discussions with regard to failure mechanisms and fracture morphologies, which are presented in chapter 7, Geogrid Failure Mechanisms, give qualitative indications of repeatability. However, no scientifically planned, statistical studies of repeatability were included in the scope of work or performed in this research program. Calculations of standard deviations were assumed to be sufficient for the purposes of this study. Also, the amounts of data scatter in the strength rupture curves presented in chapter 7 give some indication of repeatability. Finally, it should be pointed out that all tests in this program were performed by one technician.

Reproducibility testing is testing performed by different laboratories, each laboratory using its own technicians and apparatus, but all laboratories following the same procedure(s). Reproducible results means that, if a different laboratory (or laboratories) was to test more like specimens on their apparatus using the same procedures (as the laboratory that produced the original results), then that (different) laboratory could expect to produce results that are the same, or very similar to, the results obtained by the original laboratory. The reproducibility of data presented in this report is unknown because only one laboratory performed testing for the program. No scientifically planned, statistical studies of reproducibility were included in the scope of work or performed in this research program.

Variability of Test Data

Due to equipment precision levels and normal specimen morphology variations, laboratory test results will always reflect some degree of variability in test results. Therefore, not all variability is error. Variability in test results is normally represented by a computation of standard deviation. In this program, standard deviations were calculated for test results obtained from specimens tested under the same conditions.

Number of Tests

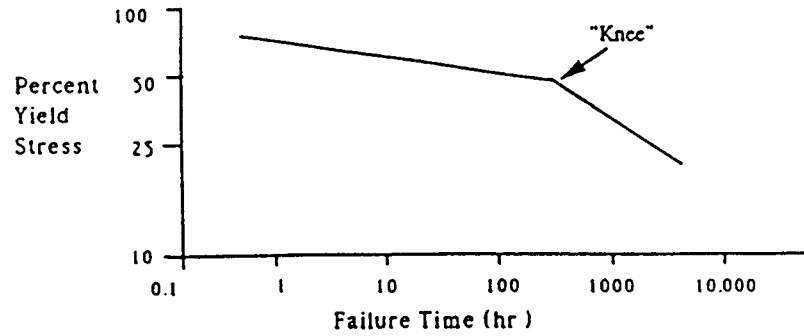
The NCTL standard method ASTM D 5397 specifies testing three specimens per strength level. In the CTL testing performed for this program, however, sometimes only one or two specimens were tested per strength level because full-strength rupture curve development to 10,000 hours was discovered to require testing over a greater range of strength levels than specified in ASTM D 5397 for most of the materials in the program. Nevertheless, it should be recognized that the fact that not enough specimens were tested at each strength level to always meet ASTM requirements is a limitation of the project funding and budget. As such, it must permeate and temper the conclusions.

b. Interpretation of NCTL Strength Rupture Curves

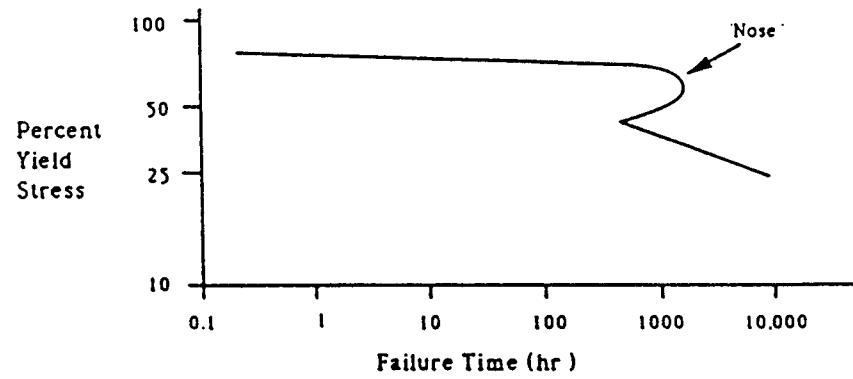
Appearance of Curves

Strength rupture curves of NCTL data generally consist of two linear portions (with different slopes) that meet to form one of three characteristic shapes, referred to as knee, step, or nose profiles. Idealized NCTL strength rupture curves demonstrating these shapes are presented in figure 4 of ASTM D5397-93. This figure is reproduced in this report as figure 6.3. As stated previously, the strength rupture curve is the primary data presentation format that is used to interpret the stress cracking resistance of notched specimens.

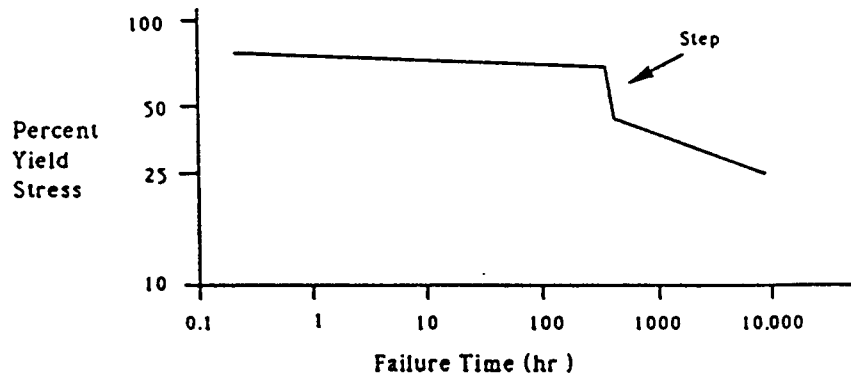
In the individual strength rupture plots presented in this report, all data points are shown, and the plots of data averages are represented by solid, dashed, or dotted lines. The plots of data averages were drawn through averages of the data points for a given strength level. The points and averages documented in the data tables are included in appendices B and C at the end of the report.



(a) A Bi-Linear (or "Knee") Response Curve



(b) A Overshoot (or "Nose") Response Curve



(c) A Tri-Linear (or "Step") Response Curve

FIG. 4 Possible Response of Curves Resulting from a Complete Notched Constant Tensile Load (NCLT) Test

Figure 6.3. Reproduction of Figure 4 of ASTM D5397-93 showing idealized shapes of NCTL strength-rupture curves.

Significance of Curve Shape

The upper left linear portion of an NCTL strength rupture curve represents material response when there is a ductile fracture in the material. The lower right linear portion represents material response when there is a quasi-brittle fracture in the material. The angled or curving juncture (i.e., knee, step, or nose) of these two linear portions represents material response when there is a transitional rupture.

Transition Point Selection

It is common within the geosynthetics industry to select a transition point from an NCTL strength rupture curve. A transition point is selected at the apparent beginning of the lower right linear portion representing the highest strength where a brittle fracture occurs. Examples of transition point selection from a strength rupture curve can be found in appendix A of Standard Method GRI-GM5(a). Figure 6.4 is reproduced from this reference. However, apparent transition points are not always readily distinguishable in an NCTL strength rupture curve, and judgment combined with visual examination of the fracture faces is necessary.

Verification of Interpretations by Fracture Face Examinations

Failure mode and transition point interpretations made from a strength rupture curve should be verified by examination of the fracture faces associated with each of the test specimens. It is helpful to arrange the ruptured specimens in order of decreasing strength level (applied during testing) in order to observe the often gradual changes from ductile to transitional fracture, and from transitional to brittle fracture.

Extrapolation

Any extrapolation of an actual test data trend to times or conditions beyond the tested times/conditions is made only with caution. When extrapolations of CTL strength rupture curves are made, the extrapolated results are qualified by an estimation, or by a discussion, of uncertainty.

Prediction

Mathematical methods are commonly used to provide predictions of CTL test results under strength levels and/or testing conditions that differ from those actually tested. Like

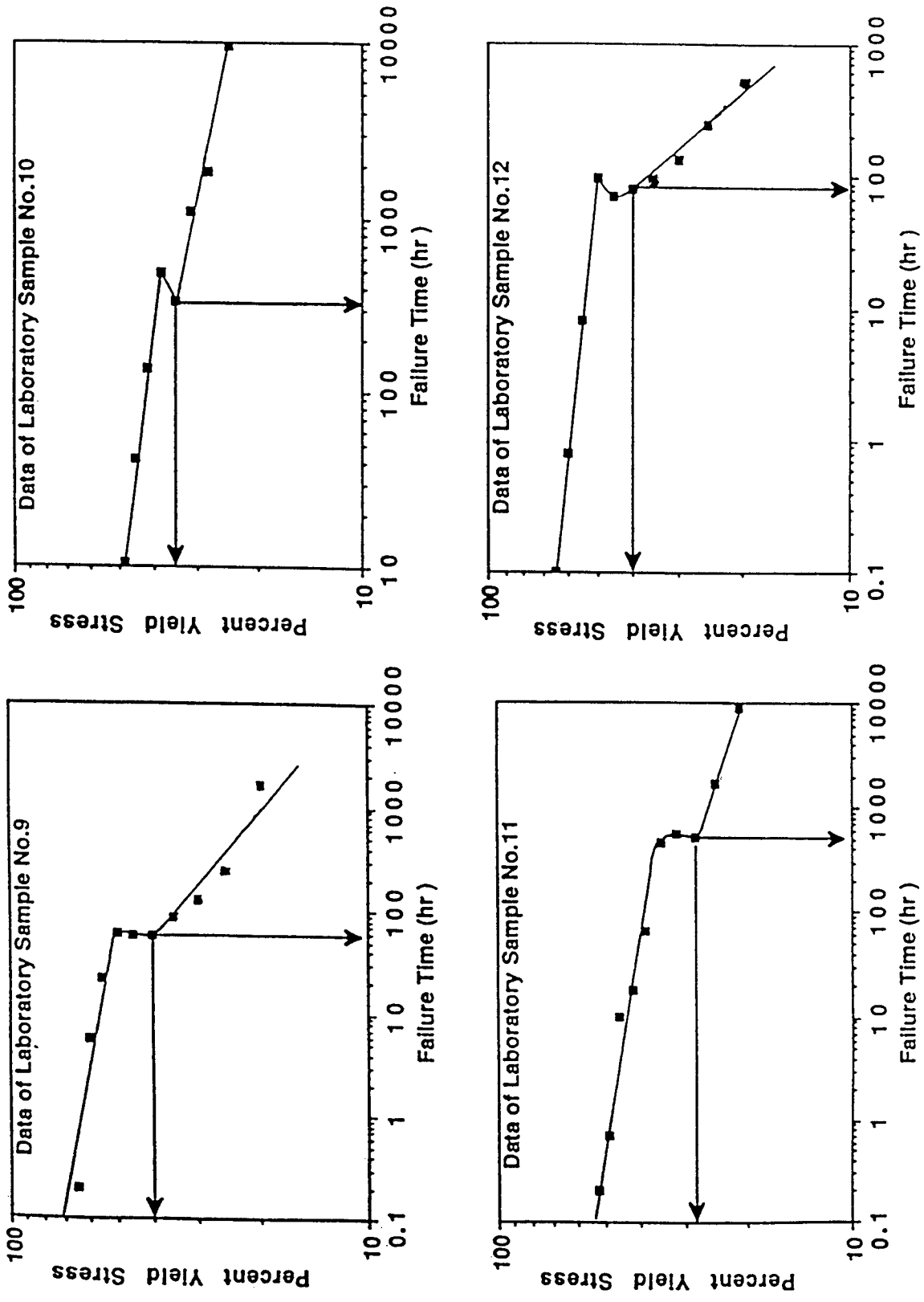


Figure 6.4. Reproduction of a selected page from Appendix B of Standard Method GRI-GM5(a) showing four examples of transition point selection from NCTL strength-rupture-curves.

extrapolations, predictions are also made with caution because they provide estimates of performance at times or conditions where no testing was performed. Mathematical methods also require that an idealization of the actual test data be represented in the model. One such mathematical method, used for predicting strength rupture times in HDPE at temperatures that are different than the actual testing temperatures, is the rate process method (RPM). The RPM uses the principle of time temperature superposition and involves developing a prediction by solving three simultaneous equations representing laboratory test data. The RPM was used in this research program for the P-1 geogrid product to make strength rupture predictions to 20°C from 50°C, 65°C, and 80°C laboratory test data. Detailed discussion of the RPM method and predicted 20°C strength rupture curves are presented in chapter 8.

Another mathematical method used for making a prediction is Popelar et al. bidirectional shifting.⁽¹⁶⁾ Like the RPM, Popelar et al. shifting also can be used to predict strength rupture times in HDPE at temperatures that are different from the actual testing temperatures. Popelar et al. shifting is horizontal and vertical shifting, proportional to temperature, in the log time and log stress axes. Popelar et al. shifting was empirically developed based on numerous stress relaxation studies of MDPE and HDPE gas pipe materials.⁽¹⁷⁾ Detailed discussion of Popelar et al. shifting and 100-yr/20°C strength rupture predictions also are presented in chapter 8.

The RPM and Popelar et al. bidirectional shifting were the mathematical prediction methods selected for analyzing the elevated temperature P-1 geogrid data generated in this program.

c. Interpretation of UCTL Strength Rupture Curves

This section provides a discussion of key considerations regarding the interpretation of UCTL test results. This section extends the discussion of the interpretation of NCTL test results.

Changes made to a material or product during UCTL specimen preparation may significantly impact time to rupture. For example, the process of die cutting a specimen from a resin plaque leaves microscopic vertical grooves on the sides of each specimen that are created by the imperfect nature of the metal die's cutting edge. In the absence of other notches or scratches on the plaque's natural top and bottom surfaces, these grooves can potentially act as artificial stress raisers. This is not a desirable effect, and is one reason for introducing a controlled notch in the NCTL test. In the UCTL test performed on resins for this research program, resins L and M were believed to experience an unquantified degree of prematurity in rupture times due to sidewall grooves made by the die. Resin H rupture times were less

impacted by microscopic side wall grooves because resin H was very resistant to stress cracking and developed no brittle ruptures during the UCTL testing.

Changes made to the shape or configuration of a product during specimen preparation may also create artificial stress raisers that can affect time to rupture. For example, cuts necessarily made to trim a product specimen for testing may provide artificial stress raisers. In the UCTL testing performed on the P-1 geogrid, some brittle fractures were initiated on the razor cut ends of the center node bar, despite the efforts to make very smooth cuts.

Appearance of UCTL Curves

It has been the authors' experience that UCTL strength rupture curves typically consist of two approximately linear portions with similar slopes that meet at ends in a generally step-shaped profile. In this way, they are similar to NCTL strength rupture curves. However, the transition zone portion of a UCTL curve is typically not as well defined as the transition zone in an NCTL curve. In addition, the difference in slope between the two linear portions of a UCTL curve is typically much less obvious than the slope difference between the ductile and brittle lines of a NCTL curve. The subtle nature of most UCTL curves hinders transition point selection by curve appearance, and places added reliance on the visual assessment of failure mode.

Transition Point Selection

The transition point from a UCTL strength rupture curve is selected in a manner similar to that used for an NCTL curve. However, because the transition zone portion of a UCTL curve is usually difficult to interpret, UCTL transition point selection presents a higher risk for error and should be verified by fracture face examinations.

Extrapolation and Prediction

The discussions presented in the previous section regarding extrapolations and predictions made from NCTL strength rupture curves applies equally to UCTL curves. However, additional cautions are placed on interpretations made from UCTL curves due to the greater possibility for fractures to occur at inconsistent locations or in apparently non-repeatable failure modes.

CHAPTER 7

CTL RESIN AND GEOGRID TEST RESULTS AND DATA ANALYSIS

7.1 INTRODUCTION

The following sections present NCTL and UCTL test results and data analysis for the three resin samples and the P-1 geogrid sample.

Brittle zone points and trends best describe a material's stress cracking resistance. Analysis of the brittle zone will be emphasized over ductile or transitional zone analysis. For most CTL testing series, a number of specimens tested at the lowest strength levels did not rupture in the time frame of the testing program. Testing a wide range of low-strength levels was intentional in order to identify the strength levels that produce 5,000 to 10,000 hr rupture times. Obtaining low-strength unruptured points was, therefore, intentional. The plotted points representing these low-strength unruptured specimens are represented by solid markers, such as a solid circle. For CTL series that demonstrated brittle failures at strength levels higher than these unruptured points, it is assumed that the lower strength level unruptured specimens would have also failed in a brittle manner if the testing had been allowed to continue for an indefinite time span. Therefore, on plots containing unruptured points, preceding brittle zone trend lines were drawn so that they end slightly above the highest solid marker plotted (with the exception of the UCTL 65°C geogrid series).

For each strength rupture curve presented, the fracture faces of ruptured specimens were visually examined to verify, or to determine, strength levels at which ductile, transitional, or brittle fractures occurred. This was performed in the following manner:

- (1) ruptured specimens for a given test series were laid out on a table in order of decreasing strength level and visually examined;
- (2) the observed trends in fracture type (for the given test series) were compared with the strength rupture curve for that series; and
- (3) each portion of the given strength rupture curve was, thereby, either verified or determined to have resulted from a failure mechanism corresponding to the observed fracture types associated with that portion of the curve.

For the resin L and M series, transition point selection was based on strength rupture curve shape and verified by fracture face examinations. For the resin H series, fracture face examinations revealed no brittle ruptures, and, therefore, no transition point was achieved or identified for either of the resin H series. For the three P-1 NCTL geogrid series, transition point selection was based on strength rupture curve shape and verified by fracture face examinations. For the three UCTL P-1 geogrid series, for which the strength rupture curves showed no clear steps, transition point selection was based solely on fracture face examinations. Therefore, visual examinations of fracture faces provided vital information to this research program.

7.2 CTL TEST RESULTS FOR THE RESINS

a. Overview

The NCTL and UCTL test results for resins L, M, and H are presented as strength rupture curves. The strength rupture curves for the NCTL tests on resins L, M, and H are presented in figures 7.1 to 7.4. The strength rupture curves for the UCTL resin tests are presented in figures 7.5 to 7.8. A tabulated summary of all strength rupture curve interpretations is presented in table 6. The raw data for each resin test series are contained in tables in appendix B.

All slopes in table 6 are reported without units because the slopes were calculated from log-log scale values. Transition point selections for the resin L and M series were based on strength rupture curve shape and verified by fracture face examinations. For both resin H series, however, fracture face examinations revealed no brittle ruptures, and, therefore, no transition point was achieved or identified for either of the two resin H series.

b. NCTL Test Results for the Resins

Presentation of the Results

Resin L. The NCTL test results produced a strength rupture curve with a mild step-type response, as shown in figure 7.1. A transition point of 8.4 hr, 21 percent was selected in accordance with the transition point selection procedure previously described. Resin L exhibited a relatively low resistance to stress cracking propagation, as demonstrated by brittle zone average failure times of 15.3 hr at 18 percent and 111.0 hr at 15 percent of yield strength (these values being read on the quasi-brittle fracture portion of the strength rupture curve in figure 7.1).

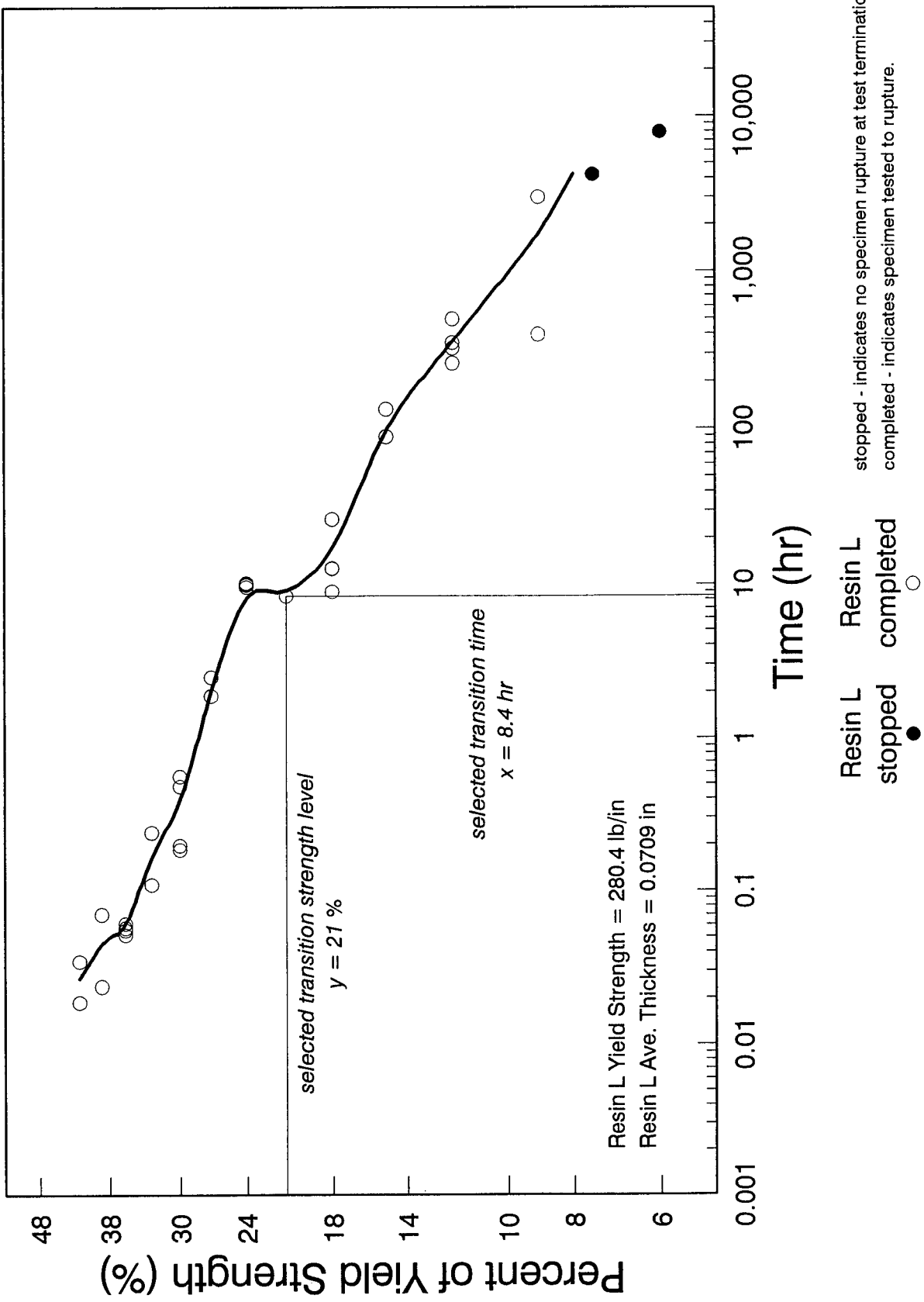


Figure 7.1. NCTL data for resin L, tested at 50°C in water.

L:MNPERC1

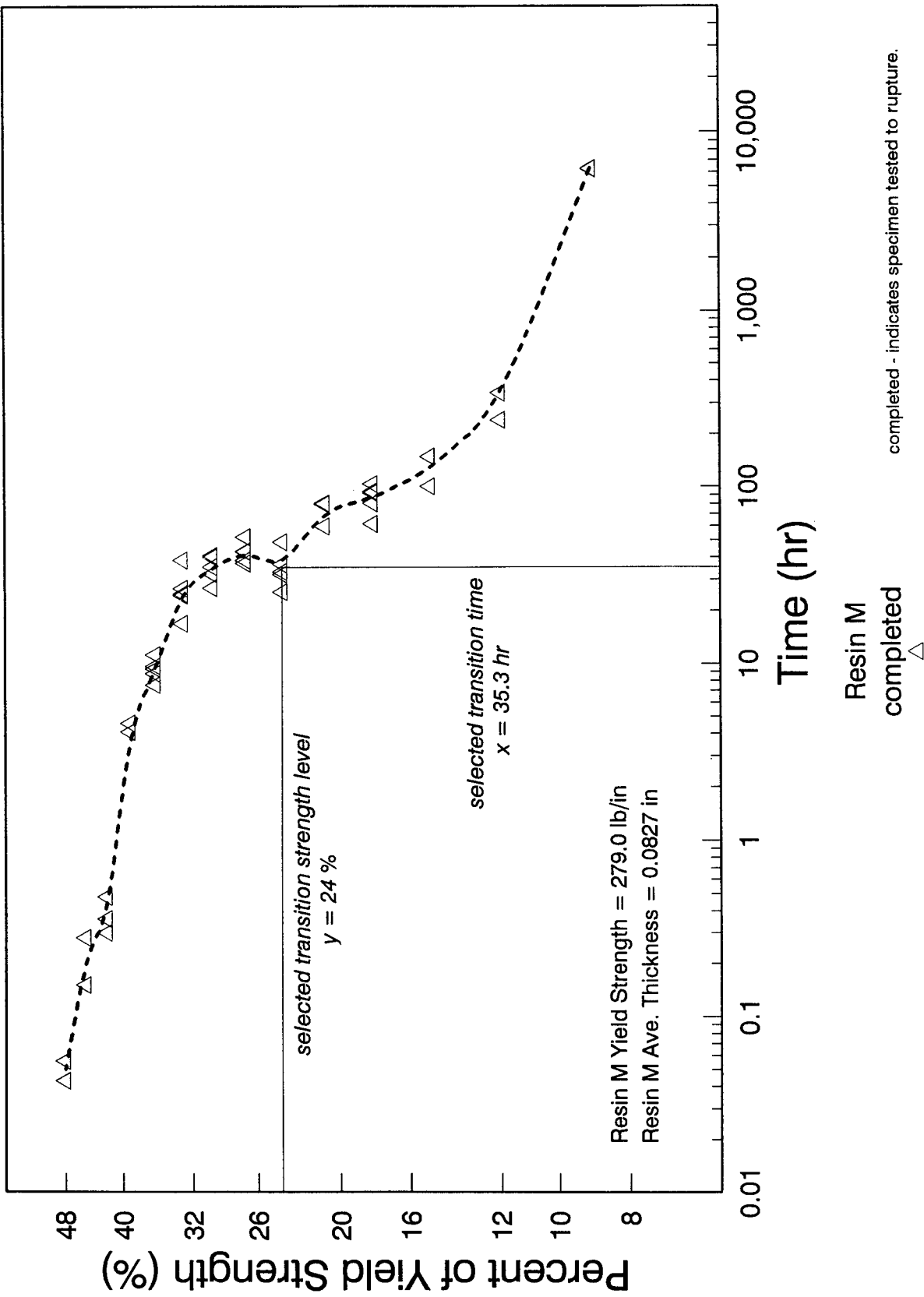


Figure 7.2. NCTL data for resin M, tested at 50°C in water.

L:LMHPERC1

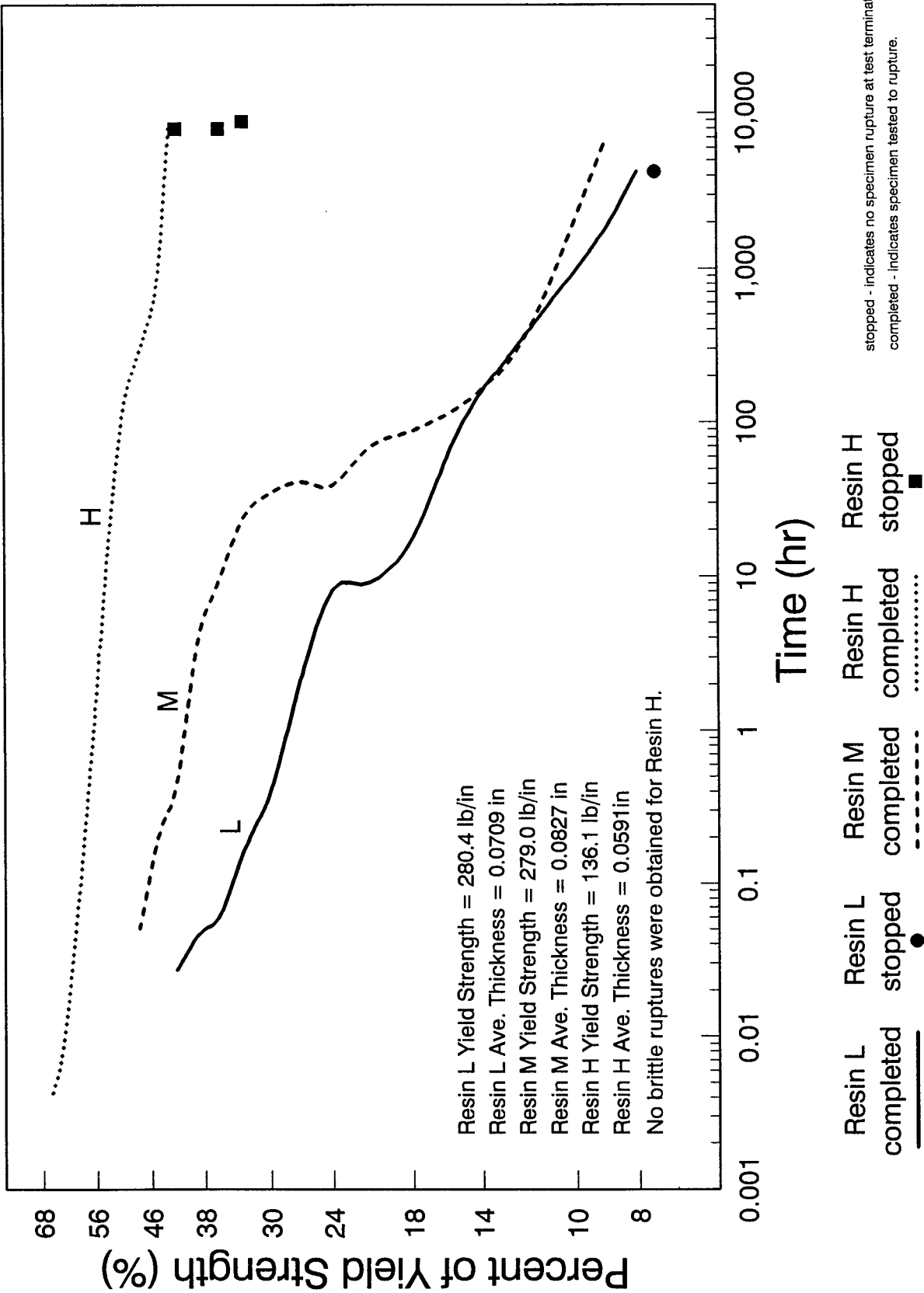


Figure 7.4. NCTL data for resins L, M, and H, tested at 50°C in water.

L:LUNPERC1

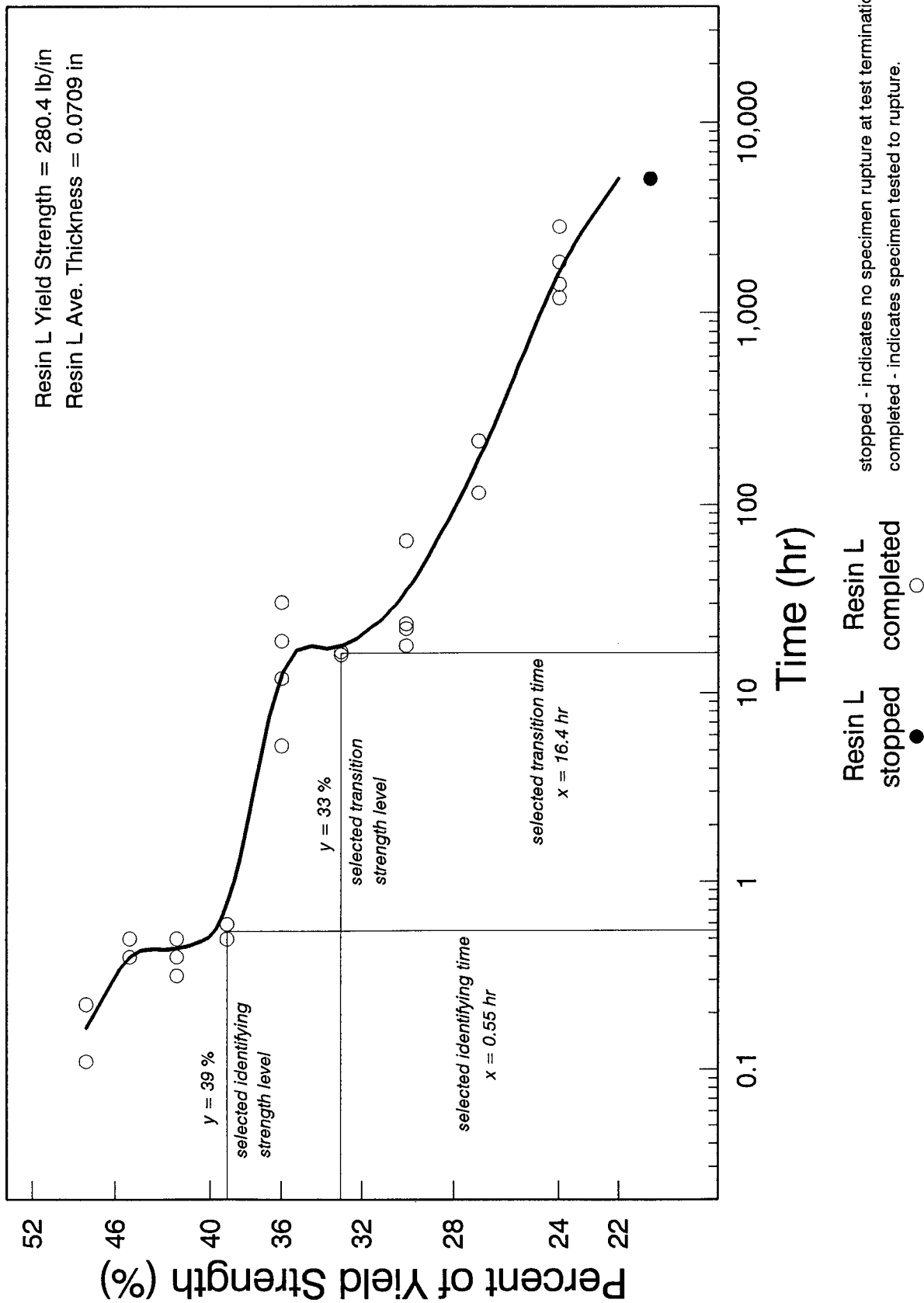


Figure 7.5. UCTL data for resin L, tested at 50°C in water.

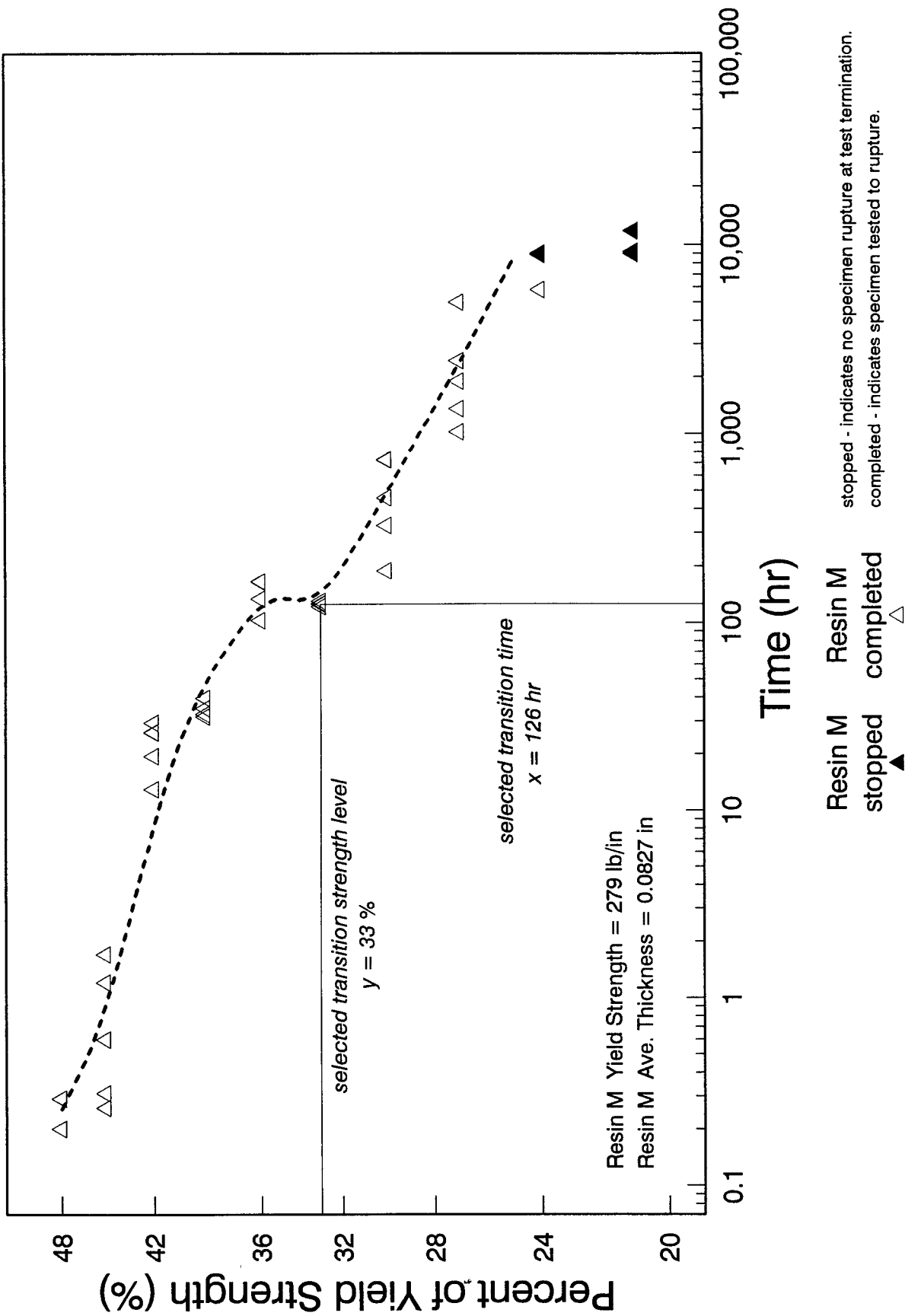


Figure 7.6. UCTL data for resin M, tested at 50°C in water.

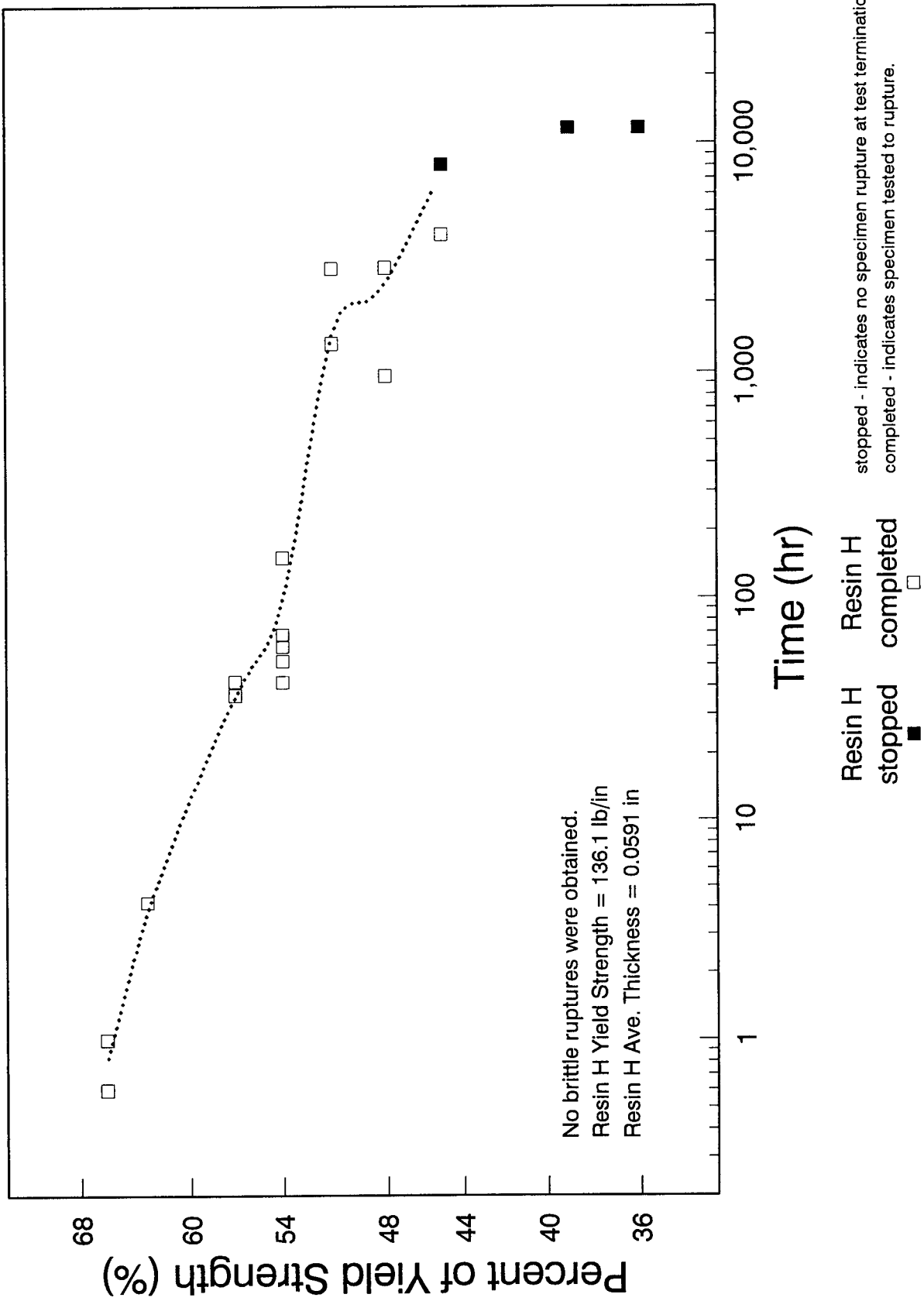
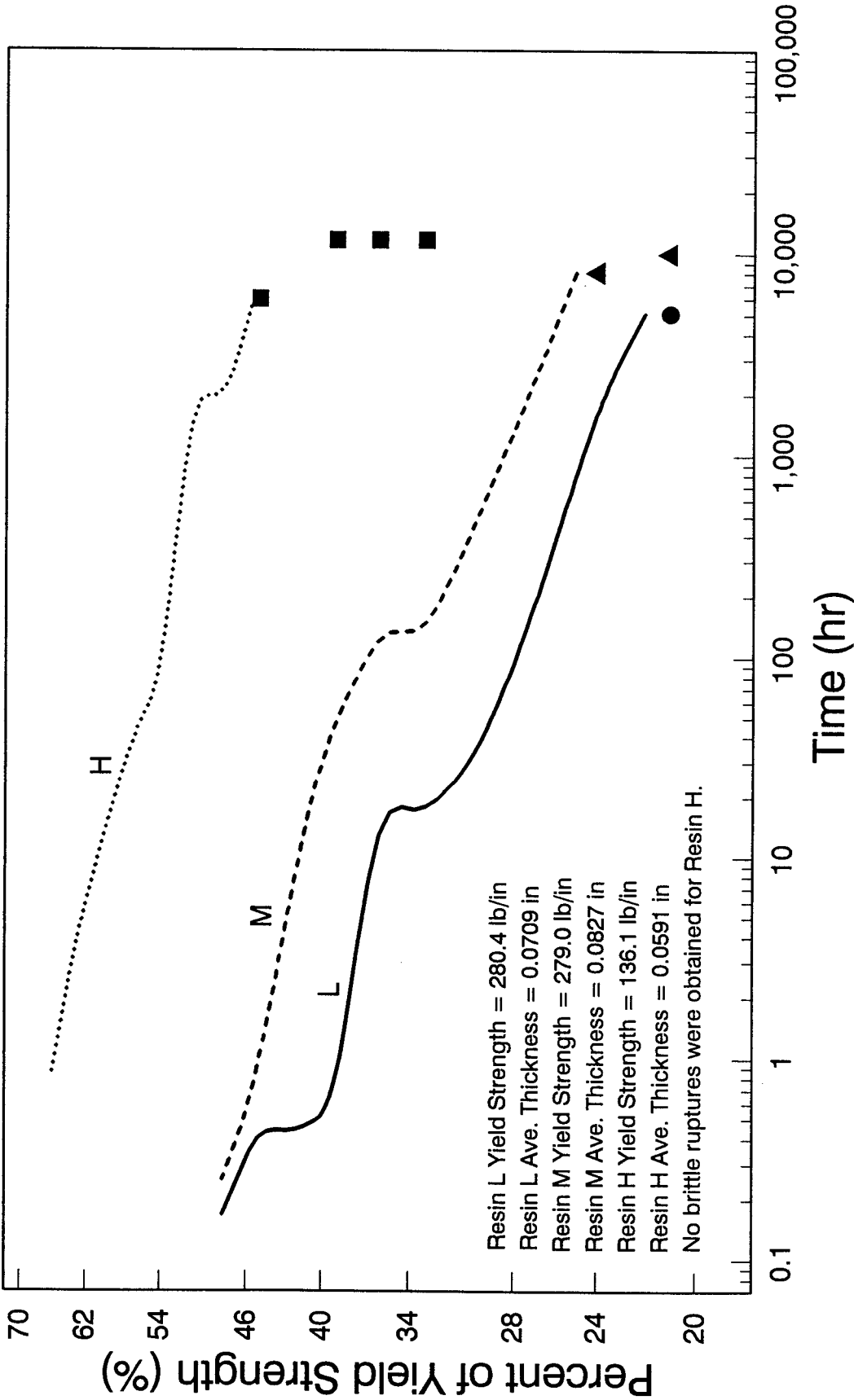


Figure 7.7. UCTL data for resin H, tested at 50°C in water.

L:LMHUPER1



Resin L Yield Strength = 280.4 lb/in
 Resin L Ave. Thickness = 0.0709 in
 Resin M Yield Strength = 279.0 lb/in
 Resin M Ave. Thickness = 0.0827 in
 Resin H Yield Strength = 136.1 lb/in
 Resin H Ave. Thickness = 0.0591 in
 No brittle ruptures were obtained for Resin H.

stopped - indicates no specimen rupture at test termination.
 completed - indicates specimen tested to rupture.

Resin L completed
 Resin L stopped
 Resin M completed
 Resin M stopped
 Resin H completed
 Resin H stopped

Figure 7.8. UCTL data for resins L, M, and H, tested at 50°C in water.

Table 6. Summary of slopes and transition points for CTL results.

Material (Temp.)	Slope Ductile ¹ Zone	Slope Brittle Zone	Transition Point	
			Time (hr)	Strength (%)
Resin L (50°C) NCTL UCTL	-0.0909	-0.1510	8.4	21
	-0.0655	-0.0589	16.4	33
	-0.0225			
Resin M (50°C) NCTL UCTL	-0.0565	-0.1681	35.3	24
	-0.0417	-0.0667	126.3	33
Resin H (50°C) NCTL UCTL	-0.0284	N/D	> 8,000	N/D
	-0.0398	N/D	> 11,000	N/D
P-1 Geogrid (80°C) NCTL UCTL	-0.0569	-0.0729	22.5	11.96
	-0.0783	-0.1728	351.2	23.14 ²
P-1 Geogrid (65°C) NCTL UCTL	-0.1084	-0.0888	66.4	12.11
	-0.0626	-0.1162	602.1	28.00 ²
P-1 Geogrid (50°C) NCTL UCTL	-0.0971	N/D	187.0	16.87
	-0.0793	-0.1445 ³	13,000 ⁴	31.2 ⁴
			40,000 ⁴	31.0 ⁴

¹ For UCTL geogrid specimens, this column refers to the shear rupture zone.

² Transition point selection was based on change in primary rupture mechanism; i.e., shear to brittle. Transition point selection for all other materials was based on the shape of the curve (plotted results) as per GRI-GM5 appendix B.

³ No brittle fractures were obtained. (Only shear rupture failures were obtained.) The 50°C UCTL slope was calculated by averaging the 65°C and 80°C UCTL slopes.

⁴ A conservative brittle rupture zone window was assumed, with an assumed transition point between 13,000 hr, 31.2 percent and 40,000 hr, 31.0 percent.

N/D = Not Determined.

Resin M. The NCTL test results produce a strength rupture curve with a broad nose-type response, as shown in figure 7.2. The transition zone appears to extend further down the strength rupture curve than most typical nose-type response curves for HDPE geomembranes. A transition point of 35.3 hr, 24 percent was selected. Even though resin M exhibited higher ductile and transitional times to failure than resin L, resin M exhibited low brittle zone times to failure like resin L. Resin M, therefore, also is considered to have exhibited a low resistance to stress cracking propagation, as demonstrated by brittle zone average failure times of 86.7 hr at 18 percent and 124.6 hr at 15 percent of yield strength (these values being read on the quasi-brittle fracture portion of the strength rupture curve in figure 7.2).

Resin H. No brittle ruptures were obtained for resin H, as shown in figure 7.3; this was determined by fracture face examinations. A transition point could not, therefore, be selected, although a transition time approximately >8000 hr is inferred. Resin H, therefore, exhibited a relatively very high resistance to stress cracking propagation.

General Discussion

The ability of a deviated testing protocol (i.e., water environment) to distinguish variance in stress cracking resistance between resins was verified. Verification was achieved in NCTL strength rupture curves capable of revealing subtle differences and similarities between resins.

Adequate strength rupture data were obtained for resin M to provide for a quantitative comparison of the stress cracking resistances of resin M with P-1 node material. (Both resin M and the base resin used to manufacture P-1 geogrid were commercially identified as D1248-III A5-E5 resins.)

The index results, summarized in table 3, do not indicate a potential reason for the large extent of the NCTL resin M transition zone, as evidenced by the shape of the curve in figure 7.2.

The NCTL selected transition times for resins L and M, and for P-1 node material tested at 50°C, are plotted on a log-linear scale as a function of resin percent crystallinity in figure 7.9. Linear regression analysis of these data produced a very good correlation coefficient of 0.99978. It is acknowledged, however, that this agreement may be a fortuitous accident because the selection of transition times is subjective in nature. Nevertheless, this comparison indicates that selected transition times consistently decrease with increasing crystallinity (and corresponding density). This trend is consistent with data from literature and experience that indicate that stress cracking resistance generally decreases with increasing resin density and crystallinity.⁽¹⁸⁾

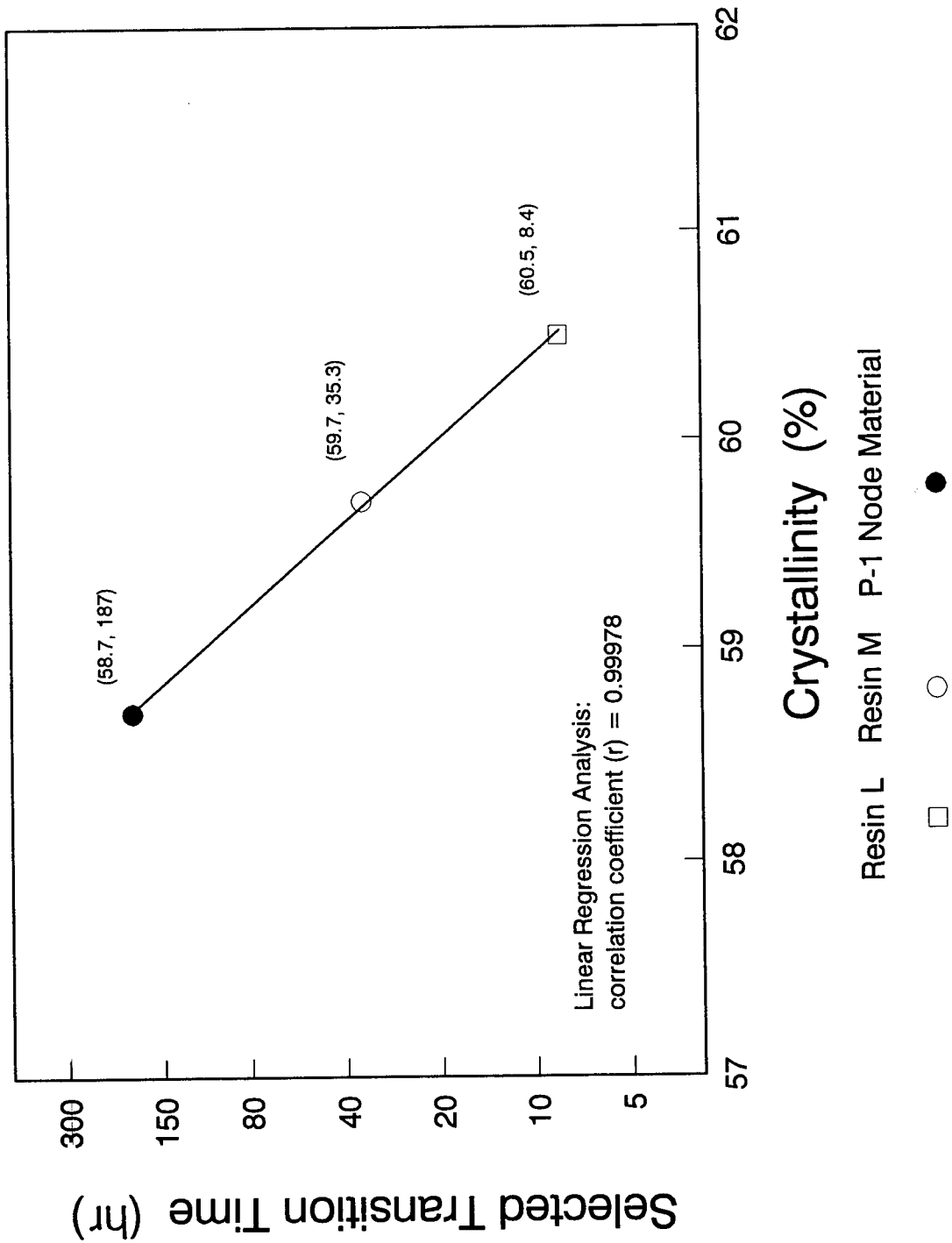


Figure 7.9. Selected transition time versus crystallinity, for 50°C NCTL resins L and M, and P-1 geogrid.

The NCTL selected transition strengths for resins L and M, and for P-1 node material tested at 50°C, are plotted on a log-linear scale as a function of resin melt flow index in figure 7.10. Melt flow responses reflect molecular weight and density, and stress cracking resistance correlates strongly with density.^(6,7,8) Linear regression analysis of these data produced a correlation coefficient of 0.84427. It has been pointed out that a possible linear correlation between transition strength and melt flow may not be real since there are other [micro-]structural factors that can contribute to strength but that don't show up in a single point melt index test. Nevertheless, because melt flow reflects density to some degree, and because stress cracking resistance correlates strongly with density, a possible correlation of melt flow with transition strength is presented in figure 7.10.

Resin M

The NCTL testing on resin M, performed in a water bath maintained at 50°C, produced the following quantitative indicators of resin M level of stress cracking resistance:

- a 900 *psi* (6200 kPa) failure time of approximately 75 hr;
- a 30 percent of yield *stress* failure time of approximately 49 hr;
- a selected transition time of 35.3 hr; and
- a brittle zone strength rupture response (curve) very similar to that observed for resin L in the 11 to 16 percent strength window.

Stress values are included in the above list of quantitative indicators for resin M because stress is an independent variable often used by the geosynthetics industry to rank HDPE geomembranes in regard to stress cracking resistance. One example of a ranking procedure can be found in a study for the Electric Power Research Institute that recommends a 900 *psi* (6200 kPa) stress level in the NCTL test for geomembranes and recommends consideration of a minimum pass criterion of 200 to 500 hours (in a 1 percent Igepal bath maintained at 50°C).⁽²⁷⁾ These recommendations are consistent with the current industry trends of comparing HDPE geomembrane materials at stress levels equivalent to 30 percent of room temperature yield *stress*, typically a stress level of 750 to 950 *psi* (5200 to 6600 kPa) and to specify a minimum pass criterion of 200 to 400 hours (in a 10 percent Igepal bath maintained at 50°C).

Current industry standards and common practices for determining stress cracking resistance of HDPE geomembrane materials include exposure to an Igepal solution. Igepal solutions are more aggressive than water (or air) with regard to accelerating stress cracking in HDPE. For example, an HDPE material failing in 100 hr in an Igepal solution can be expected to require more time to fail in a water bath (all other conditions being the same). Hsuan et al. found that, relative to transition point failure times in 100 percent tap water, transition point failure times in 10 percent Igepal solution are reduced by approximately 40 times for HDPE geomembrane sheet material.⁽¹⁴⁾

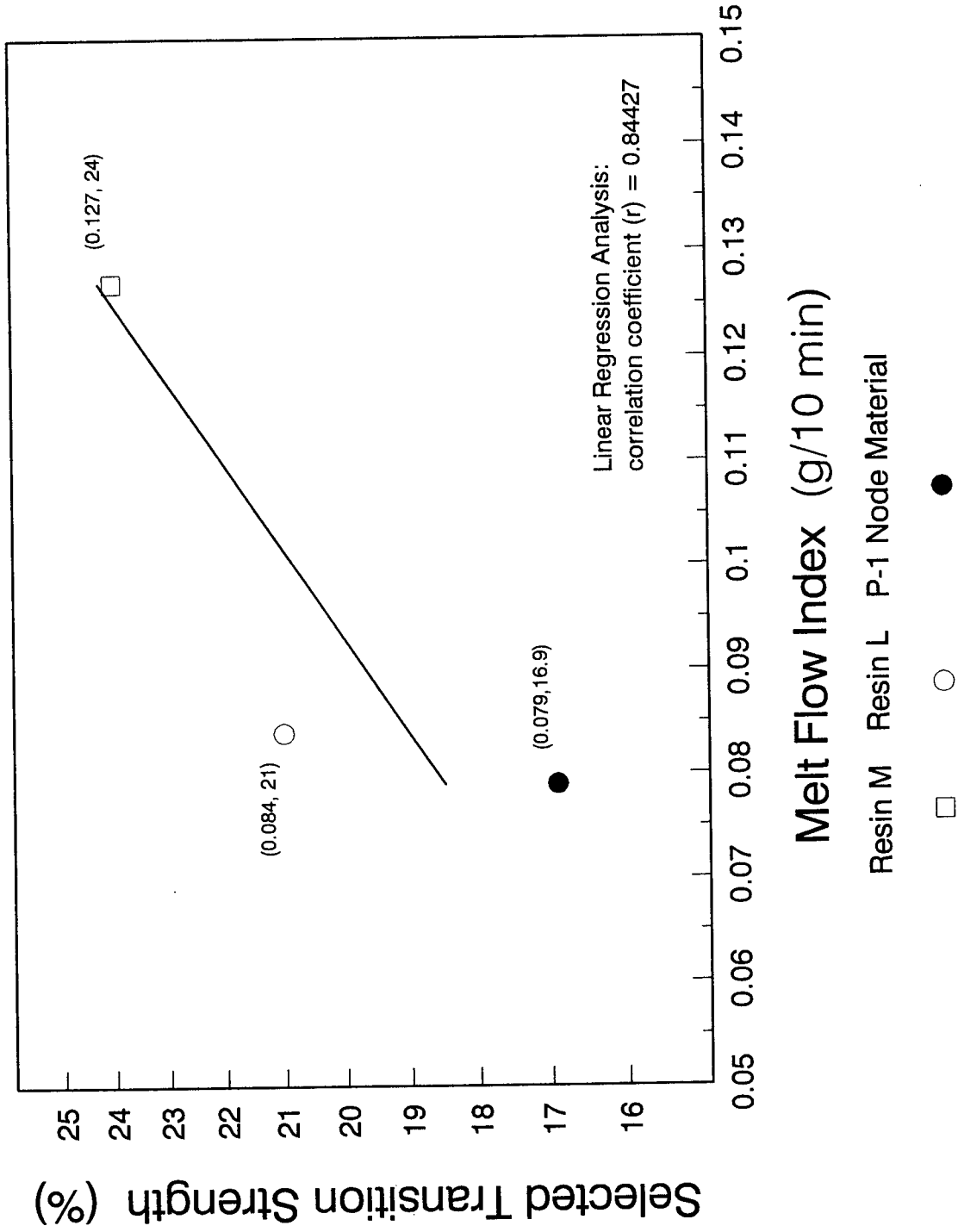


Figure 7.10. Selected transition strength versus melt flow index, for 50°C NCTL resins L and M, and P-1 geogrid.

These findings are consistent with research performed by Ward et al. who found that, relative to failure times in air at 50°C and at 4.2 MPa (609 psi), failure times in 10 percent Igepal at 50°C and at 4.2 MPa (609 psi) were reduced by 25 to 50 times for 22 PE gas pipe resins.⁽¹⁹⁾ Therefore, the current industry practice of 200 to 400 hours in Igepal at 30 percent of yield stress corresponds to more than 200 to 400 hr in water at the same temperature and stress level. Resin M, however, produced a 30 percent of yield stress failure time of only 49 hr in a water bath.

Another example of a procedure for ranking HDPE geomembranes in regard to stress cracking resistance can be found in Geosynthetic Research Institute's report to the U.S. Environmental Protection Agency titled, "*Stress Cracking Behavior of HDPE Geomembranes and Its Prevention.*"⁽¹⁴⁾ This report recommends a criterion of transition time ≥ 100 hr, for HDPE material tested according to GRI Standard Test Method GM5(a). GRI-GM5(a) specifies 10 percent Igepal and 50°C based on numerous tests performed on 7 field-retrieved HDPE geomembrane samples and on 18 new geomembrane samples. The selected transition time for resin M was 35.3 hr, which is significantly less than the recommended criterion.

In light of the above discussions, the quantitative indicators listed for resin M indicate that the stress cracking resistance of resin M was low by the industry's current geomembrane standards. With respect to the brittle zone, which is emphasized in this program, the stress cracking resistance of resin M was similar to that of resin L.

Since resin M and P-1 base resin are deduced to be very similar, the observation that stress cracking resistance of resin M was low by the industry's current geomembrane standards would suggest at first, the same for the P-1 base resin. This, however, is a preliminary conclusion based only on the similarities of resins deduced and comparative NCLT testing.

c. UCTL Test Results for the Resins

Resin L. The UCTL test results produce a strength rupture curve with two step-type responses, as shown in figure 7.5. An identifying point of 0.55 hr, 39 percent was selected for the first step. Fracture face examinations determined that the identifying point's strength level coincided with the approximate maximum strength level at which microscopic sidewall grooves on the die-cut specimens appeared to impact rupture mechanisms and, therefore, times to failure. At the second step, a transition point of 16.4 hr, 33 percent was selected. If the unquantified effect of the grooves is ignored, then resin L can be said to have exhibited low resistance (relative to resins M and H) to stress cracking initiation and propagation as demonstrated by brittle zone average UCTL failure times of 32.1 hr at 30 percent and 167.2 hr at 27 percent of yield strength.

Resin M. The UCTL test results produced a strength rupture curve with a mild step-type response, as shown in figure 7.6. A transition point of 126 hr, 33 percent was selected. Unlike the NCTL transition zone for resin M (figure 7.2), the UCTL transition zone for resin M (figure 7.6) does not significantly extend downward. Fracture face examinations revealed that microscopic sidewall grooves on the die-cut specimens also impacted resin M rupture mechanisms and times to failure to an unquantified degree. If the unquantified effect of the grooves is ignored, then resin M can be said to have exhibited medium resistance (relative to resins L and H) to stress cracking initiation and propagation, as demonstrated by brittle zone average UCTL failure times of 486.8 hr at 30 percent and 2,339 hr at 27 percent.

Resin H. No brittle ruptures were obtained for resin H (figure 7.7); this was determined by fracture face examinations. A transition point could not, therefore, be selected, although a transition time approximately >11,000 hr is inferred. The microscopic sidewall grooves on the die-cut resin H specimens did not appear to impact resin H ductile rupture mechanisms or times to failure. Resin H, therefore, exhibited very high resistance to stress cracking initiation and propagation.

General Discussion

The ability of a deviated testing protocol (i.e., water environment plus no notch) to distinguish subtle variance in stress cracking resistance between resins, with the added step of crack initiation, was not verified. However, the ability to distinguish general variance was verified, as seen in figure 7.8. Resins L and M evidenced an unquantified degree of prematurity in UCTL rupture times, possibly due to microscopic sidewall grooves left by the metal die used to punch out the specimens. The obvious cracked appearance of the sidewalls of most of the plastically-deformed UCTL resin L and M specimens generally suggests sidewall grooving as a likely source of premature failure. It is pointed out that no quantifiable data are provided to support this claim of prematurity in rupture time because of side scratches from die cutting.

Brittle fractures occurred in resin L and M specimens tested at relatively high strength levels (i.e., strength levels above the selected transition point) as well as at relatively low strength levels (i.e., strength levels below the selected transition point). The relatively high strength level specimens are used in the subsequent discussion because these cases included exceptions to what was reasonably expected, thereby offering insight into hitherto unexplained observations, such as the first step in the resin L UCTL curve shown in figure 7.5.

The initiation loci of brittle fractures in high strength level specimens appeared to coincide with thin, parallel grooves on the specimen sidewalls. These grooves were presumably

created by the cutting edge of the sharpened metal die as it was punched down, into, and through the plaque during specimen preparation. The occurrence of these brittle fractures in specimens tested at higher strength levels was not expected; rather, bulk ductile failure by necking (i.e., plastic deformation) was expected to be the only, or at least the main, failure mechanism. The actual failure process, however, appeared to be as follows: failure occurred first by a brittle fracture mechanism initiating in thin grooves on specimen sidewall surfaces and progressing inward until crack tip blunting occurred, followed by an increasing dominance in bulk plastic deformation as the brittle fractures progressed inward, diminishing the remaining cross-sectional area.

The brittle fractures in resin L and M UCTL sidewall surfaces created an appearance similar to the cracked-surface appearance sometimes associated with environmental stress cracking. Environmental stress cracking is the (potential) acceleration of stress cracking by an active chemical medium. The medium used in this testing, however, was water. Water is an inactive medium that has been shown to be unable to penetrate growing fissures (i.e., crack tips) sufficiently quickly to cause failure by stress cracking instead of failure in tension at high stresses.⁽²⁰⁾ Because bulk failure only/mainly by plastic deformation did not occur as expected, as water has been shown to not be a medium that can advance stress cracking quickly enough to modify the prevailing failure mechanism at high strength levels, and because the brittle fractures appeared to initiate from sidewall grooves, they appeared to impact rupture mechanisms.

If rupture mechanisms are impacted, then it is possible that times to rupture also will be impacted. For example, resin L in figure 7.5 shows that the times to rupture were reduced by the change in rupture mechanism from plastic deformation to brittle fracturing from sidewall grooves. The curve in figure 7.5 can be described as follows:

- At strength levels above approximately 39 percent, failure was primarily by bulk plastic deformation with some sidewall cracking.
- At strength levels below approximately 39 percent and above approximately 33 percent, failure occurred by an approximately equal combination of brittle fracturing from sidewall grooves and increasing bulk plastic deformation.
- At strength levels below approximately 33 percent, failure was primarily by brittle fracturing with secondary, localized plastic deformation increasing in the remainder of diminishing cross-sections below progressing fractures.

The step in the curve (39 to 44 percent strength level), therefore, represents a reduction in time to rupture because of the influence of sidewall grooves.

It is possible that resin L was more susceptible to the effects of the sidewall grooving than resin M, because resin L has higher density and crystallinity than resin M.

Future UCTL resin specimen preparation procedures should be modified to preclude sidewall grooving if possible, or should be modified to incorporate a process to remove sidewall grooves by a polishing method. Possible procedures for eliminating sidewall grooving were not investigated in this program.

Reliable UCTL strength rupture times (which include the time for the natural crack initiation to occur) were not obtained for the resins because of an unquantified degree of rupture time prematurity due to sidewall grooving caused by the metal die used to punch out the specimens. Therefore, the UCTL resin strength rupture may not yield a reliable quantitative comparison of rupture times between 50°C UCTL resin M and 50°C UCTL P-1 geogrid.

In the sense that the UCTL resin testing series succeeded in distinguishing general differences between the resins, while the NCTL testing series was reliably capable of revealing subtle differences between the resins, the UCTL resin testing can be said to further qualify the NCTL test as a preferred test for *ranking* resins with respect to stress cracking resistance.

7.3 CTL TEST RESULTS FOR P-1 GEOGRID

a. Overview

The NCTL and UCTL test results for the P-1 geogrid are presented as strength rupture curves for the NCTL tests in figures 7.11 to 7.14. The curves for the UCTL tests are presented in figures 7.15 to 7.18. A tabulated summary of all strength rupture curve interpretations is presented in table 6. The raw data for the geogrid test series are contained in tables in appendix C.

All slopes are reported without units because the slopes were calculated from log-log scale values. Transition point selections for the NCTL P-1 geogrid series were based on strength rupture curve shape and verified by fracture face examinations, while transition point selections for the UCTL P-1 geogrid series were based solely on fracture face examinations.

Brittle zone points and trends best describe a material's stress cracking resistance. Analysis of the brittle zone will, therefore, be emphasized over ductile or transitional zone analysis. For the following data plots and analyses, brittle zone lines were interpreted to pass above the highest strength level unruptured data point for a given series (with the exception of the UCTL 65°C series), as discussed previously.

L:G50NPERC

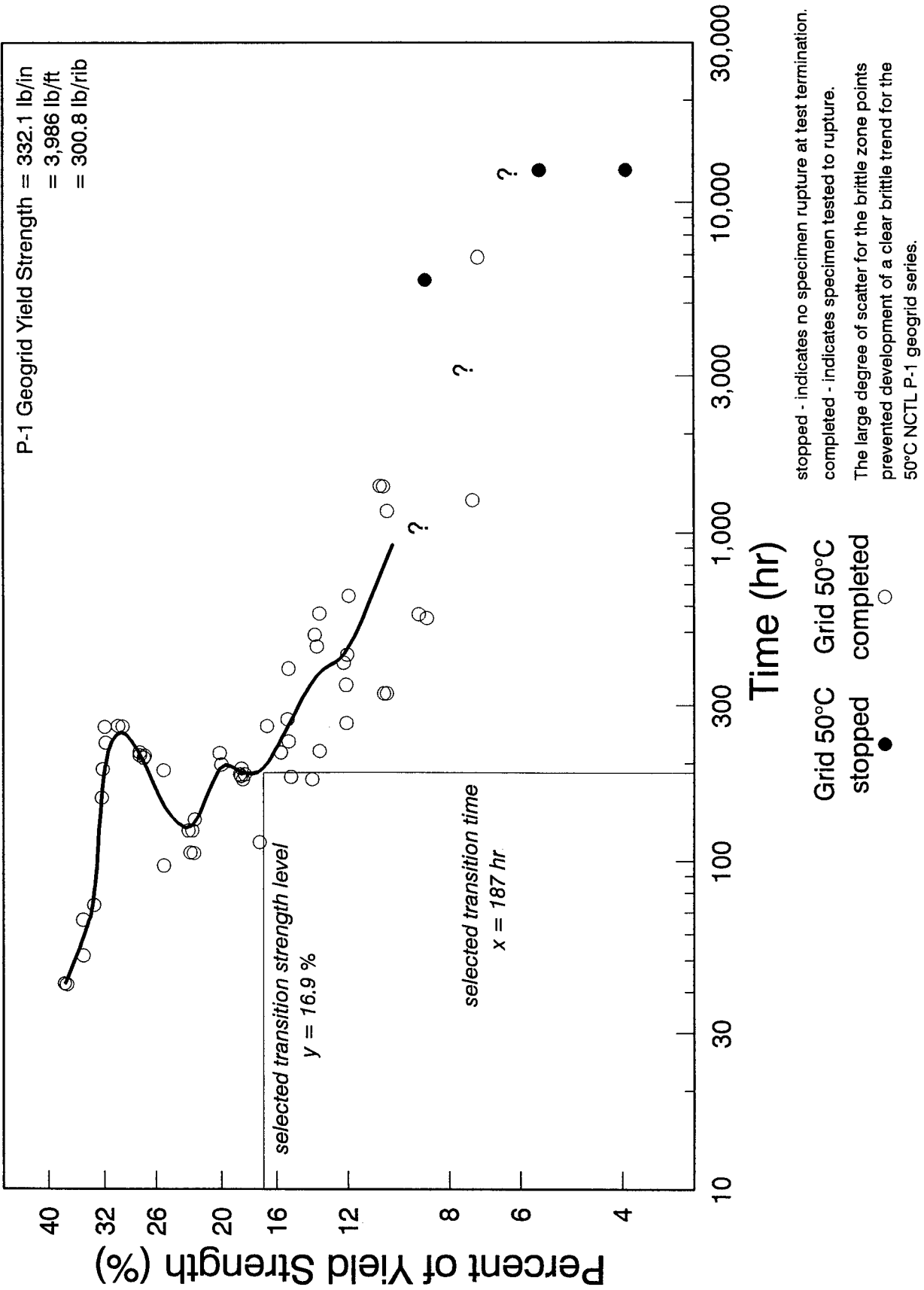


Figure 7.11. NCTL data for P-1 geogrid, tested at 50°C in water.

L:G80NPERC

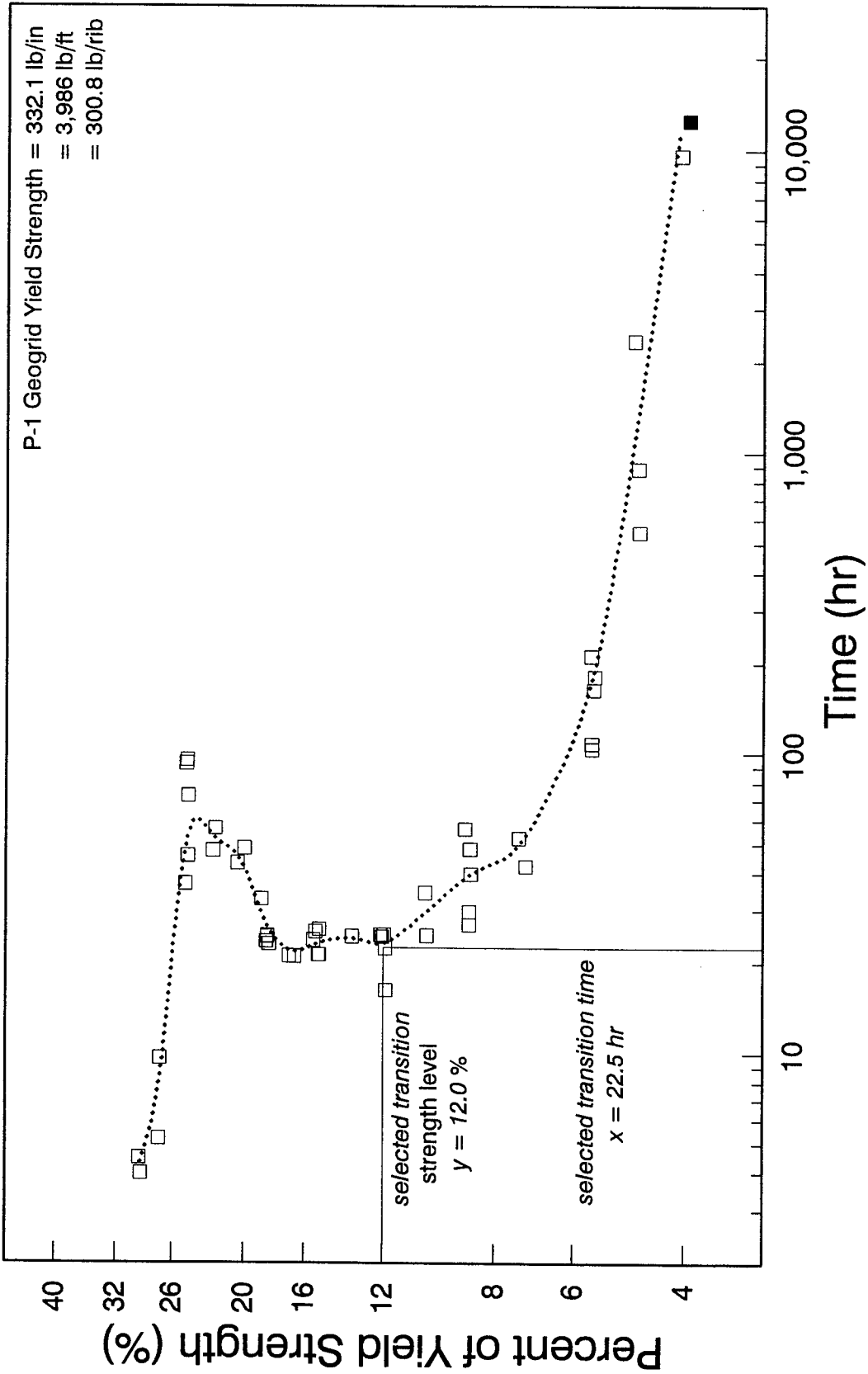


Figure 7.13. NCTL data for P-1 geogrid, tested at 80°C in water.

L:GGGNPER2 (drawing only)

P-1 Geogrid Yield Strength = 332.1 lb/in
= 3,986 lb/ft
= 300.8 lb/rib

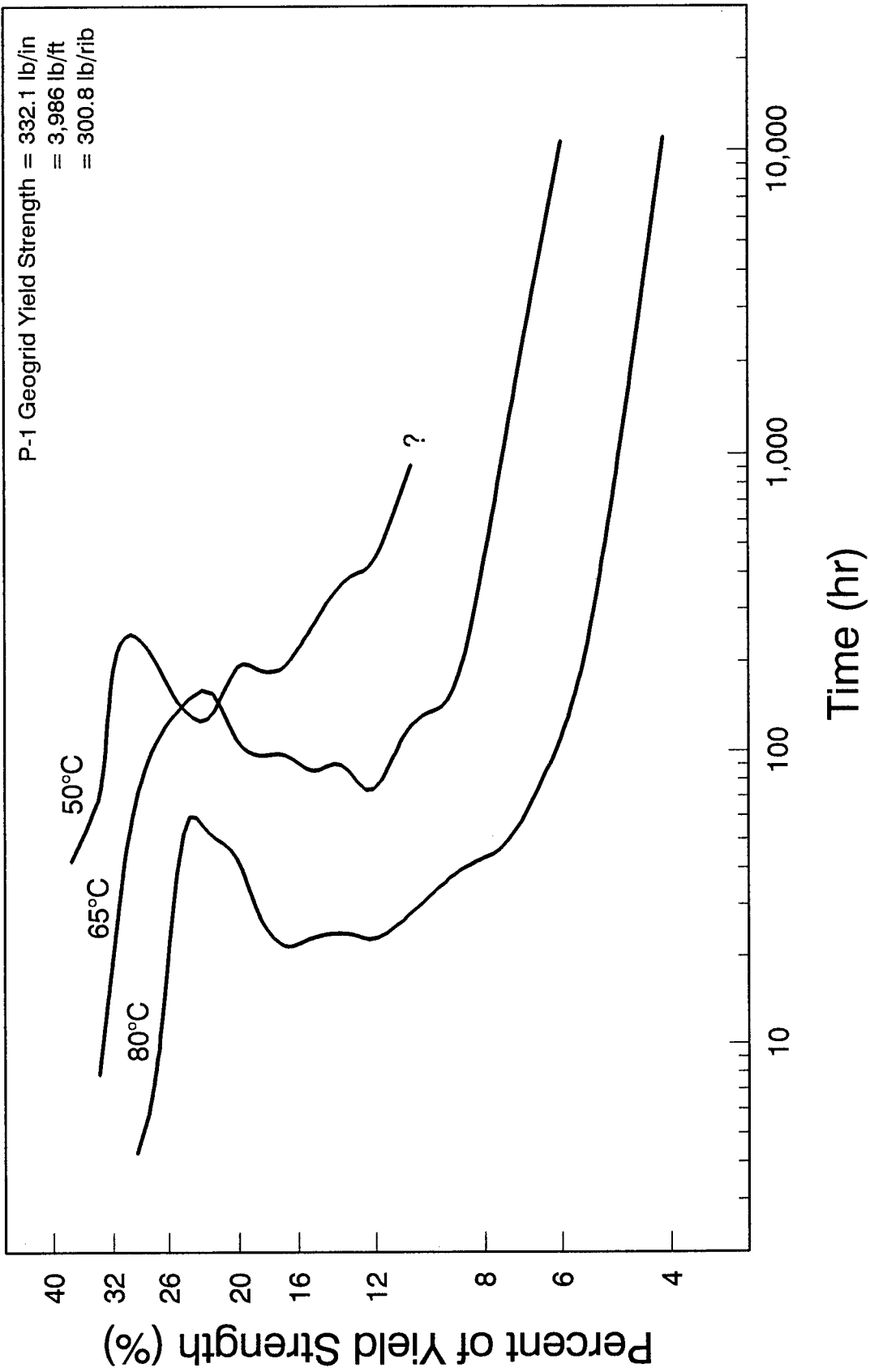
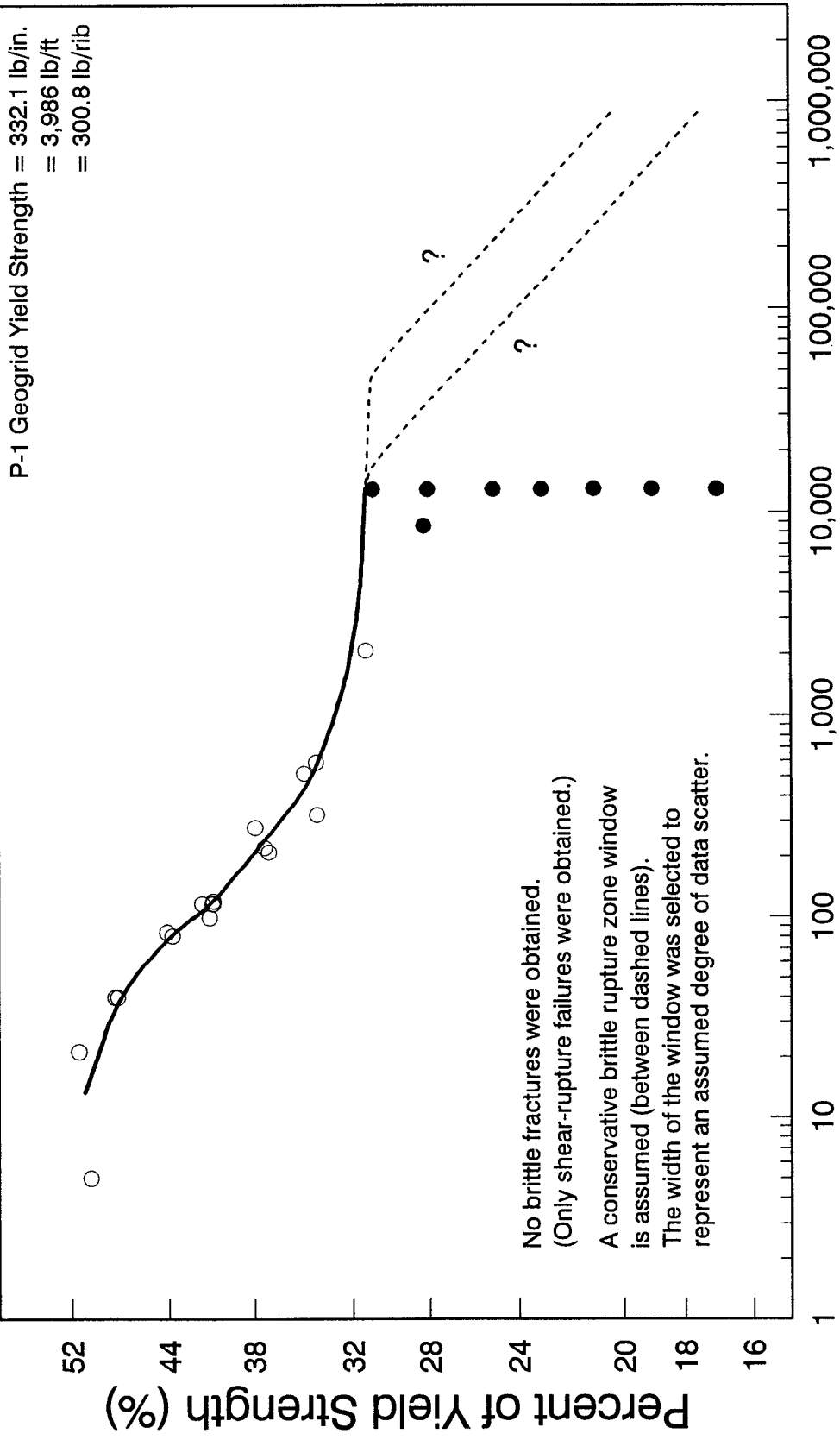


Figure 7.14. NCTL data for P-1 geogrid, tested at 50°C, 65°C, and 80°C in water.

L:G50UPERC



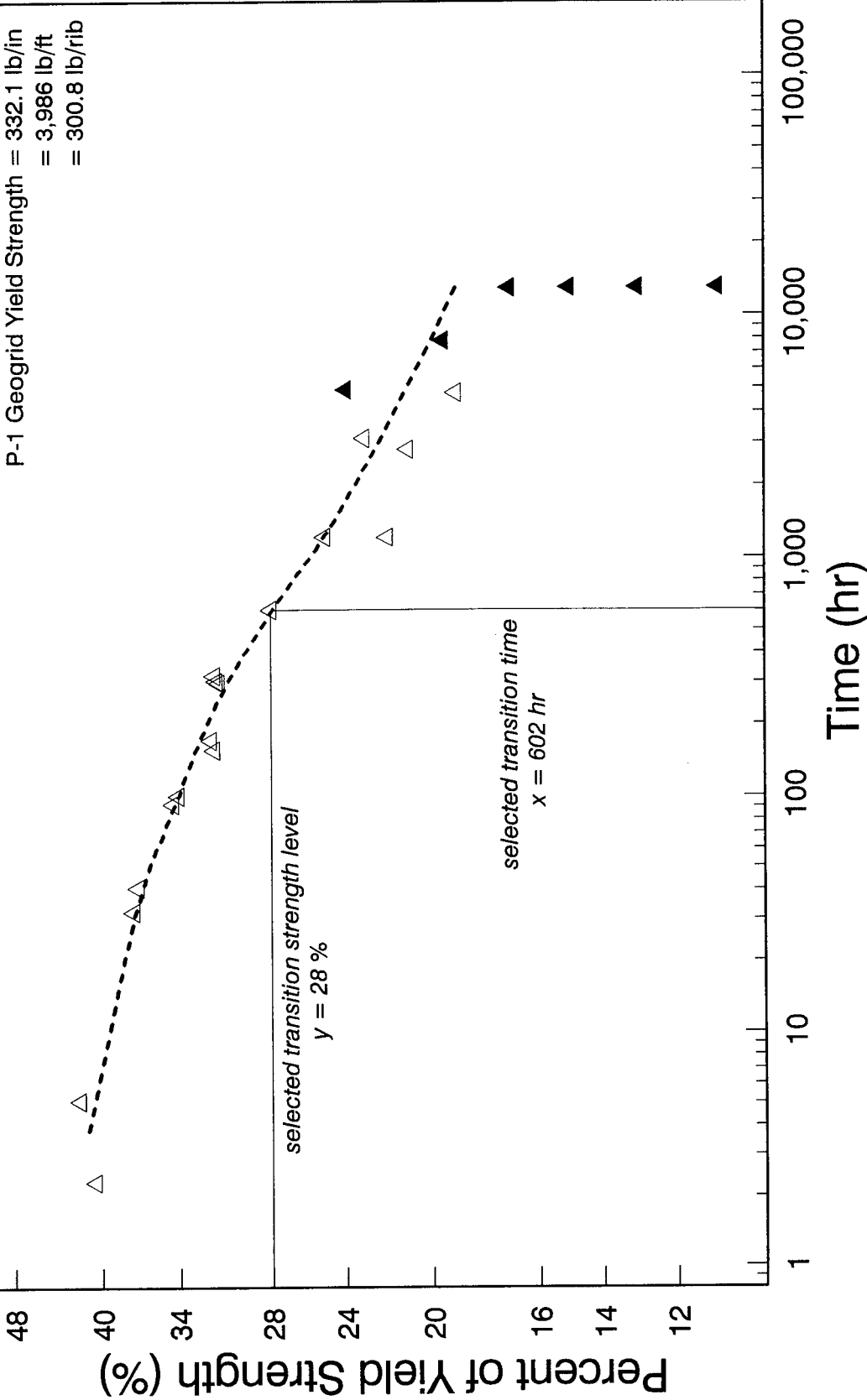
Time (hr)

Grid 50°C Grid 50°C
 stopped completed stopped completed

stopped - indicates no specimen rupture at test termination.
 completed - indicates specimen tested to rupture.

Figure 7.15. UCTL data for P-1 geogrid, tested at 50°C in water.

L:G65UPERC



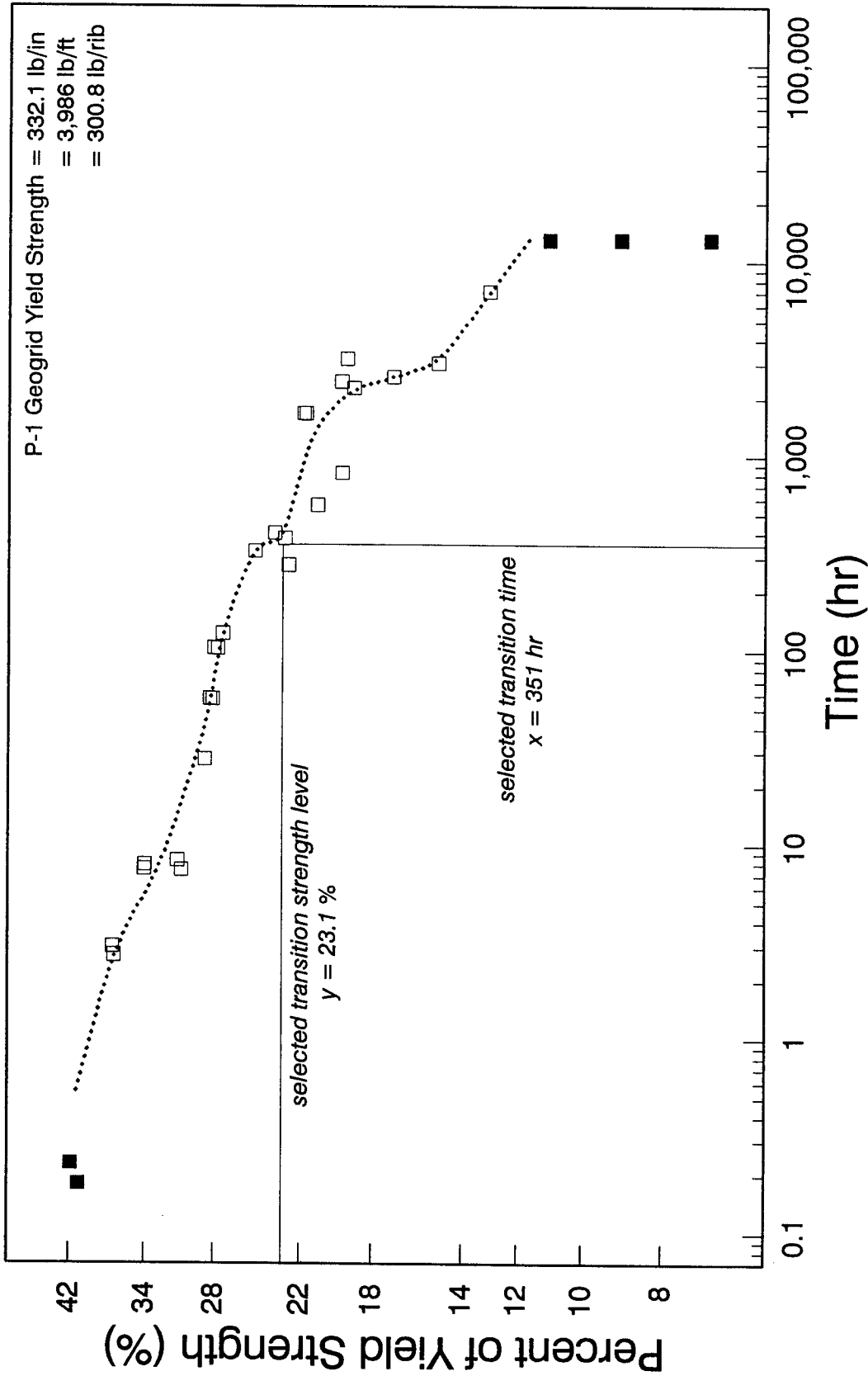
Grid 65°C Grid 65°C
 stopped completed
 stopped completed

Transition point selection was based on change in rupture mechanism, as shown by fracture face examinations.

Figure 7.16. UCTL data for P-1 geogrid, tested at 65°C in water.

L:G80UPERC

P-1 Geogrid Yield Strength = 332.1 lb/in
 = 3,986 lb/ft
 = 300.8 lb/rib

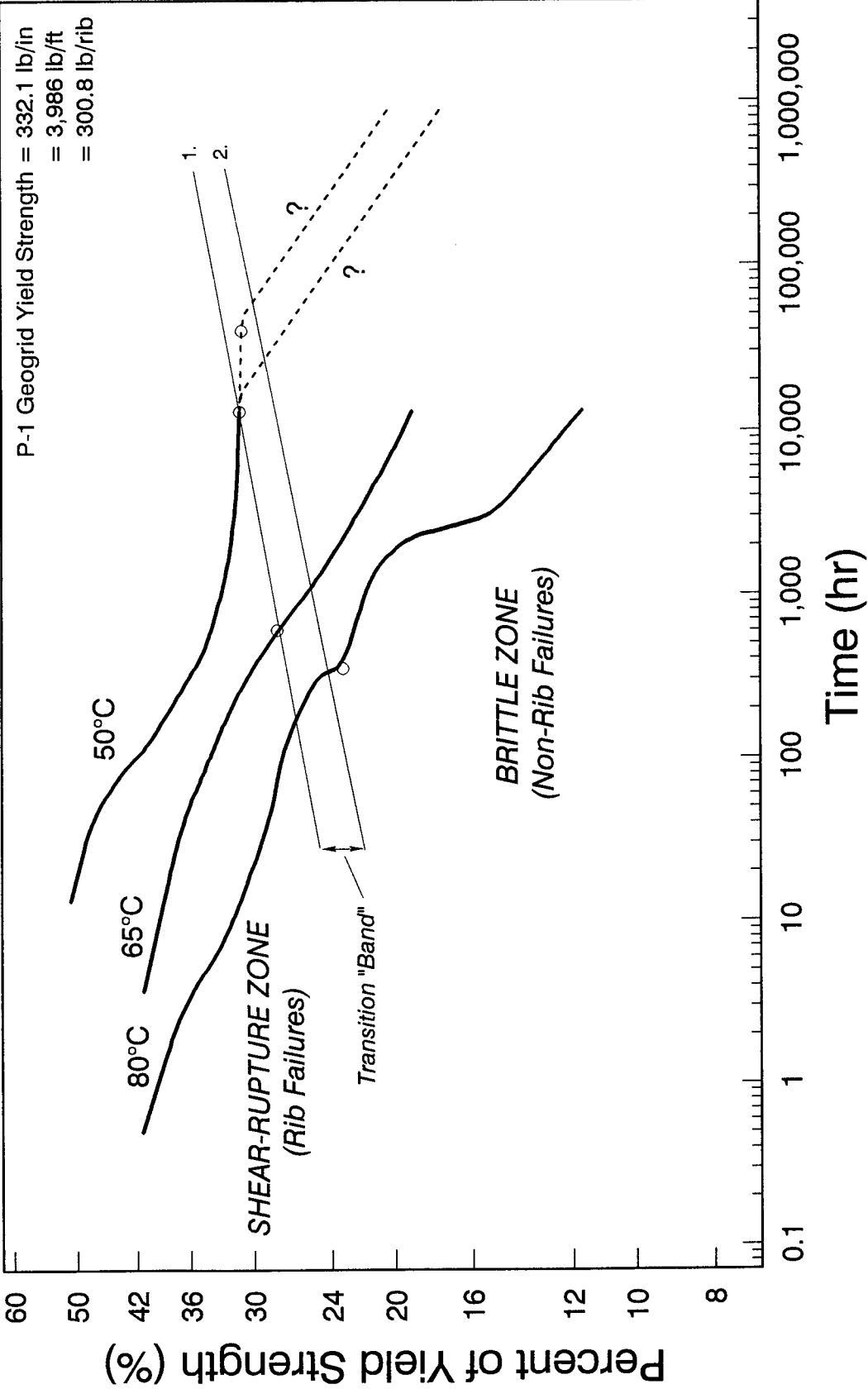


stopped - indicates no specimen rupture at test termination.
 completed - indicates specimen tested to rupture.
 Transition point selection was based on change in rupture mechanism, as shown by fracture face examinations.

Grid 80°C Grid 80°C
 stopped completed

Figure 7.17. UCTL data for P-1 geogrid, tested at 80°C in water.

L:GGGUPERC



No brittle fractures were obtained for the 50°C series.
 The thin lines 1. and 2. indicate a band in which the primary rupture mechanism changes.

Experimental Data Assumed 50°C Transition Points
 (50°C, 65°C and 80°C) Brittle Zone Window

Figure 7.18. UCTL data for P-1 geogrid, tested at 50°C, 65°C, and 80°C in water.

b. NCTL Test Results for P-1 Geogrid

NCTL Test Results for 50°C, 65°C, and 80°C

The NCTL test results for the P-1 geogrid node material produce strength rupture curves with exaggerated nose-type responses, as shown in figures 7.11, 7.12, and 7.13. The overall shapes of these curves are very similar, including the apparent extension of the transition zone further downward than most typical nose-type response curves for HDPE geomembranes. Selected transition time decreased from 187 to 66.4 to 22.5 hr as immersion temperature increased from 50°C to 65°C to 80°C, respectively. The overall, anticipated trend of decreasing time to rupture with increasing immersion temperature is evident in figure 7.14.

In spite of the overall similarities between the three curves shown in figure 7.14, the curve for 50°C is different from the other two. No explanation has been found for the difference. However, it should be noted that the testing machine used to generate the 50°C curve was the same from a technical standpoint, but had been built by a different machinist.

P-1 node material 65°C and 80°C NCTL brittle zone trends were calculated using linear regression analysis from log values of interpreted average data points, which are documented on the bottom of the summary tables in appendix C. These brittle zone trends, represented by slope (m) and y-intercept (b), are summarized below. The large degree of data scatter for 50°C NCTL brittle zone points prevented development of a clear trend.

65°C brittle zone trend:	$m = -0.0888$	$b = 1.138$
80°C brittle zone trend:	$m = -0.0729$	$b = 0.906$

A possible correlation of decreasing data scatter with increasing immersion temperature is evidenced by the decreasing standard deviations in times to rupture for 50°C to 65°C to 80°C reported in the tables in appendix C.

The general shapes of the 50°C, 65°C, and 80°C NCTL P-1 node material strength rupture curves (figure 7.14) are similar. Additionally, the extended nature of the transition zones is similar to that of resin M, a base resin used to produce this type of geogrid as shown in figure 7.2. These similarities lend credibility to the data and, thus, to the geogrid specimen selection process and testing procedures. The similar shapes of the curves also favors the application of prediction methods, such as the rate process method (RPM) and Popelar et al. shifting.

A linear trend between immersion temperature and transition time was obtained by plotting NCTL selected transition times for P-1 node material on a log-linear scale as a function of the inverse of the immersion temperature in deg. K, as presented in figure 7.19. A high correlation coefficient of $r = 0.99852$ was obtained. It is emphasized, however, that the change from transitional fracture to quasi-brittle fracture for each series was very gradual, rather than abrupt. The NCTL transition point selections are, therefore, subjective to an unquantified degree, and placing interpretive emphasis on these transition point selections is cautioned. It should be pointed out that the linear result may be due to the narrow range of temperatures studied.

The slopes of the 65°C and 80°C brittle zone trends are roughly equivalent (figure 7.14). No clear conclusion can be drawn regarding the slope of the 50°C brittle zone points because of insufficient data. Question marks have been drawn in figure 7.11 to indicate this uncertainty. However, it may be expected that the slope is similar to the slope of the 65°C and 80°C curves.

Because of an appreciable degree of data scatter obtained in the 50°C testing, future NCTL node material testing performed at lower temperatures should include more than three specimens at each strength level, especially for brittle zone determination.

The possibility of stress cracking propagation in the node material of uniaxially drawn HDPE geogrids was verified by the repeatable occurrence of quasi-brittle fracture in 50°C, 65°C, and 80°C NCTL P-1 geogrid specimens tested at the lower strength levels. Fracture planes were coincident to the remainder of the cross-section in the plane of the notch. The quasi-brittle fractures were observed in the much less oriented side portions of node material (i.e., the portions of the node material not aligned with ribs).

Adequate NCTL strength rupture data were obtained for P-1 node material to provide for quantitative comparison of 65°C and 80°C NCTL geogrid brittle zone trends with 65°C and 80°C UCTL brittle zone trends. However, 50°C NCTL data adequate for developing a clear brittle zone trend were not obtained. The NCTL data also were adequate to provide for qualitative comparison of the stress cracking resistances of resin M with P-1 node material. This comparison is presented below. The tables in appendices B and C contain the NCTL geogrid data necessary for both of these comparisons.

Previous discussion was presented showing that resin M and P-1 base resin are similar, at least in regard to density and degree of crystallinity. Because stress cracking resistance correlates strongly with density, the authors feel that reasonably valid comparisons can be made for resin M and P-1 geogrid CTL test results.

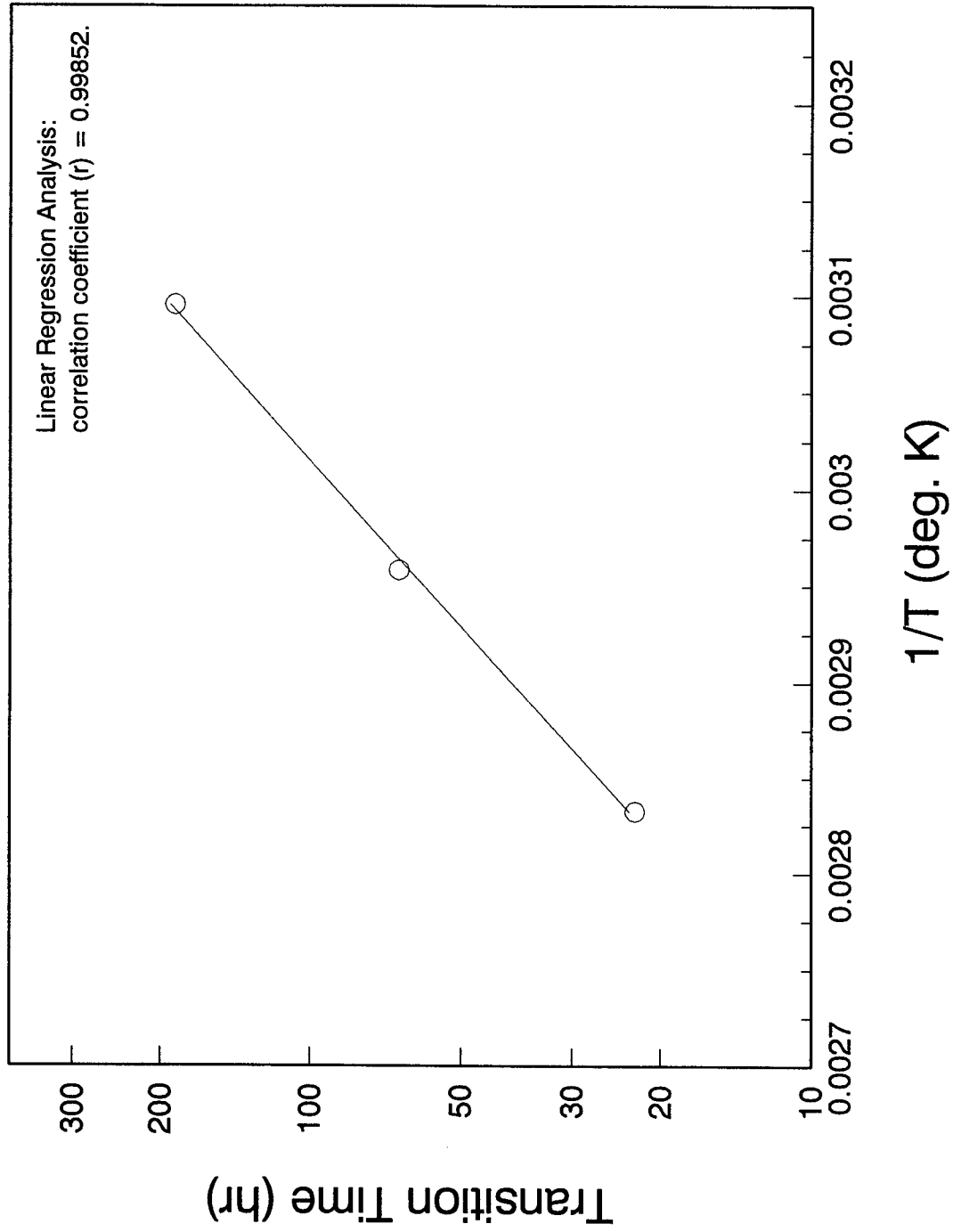


Figure 7.19. Trend in transition time for NCTL P-1 geogrid test series.

The NCTL strength rupture curves for both resin M and P-1 node material tested at 50°C are presented on the same graph in figure 7.20, which was obtained by combining figures 7.2 and 7.11. A comparison of these strength rupture curves indicates that, at strength levels greater than approximately 11 percent, P-1 node material has a higher stress cracking resistance than resin M. At strength levels less than approximately 11 percent, however, P-1 node material seems to have less stress cracking resistance than resin M. However, this conclusion should be considered with caution due to the fact that there are too few experimental data points below the 11-percent strength level to draw a firm conclusion.

c. UCTL Test Results for P-1 Geogrid

UCTL Test Results for 50°C, 65°C, and 80°C

The UCTL test results for the P-1 geogrid product produce dissimilar-looking strength rupture curves with transition points that are not apparent from curve shape, as shown in figures 7.15, 7.16, and 7.17. Transition point selection was based solely on fracture face examinations. The selected, and assumed, transition points for the UCTL geogrid series are included in table 6 and are summarized as follows:

50°C series, assumed window:	between (~ 13,000 hr , 31.2%) and (~ 40,000 hr, 31.0%);
65°C series, selected point:	(602 hr, 28.0%); and
80°C series, selected point:	(351 hr, 23.1%).

At strength levels greater than transition point strength levels, almost all specimens in every UCTL series failed in rib material by an apparently identical shear rupture mechanism; all of these shear ruptures were located in rib material at a similar distance from a node and were accompanied by twisting in the rib material. The zone above the UCTL selected transition points is herein referred to as a shear rupture zone rather than a ductile zone (figure 7.18).

A gradual transition from predominantly shear rupture failures to predominantly brittle failures was not evident in curve shape or in the examined fracture faces. Rather, the selected transition point strength levels identify the location on a strength rupture curve of a band over which primary failure mechanism changed abruptly (figure 7.18).

For the 65°C and 80°C series, stress cracking initiation and subsequent propagation (quasi-brittle fracture) occurred at low strength levels in non-repeatable fracture patterns in side node material. Side node material corresponds with the portions of the node crossbar which are not aligned with ribs. This is an important observation because it verifies that quasi-brittle fracture can occur in unnotched and undamaged P-1 geogrid material.

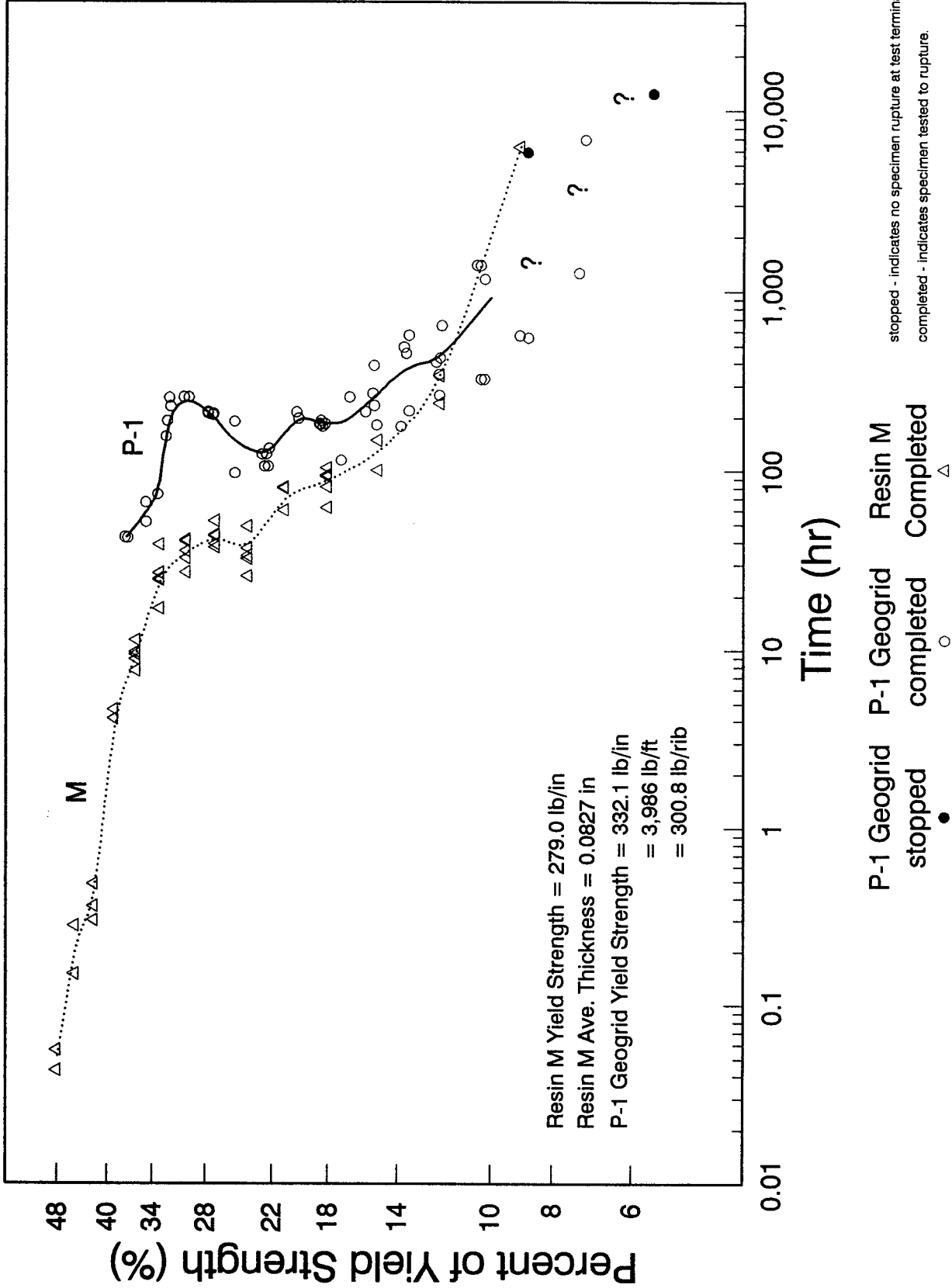


Figure 7.20. NCTL data for resin M and P-1 Geogrid, tested at 50°C in water.

For the 50°C UCTL series, no brittle fractures occurred in the portion of geogrid specimen between grips (gauge lengths) within the time frame of the testing program. The gauge lengths of the geogrid specimens are defined as the entire portion of a specimen between grips. Brittle fractures did occur in the gripped node material of specimens from all three series (i.e., 50°C, 65°C, and 80°C). However, due to the design of the geogrid grips, none of these occasional brittle fractures in gripped material led to specimen rupture in the gauge length, and, therefore, these brittle fractures in gripped node material did not impact the validity of the test results.

Since one of the objectives of this research program was to make predictions to 20°C using UCTL geogrid brittle zone data, and because 50°C is closer to 20°C than 65°C or 80°C are, it was considered desirable to include 50°C brittle data in the prediction methods. To this end, a conservative assumption was made about the 50°C brittle behavior based on the (non-brittle) stress rupture data that was obtained for the 50°C series. This 50°C brittle zone window has been plotted as a dashed line with question marks in figures 7.15 and 7.18 and in figures in chapter 8.

As indicated, unruptured points are represented by solid markers, such as a solid circle, and most brittle zone trends were drawn so that they end slightly above the highest solid marker plotted. For the 50°C UCTL geogrid results, however, no brittle fractures were obtained, and the type of failure that would eventually occur in the specimen associated with the highest solid circle (if testing had been allowed to continue indefinitely) was unknown. In order to provide for conservative predictions, it was assumed that *the highest solid circle represented a specimen that was going to fail very soon in a brittle manner*. In the context of this report, conservative means defining a strength level(s) which is(are) lower than the value(s) that could be rationally expected, with the intent of providing for a safe design. The assumption that *the highest solid circle represented a specimen that was going to fail very soon in a brittle manner* is conservative because it is a worst case assumption in regard to stress cracking (brittle) occurrence in the geogrid. The 50°C UCTL curve was therefore drawn touching the top of the highest solid circle and was then immediately angled downward on the right side of the solid circle marker. The curve was also changed to a dashed line to identify it as being based on an assumption.

Because the slope of the assumed 50°C UCTL brittle trend was unknown, a second assumption was required: it was assumed that *a 50°C brittle slope would be similar to the 65°C and 80°C brittle slopes*. Therefore, the assumed 50°C brittle slope was obtained by averaging the 65°C and 80°C UCTL brittle zone slopes. Assuming a 50°C brittle slope in this manner can be justified: brittle zone UCTL slopes for 65°C and 80°C are approximately two times steeper than their corresponding ductile slopes; and the assumed 50°C brittle slope, obtained by averaging, also results in a brittle slope that is approximately

two times steeper than its corresponding, experimentally determined 50°C ductile slope. A second dashed line, with the same slope, was drawn further to the right to create an assumed brittle zone window reflecting a third assumption: it was assumed that *a degree of data scatter would occur in 50°C UCTL brittle points similar to the data scatter observed for 65°C and 80°C brittle points.*

The 65°C and 80°C UCTL brittle zone trends were calculated using linear regression analysis from log values of interpreted average data points that are documented on the bottom of the summary tables in appendix C. The 50°C assumed (dashed lines) brittle zone slope was calculated, as described above, by averaging the 65°C and 80°C brittle zone slopes. These brittle zone trends, represented by slope (*m*) and y-intercept (*b*), are summarized as follows:

assumed 50°C brittle trend:	$m = -0.1445$	$b = 2.103$ to 2.168
65°C brittle trend:	$m = -0.1162$	$b = 1.755$
80°C brittle trend:	$m = -0.1728$	$b = 1.779$

For each UCTL series, data scatter for shear rupture zone failures was smaller than data scatter for brittle zone failures, as apparent by a visual comparison of figures 7.15, 7.16, and 7.17. Smaller data scatter occurred for shear rupture failures because these failures occurred in a very repeatable manner. The UCTL data do not support a possible correlation with regard to decreasing data scatter with increasing immersion temperature, as was made for the NCTL geogrid data.

General Discussion

The following combinations of failure mechanisms were the primary combinations obtained in the UCTL series: (1) very repeatable shear rupture in rib material at an apparent point of maximum torsion; and (2) non-repeatable combinations of quasi-brittle fracture in node material and shear rupture occurring in the center node and/or the material in the area between the rib and the node and/or rib material.

Failure to obtain 50°C UCTL brittle ruptures in this testing program was a result of stopping all testing at approximately 13,000 hr (~1.5 yr). Future 50°C UCTL geogrid testing programs should provide for testing times significantly longer than 1.5 yr.

A visual comparison of the UCTL brittle zone interpretations, as plotted on the same graph in figure 7.18, indicates that the effect of the 15° change in temperature from 50°C to 65°C is not the same as the effect of a 15° change in temperature from 65°C to 80°C. This observation reinforces the importance of including reliable 50°C brittle data points in predictions made by extrapolation to 20°C using the RPM and Popelar et al. shifting.

The possibility of stress cracking initiation and propagation in unnotched and undamaged uniaxially drawn HDPE geogrids was verified by the occurrence of quasi-brittle fractures of P-1 geogrid specimens tested at 65°C and 80°C in UCTL tests performed at the low strength levels. Quasi-brittle fractures occurred in non-repeatable locations and directions in P-1 node material. A small number of the quasi-brittle fractures observed in UCTL specimen node material were similar to the quasi-brittle fractures observed in NCTL specimen node material. This observation further verifies the capacity of unnotched and undamaged P-1 node material for stress cracking initiation and propagation.

No quasi-brittle modes of failure were evidenced, however, in fractures occurring in, or progressing through, P-1 rib material or in the material in the area between the rib and the node. Rather, in UCTL specimens tested at strength levels below the transition strength level, failures that progressed through rib material or through the material in the area between the rib and the node were controlled by shear rupture occurring between oriented fibers parallel to the applied load.

The UCTL geogrid performance testing did not provide sufficient data for comparing 50°C UCTL geogrid performance with 50°C (UCTL) resin M performance, because no transitional or quasi-brittle failures were obtained for the 50°C UCTL geogrid test series. The purpose of this comparison was to quantify potential benefits to the base resin's stress cracking resistance as a result of the geogrid manufacturing process. The 50°C UCTL geogrid data did, however, provide data adequate for comparison of non-brittle rupture times between resin M and the P-1 geogrid product. Unfortunately, the 50°C resin M data failed to facilitate a reliable comparison because of an unquantified degree of prematurity from sidewall grooving as discussed previously. Nevertheless, if the unquantified effect of the grooves on resin M data is ignored, then the base resin can clearly be seen to benefit from strengthening on the basis of much longer rupture times for the UCTL geogrid.

The research program's ultimate purpose was to conservatively predict a strength value that engineers can use as a design parameter to preclude stress cracking failures in the considered uniaxially drawn HDPE geogrid product, exposed to an ambient temperature of 20°C for 100 yr. Ideally, for this program, predictions for 20°C should be made on the basis of experimental data for 50°C, 65°C, and 80°C. However, experimental brittle zone data were obtained only for 65°C and 80°C. Since no 50°C UCTL brittle failures were obtained, it was necessary to make a conservative interpretation of the 50°C UCTL brittle zone, as discussed. In the sense that a conservative 50°C UCTL brittle zone interpretation was possible, it is possible to state that the UCTL geogrid performance testing did provide sufficient data to enable conservative predictions to 20°C.

The NCTL geogrid testing results were compared with UCTL geogrid results, with the objective of potentially qualifying the NCTL geogrid test as an acceptable short procedure for yielding long-term, quantitative, design-oriented results. This comparison is presented below. The tables in appendix C contain the data necessary for this comparison.

Comparison of UCTL Geogrid Test Results with NCTL Geogrid Test Results

P-1 geogrid 65°C and 80°C NCTL and UCTL brittle zone trends were calculated using linear regression analysis from log values of interpreted average data points, which are documented on the bottom of the summary tables in appendix C. Comparisons of these trends are presented in figures 7.21 and 7.22. These brittle zone trends, represented by slope (m) and y-intercept (b), are summarized as follows:

65°C NCTL brittle zone trend:	$m = -0.0888$	$b = 1.14$
65°C UCTL brittle zone trend:	$m = -0.1162$	$b = 1.75$
Percent Change:	- 31 %	+ 54 %
80°C NCTL brittle zone trend:	$m = -0.0729$	$b = 0.906$
80°C UCTL brittle zone trend:	$m = -0.1728$	$b = 1.78$
Percent Change:	- 137 %	+ 96 %

The different percentage changes obtained in this comparison indicate that there are insufficient data to reliably quantify a generic relationship between the NCTL and UCTL geogrid results that can be applied to all uniaxially drawn HDPE geogrids. Future NCTL and UCTL testing of a significantly larger number of different geogrid samples is required. The potential objective to qualify the NCTL geogrid testing at elevated temperatures as an acceptable short-term procedure for yielding quantitative, design-oriented results was, therefore, not achieved.

7.4 GEOGRID FAILURE MECHANISMS

Fracture faces of ruptured NCTL and UCTL geogrid specimens were examined to determine primary failure mechanisms and failure mechanism characteristics in geogrid material. The following two sections present descriptions and representative photographs of these characteristics.

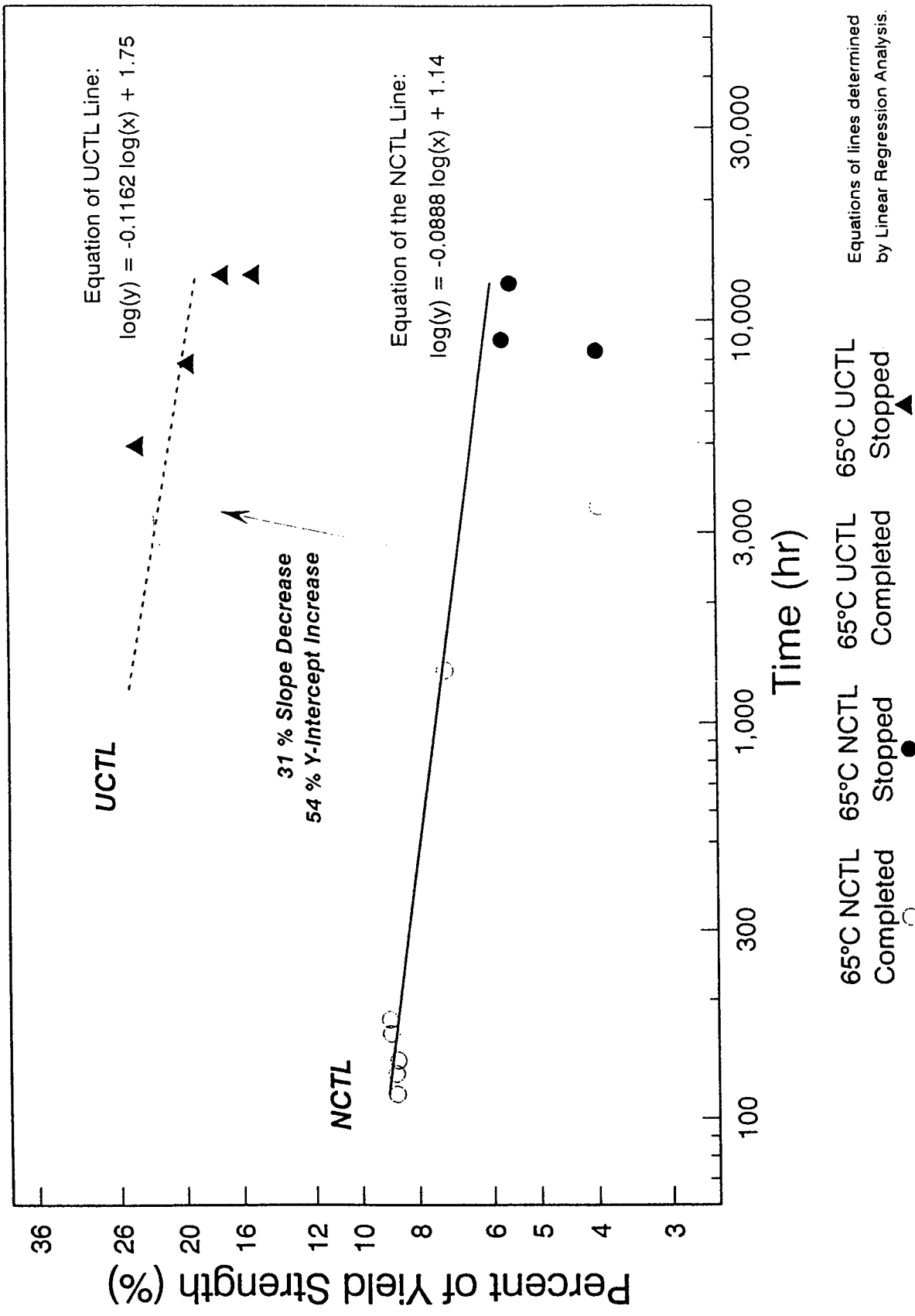


Figure 7.21. Relationship between 65°C NCTL and 65°C UCTL brittle zone P-1 geogrid data.

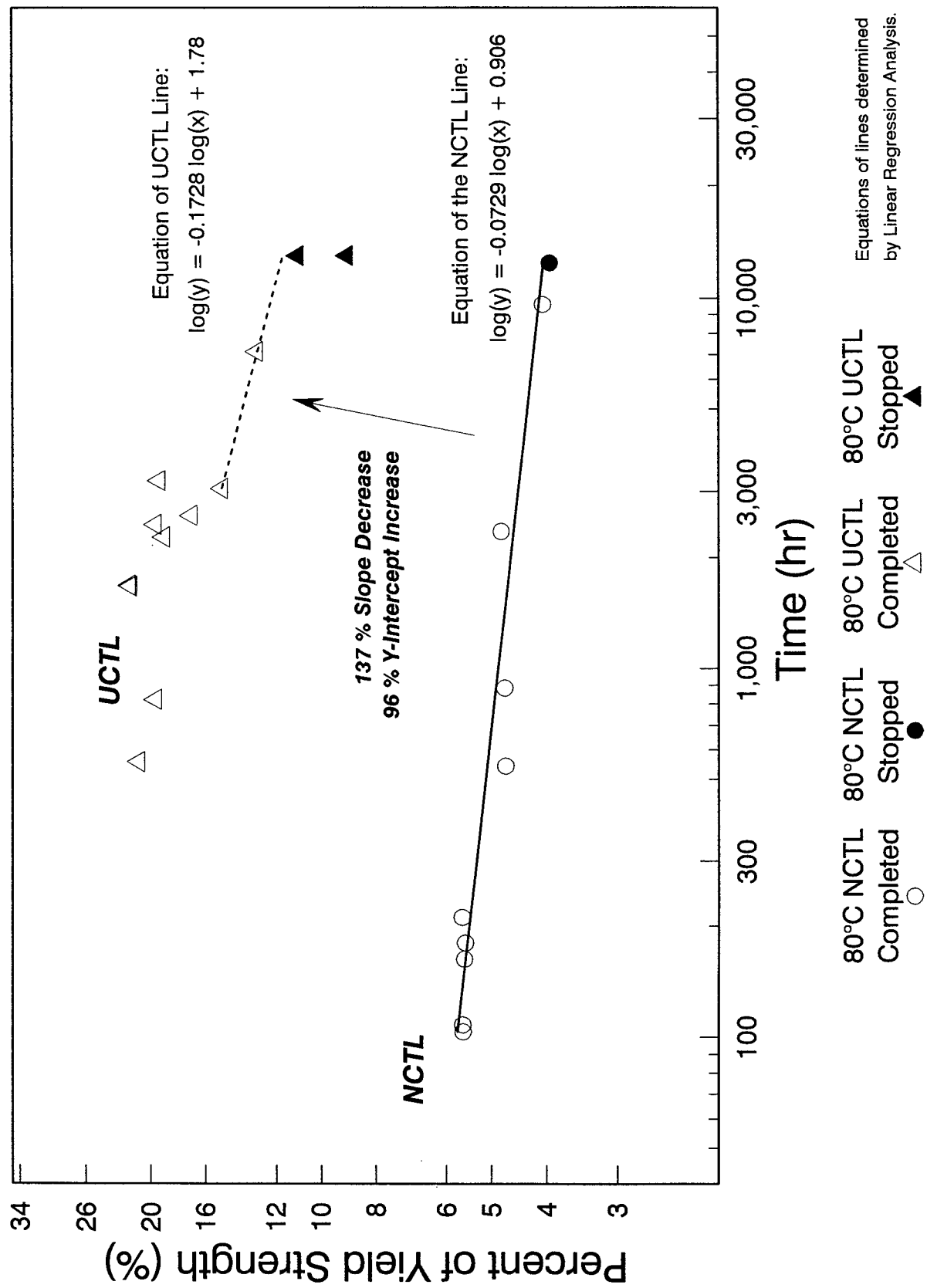


Figure 7.22. Relationship between 80°C NCTL and 80°C UCTL brittle zone P-1 geogrid data.

a. NCTL Failure Mechanisms in Node Material

The following primary failure mechanisms were observed in the notched node material of ruptured NCTL P-1 geogrid specimens: (1) ductile fracture; (2) transitional fracture; (3) quasi-brittle fracture; and (4) a combination of shear rupture and plastic deformation. These failure mechanisms occurred in very repeatable manners in the notched node material.

Ductile Fracture

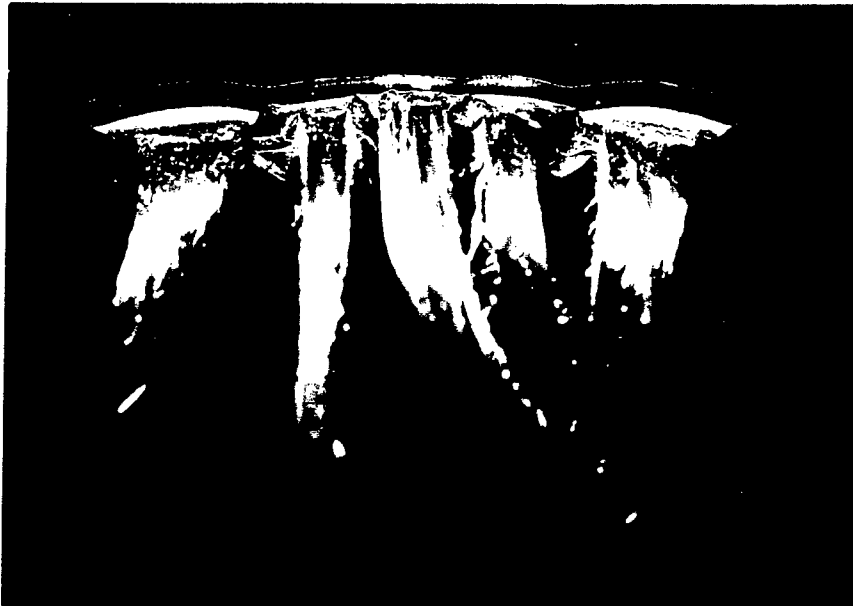
The photographs presented in figures 7.23A, B, & C show representative ductile fractures in notched node material. The ductile fractures were identified by obvious extensive plastic deformation, herein referred to as long drawn material. The long drawn material of the ductile fractures was characterized by fibrous edges and/or splintering effects resulting from molecular orientation in the node material. The splintering effects evidence a secondary shear rupture failure mechanism. Ductile fracture characteristics were consistent for the 50°C, 65°C, and 80°C series.

The long drawn material occurring in notched (geogrid) node material was different than the long drawn material occurring in notched resin M material and different than the long drawn material that occurs in typical notched geomembrane material. The long drawn material in the geogrid node material appeared to have undergone a relatively greater amount of plastic deformation prior to rupture (i.e., relative to non-oriented HDPE materials). The long drawn material in the geogrid node material was also much stiffer (more rigid) than the typically floppy long drawn material occurring in non-oriented HDPE resins.

Transitional Fracture

Each of the NCTL geogrid test series demonstrated a broad strength window over which the primary failure mechanism gradually changed (with decreasing strength level) from ductile fracture to quasi-brittle fracture. Ruptured specimens that were tested in this window evidenced roughly equal degrees of both ductile and quasi-brittle failure mechanisms; this terminal condition is termed transitional fracture. The photographs presented in figures 7.24A, B, & C show representative transitional fractures in notched node material. Transitional fracture characteristics were consistent for the 50°C, 65°C, and 80°C series.

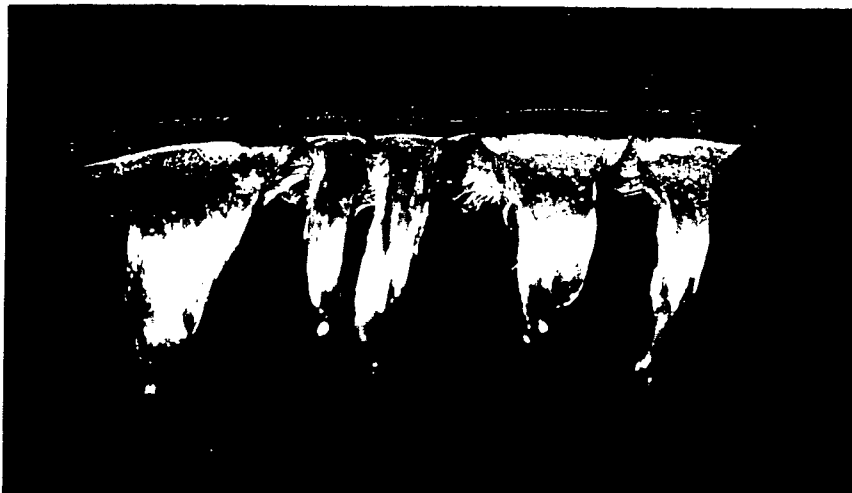
The transitional fractures were identified by a combination of long drawn material and quasi-brittle fracture surfaces. The long drawn material was significantly more pronounced in the center portion of each fracture face. (This center node material corresponds to the portion of the node crossbar that is collinear with the adjoining ribs.) The long drawn material was characterized by fibrous edges and/or splintering effects. The quasi-brittle fracture



50°C, 31.76%
Ductile
(577, × 5.6)
Figure 7.23A

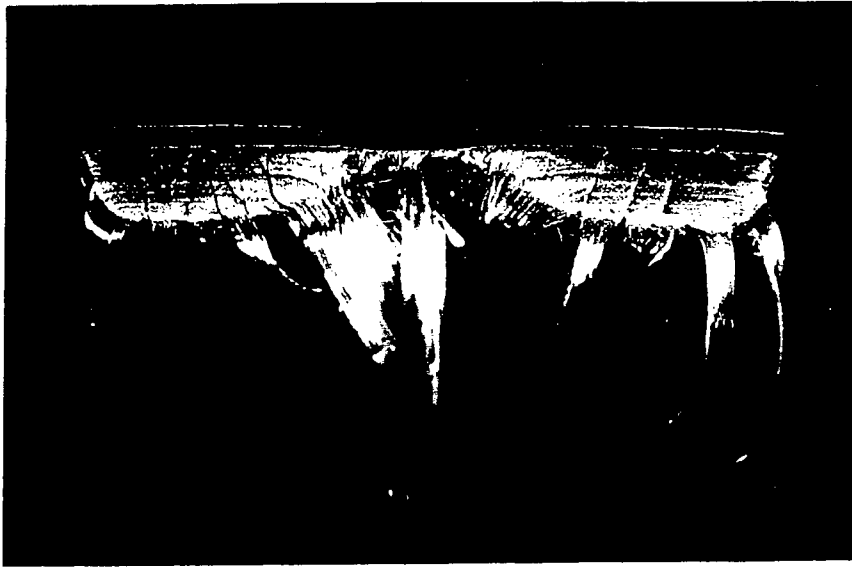


65°C, 29.54%
Ductile
(730, × 5.6)
Figure 7.23B

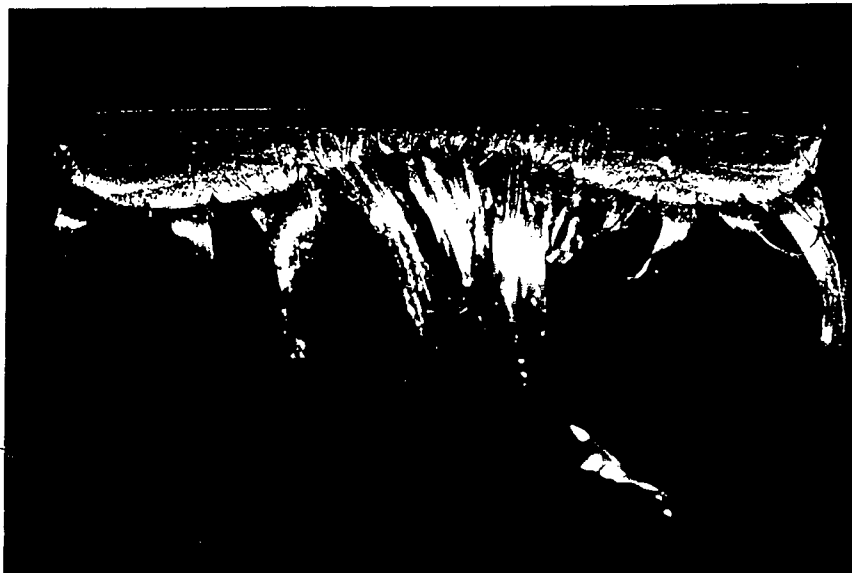


80°C, 24.68%
Ductile
(877, × 5.6)
Figure 7.23C

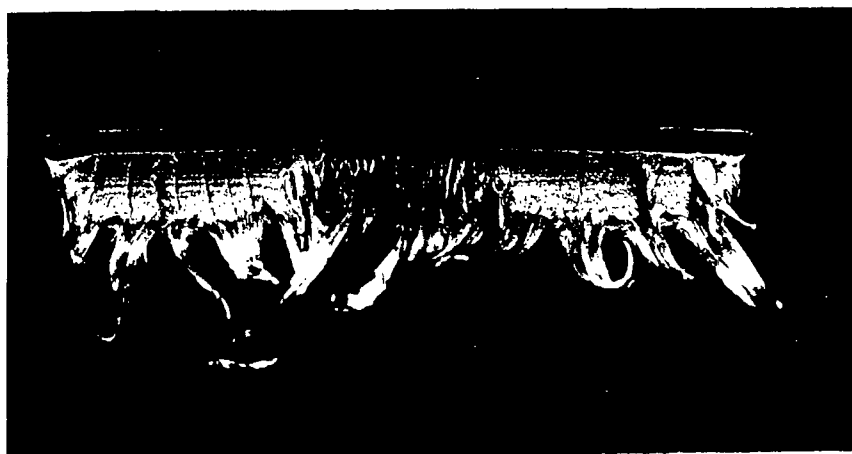
Figures 7.23A, B & C. Ductile ruptures in NCTL P-1 geogrid specimens. Note long drawn material with fibrous edges.



50°C, 19.96%
Transitional
(565, × 5.6)
Figure 7.24A



65°C, 18.68%
Transitional
(715, × 5.6)
Figure 7.24B



80°C, 16.59%
Transitional
(858, × 5.6)
Figure 7.24C

Figures 7.24A, B & C. Transitional ruptures in NCTL P-1 geogrid specimens. Note long drawn material in node center, with adjacent quasi-brittle fracture surfaces.

surfaces occurred on the side portions of each fracture face. (The side node material corresponds to the portions of the node crossbar that are not aligned with ribs, i.e., that are not collinear with the adjoining ribs.) The fracture planes were coincident to the remainder of the cross-section in the plane of the notch. These quasi-brittle surfaces appeared coarsely velvety in a manner similar to transitional fracture in non-oriented HDPE resin. The quasi-brittle surfaces also were characterized by parallel, narrow ductile veins extending downward across the side node material.

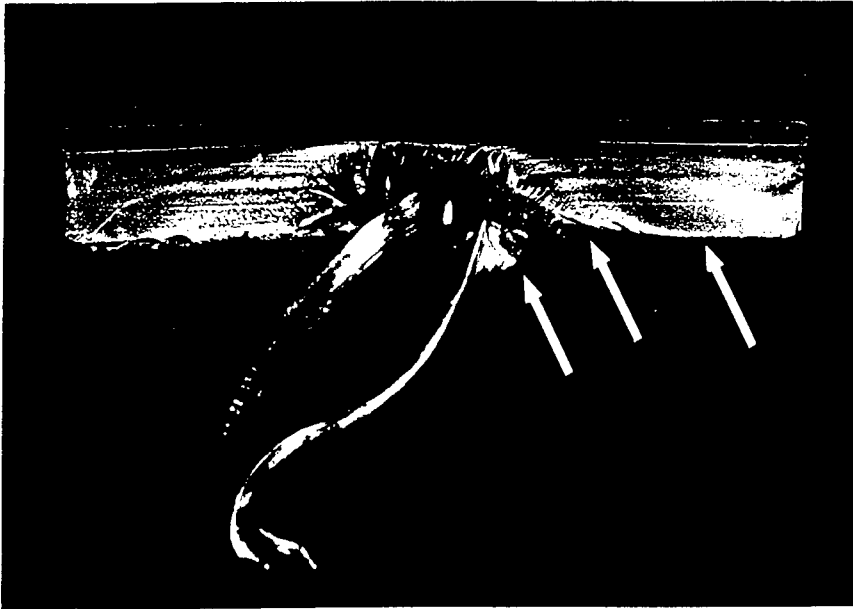
Quasi-brittle Fracture

The photographs presented in figures 7.25A, B, & C show representative quasi-brittle fractures in notched node material. The quasi-brittle fractures were identified by relatively smooth fracture faces and by a lack of obvious bulk plastic deformation. These quasi-brittle fractures exhibited characteristics generally consistent with quasi-brittle fracture characteristics observed for HDPE geomembrane and pipe materials, including a smoothly velvety appearance produced by a carpet of microscopic plastic deformation points. The quasi-brittle fracture surfaces occurred on the side portions of each fracture face, and were coincident to the remainder of the cross-section in the plane of the notch. Quasi-brittle fracture characteristics were consistent for the 50°C, 65°C, and 80°C series.

Quasi-brittle fracture was not observed, however, in the more oriented center node material. Rather, center node material evidenced primary failure by a combination of shear rupture and plastic deformation. The narrow zone occurring between the oriented center node material and the much less oriented side node material is herein referred to as the arresting zone. Effects of the arresting zone were previously observed in the geogrid specimen selection process, as presented in chapter 5. This zone is identified as a zone of rapidly changing molecular orientation. It is hypothesized that the arresting zone would present a potential advantage to the stress cracking resistance of a multiple rib, long node, bar segment by arresting stress cracking that is propagating from much less oriented side node material toward oriented center node material.

b. UCTL Failure Mechanisms in Geogrid

The following primary failure mechanisms were observed in ruptured UCTL P-1 geogrid specimens: (1) very repeatable shear rupture in rib material at an apparent point of maximum torsion; and (2) non-repeatable combinations of quasi-brittle fracture occurring in node material, and shear rupture (tearing) occurring in center node and/or the material in the area between the rib and the node and/or rib material.



50°C, 10.36%
Brittle
(540, × 5.6)
Figure 7.25A



65°C, 10.32%
Brittle
(705, × 5.6)
Figure 7.25B



80°C, 8.76%
Brittle
(843, × 5.6)
Figure 7.25C

Figures 7.25A, B & C. Brittle ruptures in NCTL P-1 geogrid specimens. Note long drawn material in node center and smooth brittle fractures on sides (arrowed), with a rougher zone between (arrowed).

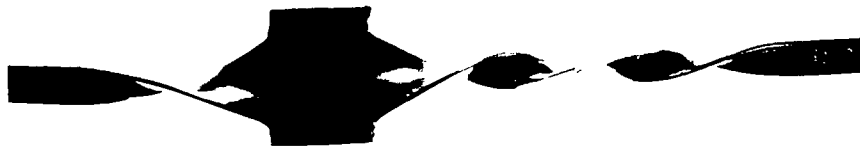
Shear Rupture

The photographs presented in figures 7.26A, B, & C show representative ruptures of unnotched and undamaged rib material tested at 50°C. These ruptures look like tears in the rib material with torn edges oriented at approximately 45° angles to the applied load. These ruptures are characterized by coarsely fibrous edges and by splinter-like fractures oriented parallel to the applied load (figure 7.27). These observations evidence shear fracturing processes. Additionally, all of the 50°C (UCTL) ruptures were accompanied by residual twisting in the rib material and occurred at a repeatable distance from a nearby node bar at an apparent point of maximum torsion. These observations evidence residual torsional stresses. (Note: the anchored ends of the specimens were not free to rotate; twisting occurred between grips.) These fracture characteristics, or evidence of shear processes and residual twisting in rib material, were consistent for specimens in the 65°C and 80°C series above a selected transition strength level, as well as for all 50°C specimens, as shown in figures 7.28A, B, & C.

The UCTL rib ruptures are labeled shear rupture failures because they possess splinter-like fractures parallel to the applied load. Evidence of other failure-contributing processes, however, indicates that the UCTL rib failure history was more complicated than a history explained only by shear processes. It is hypothesized that a combination of a relaxation-gradient phenomenon, fracturing in shear, and plastic deformation may have interacted to produce the observed UCTL rib ruptures.

The twisting phenomenon observed in rib (and in the material in the area between the rib and the node) in the higher strength level UCTL tests indicates that there are torsional stresses that are mobilized in the geogrid specimen during the CTL test. It is hypothesized that, when the uniaxially drawn rib material is heated in the immersion bath and begins to strain, internal residual stresses relax, but they relax at different rates across the width of the rib. For example, residual stresses at the outer edges of the rib may relax at a different rate than those in the center area of the rib.

These hypothesized different degrees of relaxation in rib material can be visualized as a relaxation gradient occurring across the rib material cross-section. A pronounced relaxation gradient in the rib material might induce torsional stresses to the rib. This would explain the repeatable nature of the observed rib twisting, but may not explain the repeatable locations of the rib ruptures. However, and perhaps more importantly, relatively abrupt changes in such a hypothesized relaxation gradient (across the width of a rib) would create potential shear rupture planes parallel to the applied load and normal to the induced torsional stresses. In other words, two portions of continuous rib material, which can be thought of as abutting each other on different sides of a potential shear rupture plane, would be relaxing at different



50°C, 34.05%
Shear
(525, × 0.8)
Figure 7.26A



50°C, 40.79%
Shear
(520, × 0.8)
Figure 7.26B



50°C, 51.33%
Shear
(605, × 0.8)
Figure 7.26C

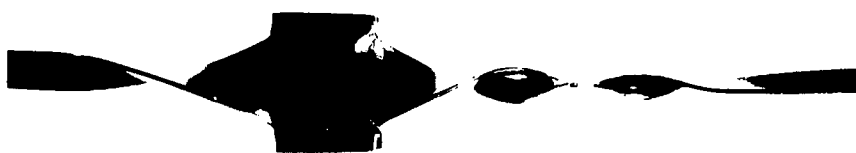
Figures 7.26A B, & C. Shear ruptures in 50°C UCTL P-1 geogrid specimens. Note twisting in the rib; also note consistent rupture location.



Figure 7.27. Close up of shear rupture in UCTL P-1 geogrid specimen. Note triangle shape of ruptured rib.



80°C, 30.66%
Shear
(823, × 0.8)
Figure 7.28A



65°C, 31.37%
Shear
(683, × 0.8)
Figure 7.28B



50°C, 34.05%
Shear
(525, × 0.8)
Figure 7.28C

Figures 7.28A, B & C. Shear ruptures in UCTL P-1 geogrid specimens. Note twisting phenomenon and rupture locations consistent for shear failures at all three test temperatures.

rates, creating a shear stress in the plane between them parallel to the applied load. This hypothesis is based on the observations of both residual rib twisting and splinter-like fractures parallel to the applied load at fracture faces.

The observation that associated pairs of fracture faces are shaped like triangles pointing toward each other indicates that failure initiated at, or near, the outer edges of the rib and gradually progressed toward the center. As fracturing in shear progressed from both edges toward the center, the remaining cross-sectional area of the rib experienced a gradually increasing stress condition. This increasing stress condition resulted in gradually increasing, localized plastic deformation in the remaining center rib material, creating a growing triangle shape. Final separation occurred in center rib material at the protruding most points of the now fully developed triangle-shaped fracture faces.

In summary, it is hypothesized that shear rupture failures were initiated near the outer two edges of rib material because of relatively abrupt changes in a residual stress relaxation gradient. This relaxation gradient was activated when testing began and the UCTL specimens were exposed to relatively high constant tensile loads and to temperatures appreciably higher than room temperature. Fracturing in shear leading to shear rupture is, therefore, considered the primary failure mechanism. Accompanying localized plastic deformation increased as the shear ruptures progressed inward, resulting in triangle-shaped fracture faces.

Transitional Fracture

Repeatable transitional fractures could not be identified. Comparison of fractures with stress rupture data indicates that there is a relatively narrow strength level band, identified as a transition band, at which the repeatable shear ruptures in rib material cease and quasi-brittle failures become more probable (as strength level decreases). Definition of a predominant transitional failure mechanism for UCTL testing (if possible) would require a significantly larger number of specimens.

Quasi-brittle Fracture, Tearing, and Rib Splitting

The 65°C and 80°C UCTL test series produced quasi-brittle fractures in unnotched and undamaged node material at low strength levels. These quasi-brittle fractures occurred in non-repeatable locations and with non-repeatable propagation directions. The photographs presented in figures 7.29A & B show two examples of these quasi-brittle fractures. The quasi-brittle fractures were identified by relatively smooth fracture faces and by a lack of associated bulk plastic deformation. These fractures exhibited characteristics generally consistent with quasi-brittle fracture characteristics observed for HDPE geomembrane and

pipe materials, including a smoothly velvety appearance produced by a carpet of microscopic plastic deformation points. The quasi-brittle fracture surfaces occurred in side node material and did not propagate through the arresting zone into center node material. Rather, brittle crack propagations appear to turn at a right angle upon contact with the arresting zone and to follow the arresting zone toward the material in the area between the rib and the node and toward rib material (figures 7.29A & B).

The photographs presented in figures 7.30A & B show a similarity between the quasi-brittle failure mechanisms evidenced in the NCTL testing and those evidenced in the UCTL testing.

A variety of other failure mechanisms occurred in various, non-repeatable combinations with brittle mechanisms in the low strength level 65°C and 80°C specimens, including tearing failures through node material and through the material in the area between the rib and the node, and rib splitting failures. Both of these mechanisms are variations of shear rupture. The photographs presented in figures 7.31A, B, C, & D show selected 80°C specimen ruptures to illustrate this variety. The 80°C UCTL specimens demonstrated a greater variety of failure mechanism combinations, rupture locations, and rupture progressions than the 65°C specimens.

7.5 SUMMARY OF NCTL AND UCTL TESTS RESULTS AND FAILURE MECHANISMS

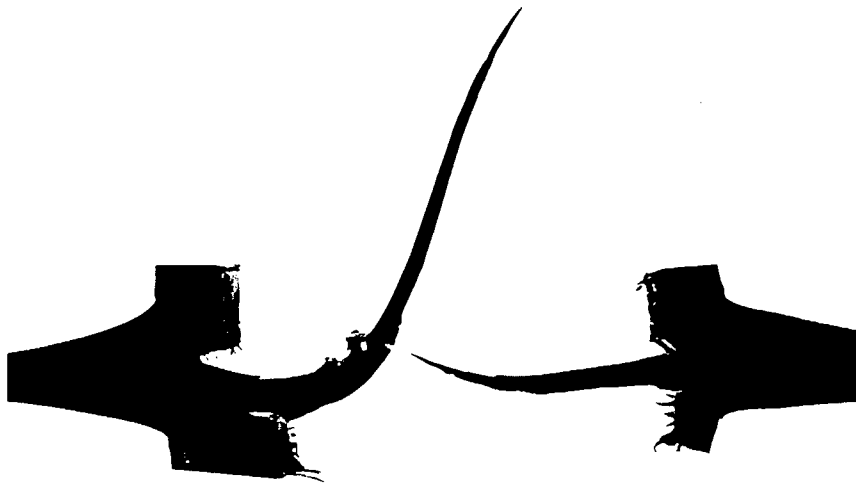
For the P-1 geogrid sample, NCTL testing was conducted on node material only, while UCTL testing was conducted on undamaged and unnotched single-rib-wide specimens.

The research program's ultimate purpose was to conservatively predict a strength value that engineers can use as a design parameter to preclude stress cracking failures in the selected uniaxially drawn HDPE geogrid product that is exposed to an ambient temperature of 20°C for 100 yr. In light of this purpose, analysis of brittle zone points and trends has been emphasized (rather than ductile zone, transition zone, or transition point analysis) because brittle zone trends best describe a material's stress cracking resistance.

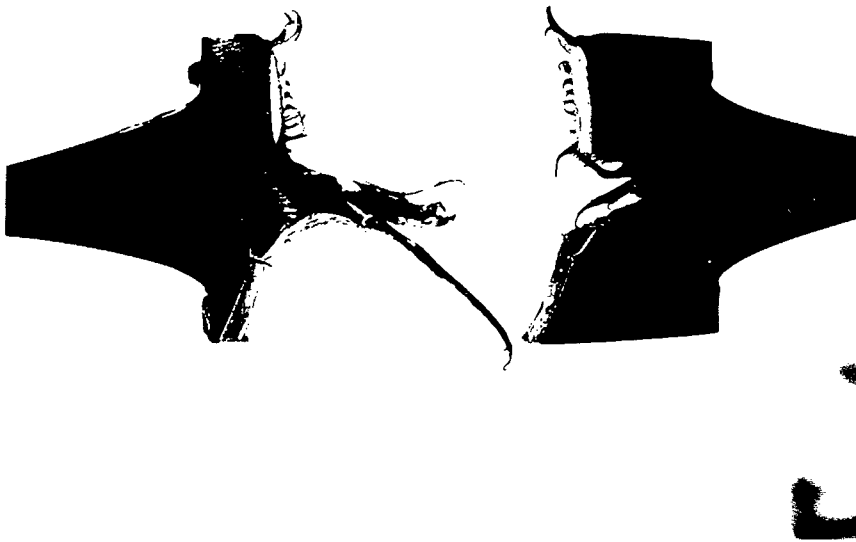
a. Summary of CTL Test Results for the Resins

NCTL Results for the Resins

- The ability of testing in water to distinguish variance in stress cracking resistance between resins was verified.



65°C, 21.00%
Brittle
(668, × 1.3)
Figure 7.29A

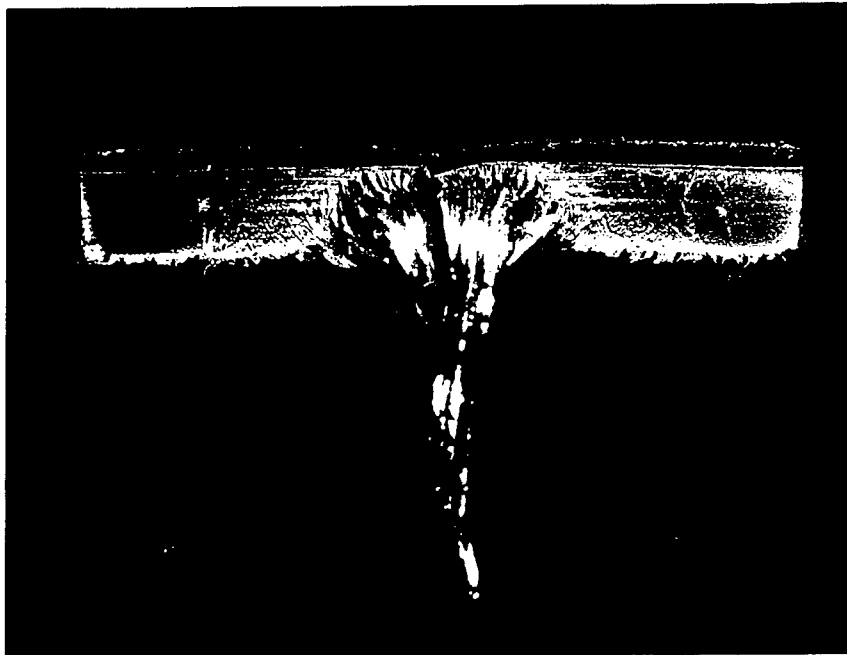


80°C, 15.00%
Brittle
(811, × 1.85)
Figure 7.29B

Figures 7.29A & B. Brittle ruptures in 65°C and 80°C UCTL P-1 geogrid specimens. Note long drawn material in node center and smooth brittle fractures on sides.

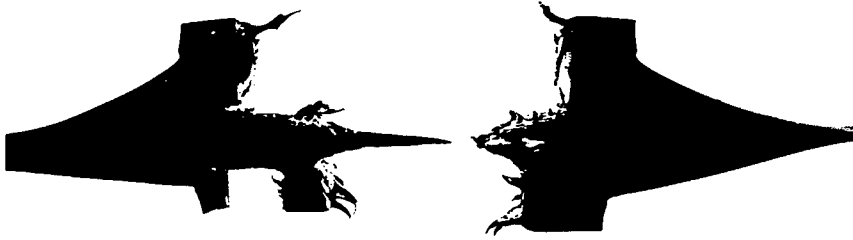


UCTL @ 80°C
Brittle, 15.00%
(811, × 4.1)
Figure 7.30A



NCTL @ 80°C
Brittle, 8.76%
(843, × 5.6)
Figure 7.30B

Figures 7.30A & B. Brittle rupture in 80°C UCTL P-1 geogrid specimen compared to brittle rupture in 80°C NCTL P-1 geogrid specimen. Note similar characteristics.



**80°C, 19.62 %
Brittle
(818, × 1.3)
Figure 7.31A**



**80°C, 19.36 %
Brittle/Tear
(904, × 1.3)
Figure 7.31B**



**80°C, 17.00 %
Brittle/Tear
(812, × 1.3)
Figure 7.31C**



**80°C, 22.76 %
Brittle/Split
(900, × 1.3)
Figure 7.31D**

Figures 7.31A, B, C & D. Brittle ruptures in 80°C UCTL P-1 geogrid specimens. Note variety of failure locations and progressions.

- Selected transition times consistently decreased with increasing crystallinity and corresponding density; this trend is consistent with published literature and experience.
- Resin L exhibited low resistance to stress cracking propagation.
- Resin H exhibited very high resistance to stress cracking propagation.
- Resin M exhibited low resistance to stress cracking propagation; even though resin M exhibited higher ductile and transitional failure times than resin L, resin M exhibited brittle failure times similar to those for resin L. Resin M stress cracking resistance was also low by current industry geomembrane standards.

UCTL Results for the Resins

- The ability of testing in water with no notch to distinguish subtle variance in stress cracking resistance between resins was not verified. However, an ability to distinguish general variance was observed.
- Resins L and M evidenced an unquantified degree of prematurity in UCTL rupture times because of microscopic sidewall grooves left by the metal die used to punch out the specimens. Therefore, reliable UCTL strength rupture times were not obtained for the resins.

If the unquantified effects of the grooves is ignored, then:

- resin L can be said to have exhibited low resistance to stress cracking initiation and propagation;
- resin M can be said to have exhibited medium resistance to stress cracking initiation and propagation; and
- resin H can be said to have exhibited very high resistance to stress cracking initiation and propagation.

b. Summary of CTL Test Results for the P-1 Geogrid Sample

NCTL Results for the P-1 Geogrid Sample

- The possibility of stress cracking propagation in the node material of uniaxially drawn

HDPE geogrids was verified by the repeatable occurrence of quasi-brittle fracture in side node material of 50°C, 65°C, and 80°C NCTL P-1 geogrid specimens tested at low strength levels.

- The general shapes of the 50°C, 65°C, and 80°C NCTL strength rupture curves were similar. The extended nature of the transition zones also were similar to the transition zone exhibited by resin M (a base resin believed to be similar to that used to produce this type of geogrid). These similarities lent credibility to the data and, thus, to the geogrid specimen selection process and testing procedures.
- The large degree of data scatter for 50°C (NCTL) brittle zone points prevented development of a clear 50°C brittle trend.
- The overall, anticipated trend of decreasing time to rupture with increasing immersion temperature was developed.
- A linear trend between transition time and immersion temperature was obtained by plotting selected transition time versus the inverse of the immersion temperature (in deg. K) on log-linear axes.
- Due to the appreciable degree of data scatter obtained in the 50°C testing, future NCTL node material testing performed at low temperatures (such as 50°C) should include more than three specimens at each strength level, especially for brittle zone determination.

UCTL Results for the P-1 Geogrid Sample

- The possibility of stress cracking initiation and propagation in unnotched and undamaged uniaxially drawn HDPE geogrids was verified by the occurrence of quasi-brittle fractures in side node material of 65°C and 80°C (UCTL) ruptured P-1 geogrid specimens tested at low strength levels. *This result verifies the capacity of unnotched and undamaged node material for stress cracking initiation and propagation.* No quasi-brittle modes of failure were evidenced, however, in fractures occurring in, or progressing through, P-1 rib material or the material in the area between the rib and the node. Rather, in UCTL specimens tested at strength levels below the transition band (figure 7.18), failures that progressed through rib material or the material in the area between the rib and the node were controlled by shear rupture occurring between oriented fibers parallel to the applied load.

- The UCTL test results for the P-1 geogrid product produced dissimilar looking strength rupture curves with transition points that were not apparent from curve shape; instead, transition point selection was determined by fracture face examinations.
- At strength levels greater than selected transition point strength levels, almost all specimens in every UCTL series failed in rib material by an apparently identical shear rupture mechanism; all of these shear ruptures were located in rib material at a similar distance from a node and were accompanied by twisting in the rib material.
- No transition zone was identified for the UCTL series because change in primary failure mechanism (with decreasing strength) from shear rupture to brittle rupture occurred relatively abruptly. A transition band was, therefore, identified as shown in figure 7.18.
- For the 65°C and 80°C series, stress cracking initiation and propagation (quasi-brittle fracture) occurred at low strength levels in non-repeatable fracture patterns in side node material.
- For the 50°C series, no brittle fractures were initiated in specimen gauge lengths within the time frame of the testing program. A brittle zone window was, therefore, assumed as occurring immediately after the highest unruptured data point in order to provide for conservative predictions to 20°C.
- Failure to obtain 50°C UCTL brittle ruptures in this testing program was a result of stopping all testing at approximately 13,000 hr (~ 1.5 yr). Future 50°C UCTL geogrid testing programs should, therefore, provide for testing times significantly longer than 1.5 yr.

c. Comparisons

Resin-Geogrid Comparison

- From NCTL test results, it may be concluded that, at strength levels higher than 11 percent, P-1 geogrid node material has higher stress cracking resistance than resin M. At lower levels, no firm conclusion can be drawn.
- From UCTL test results (ignoring sidewall groove effects on resin M specimens), P-1 geogrid has higher stress cracking resistance than resin M, suggesting the beneficial aspects of the uniaxially drawing manufacturing process.

NCTL-UCTL Geogrid Brittle Zone Trends

- The different percent changes obtained in this comparison indicated that there are insufficient data to reliably quantify a generic relationship between the NCTL and UCTL brittle zone results that can be applied to all uniaxially drawn HDPE geogrids. Future NCTL and UCTL testing of a significantly larger number of different geogrid samples is required to quantify such a relationship.

d. Summary of CTL P-1 Geogrid Failure Mechanisms

NCTL Failure Mechanisms

- The following primary failure mechanisms were observed in the notched node material of ruptured NCTL P-1 geogrid specimens: (1) ductile fracture, (2) transitional fracture, (3) quasi-brittle fracture; and (4) a combination of shear rupture and plastic deformation. These failure mechanisms occurred in very repeatable manners in the notched node material of specimens tested in all three series (i.e., 50°C, 65°C, and 80°C).
- The ductile fractures were identified by obvious extensive plastic deformation (i.e., long drawn material). The long drawn material of the ductile fractures was characterized by fibrous edges and/or splintering effects resulting from molecular orientation in the node material.
- The transitional fractures were identified by a combination of long drawn material and quasi-brittle fracture surfaces. The long drawn material was significantly more pronounced in center node material and was characterized by fibrous edges and/or splintering effects. The quasi-brittle fracture surfaces occurred in side node material and appeared coarsely velvety in a manner similar to transitional fracture in non-oriented HDPE resin.
- The quasi-brittle fractures were identified by relatively smooth fracture faces and by a lack of obvious bulk plastic deformation. These quasi-brittle fractures exhibited characteristics generally consistent with quasi-brittle fracture characteristics observed for HDPE geomembrane and pipe materials, including a smoothly velvety appearance produced by a carpet of microscopic plastic deformation points.
- Quasi-brittle fracture was not observed, however, in the more oriented center node material. Rather, center node material evidenced primary failure by a combination of shear rupture and plastic deformation.

UCTL Failure Mechanisms

- The following primary failure mechanisms were observed in ruptured UCTL P-1 geogrid specimens: (1) very repeatable shear rupture in rib material at an apparent point of maximum torsion; and (2) non-repeatable combinations of quasi-brittle fracture occurring in node material and shear rupture (tearing and rib splitting) occurring in center node and/or the material in the area between the rib and the node and/or rib material.
- The shear rupture failures in the rib material consisted of triangle-shaped fracture faces characterized by coarsely fibrous edges and by splinter-like fractures parallel to the applied load. All shear rupture failures were accompanied by residual twisting in the rib material and occurred at a repeatable distance from a nearby node at an apparent point of maximum torsion. It was shown that the shear rupture failures were initiated near the outer (two) edges of rib material because of abrupt changes in a residual stress relaxation gradient, and were accompanied by gradually increasing, localized plastic deformation as the shear ruptures progressed inward toward center rib material.
- Repeatable transitional fractures could not be identified. Definition of predominant transitional fracture characteristics for UCTL testing (if possible) would require a significantly larger number of specimens.
- The 65°C and 80°C UCTL test series produced quasi-brittle fractures in unnotched and undamaged side node material at low strength levels. These quasi-brittle fractures exhibited characteristics generally consistent with the quasi-brittle fracture characteristics observed for HDPE geomembrane and pipe materials, including a smoothly velvety appearance produced by a carpet of microscopic plastic deformation points. The quasi-brittle fracture surfaces occurred in side material only and did not propagate through the arresting zone into center node material.
- A variety of other failure mechanisms occurred in various, non-repeatable combinations with brittle mechanisms in the low strength level 65°C and 80°C specimens, including tearing failures through node material and through the material in the area between the rib and the node and rib splitting failures. Both of these mechanisms are variations of shear rupture.

CHAPTER 8

PREDICTING LONG-TERM PERFORMANCE

8.1 INTRODUCTION

The primary objective of this research program was to obtain data and develop a method for predicting the long-term performance of the P-1 geogrid in regard to stress cracking resistance. Two methods have been used to predict trends at 20°C from raw data: the RPM and Popelar et al. shifting. Predicted 20°C brittle zone trends will then be linearly extrapolated to 100 yr, and the corresponding strength level at that point will be considered a 100 yr/20°C baseline prediction in regard to brittle failure by stress cracking. A reduction of strength factor (RF and FS) to account for construction-induced damage aging and unknowns will then be applied to the UCTL baseline prediction, resulting in a strength that engineers can use for design purposes. Finally, the resulting allowable design strength will be compared with a 100 yr/20°C, safe allowable creep rupture limiting strength obtained from conventional creep testing.

In the approach described above, the tested geogrid is as manufactured. An alternative potential approach would have consisted of testing sets of geogrids that have been subjected to various levels of construction damage prior to testing. If this approach had been used, no reduction factor would have been required to account for construction damage.

The alternative approach of testing pre-damaged geogrids is fraught with practical problems as the damage to each specimen would not be uniform, introducing unquantifiable scatter to the results. Therefore, it was not deemed desirable at this stage.

It is important to note that the testing program in this report presents two boundaries for evaluating geogrids: the UCTL test corresponds to the fundamental product property and the NCTL test corresponds to a case of extreme damage to the geogrid as a result of construction operations. Actual field situations are somewhere between these two extreme cases.

Exposure to water was the test parameter selected to model anticipated in-service chemical exposure. Other common exposure media, such as dilute Igepal solutions, were not selected because they produce accelerated stress cracking and do not model in-service exposure.⁽¹⁴⁾

Mathematical Methods Used to Obtain Data at 20°C

Mathematical methods can be used to predict CTL behavior under exposure conditions that

differ from actual testing conditions; for example, predictions of behavior at temperatures lower than that used for testing can be made. From a practical standpoint, this is considered desirable because low temperature (e.g., 20°C) predictions, which may otherwise require 10 or more years of continuous testing at the low temperature, can be made from elevated temperature testing that can be performed in less than a year. The rate process method RPM is one such method used for predicting strength rupture times in HDPE at temperatures that are different from the actual testing temperatures.

The RPM uses the principle of time temperature superposition and involves solving three simultaneous equations to generate a fourth equation representing the prediction. The RPM has been used to predict long-term performance of HDPE pipes and HDPE geomembranes.^(20,21) In this research program, the RPM was used to make 100-yr predictions for an HDPE geogrid product (P-1) at an ambient temperature of 20°C. Because no testing was performed at 20°C in this research program, however, it was considered prudent to use an alternate mathematical method to verify the general accuracy of the RPM prediction. The shifting method developed by Popelar et al. and referred to as Popelar et al. shifting was selected as the alternate method for making predictions from the geogrid data.^(16,22)

Like the RPM, Popelar et al. shifting can be used to predict strength rupture times in HDPE at temperatures that are different from the actual testing temperatures. However, unlike the RPM, which uses the principle of time temperature superposition, Popelar et al. shifting uses the principle of bidirectional shifting. Shifting involves multiplying x and y values of time/strength data points by horizontal and vertical shifting functions, and generating a master curve representing the prediction. Each shifting function consists of an empirically determined natural exponential developed by Popelar on the basis of numerous tests of PE gas pipe materials and shown to be *universal* (i.e., they are applicable for developing master curves for a wide variety of crystallinity influenced physical phenomena in MDPE and HDPE gas pipe materials).

Linear regression analysis was used to calculate best-fit linear trends through logically grouped sets of data points (e.g., through the ductile data points for a given NCTL series). The term fitted data is sometimes used to refer to such a linear trend calculated using linear regression analysis. Fitted data will be referred to either as an idealized curve or simply as a trend. The accuracy of a trend is represented by the correlation coefficient (r), which is calculated during linear regression analysis. It involves calculating a line that minimizes the sum of the squares of the errors, where an error is the distance of an observed point from a potentially best fitting line.

The correlation coefficients for all trends calculated using linear regression analysis are listed on the bottom of the spreadsheets in appendices B and C.

Predicted 20°C brittle zone trends will be linearly extrapolated to 100 yr, and the corresponding strength level at that point will be considered a 100 yr/20°C prediction in regard to brittle failure by stress cracking. In the present state of knowledge about the long-term behavior of geogrids, it does not appear possible to evaluate the level of confidence that can be placed in such extrapolations.

8.2 GEOGRID PERFORMANCE PREDICTION USING THE RATE PROCESS METHOD

The RPM uses strength rupture data at two or three different temperatures to develop three equations with three unknown coefficients. The three equations provide an empirical representation of strength rupture trends at the two or three considered temperatures. A fourth equation is developed by solving the system of three simultaneous equations, thereby determining the values of the three unknown coefficients. This fourth equation is a prediction equation that can be used to predict failure times at other strength levels and temperature combinations.^(20,23) Details of steps for performing the RPM are presented below.

For this research program, the following equation is used to perform extrapolations with the RPM:

$$\log t_f = A_0 + A_1 T^{-1} + A_2 T^{-1} \log y \quad (1)$$

where:

- t_f = failure time (hours);
- y = strength level (%);
- T = bath temperature (°K); and
- A_0 , A_1 , and A_2 are constants.

Steps for Performing the RPM

The RPM can be performed as follows:

1. Select three strength/time points from two or three curves (i.e., curves that correspond to two or three different temperatures). The curves used must be of the same type (i.e., all should be brittle zone curves or all should be ductile zone curves). If two curves are used, two points should be selected on one of the curves, and one point on the other. If three curves are used, one point should be selected on each curve, and, in this case, experience shows that it is preferable to select non-collinear points.

2. Substitute the temperature, strength, and failure time values associated with one of the selected points into equation 1.
3. Continue the process described in step 2 for the other two selected points.
4. Simultaneously solve the three equations developed in steps 2 and 3 to determine constants A_0 , A_1 , and A_2 .
5. Substitute constants A_0 , A_1 , and A_2 into Equation 1 to obtain the general prediction equation for the strength rupture curves selected in step 1.
6. Substitute the temperature for which a prediction is desired (e.g., 20°C) into the general prediction equation to obtain the predicted equation for the strength rupture curve at the desired temperature.
7. Substitute a time for which a prediction is desired (e.g., 876,000 hr) into the equation of the strength rupture curve at the considered temperature (e.g., 20°C) and solve for y to calculate the predicted strength level at this temperature and at the selected time.
8. Repeat the process described in step 7 as desired or as necessary.

a. RPM Predictions from NCTL (Worst Case) Geogrid Data

Idealized NCTL P-1 geogrid strength rupture curves shown figure 8.1 were developed using the actual data trends presented in chapter 7 (figure 7.14). Equations of the straight lines in figure 8.1 are given in figure 8.2. The vertical lines between the ductile zones and the brittle zones are not representative of actual transition in the geogrid failure mode. Emphasis in this research program, and on the predictions made in this section, is on brittle zone analysis (i.e., not on transition zone or transition point analysis).

Center points and end points for each ductile and brittle trend line were calculated and are shown in figure 8.2. The NCTL points that were selected for RPM analysis are shaded black.

The RPM was performed separately for: (1) the ductile zone trends and (2) the brittle trends (using the 65°C and 80°C brittle trends only). Non-inclusion of the 50°C trend is regrettable because 50°C is closer to 20°C than 65°C and 80°C, and inclusion of a reliable 50°C trend would therefore decrease the uncertainty of the RPM prediction for 20°C. Results of the RPM calculations are summarized in table 7 and are presented in figure 8.3.

L:GNSLOPES

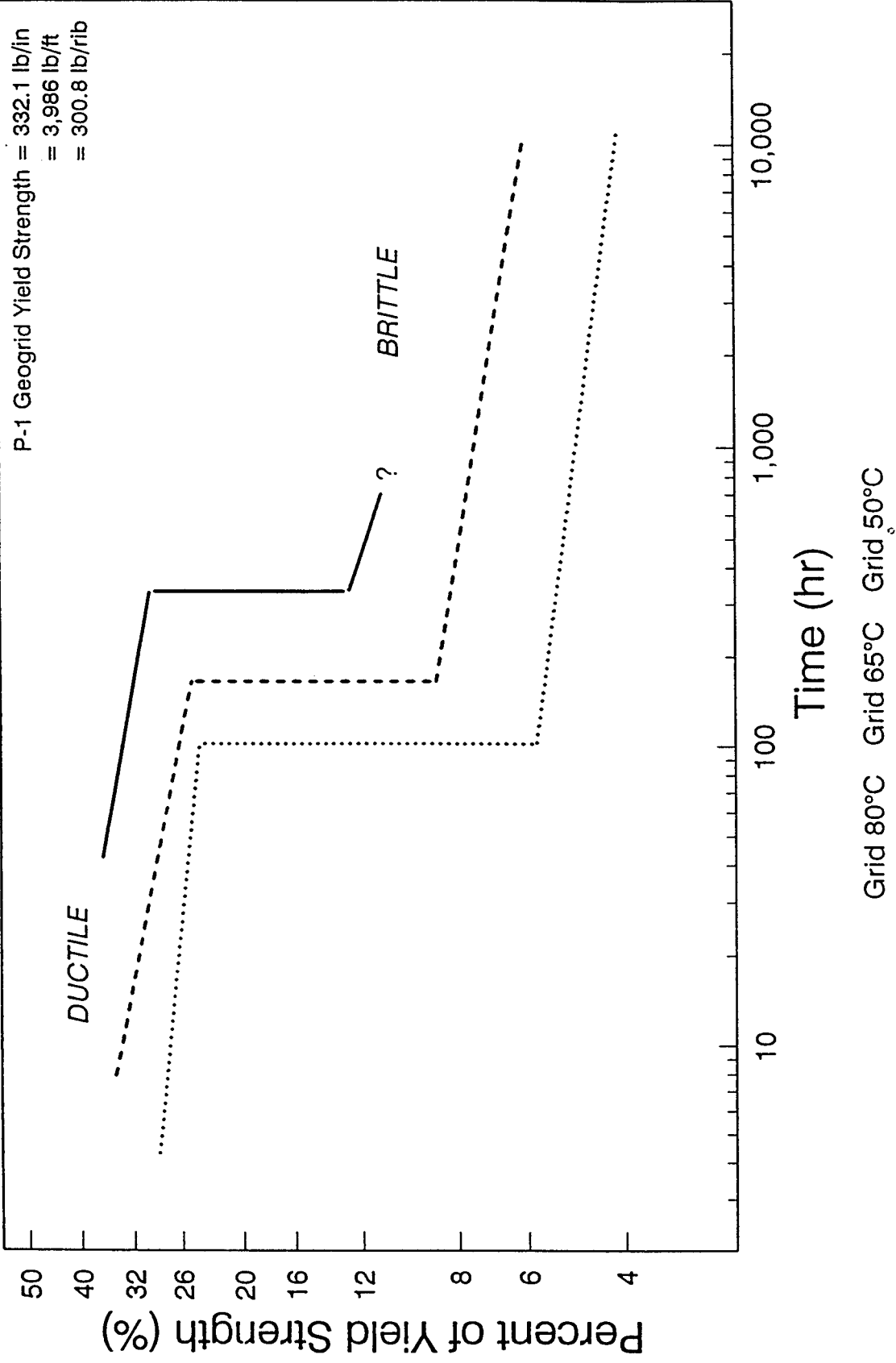


Figure 8.1. Idealizations of NCTL ("worst case") P-1 node material test data.

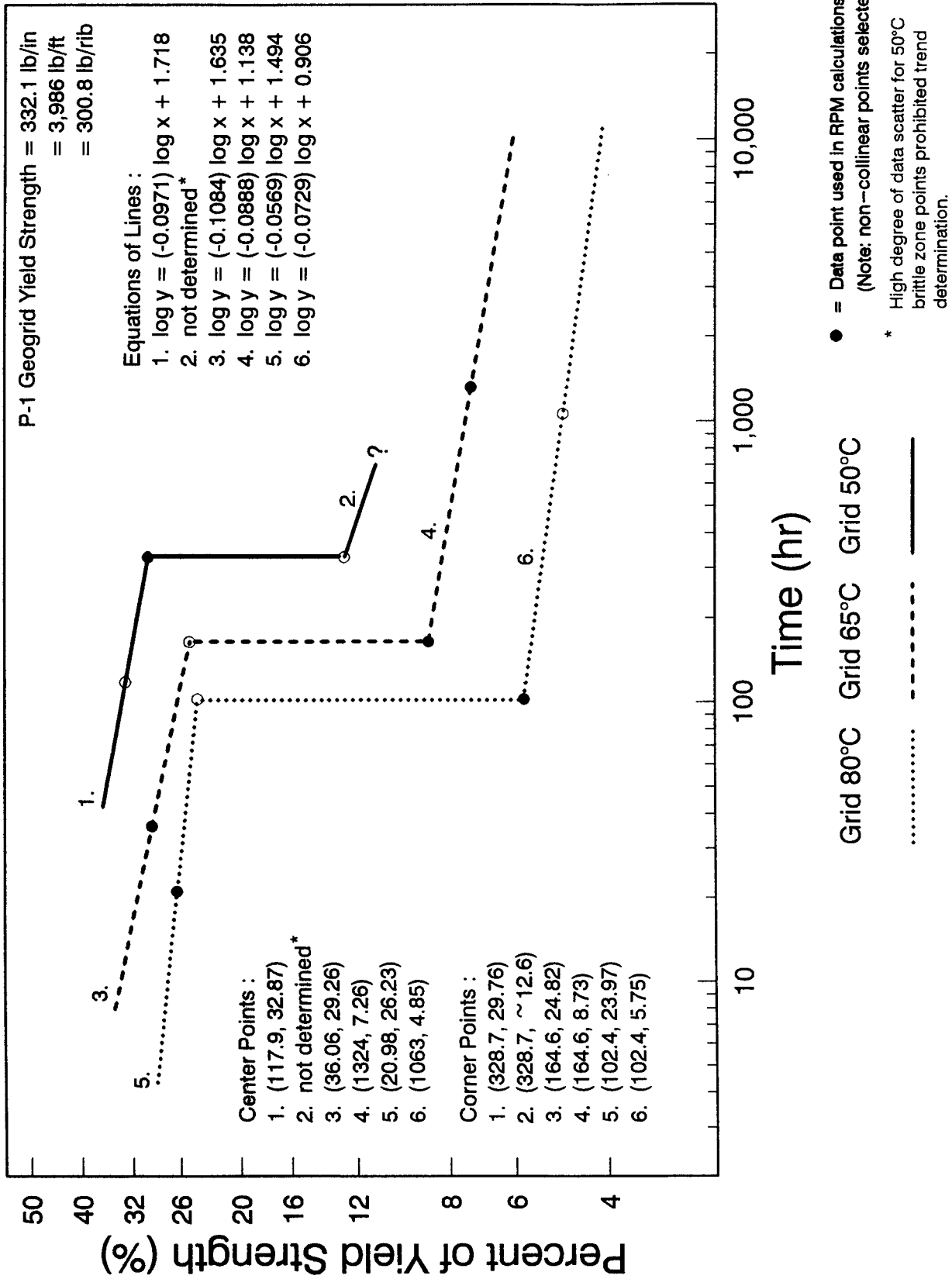


Figure 8.2. Idealizations of NCTL ("worst case") P-1 node material test data, showing equations of lines, center points, and corner points.

L:GNSLOPE3

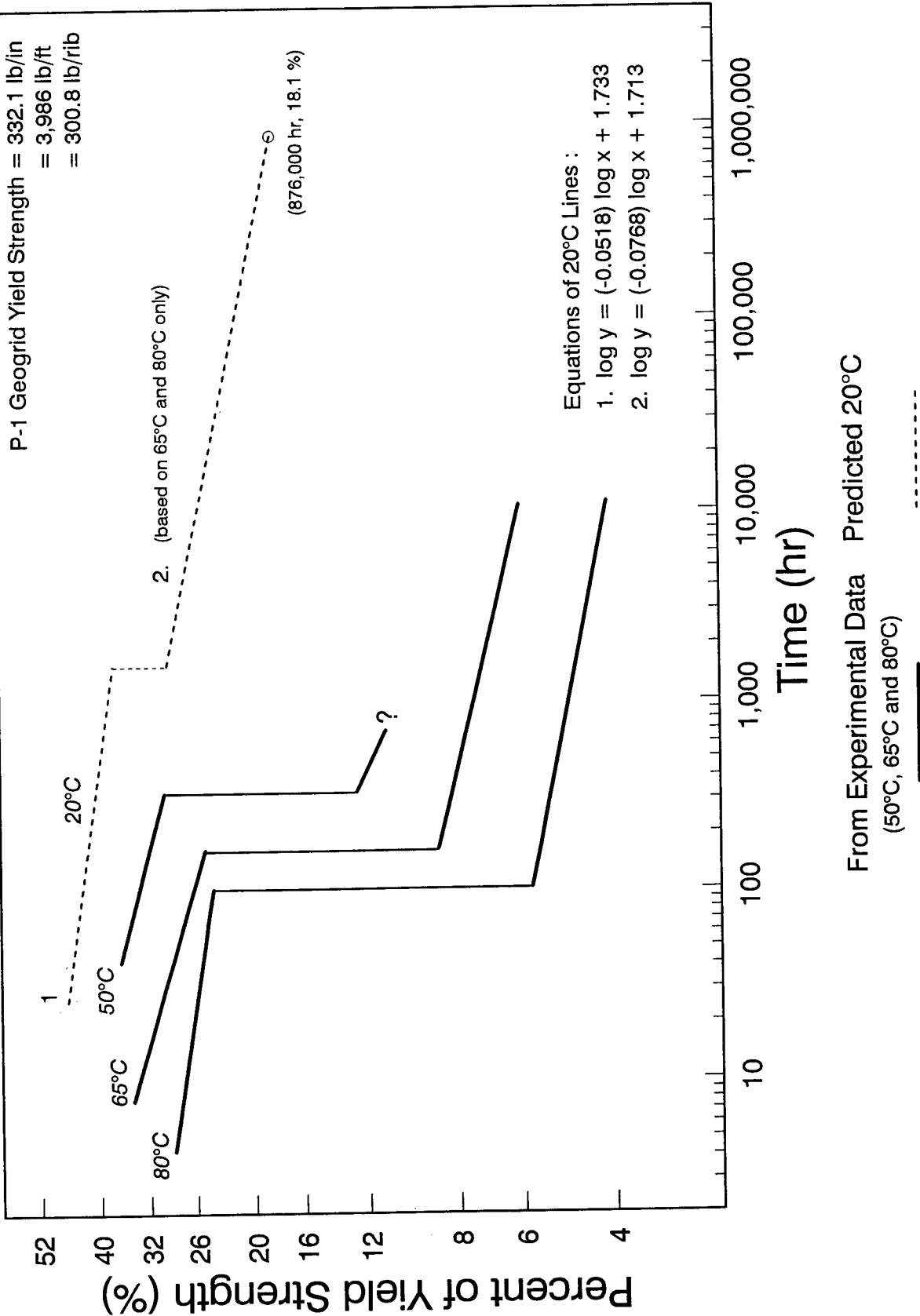


Figure 8.3. Predicted NCTL ("worst case") behavior of P-1 node material using the RPM (20°C).

Table 7. NCTL (worst case) geogrid data used for RPM calculations.

Data Grouping	Temperature T		Strength Level (%)	Time to Rupture t_f (hr)	RPM Constants (for 20°C)
	(K)	(°C)			
Ductile Zone	323	50	29.76	328.7	$A_0 = -21.886$
	338	65	29.26	36.06	$A_1 = 16,219$
	353	80	26.23	20.98	$A_2 = -5,657.7$
Brittle Zone (50°C excluded)	338	65	7.26	1324	$A_0 = -48.840$
	338	65	8.73	164.6	$A_1 = 20,853$
	353	80	5.75	102.4	$A_2 = -3,821.9$

The following 100 yr/20°C NCTL P-1 geogrid brittle zone prediction was obtained using the RPM (figure 8.3):

prediction using only 65°C and 80°C data: $t_f = 876,000$ hr, $y = 18.1\%$.

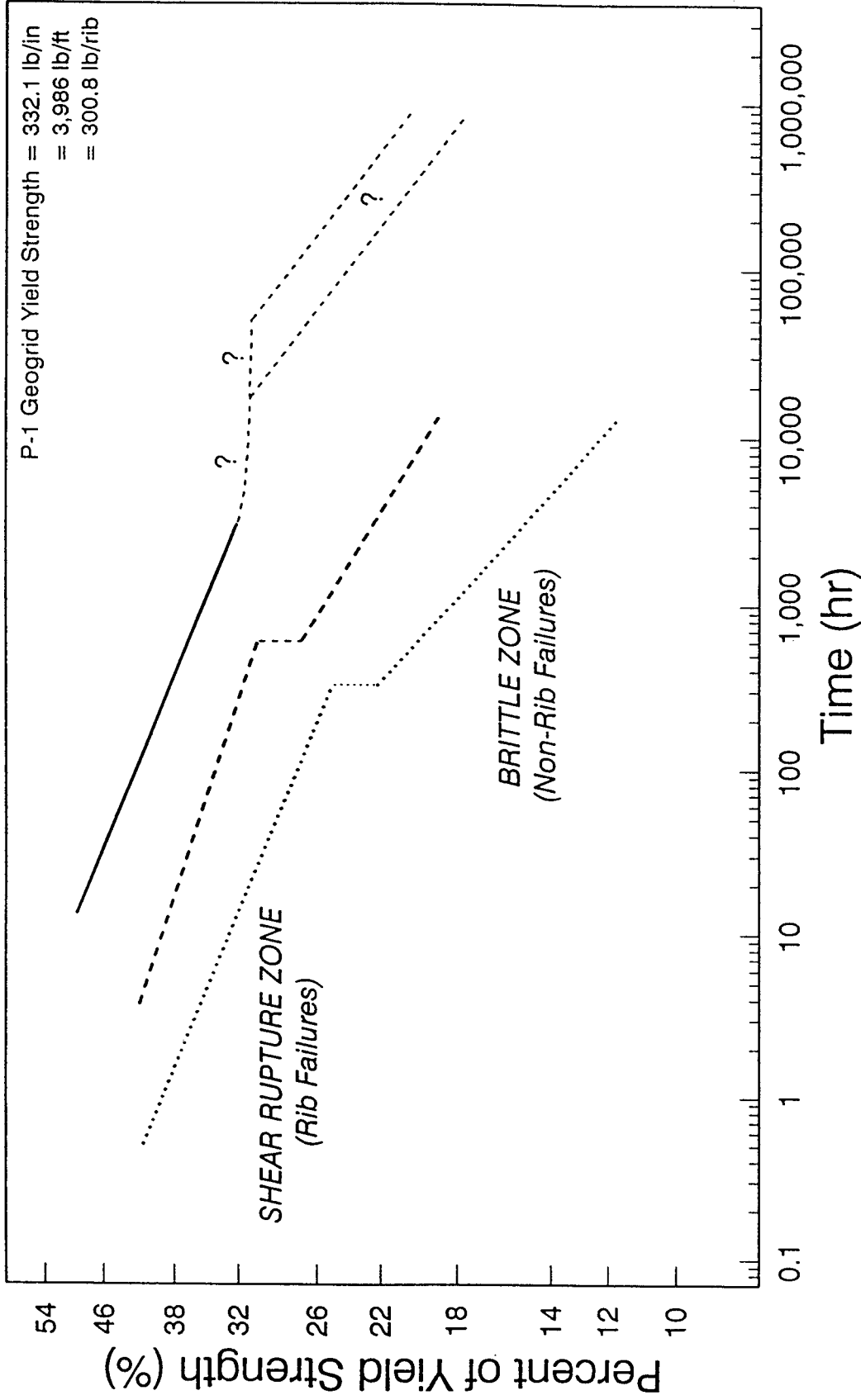
A strength level of 18 percent will, therefore, represent the 100-yr/20°C NCTL P-1 prediction. This means that a notched P-1 geogrid specimen, loaded at 18 percent of its room temperature yield strength, is predicted to experience ultimate rupture after 100 yr of exposure in 20°C water.

b. RPM Predictions from UCTL Geogrid Data

Idealized UCTL P-1 geogrid strength rupture curves, as shown in figure 8.4, were developed using the actual data trends presented in chapter 7 (figure 7.18). Emphasis in this research program, and on the predictions made in this section, is on brittle zone analysis.

L:GUSLOPES

P-1 Geogrid Yield Strength = 332.1 lb/in
= 3,986 lb/ft
= 300.8 lb/rib



Grid 80°C Grid 65°C Grid 50°C

..... - - - - - _____

Figure 8.4. Idealizations of UCTL P-1 geogrid test data.

The short vertical lines drawn between shear rupture and brittle trends at 65°C and 80°C do not represent transition zones because no appreciable transition could be identified by fracture face examinations for any of the UCTL geogrid series. (Transition means a gradual change in failure mechanism.) Fracture face examinations of ruptured UCTL geogrid specimens revealed that the failure mechanism changed relatively abruptly (with decreasing strength) from repeatable shear rupture in rib material to non-repeatable combinations of brittle and shear rupture through node material and through the material in the area between the rib and the node.

Center points and end points for each shear rupture and brittle trend line were calculated and are shown in figure 8.5. The UCTL points that were selected for RPM analysis are shaded black.

The RPM was performed separately for: (1) the shear rupture zone trends; (2) the brittle trends, using the assumed line 2a 50°C brittle trend; and (3) the brittle trends, using the assumed line 2b 50°C brittle trend. Results of the RPM calculations are summarized in table 8 and are presented in figure 8.6.

The following 100-yr/20°C UCTL P-1 geogrid brittle zone predictions were obtained using the RPM (figure 8.6):

prediction including line 2a 50°C assumption: $t_f = 876,000$ hr, $y = 43.1\%$; and
prediction including line 2b 50°C assumption: $t_f = 876,000$ hr, $y = 48.9\%$.

The assumed 50°C UCTL brittle zone window is considered a conservative assumption, as indicated previously. In the context of this report, conservative means defining a strength level that is lower than the value that could rationally be expected, with the intent of providing for a safe design. A window of 43 to 49 percent will, therefore, represent a conservative 100-yr/20°C UCTL P-1 prediction.

Finally, it should be noted that, although the 50°C UCTL brittle zone data were not as complete as they could have been if significantly more tests had been conducted, it was necessary to use them because inspection of figure 7.18 shows an important trend: the effect of a 15° change in temperature from 50°C to 65°C appears greater than the effect of a 15° change in temperature between 65°C and 80°C. This important trend would not have been reflected in the final predictions made using the RPM if the 50°C data had been excluded from use in the RPM.

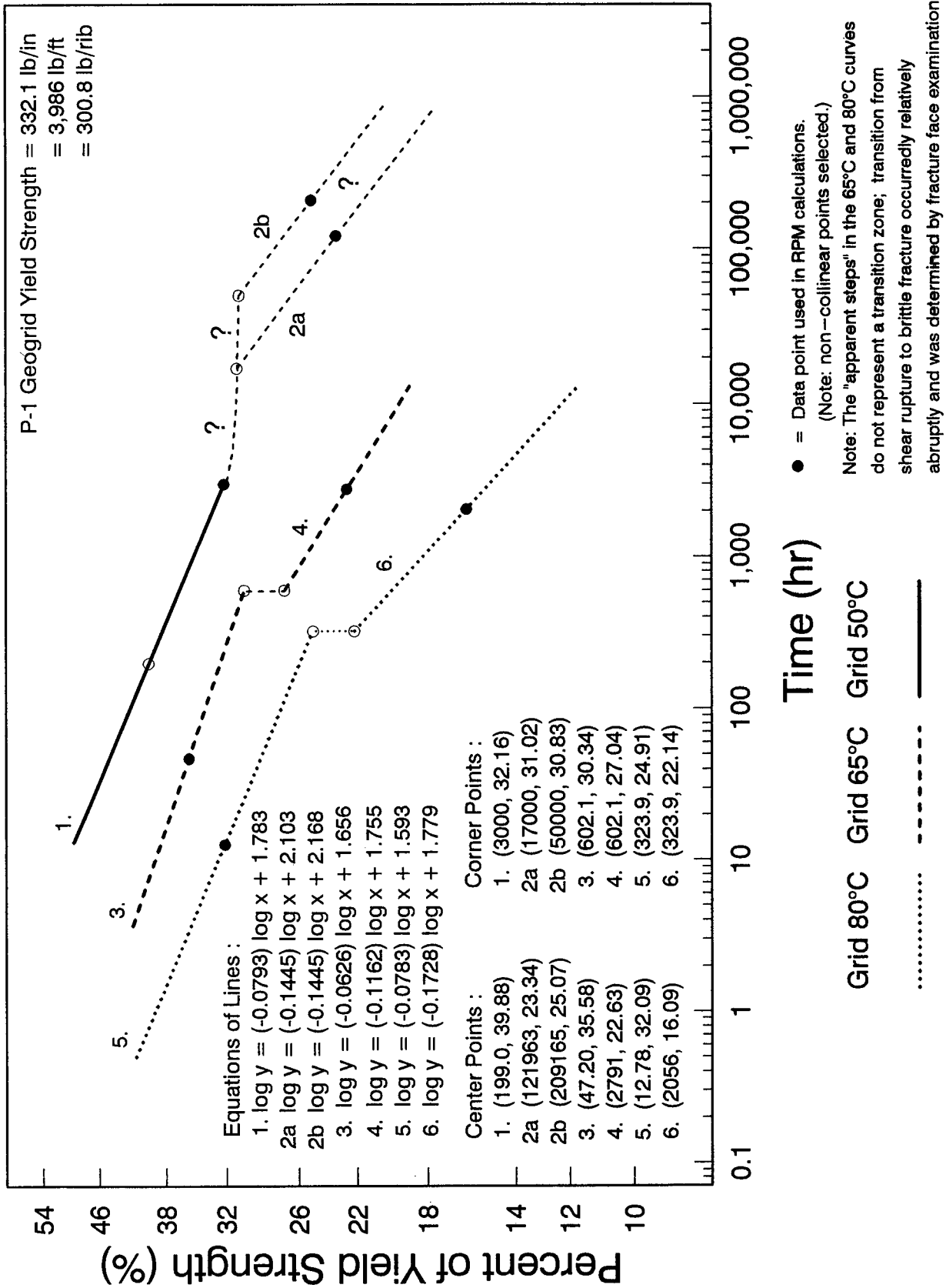


Figure 8.5. Idealizations of UCTL P-1 geogrid test data, showing equations of lines, center point, and corner points.

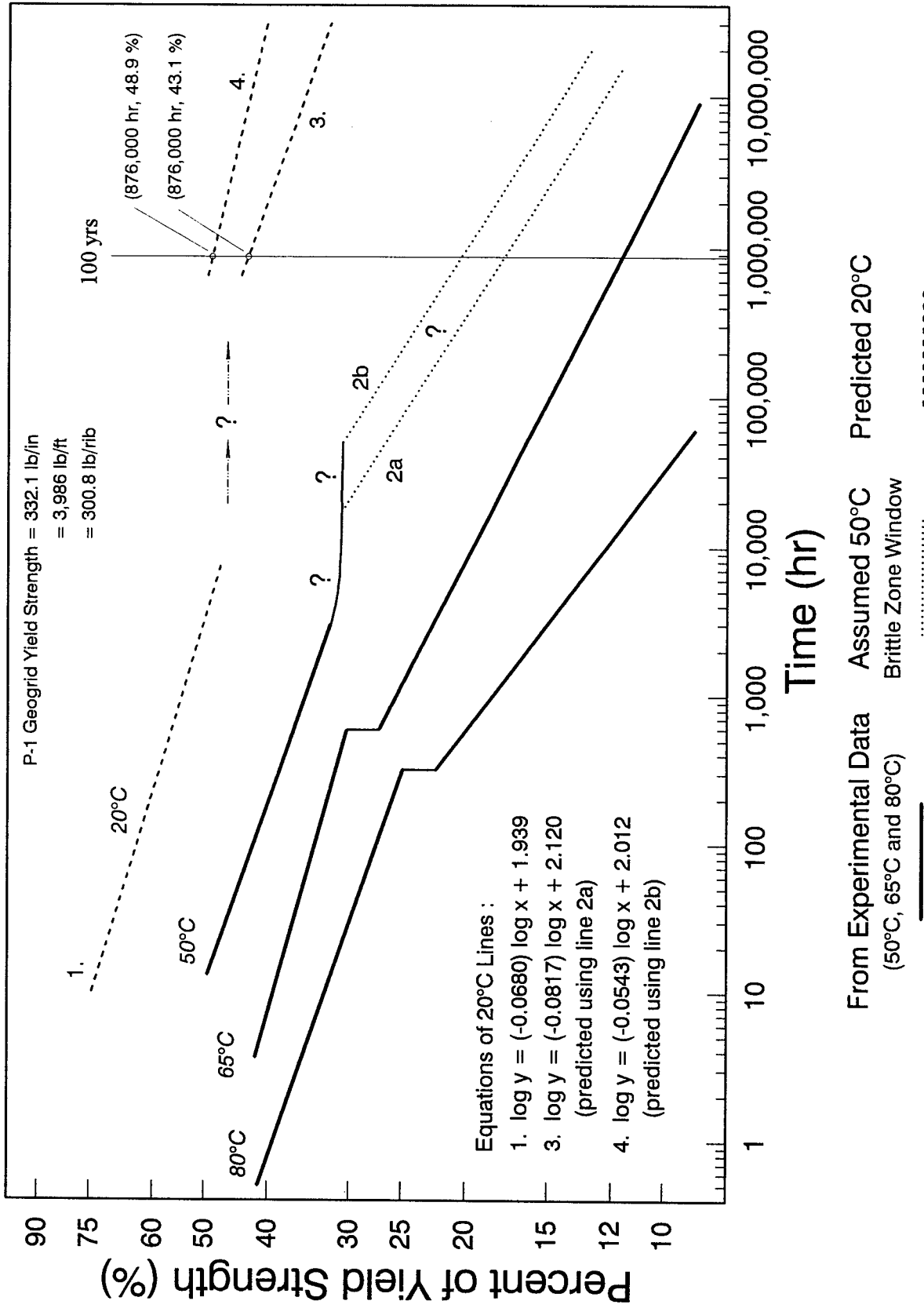


Figure 8.6. Predicted UCTL behavior of P-1 geogrid product using the RPM (20°C).

Table 8. UCTL geogrid data used for RPM calculations.

Data Grouping	Temperature T		Strength Level (%)	Time to Rupture t_f (hr)	RPM Constants (for 20°C)
	(K)	(°C)			
Shear Rupture Zone	323	50	32.16	3000	$A_0 = -24.553$
	338	65	35.58	47.20	$A_1 = 15,545$
	353	80	32.09	12.78	$A_2 = -4,306.9$
Brittle Zone (with line 2a)	323	50	23.34	121963	$A_0 = -35.086$
	338	65	22.63	2791	$A_1 = 17,881$
	353	80	16.09	2056	$A_2 = -3,585.5$
Brittle Zone (with line 2b)	323	50	25.07	209165	$A_0 = -52.902$
	338	65	22.63	2791	$A_1 = 26,347$
	353	80	16.09	2056	$A_2 = -5,389.6$

8.3 PERFORMANCE PREDICTION USING POPELAR ET AL. 1991 BIDIRECTIONAL SHIFTING

The bidirectional shifting method developed by Popelar et al. is a mathematical method selected and performed to fulfill this program's requirement of using an alternate method to predict a 20°C UCTL P-1 geogrid brittle trend from elevated temperature UCTL brittle stress rupture data.

Popelar et al. shifting is a mathematical procedure to shift time/strength rupture data points obtained at two or more temperatures (e.g., 50°C, 65°C, and 80°C) both vertically and horizontally in order to develop a master curve for a different untested temperature (e.g., 20°C). Popelar et al. shifting is horizontal and vertical shifting, proportional to temperature, in the log-time and log-strength axes.

The shifting functions were empirically determined on the basis of stress relaxation studies of MDPE and HDPE gas pipe materials.^(16,17) Note that the shifting functions are not an approximation to the Arrhenius equation, because the Arrhenius equation only considers a horizontal (time) shift and does not account for a vertical (strength) shift due to the polymer becoming more amorphous as temperature increases.⁽²⁴⁾ The shifting functions were not derived; they are empirical and are best line fits to stress relaxation data of PE gas pipe materials. Popelar concluded that their shift functions are *universal* (i.e., are applicable for developing master curves for a wide variety of crystallinity influenced (and rate process influenced) physical phenomena in MDPE and HDPE gas pipe materials).

The following equation represents the shifting function for horizontal (time) shifting:

$$x_R = x \times e^{0.109(T-T_R)} \quad (2)$$

where:

- x_R = time at reference temperature (hr);
- x = time at test temperature (hr);
- T = test temperature (°C);
- T_R = reference temperature (e.g., 20°C); and
- e = the base of the natural logarithm (2.718282. . .).

The following equation represents the Popelar et al. shifting function for vertical (strength) shifting:

$$y_R = y \times e^{0.116(T-T_R)} \quad (3)$$

where:

- y_R = strength at reference temperature (%);
- y = strength at test temperature (%);
- (x, y) = data point at test temperature; and
- (x_R, y_R) = shifted data point at reference temperature.

Table 9 summarizes the calculated natural exponentials used for shifting to 20°C.

Table 9. Summary of calculated natural exponentials used for Popelar et al. shifting.

Direction of Shifting	Temp. Shift from 50°C to 20°C	Temp. Shift from 65°C to 20°C	Temp. Shift from 80°C to 20°C
Horizontal (Time) Shifting	$e^{3.27} = 26.3113$	$e^{4.905} = 134.963$	$e^{6.54} = 692.287$
Vertical (Strength) Shifting	$e^{0.348} = 1.41623$	$e^{0.522} = 1.68540$	$e^{0.696} = 2.00571$

Steps for Performing Popelar et al. Shifting

1. Select the reference temperature (T_R) for which predictions are to be made (e.g., 20°C).
2. For each time/strength data point (x, y) obtained in CTL testing for specimens tested to complete rupture at each test temperature (T), substitute each time value (x) in equation 2 to obtain a new horizontally shifted time value (x_R) for the reference temperature (T_R).
3. Similarly, for each time/strength data point (x, y) obtained in CTL testing for specimens tested to complete rupture at each test temperature (T), substitute each strength value (y) in equation 3 to obtain a new vertically shifted time value (y_R) for the reference temperature (T_R).
4. Combine all associated x_R and y_R values obtained in steps 2 and 3 above, to make one new data set ^{(1) (2)} consisting of bidirectionally shifted points (x_R, y_R) for the selected reference temperature (T_R).

⁽¹⁾ Note: Primary rupture mechanisms associated with each point should be distinguished in order to calculate separate trends, based on primary rupture mechanism, within the new data set. Because numerous researchers have shown that ductile and brittle trends have distinctly different slopes, distinguishing these two trends is important and necessary. For example, shading in a plotted symbol can be used to represent a brittle rupture mechanism.

(2) Note: The shifting functions are intended to merge, as well as shift, elevated temperature test data. To better visualize the degree of merging of the data (also referred to as the coherency of the master curve), it is helpful to associate a unique symbol with a given actual testing temperature for plotting shifted points. For example, an open circle can be used to represent the shifted location of a 50°C data point.

5. Plot the data set obtained in step 4 on log-log scale axes; see notes (1) and (2) above. Examine the shape of the merged data set, now referred to as a master curve obtained in step 4, and examine fracture faces to determine ductile and brittle zone points.
6. Apply linear regression analysis separately to the data represented by the ductile zone points (distinguished in step 5) to develop an equation for a predicted ductile trend at the selected reference temperature.

Apply linear regression analysis separately to the data represented by the brittle zone points (distinguished in step 5) to develop an equation for a predicted brittle trend at the selected reference temperature.

Use the following equation to represent a straight line in log-log axes. The equation obtained for the brittle trend will then be referred to as the predicted reference temperature line equation.

$$\log y = m \log x + b \quad (4)$$

where:

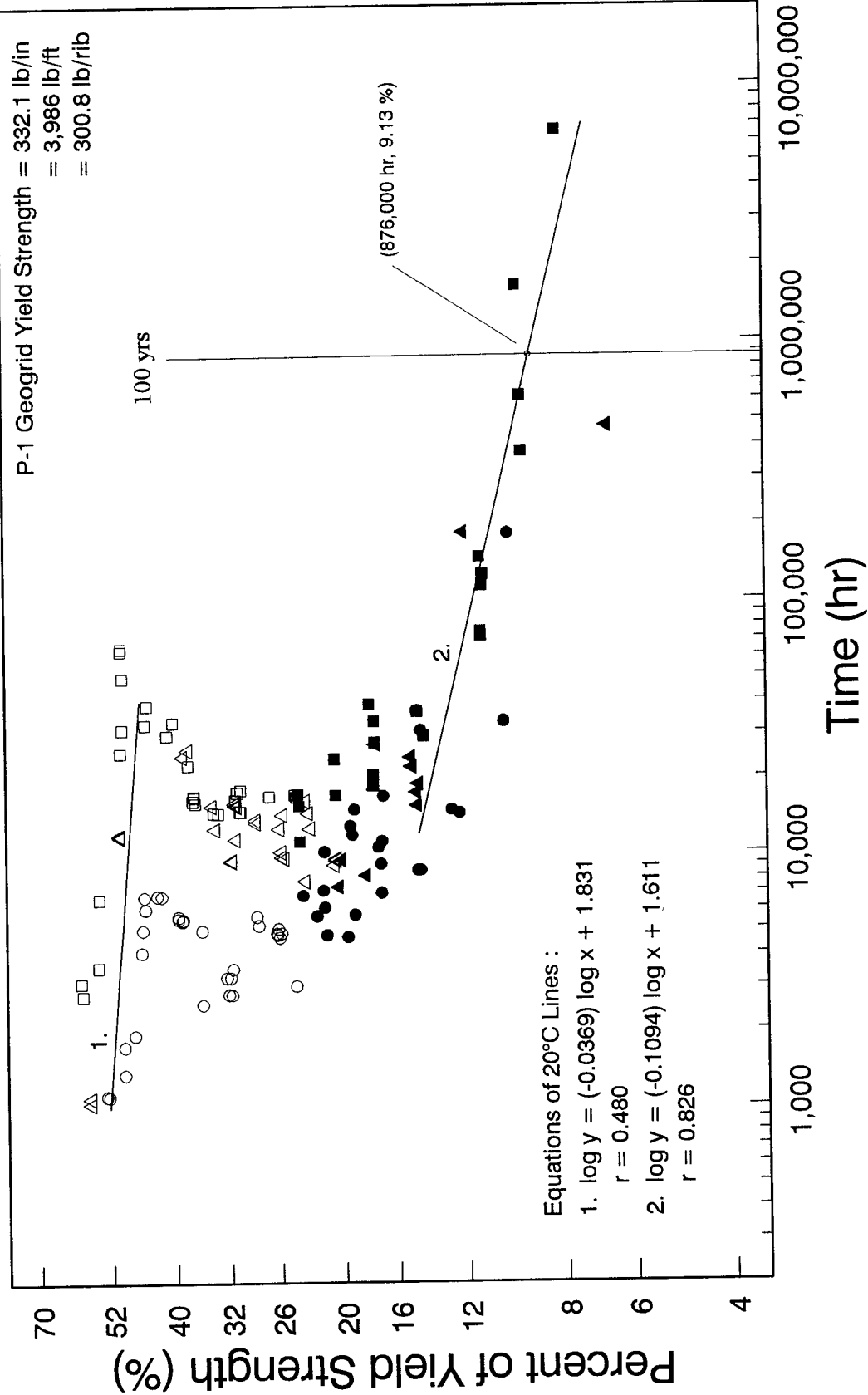
- x = failure time (hr) ;
- y = strength level (%) ;
- m = slope of the line (dimensionless); and
- b = y-intercept of the line (dimensionless).

7. Substitute a failure time for which a prediction is desired (e.g., 876,000 hr) into the predicted reference temperature line equation developed in 6 and solve for y to calculate an associated (predicted) strength level.

a. Popelar et al. Shifting of NCTL Geogrid Data

In order to obtain an alternate NCTL prediction to 20°C/100-yr for P-1 node material, Popelar et al. shifting was applied to the elevated temperature NCTL P-1 data and plotted in figure 8.7. Shifting was only applied to data for specimens tested to complete rupture.

L:MASTERN4



Shifted 50°C above T.P. below T.P. ● ○
 Shifted 65°C above T.P. below T.P. ▲ △
 Shifted 80°C above T.P. below T.P. ■ □

Figure 8.7. Predicted NCTL ("worst case") behavior of P-1 node material using Popelar et al. shifting functions (20°C).

Observation of the 20°C NCTL master curve indicates that the shifted NCTL points do not completely merge together into a coherent master curve; the 80°C points appear to be shifted too far and/or the 50°C points do not appear to be shifted far enough. This apparently incomplete merging indicates that the shifting functions do not provide for a completely coherent master curve at 20°C for notched P-1 node material. However, shifting function may provide for an accurate overall, 20°C shifting *distance* for notched P-1 node material. Unfortunately, the accuracy of the overall 20°C shifting distance could not be verified because no testing was performed at 20°C in this program.

The following 20°C NCTL P-1 node material trends were obtained by applying linear regression analyses to the Popelar et al. shifted NCTL data:

$$\begin{aligned} 20^\circ\text{C ductile trend:} \quad & \log y = (-0.0369) \log x + 1.831 \\ & r = 0.480 ; \text{ and} \end{aligned}$$

$$\begin{aligned} 20^\circ\text{C brittle trend:} \quad & \log y = (-0.1094) \log x + 1.611 \\ & r = 0.826. \end{aligned}$$

The following 20°C/100-yr NCTL P-1 node material brittle zone prediction was obtained from the Popelar et al. shifted NCTL brittle trend:

$$20^\circ\text{C}/100\text{-yr prediction:} \quad (876,000 \text{ hr, } 9.13\%).$$

A strength level of 9 percent will, therefore, represent an alternate potential worst case (NCTL) 20°C/100-yr prediction for the P-1 geogrid product. This 9 percent value is not consistent with the 20°C/100-yr value of 18 percent determined using the RPM.

b. Popelar et al. Shifting of UCTL (Performance) Geogrid Data

In order to obtain an alternate UCTL performance prediction to 20°C/100-yr for P-1 geogrid product, Popelar et al. shifting was applied to the elevated temperature UCTL P-1 data. Shifting was only applied to data for specimens tested to complete rupture. Results of the shifting of UCTL data are plotted in figure 8.8.

Observation of the 20°C NCTL master curve indicates that the degree of merging of shifted UCTL data points appears better than the degree of merging obtained with the NCTL data. Again, as with the shifted NCTL data, the shifted UCTL 80°C points appear to be shifted too far and/or the 50°C points do not appear to be shifted far enough.

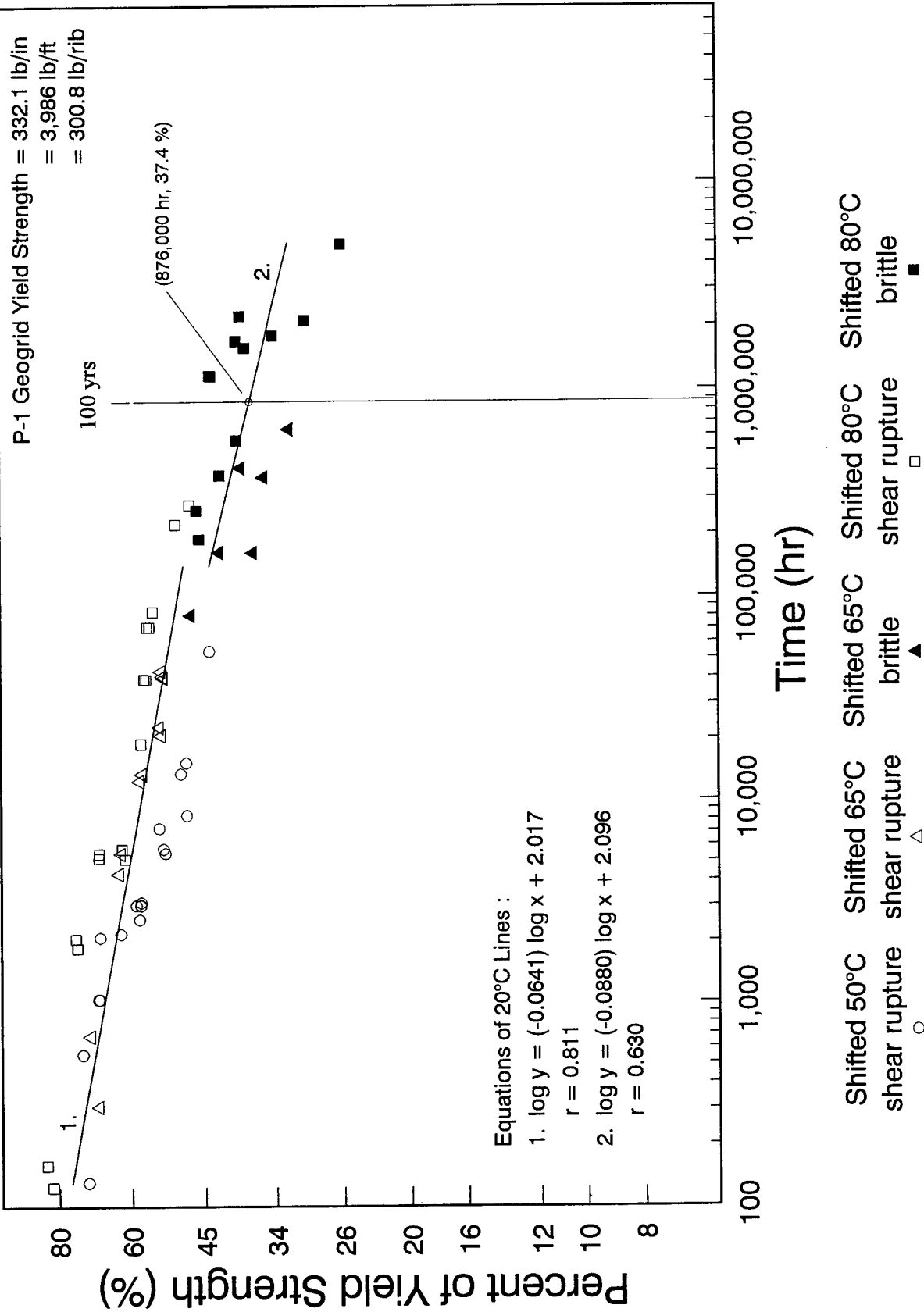


Figure 8.8. Predicted UCTL behavior of P-1 geogrid product using Popelar et al. shifting functions (20°).

This apparently incomplete merging indicates that the shifting functions may not provide for a completely coherent master curve at 20°C for undamaged P-1 geogrid product. However, the Popelar et al. shifting function may provide for an accurate overall, 20°C shifting *distance* for undamaged P-1 product. Unfortunately, the accuracy of the overall 20°C shifting distance could not be verified because no testing was performed at 20°C in this program.

It was interesting that the 20°C UCTL master curve demonstrated an overall linear trend, rather than the overall knee-shaped trend that is normally produced by notched stress rupture testing. Linear regression analysis can be used to find a best fit line through all of the shifted UCTL points. The results presented in figure 8.9 do not substantially alter the conclusions.

The following 20°C UCTL performance P-1 product trends were obtained by applying Linear regression analyses to the shifted UCTL data, as presented in figure 8.8 rather than 8.9 although they appear equally valid:

$$20^\circ\text{C shear rupture trend: } \log y = (-0.0641) \log x + 2.017, \quad r = 0.811 ; \text{ and}$$

$$20^\circ\text{C brittle trend: } \log y = (-0.0880) \log x + 2.096, \quad r = 0.630 .$$

The following 20°C/100-yr UCTL P-1 geogrid brittle zone prediction was obtained from the shifted UCTL brittle trend, as presented in figure 8.8:

$$\text{prediction: } (876,000 \text{ hr, } 37.4\%).$$

A strength level of 37 percent will, therefore, represent an alternate performance (UCTL) 20°C/100-yr prediction for the P-1 geogrid product, obtained using Popelar et al. shifting. This 37 percent value is less than the 20°C/100-yr value of 43 to 49 percent determined using the RPM.

c. Comparison of 20°C NCTL and UCTL Master Curves

P-1 geogrid 20°C NCTL and UCTL trends obtained from Popelar et al. shifted data points, were compared. This comparison is illustrated in figure 8.10 and is summarized as follows:

20°C NCTL ductile zone trend:	$m = -0.0369$	$b = 1.831$
20°C UCTL shear rupture zone trend:	$m = -0.0641$	$b = 2.017$
Percent Change:	- 74%	+ 10%
20°C NCTL brittle zone trend:	$m = -0.1094$	$b = 1.611$
20°C UCTL brittle zone trend:	$m = -0.0880$	$b = 2.096$
Percent Change:	+ 19.5%	+ 30%

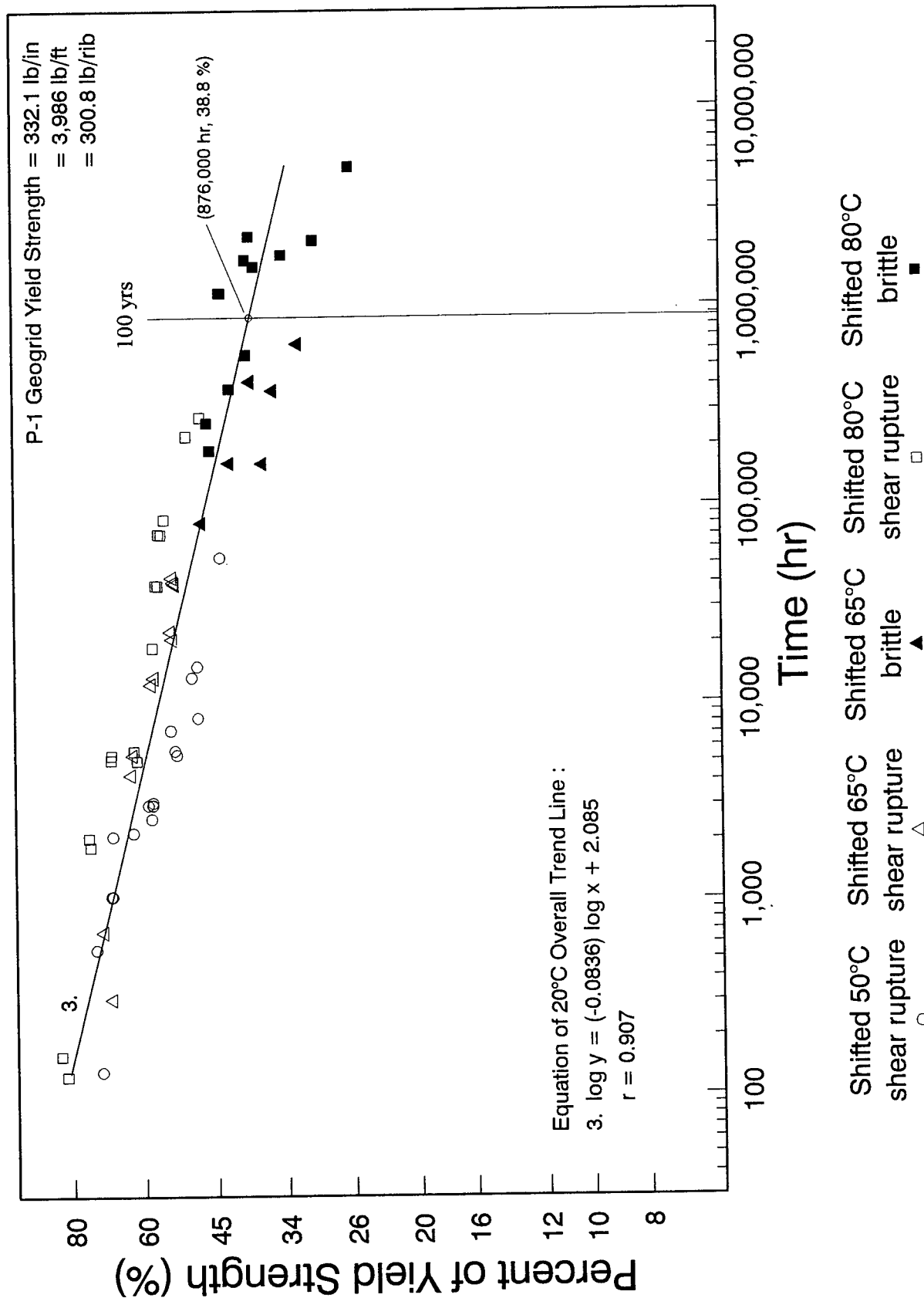


Figure 8.9. Predicted UCTL behavior of P-1 geogrid product using Popelar et al. shifting functions (20°), based on an overall trend.

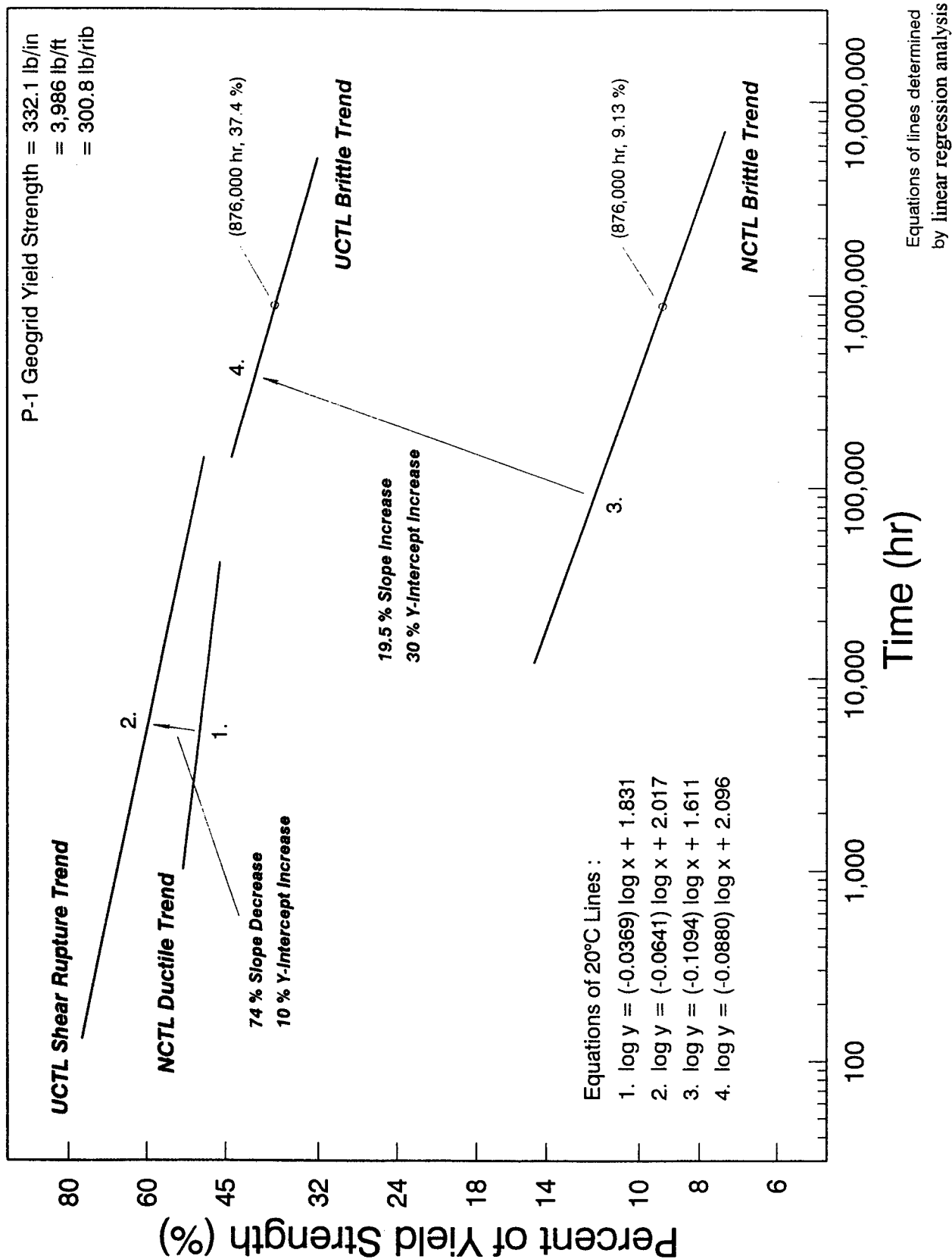


Figure 8.10. Relationship between 20°C NCTL and 20°C UCTL P-1 geogrid trends obtained using Popelar et al. shift functions.

The comparisons of 65°C and 80°C UCTL brittle zone trends previously presented are shown here for simplified reference:

65°C NCTL brittle zone trend:	$m = -0.0888$	$b = 1.14$
65°C UCTL brittle zone trend:	$m = -0.1162$	$b = 1.75$
Percent Change:	- 31%	+ 54%
80°C NCTL brittle zone trend:	$m = -0.0729$	$b = 0.906$
80°C UCTL brittle zone trend:	$m = -0.1728$	$b = 1.78$
Percent Change:	- 137%	+ 96%

Examination of the brittle zone percent changes for 20°C, 65°C, and 80°C indicates two possible concurrent, intrinsically linked trends:

- the percent change in brittle zone trend slope (m) (from NCTL slope to UCTL slope) decreased with increasing temperature; and
- the percent change in brittle zone trend y -intercept (b) (from NCTL y -intercept to UCTL y -intercept) increased with increasing temperature.

These trends in percent change hold promise as a method to link NCTL testing with UCTL testing in order to reduce the laboratory testing time required to achieve performance limits. Unfortunately, an insufficient number of different samples (i.e., only one sample of the P-1 product) were tested in this program to reliably quantify a generic relationship between the NCTL and UCTL geogrid results that can be applied to all uniaxially drawn HDPE geogrids. Future NCTL and UCTL testing of a significantly larger number of different geogrid samples is required for this purpose.

8.4 CONCLUSIONS ON GEOGRID PERFORMANCE PREDICTIONS

a. Comparison Between CTL Predictions

As indicated, two methods were used to make geogrid performance predictions: the RPM and Popelar et al. shifting. The RPM is the more generally accepted method for this type of prediction. Popelar et al. shifting, which is empirically based on PE gas pipe resins, was used as an alternate method. The 20°C/100-yr strength levels obtained using the two above methods with the data from CTL tests (NCTL and UCTL) are presented in table 10.

Table 10. 20°C, 100-yr strength levels predicted using different methods.

Method	NCTL	UCTL
Rate Process Method	18.1%	43+ %
Popelar et al. Shifting	9.1%	38.8%

The following comments can be made on the results presented in table 10:

- The presently obtained results by either method must be tempered by the fact that the use of a test temperature of 80°C is retrospectively too high as evidenced by significant changes in modulus observed for the P-1 geogrid in the oxidative stability studies under Task D, separately reported. In addition for lower temperature UCTL studies, test duration times in excess of 10,000 hrs are required to obtain rupture and subsequent analysis.
- The results obtained with Popelar et al. shifting suggest lower threshold strengths than the RPM results. As discussed, apparently incomplete merging, observed in the Popelar et al. shifted NCTL and UCTL master curves, indicated that the shifting functions may not provide for bidirectional shifting to 20°C for the P-1 uniaxially drawn geogrid product as *universally* as it does for PE gas pipe materials, which are not drawn to the same degree. This appears to be especially significant for NCTL results. Additionally, since no 20°C testing was performed in this program, the shifting distance, obtained using Popelar et al. shifting, could not be independently verified.

A comparison of the RPM with Popelar et al. shifting has been published by C.H. Popelar in, "*A Comparison of the Rate Process Method and the Bidirectional Shifting Method*".⁽²²⁾ He concludes that there is a good agreement between RPM predictions and bidirectional shifting predictions made from elevated temperature, pressurized PE gas pipe tests performed on 10 different MDPE and HDPE pipe samples, including notched specimens.

In contrast to these conclusions, this program did not find a good agreement between RPM predictions and Popelar et al. shifting predictions for the P-1 uniaxially drawn geogrid product tested in this program, *especially for the NCLT testing*. Therefore, the authors consider NCTL results obtained using the RPM, which is the presently generally accepted method to be the more valid results.

b. Creep Prediction from the Literature

It had been industry practice to perform creep tests for geosynthetics in air to define a long term strength on the basis of creep strain data. Recently creep rupture has been adopted by AASHTO as the criteria basis which is consistent with the UCTL tests performed except that the latter were performed in water rather than in-air, and at substantially higher temperatures.

Therefore, creep limiting strength based on creep-rupture is a key criteria in establishing a design allowable strength.

Creep limiting strengths for this HDPE geogrid were obtained from the literature.^(25,28) A long-term design strength of 38 percent was inferred by one-directional shifting. The following list of steps describes the procedures used to obtain this value:

- Based on the manufacturer’s information, it was inferred that the SR geogrid data published are equivalent to data that would be obtained if the same tests were performed on the P-1 geogrid product, which is the current equivalent of the SR-55 product. In fact, the wide width strengths are similar and the manufacturer has stated that the resin and draw ratios for the P-1 and SR-55 product are the same.
- Long-term design strengths for 20°C/100-yr were estimated from the curves presented, recognizing that the published research produced creep limiting strengths based both on a maximum strain of 10 percent and creep rupture data. The values were quite similar when extrapolated to 100 yr/20°C.
- The estimated long-term design strengths for 20°C/120-yr were then divided by the short-term strengths to obtain a creep limiting strength expressed as a percentage of the short-term strength.

This information is summarized as follows:

Product	Short-term Strength (kN/m)	Long-term Design Strength (kN/m)	Long-term divided by Short-term
SR 55	55	20.5	37.3 %
SR 80	80	30.5	38.1 %
SR 110	110	42.0	38.2 %
		Average:	38%

c. Comparison Between CTL and Literature Creep Predictions

The creep limit for the P-1 geogrid from the literature was established at 38 percent of the geogrid short-term strength considering creep rupture and/or a maximum strain of 10 percent. This creep limit is for an intact P-1 geogrid.

By comparison the UCTL results using the Popelar shifting method are consisted and without an abnormal amount of data scatter ($r = 0.907$) as shown on figure 8.9, while the RPM results based primarily on the high temperature creep-rupture data are somewhat less reliable, although reasonable (see figure 8.6).

It was therefore concluded that for this intact geogrid creep-rupture data conventionally obtained *defines a creep limiting or stress cracking strength*. By contrast NCTL predictions appear less reliable. The Popelar shifted data exhibits significant amount of scatter as evidence by the correlation coefficients shown on figure 8.7. The RPM developed results based primarily on the two higher temperature tested appears more credible as shown on figure 8.3.

It was therefore concluded that the RPM predictions appear to be more valid in assessing the significance of NCTL testing.

d. Significance of NCTL Testing

No studies have been performed to date to establish the creep limiting or stress cracking strength of damaged geogrids. NCTL testing is a first attempt at modeling extreme damage under the most severe controlled laboratory conditions and developing a potential interpretation procedure useful to the design engineer.

It should be understood that it is highly unlikely that severe damage will uniformly occur at every node during construction reflecting the reduced strength levels indicated by NCTL testing. Furthermore, it should be pointed out that even if a significant notch occurs during construction at a node, or locations which accelerate stress rupture, the rupture would not constitute a failure of the "whole" product, which is roll-width wide and functions in concert with its adjoining section, especially in soil reinforcement applications.

A possible interpretation of the significance of NCTL results is suggested by reviewing the current procedure for obtaining an allowable design load (T_a) for geogrid soil reinforcing elements in retaining wall design contained in AASHTO. Under the AASHTO procedure the creep limiting strength is reduced by reduction factors (RF) which assess the effects of construction damage, long term aging losses due to oxidation and an overall factor of safety (FS) of 1.5. Based on data developed by FHWA for a P-1 type geogrid, the construction damage reduction factor (RF_{ID}) can vary from 1.1 to 1.45 and the aging reducing factor (RF_D) is 1.1.⁽²⁹⁾

Application of this criteria results in an allowable design strength level of 16 to 21 percent of the reference short term strength, the lower strength level associated with the greatest measured level of construction damage.

The above would suggest that if the 100 yr/20°C NCTL strength level is at least equal to the minimum allowable design strength (T_a), the *possibility of stress cracking failure is statistically remote* considering that the NCTL strength level is based on continuous damage over the total length of the nodes in the width of geogrid used. For NCTL strength levels significantly lower than the design allowable strength, significant additional testing and development is necessary to define a minimum NCTL strength level. This was not achieved in this program.

Based on the proposed interpretation procedure and data obtained, it is preliminary concluded that the P-1 geogrid is not affected by potential stress cracking at the nodes or ribs, unless extremely coarse angular fill is used as backfill. The beneficial effect of drawing the geogrid has been indicated.

The comparison between creep limits and limits predicted from CTL tests is summarized in table 11.

Table 11. Long-term Performance Strength Levels at 20°C.

Failure Mechanism	Strength Level
Stress cracking of intact geogrid	39 to 43+ %
Creep limit of intact geogrid	38%
Design allowable strength, T_a	16 to 21 %
Stress cracking of geogrid notched in the nodes	18% ⁽¹⁾

¹ Strength limit determined using the RPM.

e. Conclusions

The following shortcomings in this research program should be considered to temper the conclusions for design presented:

1. As presented, adequate 50°C P-1 geogrid brittle zone data for developing 50°C brittle trends were not obtained. Rather, for the UCTL P-1 results, a *conservative* 50°C brittle zone window was assumed. This assumed, conservative, 50°C UCTL brittle zone window was used in the RPM calculations.

2. A testing temperature of 80°C appears too high.
3. No scientifically planned, statistical study of repeatability was included in the scope of work or performed in this research program.
4. Not enough specimens (i.e., three) were tested at each strength level to always meet ASTM D 5397 requirements.
5. The specific conclusions developed for the P-1 geogrid should be considered preliminary in light of the testing shortcomings outlined above.
6. NCLT testing can be used to compare geogrid performance and as a QA procedure.

Conclusions for Design

The following conclusions have been drawn on the basis of the developed data:

1. It has been demonstrated that stress cracking is a potential failure mode for HDPE uniaxially drawn geogrids at their nodes. Rib damage does not initiate stress cracking.
2. It has been demonstrated that stress cracking is a less stringent or equal consideration than creep for intact geogrids. Therefore, no NCLT testing is indicated for allowable strength determinations.
3. The potential for stress cracking in severely damaged geogrids has been demonstrated at load levels lower than inferred by the material creep limit. A preliminary interpretation procedure has been proposed.
4. Damage to geogrids can be significantly limited by using backfills with a maximum size on the order of 20 mm.⁽²⁶⁾ The resulting more limited damage is unlikely to reduce the allowable strength from stress cracking considerations to the levels indicated by NCLT testing.

8.5 CLOSURE OF THE RESEARCH PROGRAM

The primary objectives of this research program were achieved:

- a methodology for stress crack testing of HDPE geogrids was developed and is presented in chapters 5 and 6;
- strength rupture testing of resins and P-1 geogrid was completed and provided the observations and data necessary for understanding failure mechanisms and obtaining experimental strength rupture data, as presented in chapter 7;
- 20°C, 100-yr predictions based on the experimental data were made for the P-1 geogrid product only; and
- an interpretation procedure based on NCTL testing has been proposed.

The predictions presented in chapter 8 achieve the ultimate purpose of this research program which was to propose a strength level that could be used by engineers as a design parameter to preclude stress cracking failures in undamaged, uniaxially drawn, HDPE P-1 geogrid.

Although the objectives were achieved and far more testing than planned was conducted, it appears in retrospect that more testing would have been useful. For example, testing a larger number of geogrid specimens at 50°C and at low strength levels for 2 or 3 years would have been beneficial, though adequate 50°C data were obtained to provide for a conservative extrapolation to 20°C. Also, obtaining at least one reliable 20°C brittle point for the geogrid would have been beneficial, although the required testing time may not be realistic.

During the application of Popelar et al. shifting to the CTL geogrid data, an apparent inadequacy in the type of function or in the type of coefficient used in Popelar et al. shifting was suggested by incompletely merged master curves. It is suggested that further critical analysis of Popelar et al. shifting as it can be applied to highly drawn HDPE geogrid material should be performed.

The work presented in this report is believed to be useful to engineers since it provides a clear and simple design recommendation, and it should be useful to researchers because it provides a detailed documentation of experimental methods, observations, and results.

REFERENCES

1. ASTM D 883-90, "Standard Definitions of Terms Relating to Plastics," *1991 Annual Book of ASTM Standards*, Volume 08.01, Plastics (I), pp. 324-336.
2. Levinson, I.J., *Statics and Strength of Materials*, Prentice-Hall, Inc., Englewood Cliffs, NJ, 1971, pp. 161, 461-470.
3. Collins, J.A., *Failure of Materials in Mechanical Design*, John Wiley & Sons, Inc., New York, NY, 1993, pp. 1-53.
4. ASTM D 5397-93, "Standard Test Method for Evaluation of Stress Crack Resistance of Polyolefin Geomembranes Using Notched Constant Tensile Load Test," Edition approved April 15, 1993, pp. 1-4.
5. Mandelkern, L., "The Crystalline State," Chapter 4 in *Physical Properties of Polymers*, Second Edition, Mark, Eisenberg, Graessley, Mandelkern, Samulski, Koenig, and Wignall, American Chemical Society, Washington, DC, 1993, pp. 145-200.
6. Bourgeois, R. and Blacket, P., "HMW-High-Density Polyethylene," *Modern Plastics Encyclopedia*, ed. Rosalind Juran, McGraw-Hill, Inc., New York, NY, 1989, Vol. 66, No. 11, pp. 75-76.
7. Plastic Pipe Institute (PPI), "Engineering Properties of Polyethylene," Chapter 3 of *Handbook of Polyethylene Pipe*, PPI, Washington, DC, 1993, pp. 3-1 - 3-25.
8. Apse, J.I., "Polyethylene Resins for Geomembrane Applications," *Durability and Aging of Geosynthetics*, ed. R.M. Koerner, Elsevier Applied Science, London, England, 1989, pp. 159-176.
9. ASTM D 1248-84, "Standard Specification for Polyethylene Plastics Molding and Extrusion Materials," *1986 Annual Book of ASTM Standards*, Volume 08.04, Plastic Pipe and Building Products, pp. 38-47.
10. ASTM D 5262-92, "Standard Test Method for Evaluating the Unconfined Tension Creep Behavior of Geosynthetics," *ASTM Standards of Geosynthetics*, Third Edition, 1993, pp. 104-109.
11. Segrestin, P. and Jailloux, J-M., "Temperature in Soils and its Effect on the Aging of Synthetic Materials," *Geotextiles and Geomembranes*, Elsevier Science Publishers, England, 1988, Vol. 7, pp. 51-69.
12. Nagy, F.A., Personal Communication, 1996.

13. Giroud, J.P., "Relationship Between Geomembrane Density and Carbon Black Content," *Geosynthetics International*, 1994, Vol. 1, No. 1, pp. 93-98.
14. Hsuan, Y.G., Koerner, R.M., and Lord, A.E., Jr., "*Stress Cracking Behavior of HDPE Geomembranes and Its Prevention*," Cooperative Agreement No. CR-815692, Municipal Solid Waste and Residuals Management Branch Waste Minimization, Destruction and Disposal Research Division, U.S. Environmental Protection Agency, Cincinnati, OH, June 24, 1993.
15. Lu, X. and Brown, N., "The Transition from Ductile to Slow Crack Growth Failure in a Copolymer of Polyethylene," *Journal of Material Science*, Vol. 25, 1990.
16. Popelar, C.H., Kenner, V.H., and Wooster, J.P., "An Accelerated Method for Establishing the Long Term Performance of Polyethylene Gas Pipe Materials," *Polymer Engineering and Science*, Vol. 31, No. 24, Dec. 1991, pp. 1693-1700.
17. Popelar, C.F., Popelar C.H., and Kenner, V.H., "Viscoelastic Material Characterization and Modeling for Polyethylene," *Polymer Engineering and Science*, Vol. 30, No. 10, May 1990, pp. 577-586.
18. Gruenwald, G., *Plastics: How Structure Determines Properties*, Hanser Publishers, Munich, 1993, p. 97.
19. Ward, A.L., Lu, X. and Brown, N., "Accelerated Test for Evaluating Slow Crack Growth of Polyethylene Copolymers in Igepal and Air," *Polymer Engineering and Science*, Vol. 30, Sept. 1990, No. 18, pp. 1175-1179.
20. Bragaw, C.G., "Service Rating of Polyethylene Piping Systems by the Rate Process Method," *Eighth Plastic Fuel Gas Pipe Symposium*, 1983, pp. 40-47.
21. Lord, A.E., Jr. and Halse, Y.H., "Polymer Durability - The Materials Aspects," *Durability and Aging of Geosynthetics*, ed. R.M. Koerner, Elsevier Applied Science, London, England, 1989, pp. 293-329.
22. Popelar, C.H., "A Comparison of the Rate Process Method and the Bidirectional Shifting Method," *Proceedings of the Thirteenth International Plastic Fuel Gas Pipe Symposium*, American Gas Association, San Antonio, Texas, 1993, pp. 151-161.
23. Halse, Y.H., Lord, A.E., Jr., and Koerner, R.M., "Ductile-to-Brittle Transition Time in Polyethylene Geomembrane Sheet," *Geosynthetic Testing for Waste Containment Application*, ASTM STP 1081, ed. R.M. Koerner, American Society for Testing and Materials, Philadelphia, 1990.
24. Popelar, C.H., Personal Communication, 1997.

23. Halse, Y.H., Lord, A.E., Jr., and Koerner, R.M., "Ductile-to-Brittle Transition Time in Polyethylene Geomembrane Sheet," *Geosynthetic Testing for Waste Containment Application*, ASTM STP 1081, ed. R.M. Koerner, American Society for Testing and Materials, Philadelphia, 1990.
24. Popelar, C.H., Personal Communication, 1997.
25. Bush, D.I., "Variation of Long Term Design Strength of Geosynthetics in Temperatures up to 40°C," *Proceedings of the Fourth International Conference on Geotextiles, Geomembranes and Related Products*, Den Hoedt (ed.), The Hague, The Netherlands, Balkema, Rotterdam, 1990, pp. 673-676.
26. Koerner, G.R., Koerner, R.M., and Elias, V., "Geosynthetic Installation Damage Under Two Different Backfill Conditions," *Geosynthetic Soil Reinforcement Testing Procedures*, ASTM STP 1190, ed. S.C. Jonathan Cheng, American Society for Testing and Materials, Philadelphia, 1993, pp. 163-183.
27. Carlson, D.S., Charron, R.M., Winfree, J.P., Giroud, J.P., and McLearn, M.E., "Laboratory Evaluation of HDPE Geomembrane Seams," *Proceedings of Geosynthetics '93*, Vol. III, 1993, pp. 1543-1557.
28. Ingold, T.S., Montanelly, F., and Rimoldi, P., "Extrapolation Techniques for Long Term Strength of Polymeric Geogrids," *Proceedings of the Fifth International Conference on Geosynthetics*, Singapore 1994.
29. Elias, V. "Corrosion/Degradation of Soil Reinforcements for Mechanically Stabilized Earth Walls and Reinforced Soil Slopes," FHWA-SA-96-072, Washington, D.C. 1997.

GLOSSARY

To provide the reader with a clear understanding of the information presented in this report, a number of terms used to describe material behavior require definition. To this end, definitions for these terms, which appear throughout the text, are presented.

arresting zone: the narrow zone occurring between oriented center node material and much less oriented side node material. In this report, this zone is identified as a zone of rapidly changing molecular orientation.

bidirectional shifting: a visual or mathematical procedure for repositioning one or more plotted sets of data points by moving all data points in a set by a uniform quantity horizontally and by another uniform quantity vertically. One purpose of bidirectional shifting is to create a master curve that can be used to predict material behavior at times or conditions for which no testing was performed.

brittle fracture: the terminal condition of a specimen that has experienced stress - cracking or rapid crack propagation (RCP) without appreciable (i.e., visually obvious) prior plastic deformation. “Quasi-brittle” fracture in HDPE is produced by stress cracking (slow crackgrowth) and is characterized by plastic deformation on a microscopic level (i.e., not visually obvious). “Truly brittle” fracture in HDPE is produced by RCP and is characterized by smooth glass-like fracture faces. In this report, use of the term “brittle” refers to quasi-brittle fracture or rupture processes in HDPE.

brittle rupture: a mode of failure resulting in brittle fracture along with the separation of the specimen into two pieces.

center node material: the portion of the node crossbar that is collinear with the adjoining ribs.

constant tensile load (CTL): a laboratory test in which a force of constant magnitude and direction is continuously applied to one end of an anchored specimen, which force is intended to produce stretching or rupture in the specimen’s gauge length. In this report, the term CTL is used in a generic sense to encompass notched constant tensile load (NCTL) and unnotched constant tensile load (UCTL) testing.

cracking: the result of fracture extension due to mechanical failure by stress, which then produces two new surfaces (i.e., complete material separation). Cracking also is referred to as fracturing in this report.

crazing: a process of quasi-brittle fracture extension (i.e., stress cracking) due to mechanical failure by stress, producing small-scale yielding at a stress raiser such as a notch point or crack tip. A craze is denoted when: “the plastic zone size remains small compared with the dimensions of the crack.” Crazing may refer to the growth of a single craze or of a network of crazes. When a craze widens so much that the small-scale-yielded material begins to break, a relatively large void is left; thus a “crack” is said to have formed. A craze can thus be seen as the precursor of a crack. In a craze, there is no complete material separation.

creep: 1. The time-dependent part of strain resulting from stress.⁽¹⁾ 2. The flow of plastic deformation held for long periods of time at stresses lower than the normal yield strength.⁽²⁾

creep load limit: a maximum allowable load, selected by an engineer, intended to preclude creep rupture failure(s) in a given width of a material under specified design conditions. In this research program, creep load limits commonly specified for the P-1 geogrid product will be compared with the 100-yr/20°C predictions made from the UCTL P-1 geogrid test results.

ductile fracture: the terminal condition of a specimen that has experienced extensive plastic deformation.⁽³⁾ A ductile fracture in polyethylene is characterized by obvious plastic deformation. The material appears to stretch until it breaks. The resulting final cross-section is smaller than the original cross-sectional area.

ductile rupture: a mode of failure occurring when plastic deformation in a yielding specimen leads to the separation of the specimen into two pieces.⁽³⁾

environmental stress cracking (ESC): a stress cracking mode of failure that is accelerated due to the presence of a chemical environment.

fibrous: As used in this report, fibrous is defined by the appearance of elongated or ruptured geogrid material, characterized by clumps of loosened fiber-like splinters and by rupture in shear along planes running parallel to the direction of fiber alignment. It is noted that the degree of fibrous appearance provides one of the means for qualitative comparison of the degree of orientation between rib, transition, and node material.

fracture: the terminal condition of a specimen following a history of prior plastic deformation; generally characterized as being either brittle or ductile.⁽³⁾ The term fracture implies sufficient material separation to create two (new) surfaces in the material; it does not necessarily indicate complete separation of the bulk material into two pieces.

high-density polyethylene (HDPE): 1. a semicrystalline polyethylene material consisting of two phases: crystalline and amorphous. “In the crystalline phase, polyethylene molecules are packed into organized plates also called lamellae. Adjacent lamellae are held together by the amorphous phase, consisting of tie molecules, which include: (1) polyethylene molecules that extend from one lamella to another; and (2) physically entangled molecules that extend out of adjacent lamellae but that do not extend from one lamellae.” 2. those linear polyethylene plastics, g.v., having a standard density of 0.941 g/cm³ or greater.⁽¹⁾

Igepal CO-630: 100 percent nonylphenoxy poly(ethylene-oxy) ethanol, manufactured by General Aniline Film (GAF) Corporation. Igepal CO-630, diluted to 10 percent and maintained at 50°C, is the standard bath required in ASTM D 5397-93, titled *Notched Constant Tensile Load (NCTL) Testing for HDPE Resins*. Note: Igepal CA-720 is a similar surfactant used for testing at 70°C or 80°C when testing in Igepal is called for.

knee: one of three characteristic shapes of a stress rupture curve, consisting of two linear portions (with different slopes) meeting at ends (i.e., intersecting) to form a “knee” profile.⁽⁴⁾

necking: the localized reduction in cross-section that may occur in a material under tensile stress.⁽¹⁾

node: the non-elongated, much less oriented, crossbar zone of oriented HDPE geogrid. The material in the node generally represents the precursor sheet from which the ribs were stretched.

notch blunting: a process of notch acuity reduction due to plastic deformation (i.e., creep) between the walls of the notch. In other words, creep at the notch root blunts the notch, greatly reducing its effectiveness as a stress concentrator.

notched stress rupture test: a laboratory test intended to evaluate a material’s resistance to stress cracking (i.e., quasi-brittle fracture), employing a constant tensile load and an uniform stress concentrator (i.e., a notch). This test also is referred to as Notched Constant Tensile Load (NCTL) test. The notch is intended to induce a plane strain condition, which thus promotes crazing initiation and propagation through the material.

polyolefin: a polymer prepared by the polymerization of an olefin(s) as the sole monomer(s).⁽¹⁾ Examples of polyolefins include: polyethylene, polypropylene, and polybutylene.

rapid crack propagation (RCP): a mode of failure occurring in a thermoplastic material by rapid crack extension, resulting in the truly brittle (i.e., glass-like) fracture of the material. Rapid crack propagation is characterized by crack growth speeds on the order of hundreds of feet per second.⁽³⁾

resin: a solid or pseudosolid organic material often of high molecular weight, which exhibits a tendency to flow when subjected to stress, usually has a softening or melting range, and usually fractures conchoidally.⁽¹⁾

rib: the elongated, highly oriented, structural member of oriented HDPE geogrid. During the geogrid manufacturing process, the material was “stretched” while at a warm temperature, and subsequently cooled in the stressed condition to form a rib.

rupture: a mode of failure characterized by the extension of a fracture completely through a specimen’s thickness, or by separation of the specimen into two pieces.

splintering: the rupture process observed in oriented HDPE geogrids characterized by a fibrous appearance and by rupture in shear along planes running parallel to the direction of orientation. This is a descriptive term used in this report.

stress cracking: a mode of failure occurring in a thermoplastic material that is under a sustained stress significantly lower than the material’s room temperature yield strength. This results in quasi-brittle fracture of the material. This is also known as slow crack growth. Stress cracking is characterized by crack growth speeds on the order of fractions of an inch per minute or per day.⁽³⁾

transition point: a point selected from a stress rupture curve at the apparent beginning (top) of the linear portion representing brittle fracture data points. Examples of transition point selection from a stress rupture curve can be found in appendix B of Standard Method GRI-GM5(a).

transition zone (the material in the area between the rib and the node): the sloping region between the rib and the node in oriented HDPE geogrid through which the degree of molecular orientation is changing from highly oriented (rib material) to much less oriented (node material).

unnotched constant tensile load (UCTL): a laboratory test intended to evaluate a product's resistance to stress cracking initiation and subsequent propagation. Unlike the NCTL test, no artificial stress raiser (i.e., notch) is employed; rather, the UCTL test challenges the stress concentration factors inherent in the normal contours and morphologies of the product.

APPENDIX A

INDEX DATA



GEOSYNTEC CONSULTANTS
Materials Testing Laboratory

RESIN "M" TEST RESULTS

CLIENT: Earth Engineering & Sciences, Inc.
CONTACT: Mr. Victor Elias
GEOSYNTEC JOB NO.: MP5548

MATERIAL: High Density Polyethylene, Plaque
CLIENT ID: Resin M
DATE TESTED: 10/26/1994

<u>INDIVIDUAL SPECIMENS</u>										<u>SUMMARY RESULTS</u>			
1	2	3	4	5	6	7	8	9	10	PROPERTY (STANDARD)	UNIT	MEAN	STD
0.9503	0.9511	0.9518	0.9513	0.9499						SPECIFIC GRAVITY (ASTM D792)	n/a	0.9509	0.00077
0.9479	0.9487	0.9494	0.9489	0.9475						DENSITY (ASTM D792)	g/cc	0.9485	0.00077
291.0	292.4	274.4	270.4	267.6						YIELD STRENGTH (ASTM D638) XD	lb/in	279.2	11.7
16.1	16.7	16.6	16.7	15.8						YIELD ELONGATION (ASTM D638) XD	%	16.4	0.41
0.129	0.123	0.128								MELT FLOW INDEX (ASTM D1238)	g/10 min	0.127	0.0032
59.7										DIFFERENTIAL SCANNING CALORIMETRY CRYSTALLINITY	%	59.7	N/A

COMMENTS:
XD= CROSS-ROLL DIRECTION
N/A = NOT APPLICABLE



GEOSYNTEC CONSULTANTS
Materials Testing Laboratory

P-1 GEOGRID TEST RESULTS

CLIENT: Earth Engineering & Sciences, Inc.
CONTACT: Mr. Victor Elias
GEOSYNTEC JOB NO.: MP5548

MATERIAL: High Density Polyethylene,
Uniaxially Drawn, Oriented Geogrid
CLIENT ID: P-1 Geogrid
DATE TESTED: 10/05/94

INDIVIDUAL SPECIMENS

	1	2	3	4	5	6	7	8	9	10
0.9660	0.9640	0.9630	0.9650	0.9650	0.9650					
0.9636	0.9616	0.9606	0.9626	0.9626						
0.075	0.078	0.084								
3811	3815	3966	3957	3986	3966					
317.6	317.9	330.5	329.8	332.2	330.5					
287.6	287.9	299.3	298.6	300.8	299.3					
38.5	38.0	39.2	39.1	38.2	36.5					
288.6	289.0	283.5	303.8	291.4	311.0	298.9	313.3	314.8	313.8	
3824	3829	3756	4025	3861	4121	3960	4151	4171	4158	
318.7	319.1	313.0	335.4	321.8	343.4	330.0	345.9	347.6	346.5	
58.7										

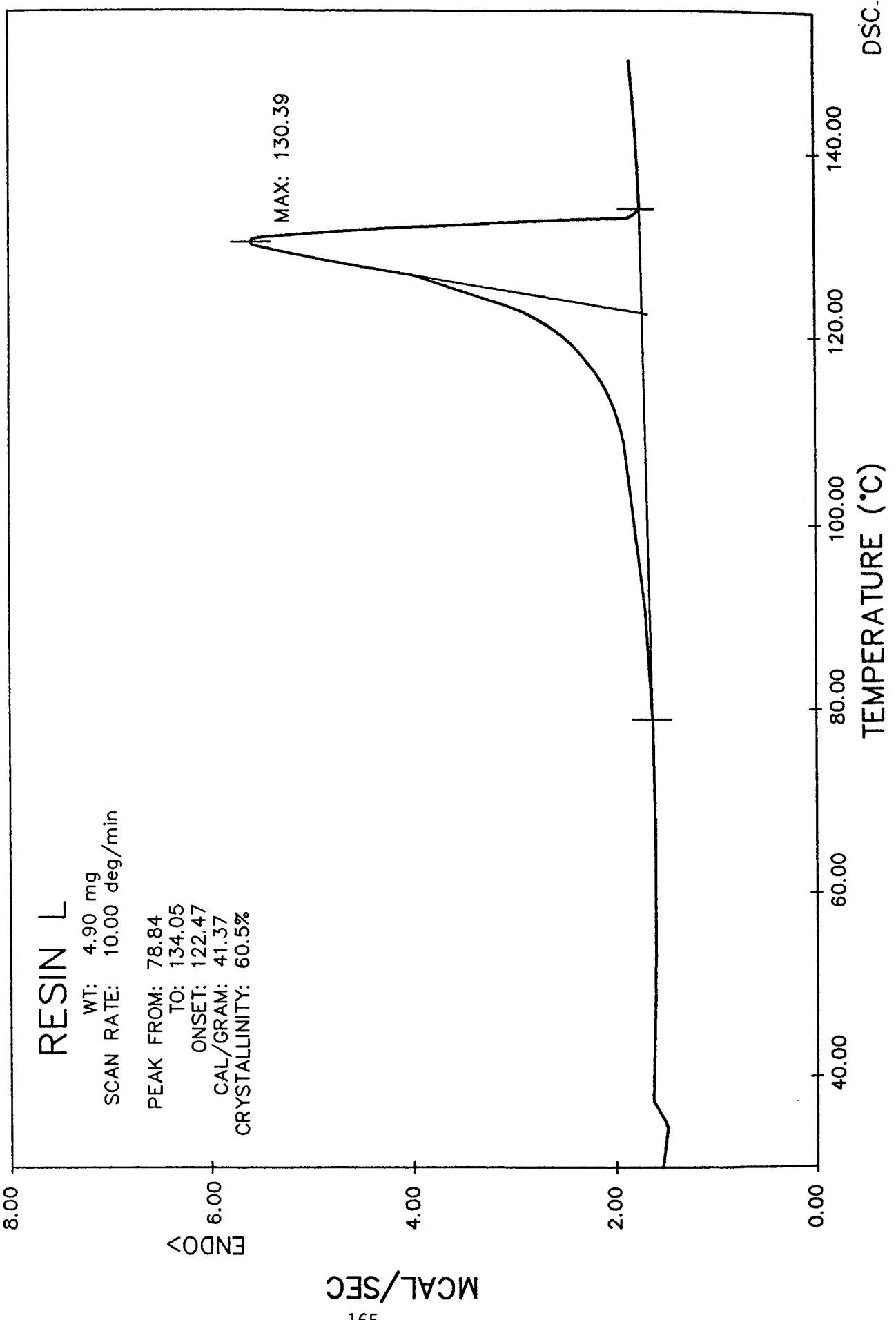
SUMMARY RESULTS

PROPERTY (STANDARD)	UNIT	MEAN	STD
SPECIFIC GRAVITY (ASTM D792)	n/a	0.9646	0.00114
DENSITY (ASTM D792)	g/cc	0.9622	0.00114
MELT FLOW INDEX (ASTM D1238)	g/10 min	0.079	0.0046
WIDE-WIDTH TENSILE PROPERTIES:			
(ASTM D4595)			
YIELD STRENGTH	lb/ft	3917	81.0
YIELD STRENGTH	lb/in.	326.4	6.75
YIELD STRENGTH	lb/rib	295.6	6.11
STRAIN @ YIELD	%	38.3	0.98
RIB TENSILE STRENGTH (GRI-GG1)			
YIELD STRENGTH	lb/rib	300.8	12.08
YIELD STRENGTH	lb/ft	3986	160
YIELD STRENGTH	lb/in	332.1	13.34
DIFFERENTIAL SCANNING CALORIMETRY			
CRYSTALLINITY	%	58.7	N/A

COMMENTS:

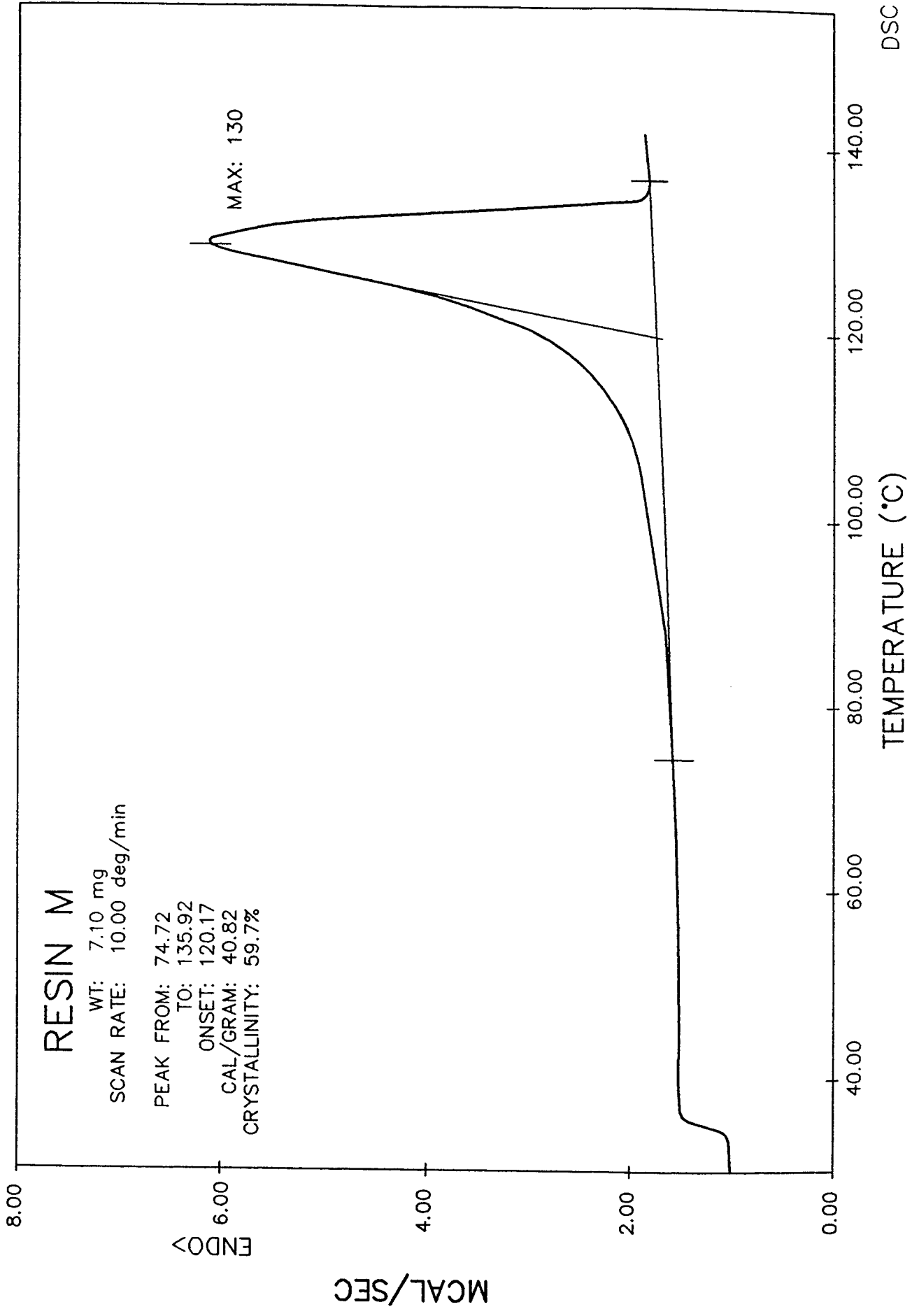
N/A = NOT APPLICABLE
Calculations used: 13.25 ribs per foot.

PROJECT: Federal Highway Administration	MATERIAL: Resin L	REPORT DATE: 9/26/96
JOB NO.: MP5548/01	TEST PARAMETERS: Scan rate = 10°C/min, in Nitrogen atmosphere.	

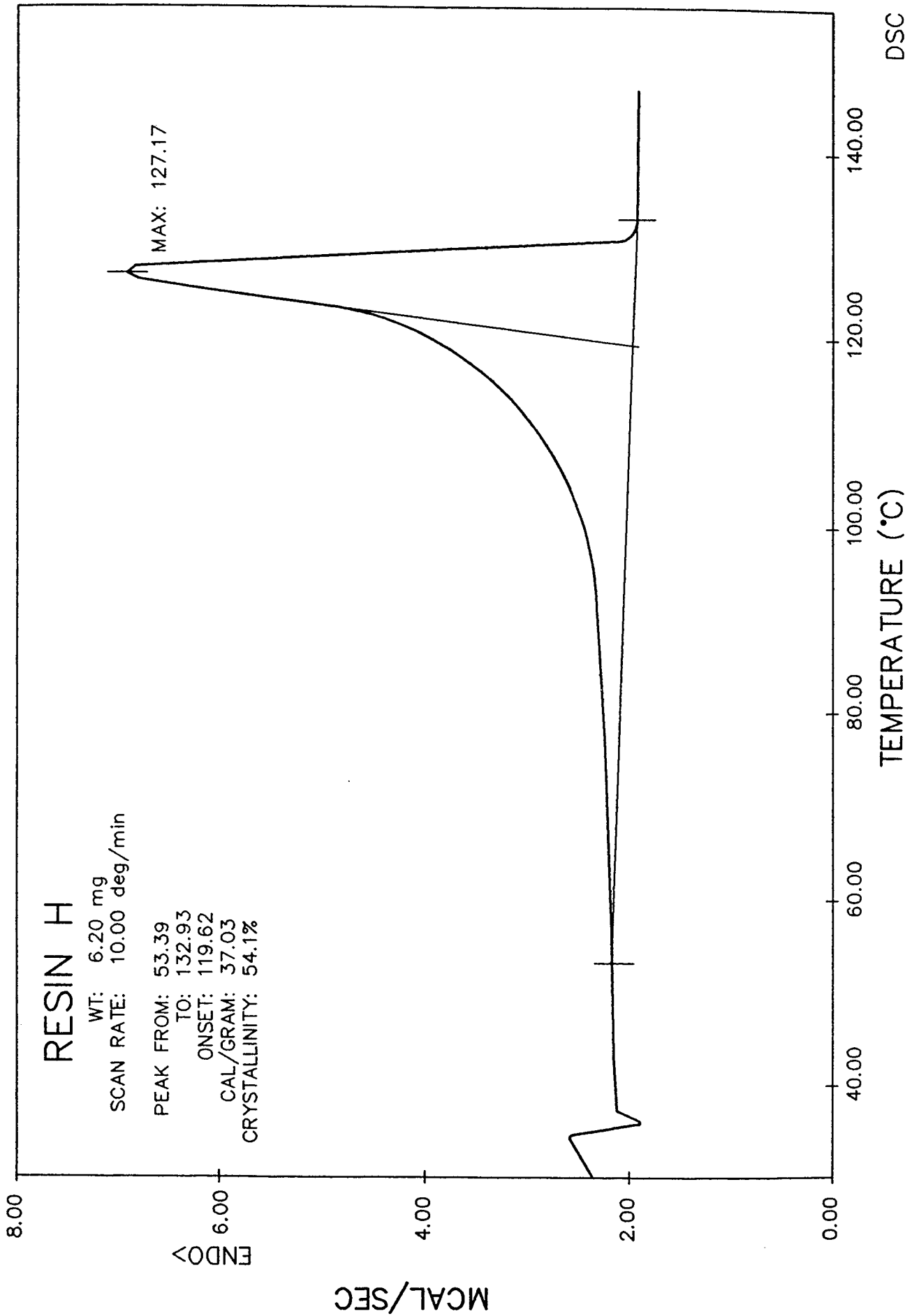


**DIFFERENTIAL SCANNING CALORIMETRY TEST
RESULTS FOR RESIN M**

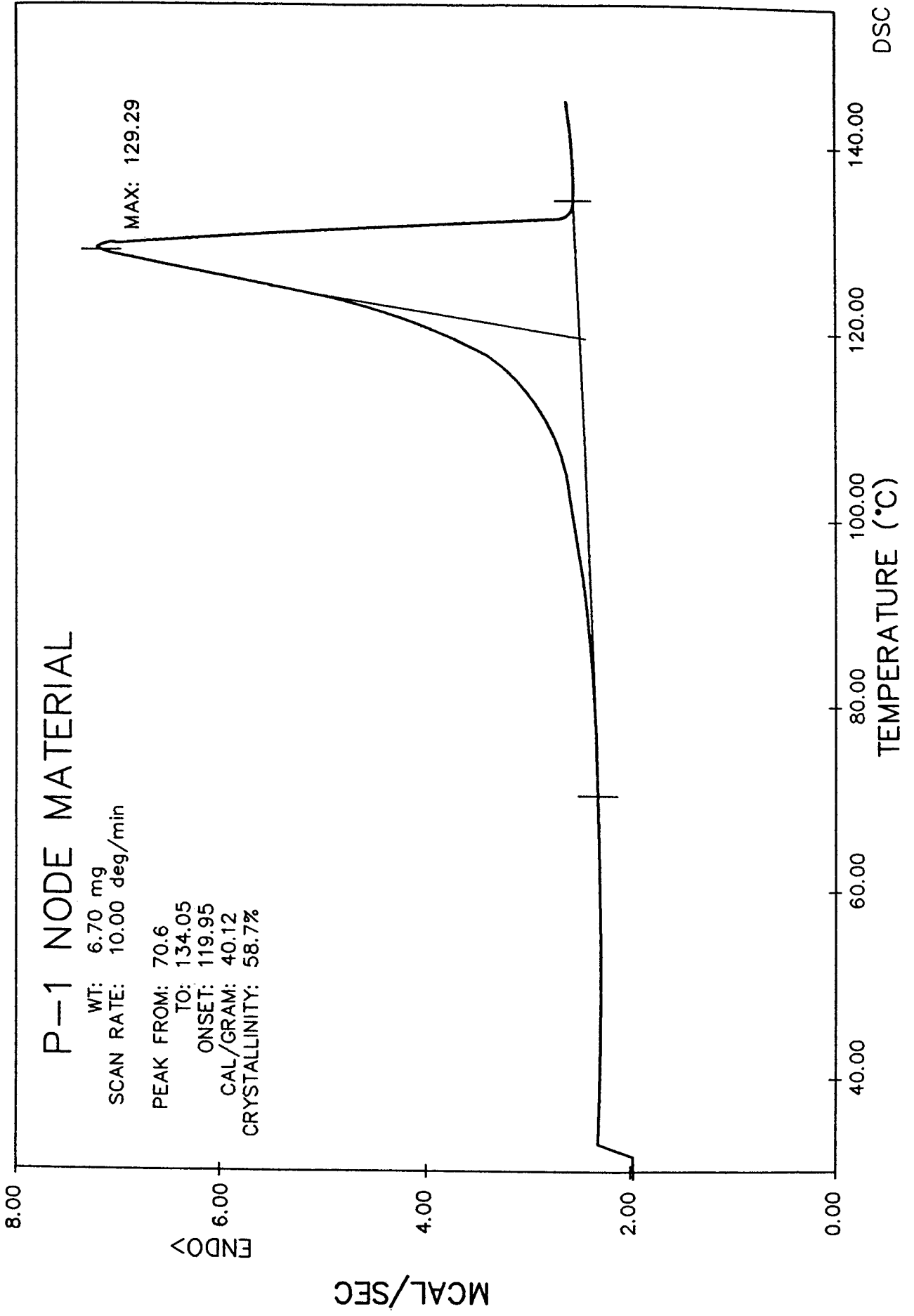
PROJECT: Federal Highway Administration	MATERIAL: Resin M	REPORT DATE: 9/26/96
JOB NO.: MP5548/01	TEST PARAMETERS: Scan rate = 10°C/min., in Nitrogen atmosphere.	



PROJECT: Federal Highway Administration	MATERIAL: Resin H	REPORT DATE: 9/26/96
JOB NO.: MP5548/01	TEST PARAMETERS: Scan rate = 10°C/min, in Nitrogen atmosphere.	



PROJECT: Federal Highway Administration	MATERIAL: P-1 Node Material	REPORT DATE: 9/26/96
JOB NO.: MP5548/03	TEST PARAMETERS: Scan rate = 10°C/min, in Nitrogen atmosphere.	



APPENDIX B

RESIN CTL DATA



GEOSYNTEC CONSULTANTS
Materials Testing Laboratory

CONSTANT TENSILE LOAD TESTS
SUMMARY REPORT: RESINS

PROJECT: Federal Highway Administration	MATERIAL: Resins L,M,H	REPORT DATE: 12/22/96
JOB NO.: MP5548 / 01	TEST PARAMETERS: 20% Notch Depth for Notched Specimens, in Water, at 50°C	

Percent of Room Temp. Yield Strength (%)	Time to Failure (hr)					
	Resin L Notched	Resin M Notched	Resin H Notched	Resin L Un-notched	Resin M Un-notched	Resin H Un-notched
6	>7940					
7.5	>4229					
9	1706	6293				
12	359.2	290.2				
15	111.0	124.6		>5093	>8689	
18	15.3	86.7		>5093	>10250	>11412
21	8.4	73.5		>5093	>10001	>11412
24	9.9	35.3		1819	>8133	>11412
27	2.2	43.0		167.2	2339	>11412
30	0.362	35.2		32.1	486.8	>11709
33	0.177	26.4	>8840	16.4	126.3	>11709
36	0.057	9.4	>7941	19.4	142.2	>11709
39	0.048	4.4		0.55	34.9	>11709
42	0.027	0.38	>7941	0.43	22.8	
45		0.22	651.1	0.45	0.81	>6026
48		0.050	288.4	0.168	0.25	1896
51			132.5			2070
54			13.2			74.5
57			0.7			39.3
60						
63			0.008			4.2
66			0.004			0.8

Notes:

* Resin L room temperature yield strength = 280.4 lb/in ;
 Resin M room temperature yield strength = 279.0 lb/in ;
 Resin H room temperature yield strength = 136.1 lb/in ;
 resin L ave. thickness = 0.0709 in ;
 resin M ave. thickness = 0.0827 in ;
 resin H ave. thickness = 0.0591 in



PROJECT: Federal Highway Administration	MATERIAL: Resin L	DATE OF REPORT: 12/22/96
JOB NUMBER: MP5548 / 01	TEST PARAMETERS: 20% Notch Depth at 50°C, In Water	

Notched Specimens

Stress (psi) ¹	311	384	460	613	765	916	1074	1218	1378	1532	1679	1838	2004	2160
Percent of Yield Strength ²	6	7.5	9	12	15	18	21	24	27	30	33	36	39	42
Specimen 1	>7940	>4229	3016	325.0	133.3	26.5	8.4	9.6	2.5	0.569	0.111	0.058	0.071	0.035
Specimen 2	>7940	>4229	395.9	260.5	88.7	12.8	8.4	10.2	1.9	0.490	0.243	0.062	0.024	0.019
Specimen 3				352.4		12.7		10.0		0.188		0.052		
Specimen 4				498.8		9.0		9.9		0.200		0.056		
Specimen 5														

Mean (hr)	>7940	1706	359.2	111.0	15.3	8.4	8.4	9.9	2.2	0.362	0.177	0.057	0.048	0.027	
S.D. (hr)	N/A	N/A	100.74	N/A	7.71	N/A	N/A	0.25	N/A	0.1964	N/A	0.0042	N/A	N/A	
	BRITTLE ZONE							TP	DUCTILE ZONE						

Notes:

- ¹ Represents an average stress.
- ² Resin L room temperature yield strength = 280.4 lb/in resin L ave. thickness = 0.0709 in
- TP = Selected Transition Point at 8.4 hr , 21 %
- L.R.A. = Linear Regression Analysis, from log (mean time) and log (percent yield strength).
- N/A = Not Applicable

Brittle Zone L.R.A.:

$m = -0.1510$
 $b = 1.4554$
 $r = -0.99068$
 $y_{100} = 3.6161 \%$

Ductile Zone L.R.A.:

$m = -0.0909$
 $b = 1.4594$
 $r = -0.98259$



GEOSYNTEC CONSULTANTS
Materials Testing Laboratory

CONSTANT TENSILE LOAD TEST AT 50°C IN WATER
RESIN M FINAL REPORT

PROJECT: Federal Highway Administration	MATERIAL: Resin M	DATE OF REPORT: 12/22/96
JOB NUMBER: MP5548 / 01	TEST PARAMETERS: 20% Notch Depth at 50°C, In Water	

Notched Specimens

Stress (psi) ¹	427	566	646	788	914	1033	1185	1335	1429	1558	1715	1880	2077	2242
Percent of Yield Strength ²	9	12	15	18	21	24	27	30	33	36	39	42	45	48
Specimen 1	6287	239.6	100.5	80.8	59.9	48.7	43.6	27.0	26.8	9.7	4.6	0.3	0.28	0.043
Specimen 2	6298	340.7	148.7	61.9	80.8	25.7	38.8	41.0	38.6	9.4	4.1	0.48	0.15	0.056
Specimen 3				92.5	79.8	32.2	43.1	32.4	25.0	7.6		0.36		
Specimen 4				103.8		33.3	37.2	40.2	24.5	11.3				
Specimen 5				94.5		36.8	52.2	35.5	17.0	8.8				
Mean (hr)	6293	290.2	124.6	86.7	73.5	35.3	43.0	35.2	26.4	9.4	4.4	0.38	0.22	0.050
S.D. (hr)	N/A	N/A	N/A	16.10	11.79	8.48	5.84	5.78	7.79	1.35	N/A	0.092	N/A	N/A
BRITTLE ZONE							TP	DUCTILE ZONE						

Notes:

¹ Represents an average stress.

² Resin M room temperature yield strength = 279.0 lb/in
resin M ave. thickness = 0.0827 in

TP = Selected Transition Point at 35.3 hr , 24 %

L.R.A. = Linear Regression Analysis,

from log (mean time) and log (percent yield strength).

N/A = Not Applicable

Brittle Zone L.R.A.:

m = -0.1681
b = 1.5662
r = -0.92267
y₁₀₀ = 3.6945 %

Ductile Zone L.R.A.:

m = -0.0565
b = 1.6101
r = -0.98416



GEOSYNTEC CONSULTANTS
Materials Testing Laboratory

CONSTANT TENSILE LOAD TEST AT 50°C IN WATER
RESIN H FINAL REPORT

PROJECT: Federal Highway Administration	MATERIAL: Resin H	DATE OF REPORT: 12/22/96
JOB NUMBER: MP5548/01	TEST PARAMETERS: 20% Notch Depth at 50°C, in Water	

Notched Specimens

Stress (psi) ¹	916	959	1153	1303	1384	1495	1563	1669	1843	1946
Percent of Yield Strength ²	30	36	42	45	48	51	54	57	60	66
Specimen 1	>9738	>7941	>7941	605.0	108.3	242.8	20.4	0.7	0.008	0.004
Specimen 2	>7941		>7941	697.2	244.1	22.2	22.2			0.004
Specimen 3					512.7		3.3			
Specimen 4							6.8			
Specimen 5										

Mean (hr)	>8840	>7941	>7941	651.1	288.4	132.5	13.2	0.7	0.008	0.004
S.D. (hr)	N/A	N/A	N/A	65.20	205.80	N/A	9.52	N/A	N/A	N/A

DUCTILE ZONE

Notes:

- ¹ Represents an average stress.
- ² Resin H room temperature yield strength = 136.1 lb/in resin H ave. thickness = 0.0591 in
No brittle fractures were obtained.
- L.R.A. = Linear Regression Analysis, from log (mean time) and log (percent yield strength).
- N/A = Not Applicable

Ductile Zone L.R.A.:

$$m = -0.0284$$

$$b = 1.7504$$

$$r = -0.98470$$



GEOSYNTEC CONSULTANTS
Materials Testing Laboratory

CONSTANT TENSILE LOAD TEST AT 50°C IN WATER
RESIN L FINAL REPORT

PROJECT: Federal Highway Administration	MATERIAL: Resin L	DATE OF REPORT: 12/22/96
JOB NUMBER: MP5548 / 01	TEST PARAMETERS: 50°C, In Water	

Un-notched Specimens

Stress (psi) ¹	604	722	846	975	1101	1226	1340	1465	1573	1702	1834	1964
Percent of Yield Strength ²	15	18	21	24	27	30	33	36	39	42	45	48
Specimen 1	>5093	>5093	>5093	1193	218.3	64.6	16.7	5.3	0.5	0.5	0.4	0.111
Specimen 2	>5093	>5093	>5093	1839	116.0	18.0	16.1	19.0	0.6	0.318	0.5	0.224
Specimen 3				2838		22.2		12.0		0.4		
Specimen 4				1406		23.5		30.4		0.5		
Specimen 5								30.5				
Mean (hr)	>5093	>5093	>5093	1819	167.2	32.1	16.4	19.4	0.55	0.43	0.45	0.168
S.D. (hr)	N/A	N/A	N/A	730.7	N/A	21.81	N/A	11.16	N/A	0.09	N/A	N/A
	BRITTLE ZONE						TP	DUCTILE ZONE "B"				
								IP				
								DUCTILE ZONE "A"				

Notes:

¹ Represents an average stress.

² Resin L room temperature yield strength = 280.4 lb/in

resin L ave. thickness = 0.0709 in

TP = Selected Transition Point at 16.4 hr , 33 %

IP = Identifying Point at 0.55 hr , 39 %

L.R.A. = Linear Regression Analysis,

from log (mean time) and log (percent yield strength).

N/A = Not Applicable

Brittle Zone L.R.A.:

m = -0.0589
b = 1.5652
r = -0.99626
y₁₀₀ = 16.4200 %

Ductile Zone "B" L.R.A.:

m = -0.0225
b = 1.5852
r = -1

Ductile Zone "A" L.R.A.:

m = -0.0655
b = 1.6305
r = -1



PROJECT: Federal Highway Administration	MATERIAL: Resin H	DATE OF REPORT: 12/22/96
JOB NUMBER: MP5548 / 01	TEST PARAMETERS: 50°C, in Water	

Un-notched Specimens

Stress (psi) ¹	413	496	568	636	705	783	842	919	1023	1104	1205	1242	1317	1462	1541
Percent of Yield Strength ²	18	21	24	27	30	33	36	39	42	45	48	54	57	63	66
Specimen 1	>11710	>11709	>11710	>11709	>11709	>11709	>11709	>11709		3959	2830	41.8	42.1	4.2	1.0
Specimen 2	>11115	>11115	>11115	>11115						>8093	961.5	150.5	36.5		0.6
Specimen 3												67.8			
Specimen 4												51.9			
Specimen 5												60.3			
Mean (hr)	>11412	>11412	>11412	>11412	>11709	>11709	>11709	>11709		>6026	1896	74.5	39.3	4.2	0.8
S.D. (hr)	N/A		N/A	1321.1	43.60	N/A	N/A	N/A							

DUCTILE ZONE

Notes:

- ¹ Represents an average stress.
- ² Resin H room temperature yield strength = 136.1 lb/in resin H ave. thickness = 0.0591 in
No brittle fractures were obtained.
- L.R.A. = Linear Regression Analysis, from log (mean time) and log (percent yield strength).
- N/A = Not Applicable

Ductile Zone L.R.A.:

$$m = -0.0398$$

$$b = 1.8179$$

$$r = -0.98192$$

APPENDIX C

P-1 GEOGRID CTL DATA



PROJECT: Federal Highway Administration	MATERIAL: P-1 Geogrid	REPORT DATE: 2/3/97
JOB NO.: MP5548 / 03	TEST PARAMETERS: 20% Notch Depth for Notched Specimens, in water	

Notched Specimens

Percent of Room Temp. Yield Strength ^{1,2} (%)	Time to Failure (hr)		
	50°C	65°C	80°C
3.98	>12474	>5958	>11038
4.78			1260
5.57	>12474	>10655	153.7
7.17	4072	1354	47.2
8.76	>2332	145.3	40.0
10.35	917.6	130.6	29.5
11.94	416.9	66.4	22.5
13.53	381.4	94.7	24.5
15.13	257.8	83.5	23.5
16.72	187.0	99.8	21.1
18.31	184.7	95.3	25.7
19.90	206.7	104.2	45.5
22.29	118.8	186.4	51.6
24.68	143.5		68.2
27.07	211.1		7.4
29.46	259.2	87.9	4.3
31.85	181.9		
34.23	58.9	7.9	
36.62	42.3		

Un-Notched Specimens

Percent of Room Temp. Yield Strength ^{1,2} (%)	Time to Failure (hr)		
	50°C	65°C	80°C
5.00		>12957	>13010
7.00	>12936	>12957	>13055
9.00	>12937	>12958	>13055
11.00	>12937	>12958	>13054
13.00	>12937	>12957	7131
15.00	>12937	>12956	3060
17.00	>12938	>12940	2590
19.31	>12937	>6299	2188
21.41	>12937	2005	1304
23.22	>12936	>4015	351.2
25.00	>12937	1213	323.9
28.05	>10739	602.1	78.3
31.23	>7500	248.8	7.9
34.17	472.3	96.3	7.7
37.24	235.1	36.3	2.9
41.09	112.9	3.7	0.50
43.89	81.8		
48.12	39.7		
50.82	13.2		

Notes:

¹ P-1 Geogrid room temp. yield strength = 332.1 lb/in (= 3,986 lb/ft, = 300.8 lb/rib).

² Represents an approximate average yield strength.



CONSTANT TENSILE LOAD TEST AT 50°C IN WATER
P-1 GEOGRID SPECIMEN FINAL REPORT

PROJECT: Federal Highway Administration	MATERIAL: P-1 Geogrid	DATE OF REPORT: 12/22/96
JOB NUMBER: MP5548 / 03	TEST PARAMETERS: 20% Notch Depth, at 50°C, in Water	

Notched Specimens

	200	280	360	440	520	600	680	760	840	920	1000	1120	1240	1360	1480	1600	1600	1720	1840	
Stress (psi)																				
Percent of Yield Strength^{1,2}	3.93	5.55	7.18	8.83	10.34	12.03	13.58	15.29	16.87	18.38	20.04	22.47	25.17	27.48	29.98	32.02	33.29	34.76	37.30	
Specimen 1	>12474	>12474	6886	551.4	325.9	265.1	217.5	181.5	114.5	178.1	215.0	124.0	96.9	211.3	259.5	257.5	73.5	66.3	42.4	
Specimen 2			1259	566.7	325.9	345.5	178.3	215.5	259.4	182.8	198.3	134.1	190.1	207.4	258.8	156.3		51.5	42.1	
Specimen 3				>5878	1384	426.1	490.2	272.0		192.6		124.0		210.1		191.3				
Specimen 4					1389	403.3	569.2	232.9		184.9		105.9		215.5		230.8				
Specimen 5					1163	644.4	451.7	387.2		184.9		106.2								

BRITTLE ZONE

	>12474	N/A	N/A	N/A	917.6	416.9	381.4	257.8	187.0	184.7	206.7	118.8	143.5	211.1	259.2	209.0	73.5	58.9	42.3	
Mean (hr)																				
S.D. (hr)																				

TP

DUCTILE ZONE

Notes:

- ¹ P-1 Geogrid room temp. yield strength = 332.1 lb/in (= 3,986 lb/ft , = 300.8 lb/rib)
- ² Represents an average yield strength.
- TP = Selected Transition Point at 187.0 hr , 16.87 % L.R.A. = Linear Regression Analysis, from log (mean time) and log (mean yield strength).
- * Large degree of data scatter for the brittle zone points prevented development of a clear brittle trend.

N/A = Not Applicable

Brittle Zone L.R.A.: ³
not determined ³

Ductile Zone L.R.A.:

m = -0.0971
b = 1.7176
r = -0.94220



PROJECT: Federal Highway Administration	MATERIAL: P-1 Geogrid	DATE OF REPORT: 12/22/96
JOB NUMBER: MF5548 / 03	TEST PARAMETERS: 20% Notch Depth, at 65°C, in Water	

Notched Specimens

Stress (psi)	200	280	360	440	520	600	680	760	840	920	1000	1120	1480	1720
Percent of Yield Strength ^{1,2}	3.95	5.61	7.22	8.79	10.55	12.11	13.69	15.19	16.91	18.47	20.11	22.54	29.57	33.60
Specimen 1	3489	>12357	1354	140.2	60.6	54.7	57.6	71.8	98.5	84.8	93.2	180.8	87.0	7.7
Specimen 2	>8426	>8954		163.7	200.6	70.7	107.6	70.9	101.1	69.1	115.2	192.0	87.9	8.1
Specimen 3				129.7		66.6	93.5	75.4		69.7			88.8	
Specimen 4				178.0		69.8	120.2	93.3		117.7				
Specimen 5				115.1		70.0		106.0		115.5				
Extra Spec.										114.7				
Mean (hr)	>5958	>10655	1354	145.3	130.6	66.4	94.7	83.5	99.8	95.3	104.2	186.4	87.9	7.9
S.D. (hr)	N/A	N/A	N/A	25.44	N/A	6.71	27.05	15.52	N/A	23.40	N/A	N/A	0.90	0.28

BRITTLE ZONE TP DUCTILE ZONE

Notes:

- P-1 Geogrid room temp. yield strength = 332.1 lb/in
(= 3,986 lb/ft , = 300.8 lb/rib)
- Represents an average yield strength.
- TP = Selected Transition Point at 66.4 hr , 12.11 %
L.R.A. = Linear Regression Analysis,
from log (mean time) and log (mean yield strength).
- Interpretation of brittle zone, using points :
(145.3, 8.79) , (1354, 7.3) , and (10655, 6).
N/A = Not Applicable

Brittle Zone L.R.A.:

$m = -0.0888$
 $b = 1.1378$
 $r = -0.99926$
 $y_{100} = 4.0738 \%$

Ductile Zone L.R.A.:

$m = -0.1084$
 $b = 1.6348$
 $r = -0.87812$



CONSTANT TENSILE LOAD TEST AT 80°C IN WATER
P-1 GEOGRID SPECIMEN FINAL REPORT

PROJECT: Federal Highway Administration	MATERIAL: P-1 Geogrid	DATE OF REPORT: 12/22/96
JOB NUMBER: MP5548 / 03	TEST PARAMETERS: 20% Notch Depth, at 80°C, in Water	

Notched Specimens

Stress (psi)	200	240	280	360	440	520	600	680	760	840	920	1000	1120	1240	1360	1480								
Percent of Yield Strength ^{1,2}	4.01	4.76	5.60	7.22	8.77	10.26	11.96	13.43	15.25	16.75	18.40	20.17	22.25	24.62	27.21	29.20								
Specimen 1	>12475	885.9	103.7	42.1	29.7	24.7	16.2	24.5	21.3	21.0	24.4	48.1	47.2	45.3	5.2	4.0								
Specimen 2	9602	544.6	163.5	52.2	26.8	34.3	22.4		21.3	21.1	24.6	42.9	55.9	72.1	9.6	4.5								
Specimen 3		2349	180.9		39.7		24.8		23.8		23.1			94.7										
Specimen 4			108.2		55.9		24.9		25.4		23.6			92.1										
Specimen 5			212.4		48.0		24.4		25.9		32.6			36.6										
Mean (hr)	>11038	1260	153.7	47.2	40.0	29.5	22.5	24.5	23.5	21.1	25.7	45.5	51.6	68.2	7.4	4.3								
S.D. (hr)	N/A	958.73	47.04	N/A	12.22	N/A	3.69	N/A	2.19	N/A	3.93	N/A	N/A	26.51	N/A	N/A								
	BRITTLE ZONE								TP								DUCTILE ZONE							

Notes:

¹ P-1 Geogrid room temp. yield strength = 332.1 lb/in
(= 3,986 lb/ft , = 300.8 lb/rib)

² Represents an average yield strength.

TP = Selected Transition Point at 22.5 hr , 11.96 %

L.R.A. = Linear Regression Analysis,
from log (mean time) and log (mean yield strength).

³ Interpretation of brittle zone, using points :
(153.7, 5.60) , (1260, 4.76) , and (11038, 4.1).

N/A = Not Applicable

Brittle Zone L.R.A.:
m = -0.0729
b = 0.9063
r = -0.99944
Y₁₀₀ = 2.9717 %

Ductile Zone L.R.A.:
m = -0.0569
b = 1.4937
r = -0.97184



GEOSYNTEC CONSULTANTS
Materials Testing Laboratory

CONSTANT TENSILE LOAD TEST AT 50°C IN WATER
P-1 GEOGRID SPECIMEN FINAL REPORT

PROJECT: Federal Highway Administration	MATERIAL: P-1 Geogrid	DATE OF REPORT: 12/22/96
JOB NUMBER: MP5548 / 03	TEST PARAMETERS: 50°C, in Water	

Un-notched Specimens

Stress (psi) ¹	226	269	323	374	458	575	609	683	716	790	875	959	1049	1152	1250	1350	1450	1550	
Percent of Yield Strength ^{2,3}	7	9	11	13	15	17	19	21	23	25	28.09	31.01	34.28	37.39	40.96	43.89	48.12	50.82	
Specimen 1	>12936	>12937	>12937	>12937	>12937	>12938	>12937	>12937	>12937	>12936	>12937	>12937	>12937	320.6	208.6	115.5	83.5	39.7	5.0
Specimen 2											>8541	2062	582.6	219.3	115.3	80.1	39.7	21.3	
Specimen 3														513.6	277.5	116.0			
Specimen 4															98.4				
Specimen 5															119.3				
Mean (hr)	>12936	>12937	>12937	>12937	>12937	>12938	>12937	>12937	>12937	>12936	>12937	>10739	>7500	472.3	235.1	112.9	81.8	39.7	13.2
S.D. (hr)	N/A	135.80	37.08	8.27	N/A	N/A	N/A												

(TP) ? SHEAR-RUPTURE ZONE

Notes:

- 1 Represents an approximate average stress across the node.
- 2 Represents an average yield strength.
- 3 P-1 Geogrid room temp. yield strength = 332.1 lb/in
(= 3,986 lb/ft , = 300.8 lb/rib)
- (TP) = Assumed Transition Point between 13,000 hr , 31.2 % and 40,000 hr, 31 % , for prediction purposes.
(No brittle fractures were obtained in this test series.)
- L.R.A. = Linear Regression Analysis,
from log (mean time) and log (mean yield strength).
- 4 Conservative assumption of brittle zone "window," using points :
Boundary Line 2a : (17000, 31) , (121963, 23.3186) , and (875000, 17.5405); and
Boundary Line 2b : (50000, 30.80) , (209165, 25.0462) , and (875000, 20.3672).

N/A = Not Applicable

Brittle Zone L.R.A., Boundary Line 2a : ⁴

$$m = -0.1445$$

$$b = 2.1027$$

$$r = -1.00000$$

$$Y_{100} = 17.5405 \%$$

Shear-Rupture Zone L.R.A.:

$$m = -0.0793$$

$$b = 1.7829$$

$$r = -0.95412$$

Brittle Zone L.R.A., Boundary Line 2b : ⁴

$$m = -0.1445$$

$$b = 2.1676$$

$$r = -1.00000$$

$$Y_{100} = 20.3672 \%$$



PROJECT: Federal Highway Administration	MATERIAL: P-1 Geogrid	DATE OF REPORT: 12/22/96
JOB NUMBER: MP5548 / 03	TEST PARAMETERS: 65°C, in Water	

Un-notched Specimens

Stress (psf) ¹	170	222	298	320	411	432	518	581	689	707	755	877	950	1067	1177	1250
Percent of Yield Strength ^{2,3}	5	7	9	11	13	15	17	19.26	21.47	23.45	25	28	31.48	34.20	37.17	41.18
Specimen 1	>12957	>12957	>12958	>12958	>12957	>12956	>12940	4773	2801	3111	1213	602.1	319.8	100.0	40.5	5.1
Specimen 2								>7825	1208	>4919			296.0	92.6	32.1	2.3
Specimen 3													170.5			
Specimen 4													155.3			
Specimen 5													302.3			
Mean (hr)	>12957	>12957	>12958	>12958	>12957	>12956	>12940	>6299	2005	>4015	1213	602.1	248.8	96.3	36.3	3.7
s.d. (hr)	N/A	N/A	N/A	N/A	N/A	N/A	79.06	N/A	N/A	N/A						

BRITTLE ZONE

TP

SHEAR-RUPTURE ZONE

Notes:

- 1 Represents an approximate average stress across the node.
- 2 Represents an average yield strength.
- 3 P-1 Geogrid room temp. yield strength = 332.1 lb/in
(= 3,986 lb/ft , = 300.8 lb/ftb)

TP = Selected Transition Point at 602.1 hr , 28.00 %

TP selection was based on change in rupture mechanism.

L.R.A. = Linear Regression Analysis,

from log (mean time) and log (mean yield strength).

4 Interpretation of brittle zone, using points :

(1213, 25) , (2800, 22.5) , (7800, 20) , and (12940, 19).

N/A = Not Applicable

Brittle Zone L.R.A.:

$$m = -0.1162$$

$$b = 1.7546$$

$$r = -0.99931$$

$$y_{100} = 11.5966 \%$$

Shear-Rupture Zone L.R.A.:

$$m = -0.0626$$

$$b = 1.6561$$

$$r = -0.98369$$



GEOSYNTEC CONSULTANTS
Materials Testing Laboratory

CONSTANT TENSILE LOAD TEST AT 80°C IN WATER
P-1 GEOGRID SPECIMEN FINAL REPORT

PROJECT: Federal Highway Administration	MATERIAL: P-1 Geogrid	DATE OF REPORT: 12/22/96
JOB NUMBER: MP5548 / 03	TEST PARAMETERS: 80°C, in Water	

Un-notched Specimens

Stress (psi) ¹	158	217	283	336	440	460	542	596	629	715	740	850	851	966	1058	1151	1250
Percent of Yield Strength ^{2,3}	5	7	9	11	13	15	17	19.41	21.51	23.14	25	27.69	28.39	30.83	33.97	37.10	41.32
Specimen 1	>13010	>13055	>13055	>13054	7131	3060	2590	2269	558.4	377.3	323.9	122.3	56.7	8.3	7.5	2.7	>0.18
Specimen 2								823.2	1673	274.4		103.0	57.0	7.4	7.9	3.0	>0.23
Specimen 3								2450	1680	401.9		103.3	27.5				
Specimen 4								3211									
Specimen 5																	
Mean (hr)	>13010	>13055	>13055	>13054	7131	3060	2590	2188	1304	351.2	323.9	109.5	47.1	7.9	7.7	2.9	0.504
S.D. (hr)	N/A	N/A	N/A	N/A	N/A	N/A	N/A	997.4	645.5	67.64	N/A	11.06	16.95	N/A	N/A	N/A	N/A

BRITTLE ZONE

TP

SHEAR-RUPTURE ZONE

Notes:

- ¹ Represents an approximate average stress across the node.
- ² Represents an average yield strength.
- ³ P-1 Geogrid room temp. yield strength = 332.1 lb/in
(= 3,986 lb/ft , = 300.8 lb/rib)

TP = Selected Transition Point at 351.2 hr , 23.14 %

TP selection was based on change in rupture mechanism.

L.R.A. = Linear Regression Analysis,

from log (mean time) and log (mean yield strength).

⁴ Interpretation of brittle zone, using points :

(3060, 15) , (7131, 13) , and (13054, 11.67).

N/A = Not Applicable

Brittle Zone L.R.A.:

$$m = -0.1728$$

$$b = 1.7788$$

$$r = -0.99989$$

$$y_{100} = 5.6501 \%$$

Shear-Rupture Zone L.R.A.:

$$m = -0.0783$$

$$b = 1.5932$$

$$r = -0.99301$$